Toxin-Induced Ordering Transitions of Liquid Crystals at Biomolecular Interfaces

TARANG GUPTA

A thesis submitted for the partial fulfillment of the degree of Doctor of Philosophy

Department of Chemical Sciences
Indian Institute of Science Education and Research Mohali
Knowledge City, Sector 81, SAS Nagar, Manauli PO, Mohali 140306,
Punjab, India.

May 2024

Dedicated to

Humanity

&

my Beloved Papa

Declaration

The work presented in this thesis entitled "*Toxin-Induced Ordering Transitions of Liquid Crystals at Biomolecular Interfaces*" has been carried out by me under the guidance of ***Prof. Santanu Kumar Pal*** at the Indian Institute of Science Education and Research Mohali. This work has not been submitted in part or full for a degree, a diploma, or a fellowship to any other university or institute. Whenever contributions from others are made, every effort is made to indicate this clearly, with due acknowledgement of collaborative research and discussions. This thesis is a bonafide record of my original work, and all sources listed within have been detailed in the bibliography.

Tarang Gupta

TARANG GUPTA

In my capacity as the supervisor of the candidate's thesis work, I certify that the above statements by the candidate are true to the best of my knowledge.

Santanu Kumar Pal

Prof. SANTANU KUMAR PAL
Professor
Department of Chemical Sciences
Indian Institute of Science Education and Research Mohali

Acknowledgements

Crafting this doctoral thesis would have remained elusive without the invaluable aid and support from the constellation of individuals orbiting me – mentors, kin, companions, and colleagues. As the curtains fall on my doctoral journey, it's with heartfelt appreciation that I extend my thanks to every contributor who, through their diverse roles, paved the way for this thesis and etched indelible memories into my academic voyage.

First and foremost, I extend my heartfelt gratitude to my mentor, **Prof. Santanu Kumar Pal**, for granting me the privilege to conduct this thesis within his laboratory and for introducing me to the captivating realm of liquid crystal-based biosensors. I am immensely appreciative of his unwavering dedication. I am grateful for fulfilling every requirement in the lab without hesitation.

I thank **Dr. Raj Kumar Roy** and **Dr. Subhabrata Maiti**, members of my doctoral committee, for timely and fruitful discussions during the annual assessment of my work. I am grateful to **Dr. Arijit Kumar De, Dr. Raj Kumar Roy, Dr. Poonam Patyar** (Punjabi University, Patiala) and **Dr. Sanjay Singh** for their teaching and constant encouragement.

I want to acknowledge the Department of Chemical Sciences and Biological Sciences of IISER Mohali for various departmental facilities like circular dichroism, spectrofluorometer, AFM, etc.

I thank our former director, **Dr. J. Gowrishankar**, for providing the space, research infrastructure, and the HOD, Department of Chemical Sciences, Dr. Sripada S. V. Ramasastry for various departmental facilities. I am thankful to CSIR, India, for a five-year research fellowship.

I also appreciate the help and cooperation of the staff members of teaching laboratories, stores, purchase office, administrative offices, account section, library, and computing facility of IISER Mohali.

I want to thank **Dr. Indu Verma, Biswajit Panda** and **Dr. Ipsita Pani** for helping with various aspects of my thesis work. I also thank lab members of **Dr. Samrat Mukhopadhyay's** group for providing cuvettes to carry out circular dichroism measurements and helping during some of the initial AFM experiments. I also thank my collaborators, **Dr. Kausik Chattopadhyay** and **Dr. Shobhna Kapoor,** for their valuable suggestions.

I am also thankful for my current and former lab-mates: Dr. Harpreet, Dr. Ipsita, Dr. Supreet, Dr. Vidhika Punjani, Dr. Rajib, Dr. Joydip De, Dr. Indu Bala, Dr. Varsha Jain, Shruti, Ritu, Shallu, Soma, Sukanya, Anshika Baghla, Madhusudan Maity and Prerna. I am blessed to have beautiful lab mates who contributed to creating a pleasant laboratory working atmosphere. I especially appreciate **Dr. Ipsita Pani** for teaching me a valuable life lesson.

I wish to thank my dear friends **Kuljeet Kaur, Kulbir Shergill, Madhusudan Maity, Anshika Baghla, Sukanya Dutta, Dr. Vidhika Punjani** and **Dr. Varsha Jain** for their positive camaraderie. They have showered love, care, and affection during the tough times. They have been great mentors and excellent moral support throughout the thesis work.

I sincerely thank my parents, M. L. Gupta and Neelam Mohan, my sister Umang Walia, Mr. Akash Walia, and my little nephew Shivay, for their never-ending support and inspiration. Their constant motivation and belief in me made me travel this longer. I sincerely acknowledge my family members for their love, support, encouragement, and care throughout my life for my welfare.

Lastly, I acknowledge **IISER Mohali** for the financial support to carry out the experimental work and for all the research facilities that facilitated the completion of my Ph.D.

I thank the Almighty for everything I have and everything I am today.

Content

CHAPTER 1: Introduction to Liquid Crystals Sensors

Chapter 1

Introduction to Liquid Crystals Sensors

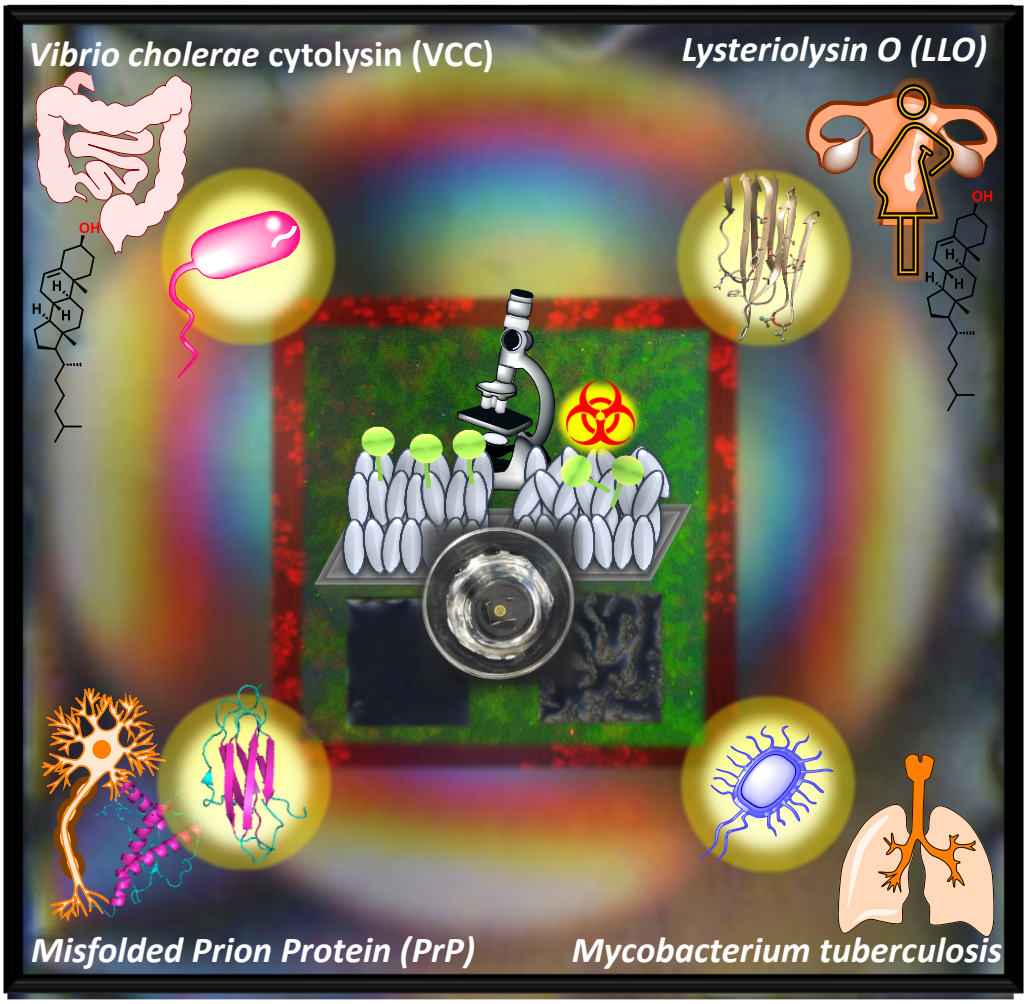

Beyond the evolution of the liquid crystal (LC) display arena, LC materials are now propelling frontiers within the vibrant realm of optical and bio-sensing systems. Unveiling biosensors crafted from LC materials, we unlock a world of label-free insights into biological marvels. LCs not only emulate biological systems but also allow us to detect their intricate behaviours. Cutting-edge investigations have unveiled a remarkable spectrum of toxin interactions with biomolecules at the LC-biomolecular interfaces.

Overview

Toxins are substances harmful to living organisms, often causing damage to cells, tissues, and organs. They can be produced by living organisms such as bacteria, fungi, plants, and animals or synthetic chemicals created by human activities.[1-9] The global COVID-19 pandemic has underscored the importance of studying toxins and comprehending their effects on diverse biomolecules. As the world grappled with the coronavirus outbreak, the significance of toxinology became glaringly evident. This crisis highlighted the need to unravel the intricate interactions between toxins and biomolecules to better prepare for and respond to emerging threats in the future. Efforts to understand the interactions of various toxins with biomolecules have led to the development and utilisation of a range of sophisticated techniques. Some of these include X-ray Crystallography,[1, 2] Nuclear Magnetic Resonance (NMR) Spectroscopy,[3, 4] Surface Plasmon Resonance (SPR),[5] Fluorescence Resonance Energy Transfer (FRET),[6, 7] and Bioinformatics and Computational Modeling.[8, 9] These techniques collectively enable researchers to decipher the intricate interactions between toxins and biomolecules, offering insights into molecular mechanisms and potential avenues for therapeutic interventions.[1-9] However, these methods face certain limitations.

Crystallization of the complex, immobilization, and specific labelling of interacting partners, which could potentially alter their behaviour, are prerequisites that restrict their applicability. Furthermore, they exhibit limited sensitivity, and the computational complexity and cost impose constraints on the scale and timeframe of systems that can be explored.[1-9] Extensive optimisation is also needed, particularly for larger or membrane-bound complexes. Despite these endeavours, simultaneous observation of lipid and protein changes remains challenging, with instances where non-covalent interactions cannot be detected. Moreover, studying these interactions at physiological concentrations proves to be a cumbersome task. The interface between the membrane and water encompasses a significant portion of the overall membrane volume, and most biological processes occur within aqueous environments. These challenges have consistently inspired researchers to develop novel sensors that operate with fewer constraints at physiological concentrations. In this regard, Liquid Crystal (LC) biosensors represent a promising avenue for advancing biomolecular detection and analysis, addressing some of the challenges posed by conventional methods and offering innovative solutions for various research and practical applications.[10-25] These sensors can be miniaturized and integrated into portable devices for point-of-care diagnostics and field applications.

In brief, LCs are a distinct state of matter that exhibits properties of both liquids and crystalline solids.[10-12] They possess a unique molecular arrangement characterized by anisotropic ordering, where the molecules within the material align in a preferred direction while still retaining some degree of fluidity.[13, 14] This ordered alignment leads to intriguing optical, electrical, and mechanical properties that make LCs useful in a variety of technological applications.[10-12] The behaviour of LCs is particularly sensitive to external factors such as temperature, pressure, and electric fields.[16, 17] This responsiveness allows them to change their optical properties, such as colour or transparency, in response to these influences. Indeed, the captivating attributes of LCs have sparked extensive exploration in the realm of biosensors.[25] Researchers have discovered that LCs offer a dynamic aqueous milieu in which biomolecular phenomena can be magnified, translating into optical signals.[10, 11] This intriguing capability has paved the way for innovative biosensing technologies that harness the responsive nature of LCs to detect and amplify molecular interactions, enabling label-free and real-time analysis of various biomolecules.

Motivated by these intriguing properties, the research compiled in this thesis endeavours to delve into the realm of LCs in order to investigate a spectrum of toxin interactions with lipids. These investigations collectively contribute to a fundamental comprehension of the stimuli-responsive LC system, shedding light on how toxins interact with a diverse array of biomolecules. To elaborate further, the utilization of LC-based systems has been the focus of exploration in this study. The objectives encompass: (i) enhanced understanding of pore-forming toxin interactions with lipid mixtures; (ii) role of lipids and cholesterol recognition motifs in *Listeriolysin O* pore formation; (iii) detection of conformational changes in biologically significant Prion protein that can lead to severe and often fatal diseases; (iv) designing an interface for studying spatiotemporally controlled lipids derived from *Mycobacterium Tuberculosis* and their interaction with antimicrobial peptides.

In essence, the research undertaken in this study aims to leverage LC-based systems to gain insights into the complex interplay between various biomolecules, toxins, and lipids, with implications for understanding diseases and advancing antimicrobial research.

1.1. Liquid Crystals (LCs)

LC is a delicate state of matter in nature. This intriguing state of matter is often found between a liquid and a solid phase, where molecules are arranged in an organized manner but are still able to move relatively freely.[13, 14] This unique state of matter exhibits properties of both liquids and solids

(Figure 1.1). They have the ability to flow like liquids yet possess some degree of order and structure characteristic of solids. In a LC, the molecules can be oriented in a specific direction or pattern, often referred to as a "mesophase," which is somewhere between the ordered structure of a solid crystal and the random arrangement of molecules in a liquid.[10-25] This ordered orientation makes LCs extremely sensitive to temperature, pressure, and electric field changes.[16, 17]

Various naturally occurring and synthetic materials can exhibit the LC phases, which possess the molecular characteristics necessary to display LC behaviour. Some common examples of substances that can exhibit LC phases include organic compounds, surfactants, polymers, and biological molecules.[8, 15] Typically, molecules that possess an anisometric shape or are arranged in an anisotropic manner tend to display LC phases. Guided by the underlying physical parameters dictating their manifestation of LC phases, they are broadly grouped into thermotropic and lyotropic categories.[16-18]

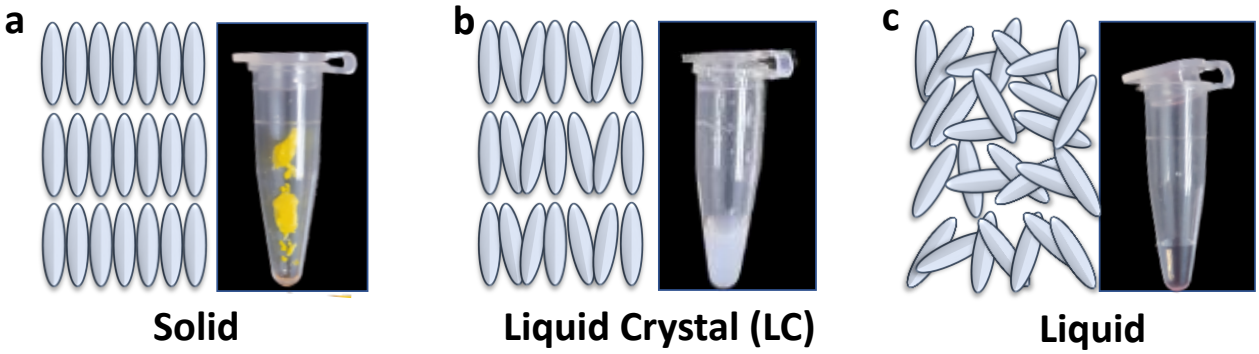

Figure 1.1 Schematic with real images of molecular arrangement in (a) solid, (b) Liquid Crystal (LC), and (c) isotropic liquids.

Thermotropic LCs are a type of LC phase that undergoes phase transitions as a result of changes in temperature.[16, 17] These transitions involve transformations between different ordered arrangements of molecules. However, lyotropic LCs are formed when specific substances, often amphiphilic molecules like surfactants or lipids, are dissolved in a solvent, usually a mixture of water and an organic solvent.[18] These LCs self-assemble into ordered structures, driven by the molecules and solvent interactions. Unlike thermotropic LCs, lyotropic LCs do not depend solely on temperature; their phases are influenced by concentration and other factors. Because thermotropic LCs present fewer constraints, our primary focus is primarily directed towards them.

Thermotropic LCs are subsequently categorized based on their shape into calamitic, bent, and disc

shapes.[14] Based on their molecular organization or symmetry within a mesophase, LCs are divided into nematics, smectics, and cholesterics mesophases (Figure 1.2).[14]

This thesis focuses explicitly on nematic LCs, which are composed of molecules with a rod-like shape. These mesophases are a combination of anisotropic physical properties like a solid and fluidity like a liquid, and hence, they possess a fascinating array of remarkable features that make them intriguing and valuable in various applications.[14] Some of these features include anisotropy, response to stimuli, birefringence, flexibility, versatility, and fast switching.

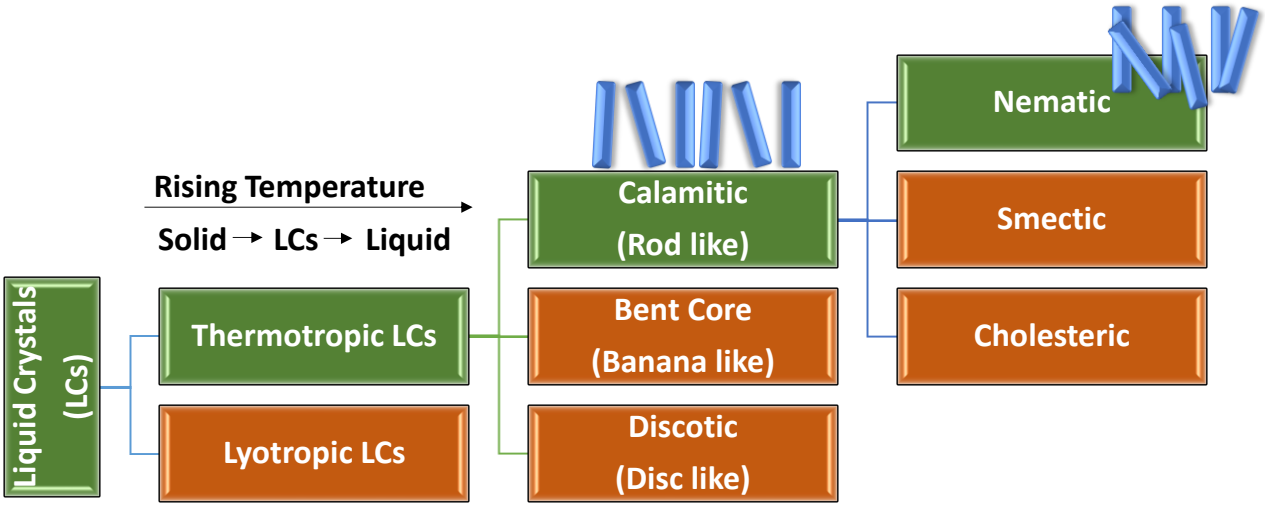

Figure 1.2 Classification of LCs based on various factors as described in the text.

The anisotropic properties mean their physical properties (such as refractive index, electrical conductivity, and thermal conductivity) vary depending on the direction. This anisotropy can be harnessed for controlled light manipulation and optical effects. They are highly responsive to external stimuli such as changes in temperature, pressure, and electric fields.[16, 17] This sensitivity allows them to be dynamically manipulated and controlled, making them ideal for use in various display technologies. LCs also have the ability to split light into two perpendicular polarizations, a phenomenon known as birefringence.[24-27] This property is exploited in optical devices, including polarization filters and waveplates.[24] Additionally, LCs can flow and adapt like liquids while retaining some level of molecular order. This flexibility and versatility make them suitable for applications ranging from display technologies to tunable lenses and smart windows.[24]

The exceptional combination of these features makes LCs an area of immense scientific exploration and technological innovation, with applications spanning from everyday consumer electronics to cutting-edge research and development.

1.2. Historical Outlook

The discovery of the LC phase and its constituent materials should not be misconstrued as an indication of its absence in the natural realm. LC phases are, in fact, omnipresent within the fabric of nature itself.[19-21] This is exemplified by the presence of LC ordering in various natural elements, such as DNA within living organisms, cell wall cellulose in plant life and fruits, collagen found in bones, corneas, and fish scales, as well as the chitin forming the protective exoskeletons of insects.[19-21] However, up to the early 19th century, the scientific community's understanding of matter's fundamental states was confined to the recognition of solids, liquids, and gases alone.[13] The awareness surrounding LC phases commenced its evolution in the latter part of the 19th century when Friedrich Reinitzer, an Austrian botanist, examined cholesterol benzoate, a derivative of cholesterol. During his investigation, he encountered a turbid liquid state at 145 ºC, which underwent a transformation into a clear liquid state upon further heating to 179 ºC.[13] Recognizing the peculiarity of this thermal behaviour, Reinitzer engaged in a collaborative exchange with Otto Lehmann, a German physicist. Lehmann subsequently conducted an exhaustive optical evaluation of the turbid phase, employing a polarizing microscope. His findings led him to the deduction that the turbid phase observed by Reinitzer exhibited attributes characteristic of both solids and liquids, thus bestowing upon it the epithet "crystalline liquid".[26] The history of LCs is a fascinating journey through scientific discovery, technological innovation, and diverse applications. The concise overview is briefly presented in various timelines.

First are the early observations in the Late 19th Century.[13] The study of LCs can be traced back to the late 19th century when researchers like Otto Lehmann and Friedrich Reinitzer observed unusual behaviours in certain organic compounds as they transitioned from solid to liquid. Reinitzer coined the term "liquid crystal" to describe these materials.

The second historical phase is the emergence of LC Science in the mid-20th Century. The true understanding of LCs started to develop in the mid-20th century. In 1927, Georges Friedel explained the anisotropic nature of LCs.[22] However, it was not until the 1960s that the molecular structure of LCs was better understood through the work of experts like Glenn H. Brown and others.[23] This laid the foundation for the science of LCs.

Third is the technological breakthrough of LCs, such as liquid crystal displays (LCDs) and displays in the 1960s-1970s. The invention of LCDs was the breakthrough that propelled LCs into the technological spotlight. In 1968, George Heilmeier and his team at RCA demonstrated the first

practical working LCD.[24] This marked the beginning of LCs' transformation into a commercially viable technology for digital displays.

Fourth, the 1980s witnessed significant advancements in LC technology, leading to improved display quality, response times, and energy efficiency. LCDs rapidly replaced older display technologies in devices like calculators, watches, and eventually computer monitors, TVs, and smartphones.[24]

In 1998, the groundbreaking research led by the Abbott group initiated a paradigm shift by unveiling an innovative framework centred on solid LC interfaces, which proved instrumental in detecting biomolecular interactions.[11] Since then, solid LC interfaces have gained substantial traction in investigating such interactions at physiological concentrations. Nevertheless, a significant challenge in this design pertains to the system's limited dynamism. Building upon this foundation, the Abbott group further demonstrated their ingenuity in 2002 by pioneering fluid LC interfaces, which provided a dynamic platform for studying binding events.[10]

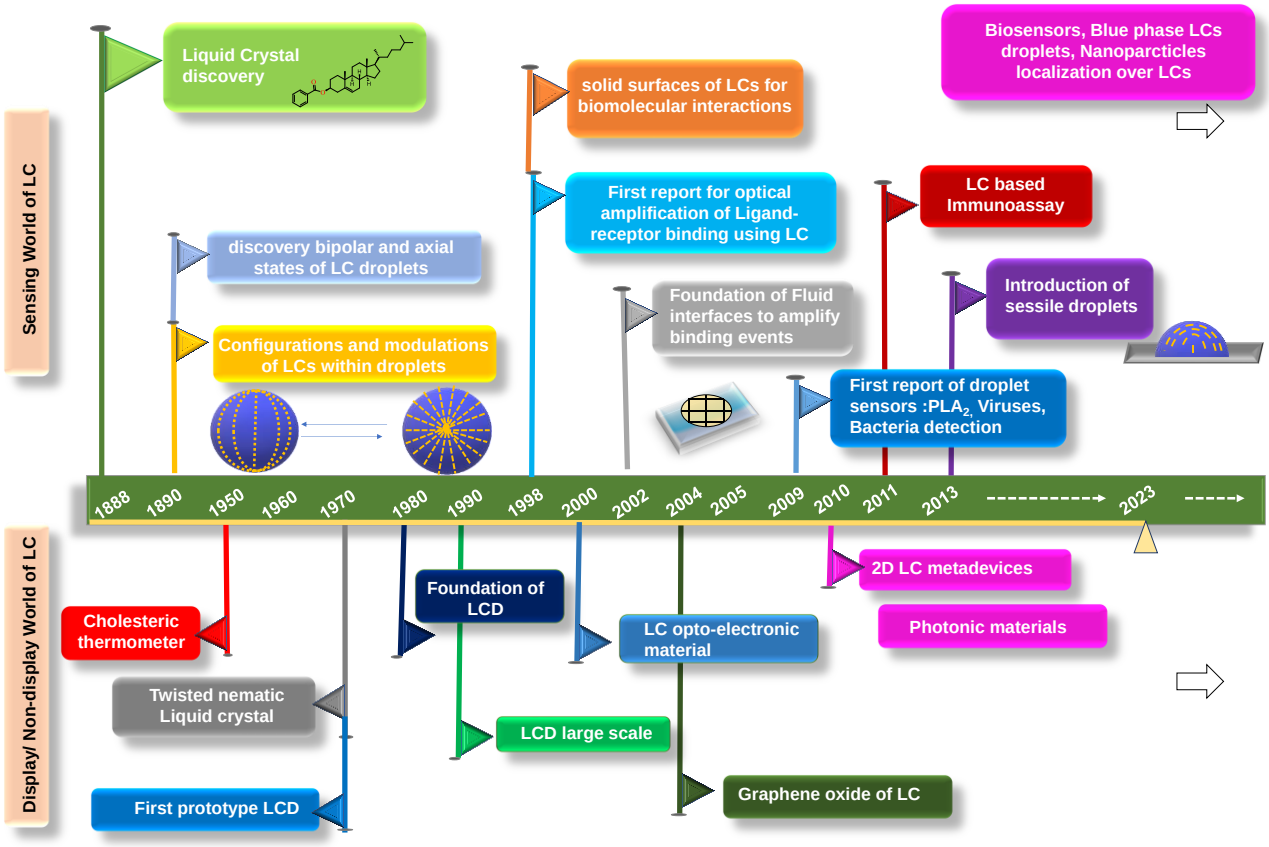

Figure 1.3 Flagpole diagram depicting the progression of LCs science.[10-14, 19-26]

Since then, the modern era of LCs has included the applications of LCs beyond displays. LCs have been commercialized and used in temperature-sensitive materials, optical devices, and tunable

lenses. LC polymers have been employed in responsive textiles and smart materials. LC also contributed to understanding complex biological systems. In collaboration with researchers from the University of Wisconsin-Madison, Platypus Technologies, a company based in Madison, has successfully brought to market an LC-based sensor designed for detecting toxic gases. Meanwhile, Crystal Diagnostics, situated in Kent (Ohio, USA), is actively pioneering advanced LC technology in partnership with researchers from the Advanced Materials and Liquid Crystal Institute (AMLCI) and Northeast Ohio Medical University (NEOMED), aimed at swiftly detecting a range of pathogens.[25] Ongoing research in LCs explores novel materials, structures, and applications. The quest for faster response times, wider viewing angles, and more sustainable technologies drive continuous innovation in the field of LC biosensing. The progression of different developments in LC is illustrated in the flagpole diagram (Figure 1.3).[10-14, 19-26]

In summary, the history of LCs is characterized by a gradual evolution from early observations of peculiar behaviours to the development of transformative display technologies and a wide range of applications in materials science, optics, and beyond. The journey continues as researchers and scientists explore new LC research and applications frontiers.

1.3. Thermotropic Nematic Mesophase

The least ordered phase of LCs is the nematic phase. In this phase, the LC molecules have a higher degree of freedom and minimal alignment.[13, 14, 22] Unlike more ordered phases, such as the smectic or cholesteric phases, where molecules have distinct positional arrangements, nematic molecules are only directionally aligned. This phase is characterized by its fluid-like behaviour while maintaining some directional ordering, making it a unique state of matter with properties that lie between those of liquids and solids. The orientation favoured locally within the medium may exhibit variation across the material, delineated by a vector denoted as n(r), representing its inherent orientation at a specific point. This vector is termed a "director".[26-28] To ensure its significance is purely directional, its magnitude is conventionally set to unity. The molecules themselves appear capable of rotation along their elongated axes, and any potential disparity in the arrangement of their two ends does not suggest a preferential alignment.

Consequently, the sign of the director holds no physical import, such that $n = -n$. In optical terms, a nematic substance behaves akin to a uniaxial material possessing a centre of symmetry. A graphical depiction of the molecular disposition within the nematic phase is shown in Figure 1.4a.

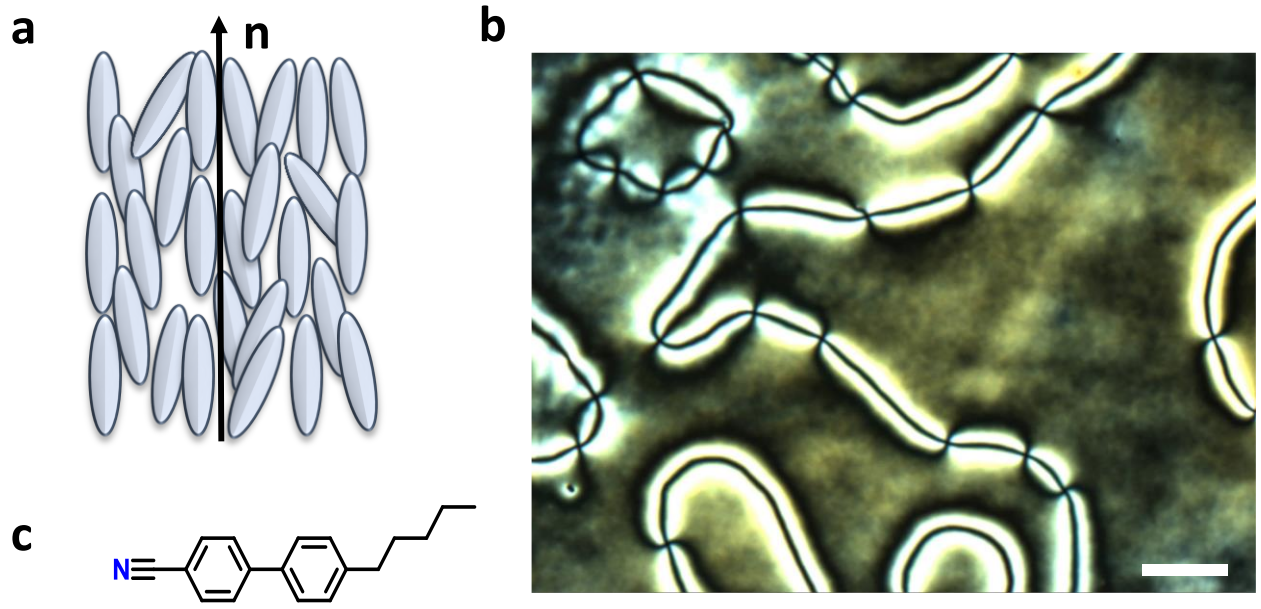

Figure 1.4 Schematic of the nematic mesophase. The nematic phase has uniaxial symmetry, as indicated by the arrow. b) The nematic texture of 5CB was captured using a 10x objective of Zeiss polarized optical microscope. Scale bar = 100 μm. c) Chemical structures of nematic LC 5CB.

The elongated, thread-like structures were observed using a polarized optical microscope (POM) with crossed polarizers, a characteristic from which nematics derive their name (Figure 1.4b).[26] Their low viscosity of nematic LCs allows for relatively easy flow and manipulation, contributing to their fluid-like behaviour and responsiveness. These characteristics give them their fluidic properties and make them suitable for biomedical applications, tunable lenses, switchable windows, and other practical applications.[29] As our study aims to investigate the effects of toxins on membranes, the phase that is most suitable for our research at room temperature is the nematic phase. One of the well-known compounds that exhibits a nematic mesophase at room temperature is 5CB (4-cyano-4'-n-pentylbiphenyl), whose structure is shown in Figure 1.4c. 5CB is in a crystalline state below 18 ºC and transitions to the nematic mesophase between 18 ºC and 35 ºC. Beyond 35 ºC, 5CB behaves like a conventional fluid.[29]

1.4. Characteristics of Thermotropic Nematic Mesophase for Sensing

Listed below are the characteristics of the nematic mesophase of calamitic LCs that render them a compelling category of materials for investigating their interfacial interactions with biological

systems.

1.4.1. Order parameter

The distinctive contrast between a nematic phase and an isotropic liquid arises from the extent of molecular orientational arrangement, which is measured by an order parameter denoted as *S*. This order parameter, defined in equation 1.1 as illustrated below, encapsulates the angular relationship (θ) between the director and the elongated molecular axis.[26]

$$\boldsymbol{S} = < \frac{\mathbf{3}\,\boldsymbol{Cos^2\theta - 1}}{\mathbf{2}} > \qquad 1.1$$

In the fully clear isotropic phase, the order parameter *S* is zero, signifying a lack of molecular alignment. Conversely, S assumes one value for a crystal phase with perfect orientational ordering. In the case of a nematic phase, the order parameter *S* typically falls within the range of 0.3 to 0.7, reflecting the intermediate level of orientational ordering exhibited by nematic LCs.

1.4.2. Optical anisotropy (Birefringence)

Birefringence, also known as double refraction, is a phenomenon observed in anisotropic materials or substances with properties that vary based on the direction in which they are measured. In the context of optics, birefringence refers to the ability of a material to split a single incident light ray into two distinct rays, each with a different refractive index, as they pass through the material.[24-31] These two rays travel with different velocities and directions, separating the light into two distinct paths.

The origin of birefringence in materials often lies in their molecular or crystalline structure. In anisotropic materials like LCs, the arrangement of molecules is not uniform in all directions, giving rise to different refractive indices for light polarized along different axes.[24-31] When anisotropic materials interact with light, the refractive index experienced by the light depends on its polarization direction relative to the material's internal structure.

In the case of LCs, molecules that can align themselves in specific directions under certain conditions, birefringence arises due to the alignment of molecules along the director or optic axis. Light travelling parallel to this axis experiences one refractive index (extraordinary index, $n_{\parallel}$), while light travelling perpendicular to this axis experiences another refractive index (ordinary index, $n_{\perp}$).[29]

Consequently, the numerical disparity, denoted as $\Delta n = n_{\parallel} - n_{\perp}$, between these refractive indices (referred to as "birefringence") is not equal to zero. Typically, nematic phases display optical positivity, meaning that the refractive index along the extraordinary axis ($n_{\parallel}$) is greater than the refractive index along the ordinary axis ($n_{\perp}$). Conversely, in an optically negative phase, the refractive index along the extraordinary axis ($n_{\parallel}$) is smaller than the refractive index along the ordinary axis ($n_{\perp}$).[29]

Birefringence has essential implications in various fields, including optics, materials science, and biology. It is used in applications such as polarizing filters, optical modulators, and waveplates in optical devices.[22-29] In biological microscopy, birefringence can provide valuable information about the structural properties of biological tissues, such as collagen fibres in connective tissues.

1.4.3. Surface-Induced Alignment of LCs

Surface-induced anchoring of LCs refers to the alignment and orientation of LC molecules at the interface or boundary between the LC material and a solid surface.[27] This phenomenon is pivotal in controlling LC systems' overall behaviour and optical properties in various applications, particularly in LCDs, optical modulators, and other electro-optical devices.[24] When a LC comes into contact with a solid surface, the LC molecules tend to align or orient themselves in a preferred direction parallel or perpendicular to the surface.[28] This alignment results from interactions between the LC molecules and the atoms or molecules of the solid surface. The way in which the LC molecules anchor or orient themselves at the surface can significantly influence the macroscopic properties of the LC material. The LC director, relative to the surface, corresponds to the orientation with the lowest free energy and is generally termed the LC's "easy axis" (Figure 1.5a).[27, 28] However, the application of an external field or the presence of a surface can induce a departure of the director from this easy axis. The energy required to move the director away from the easy axis is referred to as the "anchoring energy" (W_a), serving as a quantitative measure of the anchoring strength. Consequently, the interfacial free energy, which exhibits dependency on orientation, is often mathematically expressed as equation 1.2.[13, 29]

$$S = S_0 + \frac{1}{2} W_a \sin^2(\theta_s - \theta_e) \qquad 1.2$$

Where S represents the overall interfacial free energy, S_0 accounts for the orientation-independent

component of interfacial free energy, θ_s signifies the orientation of the surface director, and θ_e signifies the orientation of the easy axis. This interplay between surface-induced anchoring and the alignment of the LC director significantly influences the behaviour and properties of LCs at interfaces.[29]

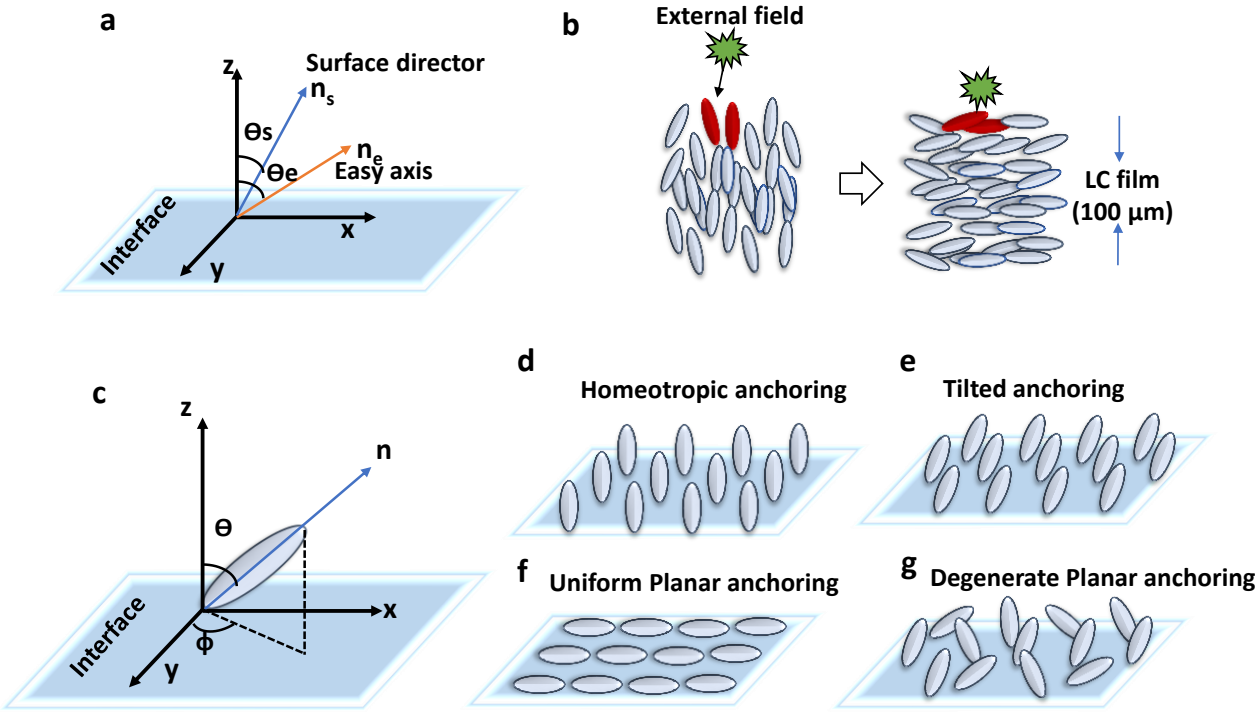

Figure 1.5 The diagram presents a visual representation: (a) of the director and the nematic LC's easy axis, while (b) demonstrates the orientational shifts of nematic LCs prompted by interfacial interactions. The schematic (c) exhibits visual depictions of two notable anchoring angles - the polar angle (θ) and the azimuthal angle (ϕ). It also explores the anchoring of nematic LCs on a surface with distinct configurations: (d) homeotropic anchoring, (e) tilted anchoring, (f) uniform planar anchoring, and (g) degenerate planar anchoring. Redrawn from reference [29, 13].

The established range for W_a typically falls between 10^{-3} and 10^{-2} mJ/m^2, as documented in previous studies.[13, 29, 30] Consequently, even subtle alterations in the topography and chemical properties of a LC interface can perturb the interfacial energetics on this scale, potentially triggering transitions in the orientational alignment of the LC molecules. Unlike isotropic liquids, this surface-induced preference for orientation extends over a considerable distance of 100 µm (significantly exceeding the size of the nematic mesogen) from the interface. This is attributed to the long-range ordering of LCs, as depicted in Figure 1.5b. The distinctive arrangement of LC molecules results in an

anisotropic optical characteristic that can be readily assessed using optical techniques.[31]

The orientation of LC molecules at a surface is defined by two angular components: azimuthal anchoring (ϕ) and polar anchoring (θ), as illustrated in Figure 1.5c. The polar angle represents the angle formed between the LC director (n) and the normal to the substrate (y). On the other hand, the azimuthal angle (ϕ) describes the in-plane orientation of the LC director relative to a reference azimuthal axis (x).[29] These distinct configurations capture the diverse ways in which the LC molecules orient themselves at the surface, influencing their overall behaviour and optical properties. Depending on the specific interactions and alignment configurations, there are different types of surface-induced anchoring, including homeotropic anchoring, planar anchoring, tilted anchoring, and degenerate planar anchoring.[28, 29] Homeotropic anchoring is the perpendicular alignment of LC molecules to the surface. This can be achieved by treating the surface with specific alignment layers or coatings that promote this perpendicular alignment. For $\theta = 0$, the LC molecules exhibit homeotropic anchoring (perpendicular to the surface).

Planar anchoring occurs when LC molecules lie parallel to the surface. This can be achieved by treating the surface with substances that encourage this parallel alignment. Planar anchoring is common in twisted nematic (T_N) LCDs, where the LC molecules are twisted between two substrates to create different optical states.[24] When $\theta = \pi/2$ and ϕ remains constant, it corresponds to a uniform planar alignment. In the case where $0 < \theta < \pi/2$ and ϕ remains constant, it represents tilted anchoring. When $\theta = \pi/2$ and ϕ take arbitrary values, it characterizes degenerate planar anchoring.[13, 32] The anchoring behaviour can be described using the director's orientation as depicted in Figure 1.5b-e.

Thus, surface-induced anchoring is crucial for the functionality of these devices. It helps to define the LC molecular arrangement, which in turn affects the devices' optical properties, response times, and viewing angles. By carefully controlling the surface treatment and the interactions between the LC molecules and the surface, engineers and researchers can design and optimize the performance of LC-based technologies.

1.4.4. Elasticity of LCs

The preferred molecular orientation within LCs gives rise to anisotropic properties, meaning that the material's properties differ depending on the measurement direction. This anisotropy is a result of the ordered arrangement of molecules.[29] Bending elasticity (K_{33}) describes how resistant the material is to bend. If the director is bent, the LC will experience a strain, and the bending elasticity quantifies

the material's resistance to this deformation. Splay elasticity (K_{11}) characterizes the material's resistance to the director being spread apart or splayed. It's associated with the variation of the director's orientation in a plane perpendicular to the deformation axis. Twist elasticity (K_{22}) reflects the material's resistance to the twisting of the director around an axis. It is related to the change in the director's orientation along the deformation axis.[29]

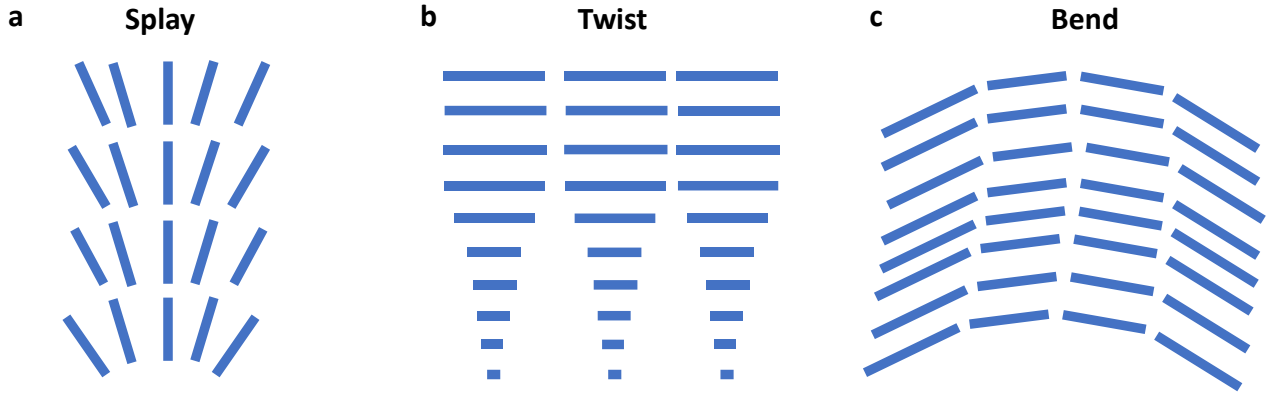

Figure 1.6 Schematic visualizations of three distinct modes of deformation within LCs: (a) splay, (b) twist, and (c) bend. Redrawn and reproduced from reference [29].

When external forces are applied to a LC, they can cause the director to deviate from its equilibrium orientation. Depending on the nature of the force, different modes of deformation (splay, twist, bend) can occur, as shown in Figure 1.6.[29] These deformations involve changes in the director's orientation and result in strain within the material.

The elastic behaviour of a confined LC system can be described using the Frank-Oseen equation. This equation relates the arbitrary curvature of the director to the different deformation modes (splay, twist, and bend) and their associated elastic constants: K_{11}, K_{22}, and K_{33}.[13, 29] These constants quantify the resistance of the LC to deformations in different directions. They are intrinsic material properties that determine how the material responds to external forces and changes in director orientation.

The LC elastic free energy density (F_d) coupled with the strain of a nematic LC is described in equation 1.3 below[13, 29]:

$$\boldsymbol{F_d = \frac{1}{2}\, K_{11}(\nabla.\hat{n})^2 + \frac{1}{2}\, K_{22}(\hat{n}.\nabla\times\hat{n})^2 + \frac{1}{2}\, K_{33}(\hat{n}\times(\nabla\times\hat{n}))^2} \qquad 1.3$$

where n represents the director of the nematic LC.

The typical magnitude of the three elastic constants is around 10^{-11} N.[26, 30] The comprehension of the elasticity characteristics of LCs plays a vital role in investigating the variations in order parameters and the stability of defects within them. The significance of the elastic energy retained within the LC

layer and the influence of orientation-dependent surface energies on the overall free energy of the LC are contingent on the system's geometric configuration. This interplay often gives rise to intriguing interfacial phenomena.[26-32]

In summary, the elastic properties of LCs are influenced by the long-range orientation of molecules within the LC phase. The anisotropic nature of LCs, created by the ordered alignment of molecules along the director, leads to specific elastic responses to different types of deformations. The bending, splay, and twist elasticities quantify the LC's resistance to deformations in different directions and play a significant role in understanding the material's behaviour under external forces.

1.5. LC sensors

LC sensors are devices that utilize the properties of LCs to detect and respond to changes in environmental conditions, physical parameters, or the presence of specific molecules.[24, 29] These sensors take advantage of the unique optical, electrical, and mechanical characteristics of LCs to achieve sensitive and selective detection. The principle of operation of LC sensors is to detect changes in these properties when the LC material interacts with a specific stimulus, such as temperature, electric fields, pressure, mechanical stress, or the presence of target molecules.[33, 34] LCs exhibit different optical properties, such as colour, birefringence, and polarization, based on their molecular alignment. These sensors have a wide range of applications in electronics, biology, chemistry, and environmental monitoring. There are various types of LC sensors, as listed:

(i) Temperature Sensors: LCs are sensitive to temperature changes, and their optical properties can be used to measure temperature variations.[35, 36]

(ii) Pressure Sensors: Applying pressure to a LC can alter its molecular alignment, changing its optical properties.[37, 38]

(iii) Chemical Sensors: LC sensors can be functionalized with specific molecules (receptors) that bind to target analytes, leading to LC optical response changes. This is often used for detecting gases, ions, or biomolecules.[39, 40]

(iv) Biochemical Sensors: LC sensors can detect specific biomolecules (such as proteins, DNA, or antibodies) by leveraging molecular recognition events that cause changes in LC alignment.[41, 42]

Given that these sensors provide label-free detection, real-time monitoring, and potential portability, along with their high sensitivity, there is a strong demand for their utilization in the rapid and

sensitive diagnosis of disease markers, viruses, and bacteria in biological samples.[35-42] As a result, the primary focus of this thesis is the comprehensive investigation of the interactions between various toxins and biomolecular interfaces.

The basic principle of operation of these LC biosensors involves exploiting the sensitivity of LCs to molecular interactions. When the LC film comes into contact with the target biomolecule, it can induce changes in the ordering or orientation of the LC molecules. These changes might lead to alterations in the LC's optical properties, such as changes in colour, birefringence, or polarization, which can be observed and quantified.[29] In a LC biosensor, the LC material is often coated onto a substrate or surface, forming a thin film. The LC film is designed to interact with target biomolecules, leading to detectable changes in the LC's properties. These changes can be translated into signals that are measured and interpreted to provide information about the presence or concentration of the target biomolecule.

In this thesis, our focus has centred on exploring interfaces that arise between aqueous phases and thermotropic LC, driven by two primary factors: (a) the deformable nature of the interface due to the immiscibility between thermotropic LCs and water and (b) the incorporation of an aqueous phase that preserves the inherent activity of biological analytes, allowing for the examination of the influence of biomolecular interactions on LCs.

1.6. Experimental platform (Aqueous-LC thin films Interfaces)

Guided by the promising applications of LCs in chemical and biological sensing, the scientific community has employed a range of methodologies to create LC-aqueous interfaces, including techniques involving stabilizing LC films within micro-fabricated structures. These interfaces are often characterized by planar and curved geometries. Given that our primary emphasis is on studying the diverse conformational changes of toxins at biomolecular interfaces, which can be effectively showcased using thin films of LCs, our research predominantly revolves around the utilization of LC thin film interfaces. Brake and Abbott's pioneering work in 2002 serves as a prototype for planar interfaces between LCs and aqueous phases.[10] A visual representation of this concept is provided in Figure 1.7. This methodology involves placing a metallic transmission electron microscopy (TEM) grid onto a glass substrate. Before implementation, the glass substrate is chemically modified to dictate the orientation of the LC at the lower surface. Octadecyltrichlorosilane (OTS) or dimethyloctadecyl[3(trimethoxysilyl)propyl]ammonium chloride (DMOAP) are the preferred

silanes for glass treatment, as they induce strong homeotropic (perpendicular) anchoring of most nematic LCs.

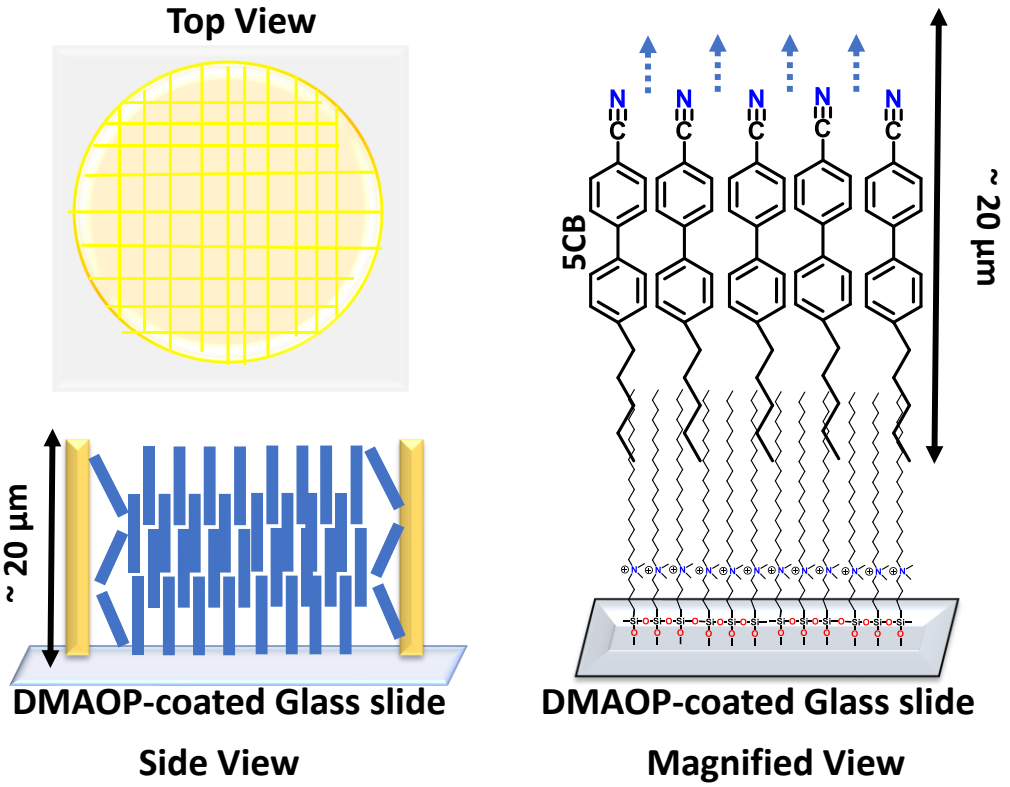

Figure 1.7 Experimental configuration of LC thin films employed in a biosensor, showcasing top, side, and magnified views.

Subsequently, the LC material is introduced into the grid's pores, facilitating mechanical support against the aqueous phase through capillary forces between the LC and the metal. In the absence of excess LC, the film's thickness is approximately equivalent to the grid's dimension. Within each grid square, the bottom substrate of the LC film makes contact with DMOAP, aligning LC molecules perpendicular to the surface plane.[29] The upper LC surface interacts with air, promoting homeotropic anchoring, resulting in a uniform perpendicular alignment of the director throughout the bulk. This configuration produces a black image under crossed polarizers (Figure 1.8a). The supported LC film is then submerged in an aqueous solution to establish an approximately uniform LC-aqueous interface (Figure 1.8b). Water or an aqueous buffer typically aligns the LC director parallel to the substrate, generating a hybrid configuration in bulk. Consequently, hybrid conditions yield non-zero effective birefringence, causing the optical texture to appear bright and nonuniform between crossed

linear polarizers (Figure 1.8b). Upon the self-assembly of surfactants into the aqueous phase, a dark optical appearance emerges, consistent with the homeotropic orientation of LC (Figure 1.8c).

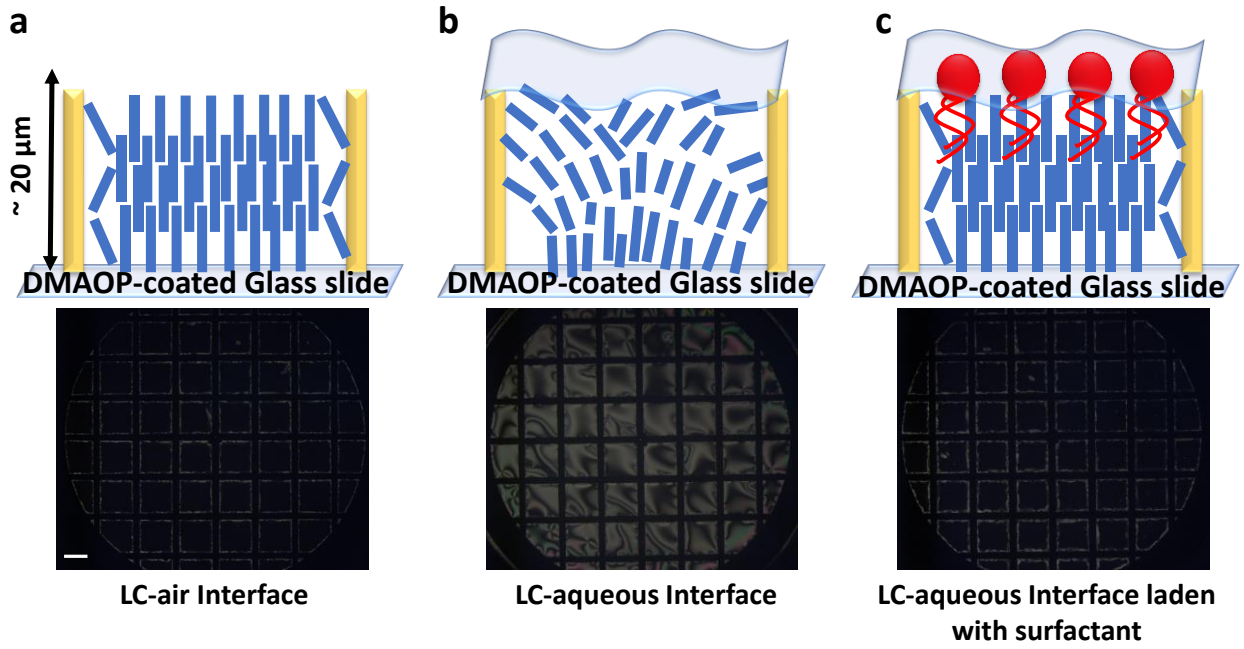

Figure 1.8 The Exemplary POM images and corresponding illustrative depictions of LC alignments upon interaction with (b) air, (c) water, and (d) 9 µM cetyltrimethylammonium bromide (CTAB) surfactant (amphiphile) in the aqueous medium. Scale bar = 200 µm.

Progressive exploration has firmly established that the adsorption of amphiphiles triggers the homeotropic orientation of LCs at interfaces between LCs and aqueous phases.[28, 43, 44] A Thorough investigation has been devoted to scrutinizing the detailed influence of molecular attributes (such as branching and chain length) and the organizational dynamics of adsorbed amphiphiles. This inquiry has yielded a comprehensive understanding of the intricate correlation between LC ordering and the intermolecular interactions occurring among adsorbates/mesogens. The investigation has also furnished compelling evidence, underscoring that the predominant driving force behind the homeotropic LC ordering at aqueous interfaces is the lateral hydrophobic interactions between the hydrocarbon chains of mesogens and the amphiphile. It follows a logical pattern that the hydrophilic portion of the amphiphile aligns with the aqueous phase while the hydrocarbon tails intercalate within the LC medium. Notably, the nematic elasticity of the LC has been identified as a pivotal factor shaping the interfacial arrangement of molecular assemblies.[45]

The LC-aqueous interface is remarkably sensitive to the presence of amphiphiles, including naturally

occurring phospholipids that constitute a key component of biological membranes. As a result, numerous investigations have been conducted utilizing these interfaces to explore various biomolecular interactions. Leveraging the biomimetic attributes inherent in this interface, a diverse array of designs has emerged, harnessing its potential for sensing biomolecular phenomena. In particular, the reorganization of phospholipids induced by specific biomolecular interactions with proteins has been observed to initiate transformative ordering transitions within LCs. Furthermore, it is well-documented that the highly specific event of DNA hybridization at the LC-aqueous interface induces a distinct orientational transition of LCs.[46] The dynamic responsiveness of LCs, which undergo ordering transitions contingent on the molecular structure of analytes present at the interface, holds significant implications for sensing applications. For example, while lipids induce a homeotropic ordering of LCs, proteins incite a planar anchoring of LCs at the aqueous interface. Furthermore, LCs exhibit distinct ordering profiles dictated by the aggregated states of proteins.[47]

In recent years, LC-based interfaces have been ingeniously leveraged as optical tools for detecting an array of biomolecules, biomarkers, and toxic analytes. These encompass acetylcholinesterase,[48] bile acids,[49] cellulase, cysteine,[50] pesticides,[51] glucose,[52] heavy metal ions such as Cu^{2+},[53] Hg^{2+},[54, 55] human breast cancer cells,[56] and more. Leveraging their remarkable ability to discern subtle interfacial variations, the interfaces formed between LCs and aqueous phases embody a captivating and promising category of stimuli-responsive materials that hold the potential to advance various technologies. As the field progresses, experimental and theoretical studies of the alignment process in LCs, which serves as the foundational framework of LC biosensors, will undoubtedly continue to offer invaluable insights into interfacial interactions. This ongoing endeavour is poised to enhance sensitivity and efficiency in utilizing alignment mechanisms to their full potential.

In summary, LC sensors are versatile devices that leverage the unique properties of LCs to detect changes in various parameters. LC biosensors offer advantages such as label-free detection, real-time monitoring, and potentially high sensitivity. However, they also come with challenges related to optimizing sensitivity, specificity, and reproducibility and addressing potential interference from complex biological matrices.

1.7. Decoration of Amphiphiles at aqueous-LC Interfaces

Assembling amphiphiles plays a crucial role in various scientific and technological applications, particularly at LC-aqueous interfaces. These interfaces involve the interaction between LC molecules

and aqueous phases, and assembling amphiphiles can influence the behaviour and properties of these interfaces.[29]

Amphiphiles are molecules that possess both hydrophilic (water-attracting) and hydrophobic (water-repelling) components. These assemblies of amphiphiles are responsive to external stimuli, such as changes in temperature, pH, or ion concentration. This responsiveness can be harnessed to control the properties of the LC-aqueous interface.

As previously mentioned, our aim is to investigate the interactions between diverse toxins and biological membranes primarily consisting of lipids laden at the LC-aqueous interface. In the subsequent section, we will elucidate two approaches for arranging amphiphiles at these interfaces.

1.7.1. Vesicle Fusion

Understanding vesicle fusion at the LC-aqueous interface has implications for various fields, including materials science, drug delivery, and biophysics. It could contribute to the development of innovative drug delivery systems, the design of biomimetic materials, and the fundamental understanding of membrane interactions in complex environments. Studying vesicle fusion at the LC-aqueous interface can offer unique insights into the interplay between lipid bilayers, LC, and aqueous environments.

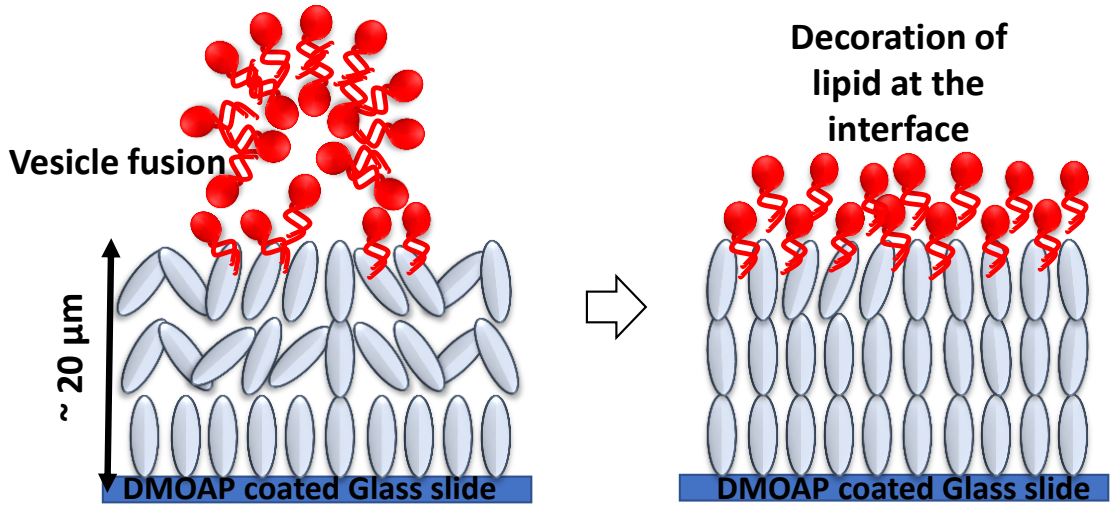

Figure 1.9 Schematic demonstrating the spontaneous lipid vesicle fusion at LC-aqueous interface.

The LC phase introduces an additional dimension of complexity due to its ordered molecular arrangement and responsiveness to external stimuli. The interaction between vesicles and the LC

phase can influence vesicle fusion dynamics, energetics, and mechanisms.[57-58] Vesicle fusion at the LC-aqueous interface refers to the process in which lipid vesicles (small, spherical lipid bilayer structures) interact and merge their membranes within the context of the interface between a LC phase and an aqueous phase.[57] This process involves the fusion of lipid bilayers from two or more vesicles, resulting in the formation of larger vesicles or the exchange of their contents. The lateral arrangement of lipids was motivated by the aim to reduce the elastic energy stored within the nematic LC layer.[58] Figure 1.9 illustrates the natural fusion of a lipid vesicle with the LC-aqueous interface. This transition occurs by creating vertically aligned domains, which gradually spread across the entirety of the interface.

1.7.2. Langmuir-Blodgett Monolayer Technique

The Langmuir-Blodgett monolayer technique involves the controlled deposition of a monolayer of amphiphilic molecules from an air-water interface onto a substrate.[59] This technique allows for the precise formation of well-ordered and organized molecular layers, offering insights into interfacial phenomena, molecular interactions, and the creation of functional materials.

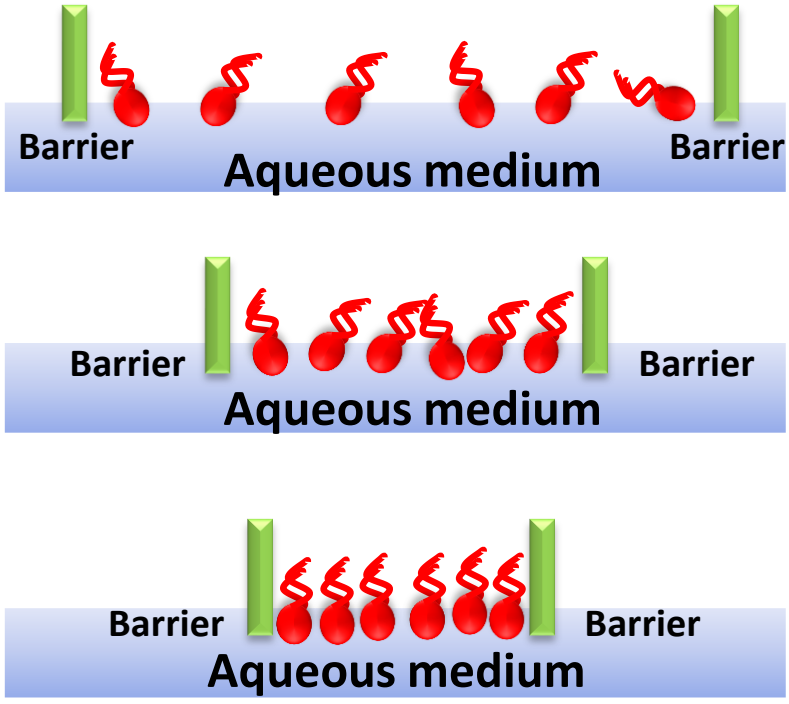

Figure 1.10 Schematic representation demonstrating the formation of the monolayer by compression of the barriers using the Langmuir-Blodgett technique.

The Langmuir-Blodgett (LB) method has been extensively employed in various scientific and technological applications. In the Langmuir-Blodgett monolayer technique, amphiphilic molecules with both hydrophilic and hydrophobic parts are spread as a monolayer on the water surface within a Langmuir trough.[60] The molecules self-organize due to their affinity for the air-water interface, with the hydrophobic tails oriented toward the air and the hydrophilic heads interacting with water. The monolayer is compressed or expanded by moving the barriers of the Langmuir trough. This manipulation increases or decreases the surface density of the monolayer, affecting the packing and orientation of the amphiphilic molecules. The Langmuir-isotherm describes the behaviour of molecules or nanoparticles that spontaneously adsorb at the air-water interface. When molecules are spread on the water surface, they can form a monolayer, and the surface pressure increases as more molecules are added.

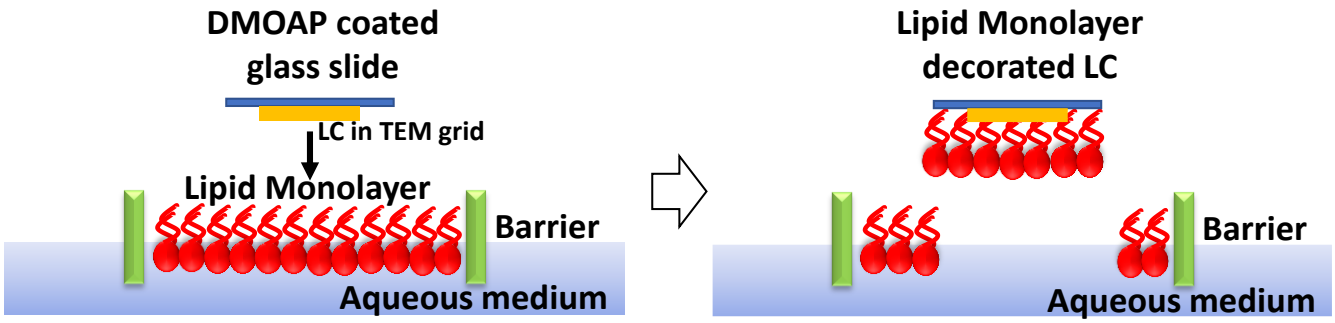

Figure 1.11 Diagram illustrating the Langmuir-Schaefer technique of transferring lipid monolayer at LC interface.[59, 60]

The isotherm helps to understand how molecules or particles adsorb and arrange themselves at the interface and how the surface pressure changes as a function of the amount of material added. Figure 1.10 illustrates the formation of the monolayer by compression of the barriers using Langmuir-Blodgett technique. A LC supported by a TEM grid and DMOAP-coated glass slide is carefully dipped through the monolayer at the air-water interface. A LC supported by a TEM grid and DMOAP-coated glass slide is carefully dipped through the monolayer at the air-water interface. As the substrate is withdrawn, it carries a portion of the monolayer with it, resulting in a single molecular layer deposition on the substrate. The schematic in Figure 1.11 illustrates the Langmuir-Schaefer technique of transferring the monolayer at the LC interface.

1.8. Introduction to various toxins and biomolecules addressed in the studies

Within this thesis, we have delved into the nanoscale examination of aqueous interfaces of LC concerning a range of toxins interacting with lipid membranes. We focus on elucidating specific interactions occurring at these LC-aqueous interfaces in each inquiry. The ensuing section serves to acquaint the readers with the significance of the interactions explored in their respective chapters.

1.8.1 *Vibrio Cholerae* Ccytolysin (VCC)

Vibrio Cholerae Cytolysin, also known as VCC or V. cholerae cytolysin, is a protein toxin produced by the bacterium *Vibrio cholerae*. *Vibrio cholerae* is the causative agent of cholera, a severe diarrheal disease that can lead to dehydration and potentially fatal outcomes if not treated promptly.[61]

VCC is a pore-forming toxin, which means that it can create pores in the membranes of target cells, disrupting their integrity and leading to cell lysis (rupture).[61, 62] The toxin is involved in the pathogenesis of cholera by contributing to the damage of intestinal epithelial cells, which are the cells lining the gut.[62-64] This damage to the gut lining contributes to the massive fluid loss characteristic of cholera diarrhoea. VCC's exact mechanism of action involves its binding to target cell membranes, oligomerization (formation of protein complexes), and insertion into the cell membrane, where it creates pores.[62-64] These pores disrupt the osmotic balance of the cell, leading to the influx of water and ions and eventually causing cell lysis. The action of VCC is highly impacted by the presence of cholesterol in the lipid membranes.[65] The interaction between VCC and cholesterol molecules in the membrane enhances the stability and effectiveness of the toxin's pore-forming activity.[66, 67] Cholesterol serves as a co-factor that helps stabilize the VCC structure and promotes its integration into the membrane, thereby increasing the toxin's cytotoxic effects on the target cells.[66, 67] The study of VCC is essential for understanding the molecular mechanisms behind the virulence of *Vibrio cholerae* and the pathogenesis of cholera. Researchers aim to elucidate the toxin's interactions with host cells, its role in disease progression, and its potential as a target for therapeutic interventions.

1.8.2. Lysteriolysin O (LLO)

Lysteriolysin O (LLO) is a protein toxin produced by the bacterium *Listeria Monocytogenes*. *Listeria*

monocytogenes is a pathogenic bacterium that can cause listeriosis, a foodborne illness that primarily affects individuals with weakened immune systems, pregnant women, newborns, and the elderly.[68, 69] LLO is a key virulence factor of *Listeria monocytogenes*, playing a critical role in the bacterium's ability to invade and survive within host cells. LLO is classified as a pore-forming toxin because it has the ability to create pores in cell membranes.[69] These pores disrupt the integrity of the membrane, leading to changes in membrane permeability, ion imbalance, and cellular damage.[68]

Listeria monocytogenes is engulfed by host cells through phagocytosis, a process where the bacterium is enclosed within a cellular compartment called a phagosome.[68-70] *Listeria monocytogenes* secrete LLO and plays a crucial role in breaking down the phagosomal membrane, allowing the bacterium to escape into the host cell's cytoplasm. This escape is critical for the bacterium's ability to replicate and spread within the host. Once *Listeria monocytogenes* escape the phagosome, it can replicate within the host cell's cytoplasm. LLO contributes to the bacterium's intracellular survival and growth by disrupting cellular membranes and facilitating nutrient uptake.[68-70] By escaping the phagosome and replicating in the host cell's cytoplasm, *Listeria monocytogenes* can evade detection by the immune system, allowing it to establish a persistent infection.[70] The study of LLO provides insights into the mechanisms of bacterial pathogenesis and host-pathogen interactions. Researchers have also explored the potential use of LLO in various biomedical applications, such as drug delivery.[70]

Understanding the function and mechanisms of LLO is crucial for developing strategies to combat listeriosis and for gaining insights into how bacteria manipulate host cells to cause disease.

1.8.3. Prion Protein (PrP)

The prion protein, often abbreviated as PrP, is a unique and enigmatic type of protein that can undergo a misfolding process, leading to the development of prion diseases.[71] Prions are responsible for a group of rare and fatal neurodegenerative disorders known as transmissible spongiform encephalopathies (TSEs). These diseases affect the central nervous system and are characterized by the accumulation of abnormal protein aggregates.[71, 72]

PrP is naturally present in a healthy, properly folded conformation (PrP^{C}, where "C" stands for cellular). It is primarily found on the surface of neurons and other cells. PrP^{C} has a predominantly α-helical structure.[71, 72] In prion diseases, the PrP can undergo a spontaneous conformational change, forming a misfolded, disease-associated isoform (PrP^{Sc}, where "Sc" stands for scrapie, a type of

TSE).[72] This misfolded isoform has a higher β-sheet content and is resistant to degradation. The misfolded PrP^{Sc} isoform has the ability to induce the misfolding of normal PrP^{C} molecules into the abnormal conformation. This results in the accumulation of aggregated PrP^{Sc} in the brain, forming amyloid plaques. These aggregates disrupt neuronal function and cause neurodegeneration.[71, 72]

One of the most remarkable aspects of prion diseases is their transmissible nature. Misfolded PrP^{Sc} can induce the misfolding of normal PrP^{C} in other individuals, leading to disease transmission. This property is often called "infectious protein" behaviour, which distinguishes prions from traditional infectious agents like viruses or bacteria.[71, 72]

These diseases include well-known conditions such as Creutzfeldt-Jakob disease (CJD) in humans, bovine spongiform encephalopathy (BSE) or "mad cow disease" in cattle, scrapie in sheep, and chronic wasting disease (CWD) in cervids.[71, 72] These diseases are characterized by progressive neurological symptoms, including cognitive decline, motor dysfunction, and behavioural changes.[73]

Prion diseases have attracted significant scientific interest due to their unique properties and potential public health implications. Researchers are working to understand the mechanisms of prion misfolding, propagation, and pathogenesis. Studies of prions also have broader implications for our understanding of protein misfolding and aggregation in other neurodegenerative diseases, such as Alzheimer's and Parkinson.[71, 72] The study of PrP and prion diseases has expanded our understanding of protein folding, misfolding, and the spread of pathological changes within the brain. While progress has been made in uncovering the molecular basis of prion diseases, many questions remain, and research continues to explore new insights into these intriguing and complex disorders.

1.8.4. *Mycobacterium tuberculosis* (*Mtb*)

Mycobacterium tuberculosis (*Mtb*) is a bacterium that causes tuberculosis (TB), a contagious and potentially severe infectious disease primarily affecting the lungs.[74] TB remains a significant global health challenge, particularly in areas with limited access to healthcare and resources. *Mtb* is a slow-growing, rod-shaped bacterium with a unique cell wall structure that contains high levels of lipids, which contribute to its distinctive properties and resistance to certain environmental conditions.[75] TB is primarily transmitted through the inhalation of airborne respiratory droplets containing *Mtb*. When an infected person coughs, sneezes, or talks, tiny droplets containing the bacteria can be released into the air, and individuals nearby can inhale these droplets and become infected.[76] TB can present in different forms, with pulmonary tuberculosis being the most common. Symptoms of pulmonary TB

may include a persistent cough, chest pain, coughing up blood, weight loss, fatigue, and night sweats. TB can also affect other parts of the body, leading to extrapulmonary TB.[77]

Drug-resistant strains of *Mtb*, such as multidrug-resistant TB (MDR-TB) and extensively drug-resistant TB (XDR-TB), pose challenges to effective treatment.[78-80] These strains are resistant to common antibiotics used to treat TB, making treatment more complex and challenging. TB is a significant global health burden, particularly in low- and middle-income countries.[78-80] The World Health Organization (WHO) ranks TB among the top infectious disease killers worldwide.

Its diagnosis involves various methods, including sputum microscopy, culture, and molecular tests. Treatment typically requires a combination of antibiotics taken over several months. Early diagnosis and appropriate treatment are crucial to controlling the spread of TB and preventing severe disease outcomes. Efforts to control TB include vaccination with the Bacillus Calmette-Guérin (BCG) vaccine, improving access to diagnostics and treatment, implementing infection control measures in healthcare settings, and raising awareness about TB transmission and prevention.[78] Ongoing research focuses on developing improved TB diagnostics, new drugs, and vaccines to combat *Mtb* and reduce the global burden of TB.[78-80]

1.8.5. Aurein 1.2 and Maculatin 1.1

Aurein 1.2 and Maculatin 1.1 are antimicrobial peptides (AMPs), which are small molecules that play a crucial role in the innate immune response of various organisms, including humans and animals.[80-82] These peptides are part of the host's defence system against bacterial infections and are known for their ability to kill or inhibit the growth of a wide range of microorganisms, including bacteria, fungi, and even certain viruses.[80-82]

Aurein 1.2 is a type of antimicrobial peptide found in the skin secretions of the green and golden bell frog (*Litoria aurea*).[80] It is part of a family of peptides known as aureins, known for their potent antimicrobial activity. It has been studied for its ability to disrupt bacterial cell membranes, leading to cell death.[81] It achieves this by forming pores in the membranes, disrupting their integrity, and causing leakage of cellular contents. Apart from its antimicrobial activity, aurein 1.2 has also been explored for potential applications in cancer research and drug delivery due to its ability to interact with cell membranes.

Maculatin 1.1 is an antimicrobial peptide that was originally isolated from the skin secretions of the Australian green tree frog (*Litoria genimaculata*).[82] Similar to other AMPs, maculatin 1.1 exhibits a

broad-spectrum antimicrobial activity against various pathogens, including bacteria and fungi.[82] It functions by targeting microbial cell membranes, leading to membrane disruption and cell death. In addition to its antimicrobial properties, maculatin 1.1 has also been studied for its potential in wound healing and immune modulation.[80-82]

Both Aurein 1.2 and Maculatin 1.1 are examples of nature's defence mechanisms against microbial threats. Their antimicrobial activities have attracted interest from researchers in fields such as infectious disease, biotechnology, and drug development. By understanding the mechanisms of action of these peptides, scientists aim to develop novel strategies for combating antibiotic-resistant bacteria and other pathogens.

1.9. Technique used for Optical Characterization of LCs at the interfaces

Polarizing Optical Microscopy (POM) is a widely used technique in materials science and microscopy to study birefringent materials, which are materials that exhibit double refraction due to their anisotropic properties.[14, 26]

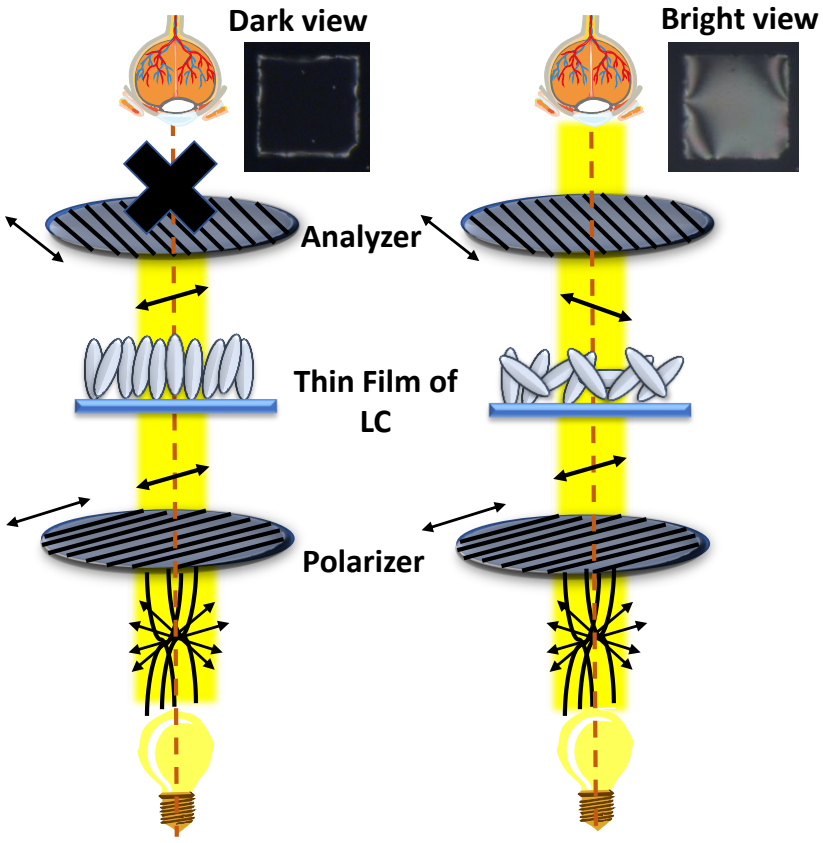

Figure 1.12 The schematic illustrates the operational concept of a polarized optical microscope

(POM) incorporating perpendicular polarizers. Unique optical characteristics arise from various orientations of LCs when examined between these crossed polarizers. The image has been drawn using powerpoint and chemdraw tools.

Birefringence occurs when light passes through a material and is split into two perpendicular polarization states, each travelling at different speeds. This effect is commonly observed in materials like crystals and LCs.[14, 26] The basic setup of POM involves using polarized light, which has its electric field oscillating in a specific direction. When this polarized light passes through a birefringent sample, the different refractive indices for the two polarization states cause a phase shift between them. This phase difference can lead to changes in the intensity and polarization of the transmitted light, which can then be visualized and analyzed. The light source emits unpolarized light, which then passes through a linear polarizer. This polarizer only allows light oscillating in a specific direction (the transmission axis of the polarizer) to pass through. This results in the light becoming polarized. The polarized light then passes through the birefringent sample, such as a LC material. The sample modifies the polarization state of the light due to its birefringence properties. After passing through the sample, the polarized light encounters another polarizer known as the analyzer. This analyzer is typically oriented at a specific angle relative to the polarizer before the sample. The analyzer can be rotated to adjust its polarization axis.

The intensity of light transmitted through the analyzer depends on the relative orientation of the polarizer and the analyzer, as well as the birefringent properties of the sample.[14, 26] In regions of the sample where there is no birefringence, the light will pass through both polarizers and appear bright in the microscope's image (Figure 1.12).

In regions with birefringence, the phase difference between the polarization states will cause changes in brightness and colour. The optical appearance of the sample under POM provides information about the orientational ordering of the birefringent material. In the case of LCs, it helps determine the arrangement and alignment of the LC molecules.

1.10. Other Techniques used in the studies

1.10.1. Atomic Force Microscopy (AFM)

Atomic force microscopy (AFM) is a versatile and high-resolution imaging technique used to study

the surface topography and mechanical properties of a wide range of materials at the nanoscale.[83] AFM operates on the principle of scanning a sharp tip over the surface of a sample while measuring the interaction forces between the tip and the surface. Applications of AFM include nanomaterial characterization, biological imaging, surface roughness analysis, mechanical properties, and chemical analysis.[84, 85]

The utilization of AFM has provided a discerning avenue for investigating the morphological characteristics of distinct protein species interfacing with various LC interfaces. Our experimental protocol typically entails the preparation of samples by subjecting proteins to an incubation process with the LC interface, subsequently recovering these samples upon elapsing the stipulated temporal duration. In a specific operational sequence, approximately 50 µl of the thus-extracted sample is meticulously deposited via drop-casting onto a silicon wafer substrate, with subsequent desiccation via air exposure to facilitate sample immobilization. This process results in the formation of a layer, which can then be examined at the nanoscale using AFM. The AFM, with its probing capabilities, enables the meticulous scrutiny of the surface topography and mechanical attributes of these protein layers, thus yielding valuable insights into their structural and interfacial characteristics.

1.10.2. Circular Dichroism (CD)

Circular Dichroism (CD) is a powerful spectroscopic technique to study chiral molecules' structural and conformational properties, such as proteins, nucleic acids, and other optically active compounds.[86, 87] CD measures the differential absorption of left-handed circularly polarized light (L-CPL) and right-handed circularly polarized light (R-CPL) by chiral molecules as a function of the wavelength of light.[88] Key features and principles of CD spectroscopy include chirality, circularly polarized light, differential absorption, secondary structure analysis, conformational changes, and quantitative analysis. CD spectrometers are typically equipped with a light source, sample compartment, and a detector to measure the intensity of transmitted light. A reference cell containing a non-chiral substance is often used to account for baseline effects. Applications of CD spectroscopy include protein structure, nucleic acid conformation, enzyme kinetics, drug binding studies, and quality control.[86-88]

Employing CD spectroscopy as our analytical methodology, we have examined the conformational transformations exhibited by toxic proteins in response to their interactions with lipid molecules. The analytical focus of our investigations has encompassed the structural alterations incurred by the

proteins in both their pre-interaction and post-interaction states. Our experimental paradigm commonly features the scrutiny of protein toxins, typically present at micromolar concentrations, in an isolated state. These proteins are subjected to an incubation process with lipid molecules, thereby mimicking the physiologically relevant conditions under which these interactions occur.

The consequential objective of our studies is to elucidate the alterations in the secondary structures of these toxic proteins, as manifested by the distinctive CD spectra before and after the lipid interaction event. The resultant CD spectra enable the quantification of changes in the protein's conformational attributes and the identification of any perturbations in the protein's secondary structural elements, such as alpha-helices, beta-sheets, or random coils, as a direct consequence of its interaction with the lipid moieties. This elucidation of conformational dynamics is paramount in comprehending toxicity's molecular basis and advancing our insights into the mechanisms underlying toxicological phenomena.

1.10.3. Confocal fluorescence microscopy

Confocal fluorescence microscopy is a sophisticated optical imaging technique employed in the scientific investigation and visualization of biological and material specimens at high resolution.[89] This method offers improved contrast, reduced background noise, and the capacity to collect three-dimensional information from the specimen. It is particularly valuable for observing fluorescently labelled structures and features within cells and tissues. Key elements and principles of confocal fluorescence microscopy encompass laser scanning, pinhole aperture, scanning mechanism, three-dimensional imaging, image formation, and fluorescence labelling.[89, 90] Applications of confocal fluorescence microscopy include cell biology, neuroscience, developmental biology, cancer research, and materials science.[90]

The application of confocal fluorescence microscopy has facilitated a comprehensive investigation into the lateral distribution of regions enriched in both proteins and lipids.[89, 90] This powerful technique has allowed us to gain profound insights into the spatial organization of these biomolecular constituents, particularly in the context of the LC and aqueous interface. Our experimental paradigm predominantly entails using fluorescently labelled proteins and lipids, a deliberate choice made to harness the enhanced sensitivity and selectivity of confocal fluorescence microscopy. In the specific context of our investigations at the LC-aqueous interface, we deploy the practice of utilizing fluorescently labelled proteins and lipids. These biomolecules, suitably tagged with fluorophores, are

introduced to the interface under scrutiny. The application of water-dipping objectives in the confocal imaging setup allows for optimal visualization and examination of the molecular constituents present at the interface. By illuminating the sample with the focused laser beam and selectively collecting the emitted fluorescence, we can discern these biomolecules' spatial arrangement and localization with exceptional precision.

The data obtained from this method is invaluable in deciphering the intricate organization of lipids and proteins at the interface. Specifically, it enables us to scrutinize and elucidate the existence of phase-segregated domains within this complex molecular milieu. Identifying and characterizing such domains provide critical information, shedding light on the partitioning and interactions of lipids and proteins, their lateral organization, and the potential implications for various biological and biophysical processes.

1.10.4. Zeta potential measurements

Zeta potential measurements, an essential analytical technique in colloid and surface science, provide valuable information regarding the surface charge and electrokinetic properties of particles and interfaces in colloidal dispersions.[91, 92] This technique offers insights into colloidal systems' stability, interaction, and behaviour. Zeta potential represents the electric potential at the shear plane, which is a hypothetical plane located at the interface of a particle or an interface with the surrounding liquid. The shear plane is the boundary where the moving fluid layer next to the particle or interface interacts with the bulk liquid. Zeta potential is typically expressed in millivolts (mV) and is an indicator of the magnitude and polarity of the electric charge carried by the particle or interface.[93]

Zeta potential is measured using techniques such as electrophoretic light scattering, laser Doppler electrophoresis, or streaming potential measurements.[94, 95] The key principle involves subjecting colloidal particles or interfaces to an electric field and monitoring the velocity or potential changes resulting from this field. The data collected during these measurements are subsequently used to calculate the zeta potential.

The application of zeta potential measurements has provided us with a powerful means to quantitatively assess the charge distribution on LC droplets when interfacing with biomolecular interfaces. This technique has proven indispensable in our efforts to gain a comprehensive understanding of the role played by electrostatic forces in mediating interactions between toxic proteins and biological membranes at the LC interfaces. Our investigative approach commonly

involves the characterization of the electrostatic properties of LC droplets before and after their interaction with biomolecular interfaces. Specifically, we examine how the electrostatic potential, as reflected by the zeta potential, changes in response to the incubation of these interfaces with toxic proteins. This detailed assessment of electrostatic potential alterations serves as a critical probe into the nature of the interactions between a diverse range of proteins and biological membranes. The insights derived from these zeta potential measurements are pivotal in unravelling the molecular interactions that transpire at the interfaces of lipid-laden LC droplets and toxic proteins. The quantification of electrostatic potential changes informs us about the driving forces governing these interactions and provides a quantitative basis for understanding the stability and dynamics of these interfacial systems.

1.10.5. Density Functional Theory (DFT)

Density Functional Theory (DFT) is a computational quantum mechanical modelling method used to study the electronic structure of molecules, atoms, and solids.[96] It's widely employed in various fields, including chemistry, physics, and materials science. DFT offers a way to predict and understand the behaviour of electrons in a system, allowing scientists to investigate the properties and behaviour of matter at the atomic and molecular levels.

The key aspects of DFT include electron density, energy minimization, and exchange-correlation functionals. DFT can be applied to a wide range of systems, from small molecules to large proteins, from solid-state materials to surfaces and interfaces. It's used to predict molecular geometries, electronic properties, and chemical reactivity.[96, 97] DFT is computationally less demanding than solving the Schrödinger equation for the many-electron wave function, which makes it a practical choice for studying large and complex systems.[97] It is widely used for studying the properties of materials, catalysis, and the design of new compounds.[96, 97] The study has provided a comprehensive and in-depth analysis of energy interactions occurring at the molecular level, particularly within the gaseous phase. This approach has allowed us to scrutinize molecular systems with meticulous attention to detail, facilitating a profound understanding of the intricate interplay of energies involved in their interactions. Within the purview of this study, we have harnessed DFT as our computational framework. The central tenet of DFT is its focus on electron density, a fundamental concept that represents the spatial distribution of electrons within a given system. By pursuing the minimization of the system's total energy, which encompasses kinetic energy, electron-electron interactions, and

interactions with external potentials such as nuclei and electric fields, we aim to elucidate the energetics underlying molecular systems.

In summation, using Density Functional Theory as the underpinning computational framework in our study has empowered us to explore molecular systems comprehensively, scrutinizing their electronic structure and the intricate energetic contributions that govern their behaviour. Through this research, we aim to shed light on the fundamental principles and molecular properties that underlie the behaviour of these systems, thereby advancing our understanding of the molecular world in the gaseous phase.

1.11. Organization of the Thesis

This thesis explores the utilization of thermotropic nematic LC for designing dynamic functional interfaces that emulate biomembranes. Leveraging the distinctive traits of LC, such as birefringence and low surface anchoring energy, enables LC to respond to stimuli.[10, 29, 31] The presence of a 100 µm cooperative effect facilitates the propagation of changes from the interface to the LC bulk, thereby magnifying physiological processes to the micro-scale.[29] The user-friendly setup, sensitivity, and smartphone-compatible analysis contribute to the advancement and utilization of LC sensors.[39] The primary goal of this thesis is to investigate the interactions of various toxins with mimicked biomembranes and to examine how proteins undergo conformational changes upon interaction. Additionally, the research sheds light on the impact of the innate immune system-derived antimicrobial peptides (AMPs) on the spatiotemporally controlled envelopes of *Mtb*.

The application of LC-aqueous interfaces for studying the action of various toxins at lipids has been detailed below.

In **Chapter 2**, the focus was on the utilization of LC-aqueous interfaces as a means to explore the cholesterol-mediated effects of a β-barrel pore-forming toxin (PFT), specifically VCC. This section of the research aims to achieve several key objectives. The first objective is to gain insight into how cholesterol influences the self-assembly of lipids at the LC-aqueous interface. The second goal is to establish a robust framework utilizing LCs to study the interactions between VCC and phospholipids with varying cholesterol amounts. Despite advancements in our understanding of the membrane pore-formation mechanisms of PFTs, numerous aspects of the protein-lipid interplay at the membrane interface remain unexplored.[69] For instance, the specific alterations induced in the membrane lipid bilayer by the membrane-damaging actions of PFTs have not been extensively

investigated.[69] The process of oligomeric pore formation by PFTs involves significant structural changes. Additionally, the mode of action of PFTs triggers a reorganization or remodelling of the membrane architecture, encompassing modifications in lipid microdomains, membrane lipid phase separation, and mixing. A comprehensive grasp of these membrane remodelling events initiated by PFTs holds significance and necessitates sensitive methodologies to observe and comprehend these intricate processes. In this study, the question revolves around whether the binding of VCC to lipid-adorned LC interfaces can reorganise lipid molecules. The principal objective is to delve into the structural transformations occurring in the interfacial VCC upon interacting with the lipid-enriched LC-aqueous interface. The findings reveal the feasibility of replicating the membrane interactions of VCC at nanomolar concentrations using lipid-decorated LC-aqueous interfaces facilitated by the surface-driven ordering transitions of LCs.

Chapter 3 of the research explores whether a biomimetic LC-aqueous interface can effectively capture the LLO-induced alterations within the distinctive amphipathic milieu. Additionally, the investigation delves into comprehending the LLO-cholesterol interaction facilitated by the cholesterol-recognition motif (CRM), which plays a pivotal role in membrane binding and activity. The inherent CRM motif within LLO is substituted with a glycine pair to generate the ΔCRM variant, thereby enabling the analysis of cholesterol-dependent membrane interactions and LLO-mediated modulations. The findings reveal a substantial impact of CRM region mutation on the physical interaction between LLO and cholesterol. Notably, this binding capacity reduction is pronounced primarily when cholesterol levels in the membranes are low, suggesting the interplay between cholesterol and membrane dynamics in influencing LLO activity.

Furthermore, cholesterol emerges as a key determinant in modulating the membranes' phase heterogeneity, lipid packing, and hydrophobicity. This study meticulously explores the potential of the LC interface to discern sequential alterations of two amino acids solely based on LC's optical responses within physiological environments. Consequently, the LC-based approach presents itself as a straightforward assay for probing bacterial protein's structural foundation and cholesterol-dependent pathogenicity. This research strives to unravel the intricate lipid-protein interactions occurring at the nano-scale aqueous interface of LC, a realm inaccessible to conventional measurement techniques. However, there remains an avenue for future investigations concerning the interplay between membrane dynamics and LLO activity.

Chapter 4 presents an approach centred around differentially charged lipid monolayer-enriched LC-aqueous interfaces. This design is geared towards investigating the intricate interfacial

binding and conformational changes of the Prion protein (PrP), a complex phenomenon integral to its etiology. PrP misfolding and aggregation underlie fatal neurodegenerative disorders affecting both humans and animals.[71-73] Previous efforts employing advanced spectroscopic techniques like circular dichroism (CD) and fluorescence have shed light on the pivotal role of specific lipid compositions in surmounting the energy barrier associated with PrP unfolding and aggregation.[71-73] This involves the transition from α-helical to β-sheet-rich isoforms. However, despite considerable insights into PrP propagation mechanisms, our understanding of the forces driving its conformational modulations remains relatively obscure.[71-73] The study elucidates three crucial facets intertwined with the foundational elements of neuropathology: (i) the influence of ionic and non-covalent forces in low and high-level PrP interactions with lipids, (ii) the role of multivalent interactions in PrP's conformational variations, and (iii) the modifications occurring in the membrane structure throughout these interactions. Moreover, the LC-based approach remarkably discerns the subtlest interactions between PrP and zwitterionic lipids, an achievement unattainable by intricate spectroscopic techniques. The findings spotlight the significant impact of electrostatic forces, contingent upon membrane interfacial properties, in orchestrating the initial binding of PrP. This enhances the effective PrP concentration and fosters short-range hydrophobic and protein-protein interactions. The hydrophobic interactions between PrP and lipid membranes prompt protein unfolding, reducing the energy barrier to PrP misfolding. Consequently, coupling PrP misfolding via hydrophobic interactions with the efficient neutralization of electrostatic charge amplifies its aggregation into oligomers. These oligomers undergo two distinct membrane-mediated aggregations catalyzed by chemoresponsive LC. This research underscores the efficacy of the LC-based methodology as a potent strategy for offering mechanistic insights into the origin and progression of prion diseases operating at physiological concentrations.

Chapter 5 endeavours are underpinned by objectives that propel our research forward. Our first objective is to comprehensively understand the contrasting attributes exhibited by the bacterium's inner (IML) and outer (OML) membrane envelopes at various interfaces. This pursuit is driven by the desire to uncover the differentials inherent in these distinct membrane layers. The second facet of our investigation hinges on the influence exerted by the growth phase of the bacteria on these envelopes, subsequently shaping their behaviours and responses at the interfaces. We delve into the intricate interplay between bacterial growth stages and membrane characteristics, aiming to unearth the intricate interdependencies between the two. Our third endeavour explores the multifaceted actions of antimicrobial peptides (AMPs) on the spatiotemporally derived membranes

of *Mtb*. This facet of our study aims to unravel the complex interactions between AMPs and *Mtb* membranes. This analysis is poised to yield valuable insights into the underlying mechanisms that govern these interactions, contributing to a deeper understanding of their implications.

Chapter 5 seeks to navigate the intricate dynamics surrounding these diverse objectives. By delving into the interplay between membrane envelopes, bacterial growth phases, and the actions of antimicrobial peptides, our research endeavours to illuminate the underlying mechanisms that drive the antimicrobial peptides and bacterial membrane interactions. Through this approach, we aim to contribute valuable insights into the complex dynamics that underlie the interactions between AMPs and *Mtb* membranes, thereby enriching our understanding of these biological processes.

1.12. Acknowledgements

T.G. acknowledges powerpoint, chemdraw, pymol and chimera tools for various cartoons and protein structures used in the table of contents (TOC) graphics and schematics.

References

1. Miller, C. E.; Majewski, J.; Watkins, E. B.; Kuhl, T. L., Part I: an x-ray scattering study of cholera toxin penetration and induced phase transformations in lipid membranes. *Biophys. J.* **2008,** *95* (2), 629-40.

2. Wu, Y.; He, K.; Ludtke, S. J.; Huang, H. W., X-ray diffraction study of lipid bilayer membranes interacting with amphiphilic helical peptides: diphytanoyl phosphatidylcholine with alamethicin at low concentrations. *Biophys. J.* **1995,** *68* (6), 2361-2369.

3. Moco, S., Studying Metabolism by NMR-Based Metabolomics. *Front. Mol. Biosci.* **2022,** *9*, 882487.

4. Emeasoba, E. U.; Ibeson, E.; Nwosu, I.; Montemarano, N.; Shani, J.; Shetty, V. S., Clinical relevance of nuclear magnetic resonance LipoProfile. *Front. Nucl. Med.* **2022,** *2*, 960522.

5. Figueira, T. N.; Freire, J. M.; Cunha-Santos, C.; Heras, M.; Goncalves, J.; Moscona, A.; Porotto, M.; Salome Veiga, A.; Castanho, M. A., Quantitative analysis of molecular partition towards lipid membranes using surface plasmon resonance. *Sci. Rep.* **2017,** *7* (1), 45647.

6. Wu, L.; Huang, C.; Emery, B. P.; Sedgwick, A. C.; Bull, S. D.; He, X. P.; Tian, H.; Yoon, J.; Sessler, J. L.; James, T. D., Förster resonance energy transfer (FRET)-based small-molecule sensors and imaging agents. *Chem. Soc. Rev.* **2020,** *49* (15), 5110-5139.

7. Sturmey, R. G.; O'Toole, P. J.; Leese, H. J., Fluorescence resonance energy transfer analysis of mitochondrial:lipid association in the porcine oocyte. *Reprod.* **2006,** *132* (6), 829-37.

8. Marrink, S. J.; de Vries, A. H.; Tieleman, D. P., Lipids on the move: simulations of membrane pores, domains, stalks and curves. *Biochim. Biophys. Acta* **2009,** *1788* (1), 149-68.

9. Siwko, M. E.; Marrink, S. J.; de Vries, A. H.; Kozubek, A.; Uiterkamp, A. J. M. S.; Mark, A. E., Does isoprene protect plant membranes from thermal shock? A molecular dynamics study. *Biochim. Biophys. Acta* **2007,** *1768* (2), 198-206.

10. Brake, J. M.; Abbott, N. L., An Experimental System for Imaging the Reversible Adsorption of Amphiphiles at Aqueous−Liquid Crystal Interfaces. *Langmuir* **2002,** *18* (16), 6101-6109.

11. Gupta, V. K.; Skaife, J. J.; Dubrovsky, T. B.; Abbott, N. L., Optical amplification of ligand-receptor binding using liquid crystals. *Science (New York, N.Y.)* **1998,** *279* (5359), 2077-80.

12. Schmidt-Mende, L.; Fechtenkotter, A.; Mullen, K.; Moons, E.; Friend, R. H.; MacKenzie, J. D., Self-organized discotic liquid crystals for high-efficiency organic photovoltaics. *Science (New York, N.Y.)* **2001,** *293* (5532), 1119-22.

13. Collings, P. J.; Hird, M., *Introduction to Liquid Crystals: Chemistry and Physics (1st ed.)*. CRC Press: 1997.

14. Collings, P. J., *Liquid crystals: nature's delicate phase of matter*. Princeton University Press: 2002.

15. Ramírez, M. A.; Jiménez, H. S.; Banat, I. M.; Díaz De Rienzo, M. A., Surfactants: physicochemical interactions with biological macromolecules. *Biotechnol. Lett.* **2021,** *43*, 523-535.

16. Miskovic, V.; Malafronte, E.; Minetti, C.; Machrafi, H.; Varon, C.; Iorio, C. S., Thermotropic Liquid Crystals for Temperature Mapping. *Front. Bioeng. Biotechnol.* **2022,** *10*, 806362.

17. Chakrabarti, D.; Bagchi, B., Energy landscape view of phase transitions and slow dynamics

in thermotropic liquid crystals. *Proc. Natl. Acad. Sci. U. S. A.* **2006,** *103* (19), 7217-21.

18. Wang, X.; Zhang, Y.; Gui, S.; Huang, J.; Cao, J.; Li, Z.; Li, Q.; Chu, X., Characterization of Lipid-Based Lyotropic Liquid Crystal and Effects of Guest Molecules on Its Microstructure: a Systematic Review. *AAPS PharmSciTech.* **2018,** *19* (5), 2023-2040.

19. Rey, A. D., Liquid crystal models of biological materials and processes. *Soft Matter* **2010,** *6* (15), 3402-3429.

20. Besseau, L.; Bouligand, Y., The twisted collagen network of the box-fish scutes. *Tissue Cell* **1998,** *30* (2), 251-60.

21. Giraud-Guille, M. M., Twisted liquid crystalline supramolecular arrangements in morphogenesis. *Int. Rev. Cytol.* **1996,** *166*, 59-101.

22. An, J. G.; Hina, S.; Yang, Y.; Xue, M.; Liu, Y., Characterization of liquid crystals: A literature review. *Rev. Adv. Mater. S* **2016,** *44* (4).

23. Brown, G. H.; Wolken, J. J., *Liquid Crystals and Biological Structures*. Academic Press, New York, **1979**.

24. Kawamoto, H., The history of liquid-crystal displays. *Proc. IEEE* **2002,** *90* (4), 460-500.

25. Xie, R.; Li, N.; Li, Z.; Chen, J.; Li, K.; He, Q.; Liu, L.; Zhang, S., Liquid Crystal Droplet-Based Biosensors: Promising for Point-of-Care Testing. *Biosensors (Basel)* **2022,** *12* (9), 758.

26. De Gennes, P. G.; Prost, J., *The physics of liquid crystals*. Oxford University Press: 1994.

27. Jerome, B., Surface effects and anchoring in liquid crystals. *Rep. Prog. Phys.* **1991,** *54* (3), 391.

28. Gupta, V. K.; Abbott, N. L., Azimuthal anchoring transition on nematic liquid crystals on self-assembled monolayers formed from odd and even alkanethiols. *Phys. Rev. E.* **1996,** *54* (5), R4540-R4543.

29. Lockwood, N.; Gupta, J.; Abbott, N., Self-assembly of amphiphiles, polymers and proteins at interfaces between thermotropic liquid crystals and aqueous phases. *Surf. Sci. Rep.* **2008,** *63* (6), 255-293.

30. Lavrentovich, O. D., Topological defects in dispersed words and worlds around liquid

crystals, or liquid crystal drops. *Liq. Cryst.* **1998,** *24* (1), 117-126.

31. Miller, D. S.; Carlton, R. J.; Mushenheim, P. C.; Abbott, N. L., Introduction to optical methods for characterizing liquid crystals at interfaces. *Langmuir* **2013,** *29* (10), 3154-3169.

32. Sengupta, A., Liquid Crystal Theory. In *Topological Microfluidics*, Sengupta, A., Ed. Springer International Publishing: Cham, 2013; pp 7-36.

33. Zhou, Y.; Dong, L.; Zhang, C.; Wang, L.; Huang, Q., Rotational Speed Measurement Based on LC Wireless Sensors. *Sensors (Basel)* **2021,** *21* (23), 8055.

34. Li, Z.; Yin, Y., Stimuli-Responsive Optical Nanomaterials. *Adv. Mater.* **2019,** *31* (15), e1807061.

35. Moreira, M. F.; Carvalho, I. C. S.; Cao, W.; Bailey, C.; Taheri, B.; Palffy-Muhoray, P., Cholesteric liquid-crystal laser as an optic fiber-based temperature sensor. *Appl. Phys. Lett.* **2004,** *85* (14), 2691-2693.

36. Algorri, J. F.; Urruchi, V.; Bennis, N.; Sanchez-Pena, J. M., A novel high-sensitivity, low-power, liquid crystal temperature sensor. *Sensors (Basel)* **2014,** *14* (4), 6571-83.

37. Feng, J.; Zhao, Y.; Li, S. S.; Lin, X. W.; Xu, F.; Lu, Y. Q., Fiber-optic pressure sensor based on tunable liquid crystal technology. *IEEE Photonics J.* **2010,** *2* (3), 292-298.

38. Kottapalli, A. G. P.; Asadnia, M.; Miao, J. M.; Barbastathis, G.; Triantafyllou, M., A flexible liquid crystal polymer MEMS pressure sensor array for fish-like underwater sensing. *Smart Mater. Struct.* **2012,** *21* (11), 115030.

39. Carlton, R. J.; Hunter, J. T.; Miller, D. S.; Abbasi, R.; Mushenheim, P. C.; Tan, L. N.; Abbott, N. L., Chemical and biological sensing using liquid crystals. *Liq. Cryst. Rev.* **2013,** *1* (1), 29-51.

40. Manna, U.; Zayas-Gonzalez, Y. M.; Carlton, R. J.; Caruso, F.; Abbott, N. L.; Lynn, D. M., Liquid crystal chemical sensors that cells can wear. *Angew. Chem. Int. Ed.* **2013,** *52* (52), 14011-14015.

41. Zhan, X.; Liu, Y.; Yang, K. L.; Luo, D., State-of-the-Art Development in Liquid Crystal Biochemical Sensors. *Biosensors (Basel)* **2022,** *12* (8), 577.

42. Hong, P. T. K.; Jang, C. H., Sensitive and label-free liquid crystal-based optical sensor for the detection of malathion. *Anal. Biochem.* **2020,** *593*, 113589.

43. Lockwood, N. A.; De Pablo, J. J.; Abbott, N. L., Influence of surfactant tail branching and organization on the orientation of liquid crystals at aqueous-liquid crystal interfaces. *Langmuir* **2005,** *21* (15), 6805-6814.

44. Brake, J. M.; Mezera, A. D.; Abbott, N. L., Effect of surfactant structure on the orientation of liquid crystals at aqueous-liquid crystal interfaces. *Langmuir* **2003,** *19* (16), 6436-6442.

45. Brake, J. M.; Daschner, M. K.; Abbott, N. L., Formation and characterization of phospholipid monolayers spontaneously assembled at interfaces between aqueous phases and thermotropic liquid crystals. *Langmuir* **2005,** *21* (6), 2218-2228.

46. Price, A. D.; Schwartz, D. K., DNA hybridization-induced reorientation of liquid crystal anchoring at the nematic liquid crystal/aqueous interface. *J. Am. Chem. Soc.* **2008,** *130* (26), 8188-8194.

47. Tercero, M. D. D.; Abbott, N. L., Ordering transitions in liquid crystals permit imaging of spatial and temporal patterns formed by proteins penetrating into lipid-laden interfaces. *Chem. Eng. Commun.* **2008,** *196* (1-2), 234-251.

48. Wang, Y.; Hu, Q.; Guo, Y.; Yu, L., A cationic surfactant-decorated liquid crystal sensing platform for simple and sensitive detection of acetylcholinesterase and its inhibitor. *Biosens. Bioelectron.* **2015,** *72*, 25-30.

49. He, S.; Liang, W.; Cheng, K. L.; Fang, J.; Wu, S. T., Bile acid–surfactant interactions at the liquid crystal/aqueous interface. *Soft Matter* **2014,** *10* (26), 4609-4614.

50. Wang, Y.; Hu, Q.; Tian, T.; Gao, Y.; Yu, L., A liquid crystal-based sensor for the simple and sensitive detection of cellulase and cysteine. *Colloids Surf. B* **2016,** *147*, 100-105.

51. Wang, Y.; Hu, Q.; Tian, T.; Yu, L., Simple and sensitive detection of pesticides using the liquid crystal droplet patterns platform. *Sens. Actuators B Chem.* **2017,** *238*, 676-682.

52. Khan, M.; Park, S. Y., Liquid crystal-based proton sensitive glucose biosensor. *Anal. Chem.* **2014,** *86* (3), 1493-501.

53. Li, G.; Gao, B.; Yang, M.; Chen, L. C.; Xiong, X. L., Homeotropic orientation behavior of nematic liquid crystals induced by copper ions. *Colloids Surf. B* **2015,** *130*, 287-91.

54. Chen, C. H.; Lin, Y. C.; Chang, H. H.; Lee, A. S., Ligand-doped liquid crystal sensor system for detecting mercuric ion in aqueous solutions. *Anal. Chem.* **2015,** *87* (8), 4546-51.

55. Singh, S. K.; Nandi, R.; Mishra, K.; Singh, H. K.; Singh, R. K.; Singh, B., Liquid crystal based sensor system for the real time detection of mercuric ions in water using amphiphilic dithiocarbamate. *Sens. Actuators B Chem.* **2016,** *226*, 381-387.

56. Ding, W.; Gupta, K. C.; Park, S. Y.; Kim, Y. K.; Kang, I. K., In vitro detection of human breast cancer cells (SK-BR3) using herceptin-conjugated liquid crystal microdroplets as a sensing platform. *Biomater. Sci.* **2016,** *4* (10), 1473-1484.

57. Tan, L. N.; Orler, V. J.; Abbott, N. L., Ordering transitions triggered by specific binding of vesicles to protein-decorated interfaces of thermotropic liquid crystals. *Langmuir* **2012,** *28* (15), 6364-76.

58. Gupta, J. K.; Meli, M. V.; Teren, S.; Abbott, N. L., Elastic energy-driven phase separation of phospholipid monolayers at the nematic liquid-crystal–aqueous interface. *Phys. Rev. lett.* **2008,** *100* (4), 048301.

59. Meli, M. V.; Lin, I. H.; Abbott, N. L., Preparation of microscopic and planar oil-water interfaces that are decorated with prescribed densities of insoluble amphiphiles. *J. Am. Chem. Soc.* **2008,** *130* (13), 4326-4333.

60. Kurniawan, J.; De Souza, J. F. V.; Dang, A. T.; Liu, G. Y.; Kuhl, T. L., Preparation and characterization of solid-supported lipid bilayers formed by Langmuir–Blodgett deposition: a tutorial. *Langmuir* **2018,** *34* (51), 15622-15639.

61. Valeva, A.; Walev, I.; Boukhallouk, F.; Wassenaar, T. M.; Heinz, N.; Hedderich, J.; Lautwein, S.; Möcking, M.; Weis, S.; Zitzer, A., Identification of the membrane penetrating domain of Vibrio cholerae cytolysin as a β-barrel structure. *Mol. Microbiol.* **2005,** *57* (1), 124-131.

62. Olson, R.; Gouaux, E., Vibrio cholerae cytolysin is composed of an alpha-hemolysin-like core. *Protein Sci.* **2003,** *12* (2), 379-83.

63. De, S.; Olson, R., Crystal structure of the *Vibrio cholerae* cytolysin heptamer reveals

common features among disparate pore-forming toxins. *Proc. Natl. Acad. Sci. U. S. A.* **2011,** *108* (18), 7385-90.

64. Zitzer, A.; Zitzer, O.; Bhakdi, S.; Palmer, M., Oligomerization of *Vibrio cholerae* cytolysin yields a pentameric pore and has a dual specificity for cholesterol and sphingolipids in the target membrane. *J. Biol. Chem.* **1999,** *274* (3), 1375-80.

65. Kathuria, R.; Mondal, A. K.; Sharma, R.; Bhattacharyya, S.; Chattopadhyay, K., Revisiting the role of cholesterol in regulating the pore-formation mechanism of *Vibrio cholerae* cytolysin, a membrane-damaging β-barrel pore-forming toxin. *Biochem. J.* **2018,** *475* (19), 3039-3055.

66. Rai, A. K.; Chattopadhyay, K., Trapping of *Vibrio cholerae* cytolysin in the membrane-bound monomeric state blocks membrane insertion and functional pore formation by the toxin. *J. Biol. Chem.* **2014,** *289* (24), 16978-87.

67. Paul, K.; Chattopadhyay, K., Single point mutation in Vibrio cholerae cytolysin compromises the membrane pore-formation mechanism of the toxin. *FEBS J.* **2012,** *279* (21), 4039-51.

68. Tweten, R. K., Cholesterol-dependent cytolysins, a family of versatile pore-forming toxins. *Infect. Immun.* **2005,** *73* (10), 6199-209.

69. Lata, K.; Singh, M.; Chatterjee, S.; Chattopadhyay, K., Membrane Dynamics and Remodelling in Response to the Action of the Membrane-Damaging Pore-Forming Toxins. *J. Membr. Biol.* **2022,** *255* (2-3), 161-173.

70. Koster, S.; Van Pee, K.; Hudel, M.; Leustik, M.; Rhinow, D.; Kuhlbrandt, W.; Chakraborty, T.; Yildiz, O., Crystal structure of listeriolysin O reveals molecular details of oligomerization and pore formation. *Nat Commun* **2014,** *5* (1), 3690.

71. Agarwal, A.; Das, D.; Banerjee, T.; Mukhopadhyay, S., Energy migration captures membrane-induced oligomerization of the prion protein. *Biochim. Biophys. Acta Proteins Proteom.* **2020,** *1868* (2), 140324.

72. Baskakov, I. V.; Legname, G.; Prusiner, S. B.; Cohen, F. E., Folding of prion protein to its native α-helical conformation is under kinetic control. *J. Biol. Chem.* **2001,** *276* (23), 19687-19690.

73. Linden, R.; Martins, V. R.; Prado, M. A.; Cammarota, M.; Izquierdo, I.; Brentani, R. R., Physiology of the prion protein. *Physiol. Rev.* **2008,** *88* (2), 673-728.

74. Saravanan, M.; Niguse, S.; Abdulkader, M.; Tsegay, E.; Hailekiros, H.; Gebrekidan, A.; Araya, T.; Pugazhendhi, A., Review on emergence of drug-resistant tuberculosis (MDR & XDR-TB) and its molecular diagnosis in Ethiopia. *Microb. Pathog.* **2018,** *117*, 237-242.

75. Gengenbacher, M.; Kaufmann, S. H. E., Mycobacterium tuberculosis: success through dormancy. *FEMS Microbiol. Rev.* **2012,** *36* (3), 514-532.

76. Ma, J.; Jiang, G.; Ma, Q.; Wang, H.; Du, M.; Wang, C.; Xie, X.; Li, T.; Chen, S., Rapid detection of airborne protein from Mycobacterium tuberculosis using a biosensor detection system. *Analyst* **2022,** *147* (4), 614-624.

77. Maurya, A. K.; Singh, P.; Kant, S., Extra Pulmonary Tuberculosis: An Overview. *J. Natl. Med. Assoc.* **2018,** *12* (01), 40-42.

78. Scriba, T. J.; Netea M. G.; Ginsberg A. M., Key recent advances in TB vaccine development and understanding of protective immune responses against Mycobacterium tuberculosis. *Semin Immunol.* **2020,** *50*, 101431.

79. Sheard, D. E.; Simpson, N. M. O'B.; Wade, J. D.; Separovic F., Combating bacterial resistance by combination of antibiotics with antimicrobial peptides. *Pure Appl. Chem.* **2019,** *91*, 199-209.

80. Chen, T.; Scott, C.; Tang, L.; Zhou, M.; Shaw, C., The structural organization of aurein precursor cDNAs from the skin secretion of the Australian green and golden bell frog, Litoria aurea. *Regul. Pept.* **2005,** *128* (1), 75-83.

81. Lee, T. H.; Hall, K. N.; Aguilar, M. I., Antimicrobial Peptide Structure and Mechanism of Action: A Focus on the Role of Membrane Structure. *Curr. Top. Med. Chem.* **2016,** *16* (1), 25-39.

82. Rozek, T.; Waugh, R. J.; Steinborner, S. T.; Bowie, J. H.; Tyler, M. J.; Wallace, J. C., The maculatin peptides from the skin glands of the tree frog Litoria genimaculata: a comparison of the structures and antibacterial activities of maculatin 1.1 and caerin 1.1. *J. Pept. Sci.* **1998,** *4* (2), 111-5.

83. Picas, L.; Milhiet, P. E.; Hernandez-Borrell, J., Atomic force microscopy: a versatile tool to probe the physical and chemical properties of supported membranes at the nanoscale. *Chem. Phys. Lipids* **2012,** *165* (8), 845-60.

84. Baer, D. R.; Gaspar, D. J.; Nachimuthu, P.; Techane, S. D.; Castner, D. G., Application of surface chemical analysis tools for characterization of nanoparticles. *Anal. Bioanal. Chem.* **2010,** *396* (3), 983-1002.

85. Guo, D.; Xie, G.; Luo, J., Mechanical properties of nanoparticles: basics and applications. *J. Phys. D: Appl. Phys* **2014,** *47* (1), 013001.

86. Ranjbar, B.; Gill, P., Circular dichroism techniques: biomolecular and nanostructural analyses- a review. *Chem. Biol. Drug Des.* **2009,** *74* (2), 101-20.

87. Zhao, X.; Wang, Y.; Zhao, D., Structural analysis of biomacromolecules using circular dichroism spectroscopy. In *Advanced Spectroscopic Methods to Study Biomolecular Structure and Dynamics*, Saudagar, P.; Tripathi, T., Eds. Academic Press: 2023; pp 77-103.

88. Wang, Y.; Harada, T.; Phuong, L. Q.; Kanemitsu, Y.; Nakano, T., Helix Induction to Polyfluorenes Using Circularly Polarized Light: Chirality Amplification, Phase-Selective Induction, and Anisotropic Emission. *Macromolecules* **2018,** *51* (17), 6865-6877.

89. Foldes-Papp, Z.; Demel, U.; Tilz, G. P., Laser scanning confocal fluorescence microscopy: an overview. *Int. Immunopharmacol.* **2003,** *3*, 1715-29.

90. St Croix, C. M.; Shand, S. H.; Watkins, S. C., Confocal microscopy: comparisons, applications, and problems. *Biotechniques* **2005,** *39*, S2-5.

91. Retamal Marín, R. R.; Babick, F.; Hillemann, L., Zeta potential measurements for non-spherical colloidal particles -Practical issues of characterisation of interfacial properties of nanoparticles. *Colloids Surf. A Physicochem. Eng. Asp.* **2017,** *532*, 516-521.

92. Sennett, P.; Olivier, J. P., Colloidal dispersions, electrokinetic effects, and the concept of zeta potential. *J. Ind. Eng. Chem.* **1965,** *57* (8), 32-50.

93. Lunardi, C. N.; Gomes, A. J.; Rocha, F. S.; D. Tommaso, J.; Patience, G. S., Experimental methods in chemical engineering: Zeta potential. *Can. J. Chem. Eng.* **2021,** *99* (3), 627-639.

94. Corbett, J. C. W.; M. Watson, F.; Jack, R. O.; Howarth, M., Measuring surface zeta potential using phase analysis light scattering in a simple dip cell arrangement. *Colloids Surf. A Physicochem. Eng. Asp.* **2012,** *396*, 169-176.

95. Mateos, H.; Valentini, A.; Robles, E.; Brooker, A.; Cioffi, N.; Palazzo, G., Measurement of the zeta-potential of solid surfaces through Laser Doppler Electrophoresis of colloid tracer in a dip-cell: Survey of the effect of ionic strength, pH, tracer chemical nature and size. *Colloids Surf. A: Physicochem. Eng. Asp.* **2019,** *576*, 82-90.

96. Sibanda, D.; Oyinbo, S. T.; Jen, T. C., A review of atomic layer deposition modelling and simulation methodologies: Density functional theory and molecular dynamics. *Nanotechnol. Rev.* **2022,** *11* (1), 1332-1363.

97. Hafner, J.; Wolverton, C.; Ceder, G., Toward Computational Materials Design: The Impact of Density Functional Theory on Materials Research. *MRS Bull.* **2011,** *31* (9), 659-668.

Chapter 2

Elucidating Liquid Crystal-Aqueous Interface for the Study of Cholesterol-Mediated Action of a β-Barrel Pore Forming Toxin

Pore-forming toxins (PFTs) produced by pathogenic bacteria serve as prominent virulence factors with potent cell-killing activity.[1-8] Most of the β-barrel PFTs form transmembrane oligomeric pores in the membrane lipid bilayer in the presence of cholesterol.[1] The pore-formation mechanisms of the PFTs highlight well-orchestrated regulated events in the membrane environment, which involve dramatic changes in the protein structure and organization.[1-3] Also, concerted crosstalk between protein and membrane lipid components appears to play crucial roles in the process. Membrane-damaging lesions formed by the pore assembly of the PFTs would also be expected to impose drastic alterations in the membrane organization, details of which remain obscure in most cases.[1-13] Prior reports have established that aqueous interfaces of liquid crystals (LCs) offer promise as responsive interfaces for biomolecular events (at physiologically relevant concentrations), which can be visualized as optical signals.[14] Inspired by this, herein, we sought to understand the lipid membrane interactions of a β-barrel PFT, i.e., *Vibrio cholerae* cytolysin (VCC), using LC-aqueous interfaces.

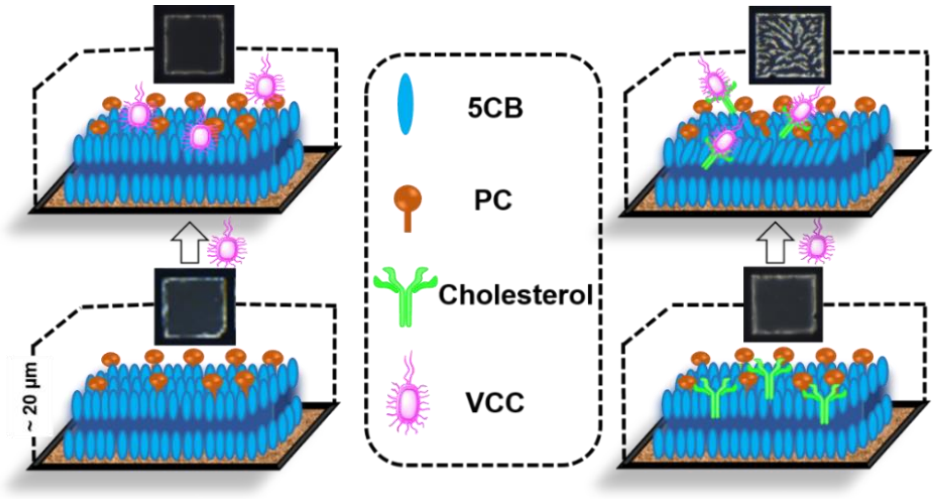

Our results show the formation of dendritic patterns upon the addition of VCC to the lipid embedded with cholesterol over the LC film. In contrast, we did not observe any LC reorientation upon the addition of VCC to the lipid-laden LC-aqueous interface in the absence of cholesterol. An array of techniques, such as polarizing optical microscopy (POM), atomic force microscopy (AFM), and fluorescence measurements, were utilized to decipher the LC response to the lipid interactions of VCC occurring at these interfaces. Altogether, the results obtained from our study provide a novel platform to explore the mechanistic aspects of the protein-membrane interactions in the process of membrane pore-formation by the membrane-damaging PFTs.

2.1. Introduction

Pore-forming toxins (PFTs) are potent virulence factors produced by pathogenic bacteria. PFTs exert pathophysiological effects by forming pores in the membrane lipid bilayer of their target cells.[1-9] PFTs have been categorized either as α-PFTs or β-PFTs,[1, 2] depending on the structural mechanisms associated with their membrane pore-formation processes. β-PFTs employ a β-barrel motif to form the transmembrane pore, whereas the membrane-spanning scaffold of the α-PFTs is constituted with an α-helical bundle. β-PFTs are the most well-studied family of membrane-disrupting cytolytic PFTs, and *Vibrio cholerae* cytolysin (VCC) is one of the most prominent members in this family.[3-7] Consistent with the β-PFT mode of action, VCC is secreted by the bacteria in the form of water-soluble monomeric molecules.[8] Upon binding to the target cell membranes, VCC forms heptameric β-barrel pores in the membrane lipid bilayer, which eventually leads to the permeation of the plasma membranes.[8] Interaction with the membrane lipid bilayer triggers major structural and organizational changes in the VCC structure. Membrane-bound toxin molecules self-associate to form a heptameric assembly, in which each of the protomers contributes pore-forming β-strands that insert into the membrane in a concerted manner to form the β-barrel scaffold of the pore.[5, 9-12] It is evident that the unique amphipathic environment of the membrane lipid bilayer is absolutely essential in facilitating the pore-formation process of the PFTs, including that of VCC.[9-12] Moreover, as observed with many PFTs, VCC exhibits specific interactions with the membrane lipid components. These membrane lipids play critical roles in regulating some of the distinct steps of the pore-formation mechanism.[13] For example, VCC employs a distinct structural motif to recognize the membrane phospholipids, and this interaction event allows the toxins to establish specific associations with the membranes.[7, 8] Membrane cholesterol has also been shown to play critical roles in regulating the membrane pore-formation mechanism of VCC. Cholesterol is essential for efficient binding, as well as functional oligomeric pore-formation by the membrane-bound toxin molecules.[9-11] Consistent with the cholesterol-dependent interaction with the target membranes, VCC has been shown to display a prominent propensity to associate with the cholesterol-rich fractions of the membrane microdomains in erythrocytes.[9-11]

Immense efforts have been made to explore the mechanistic aspects of the membrane interactions and pore-formation processes employed by the β-PFTs, including those of VCC.[7-12] Such studies have already elucidated some of the crucial details of the structural and organizational changes

induced in the β-PFT molecular architectures in the process of membrane pore-formation. However, several aspects of the protein-lipid crosstalk at the membrane interface still remain unexplored in the context of the membrane pore-formation mechanisms of the PFTs.[13] For example, details of the changes imposed on the membrane lipid bilayer itself by the membrane-damaging action of the PFTs have not been explored much. PFTs undergo major structural changes in the process of oligomeric pore formation in the membrane.[1-9] Furthermore, the PFT mode of action triggers reorganization/remodelling in the membrane architecture, which includes alterations in the lipid microdomain, membrane lipid phase separation, and/or mixing.[13] Detailed understanding of such membrane remodelling events triggered by PFTs is essential, and sensitive methodologies/techniques are required to document and understand these processes. In the present study, we ask if the binding of VCC to lipid-decorated interfaces of liquid crystals (LCs) can trigger a reorganization of the lipid molecules. We also aim to investigate the structural changes in interfacial VCC upon binding to the lipid-laden LC-aqueous interface. We report that it is possible to mimic the membrane interactions of VCC using lipid-decorated LC-aqueous interfaces at nM concentrations through surface-driven ordering transitions of LCs.

LCs possess uniquely delightful properties such as low interfacial energy, surface sensitivity, mobility, and mechanical responsiveness.[14] Due to the long-range orientational order of LC molecules, changes in the interfacial ordering of molecules can be communicated up to 100 μm distance from the interface.[14, 15] Thin films of LCs have been used for the detection of a wide range of analytes with high sensitivity without any requirement of complicated instruments and labour. Owing to these properties, LC-aqueous interfaces have been used for the detection of DNA, proteins, and so on.[15-20] Target-analyte binding at the LC-aqueous interface can be easily transformed into macroscopic optical signals even at remarkably low concentrations of the analyte.[15-20] LC-based interfaces have been used to study biomolecular interactions of endotoxin, membrane-damaging peptides, and their conformational switching in the presence of specific ions.[21, 22] However, the interactions of the PFTs with the lipid membrane on the LC-aqueous interface have not been explored. In this work, we investigated the interfacial interactions of a prototype β-PFT, VCC, with phospholipids in the presence or absence of cholesterol at the LC-aqueous interface.

2.1.1. Objectives

We strive for the following objectives in this work. First, we sought to understand the effect of cholesterol on the self-assembly of lipids on the LC-aqueous interface. Second, we sought to design

a robust platform using LCs to study the interactions of VCC with phospholipids having various amounts of cholesterol. We characterized the VCC-lipid assembly state at the lipid-laden LCs using fluorescence and atomic force microscopies. Furthermore, we quantified the LC response upon interactions of VCC with the lipid membranes supplemented with cholesterol.

2.2. Results and Discussion

To understand the behaviour of the archetypical β-PFT, VCC, at the lipid-laden LC-aqueous interface, we first investigated the self-assembly of the membrane phospholipid, 1-palmitoyl-2-oleoyl-*sn*-glycero-3-phosphocholine (PC), at these interfaces.

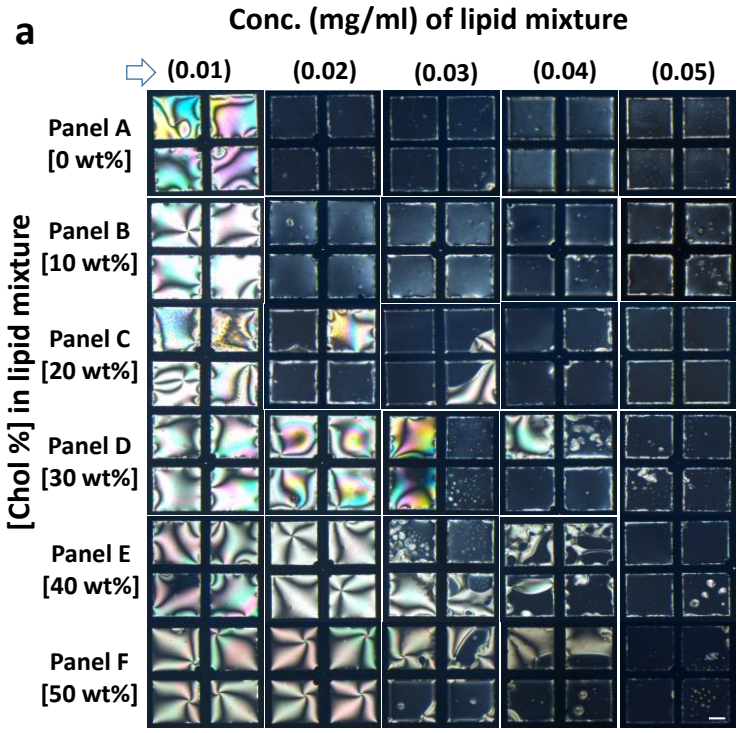

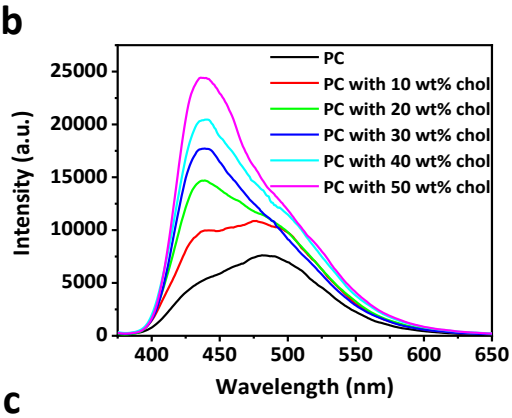

c

Liposomes with 0.5 mol% laurdan dye	Generalized Polarization (GP)
PC	-0.165
PC with 10 wt% chol	-0.017
PC with 20 wt% chol	0.153
PC with 30 wt% chol	0.242
PC with 40 wt% chol	0.247
PC with 50 wt% chol	0.291

Figure 2.2.1 (a) Polarized optical micrographs of the LC-aqueous interface captured after 10 min of addition of lipid (PC/cholesterol) mixtures at different concentrations. The images show the representative micrographs with 0-50 wt% cholesterol [panels A-F] at different concentrations of the lipid mixture (0.01-0.05 mg ml^{-1}) as indicated in the respective columns. We noted a decrease in the extent of homeotropic alignment of the LC with the increase in cholesterol (chol) amount at a particular concentration of the lipid mixture. (b) Fluorescence emission spectra of laurdan dye in the lipid (PC) vesicles having various amounts of cholesterol. The concentration of the total lipid mixture was kept at 1 mg ml^{-1} for all the fluorescence measurements. (c) Generalized polarization (GP)

factors of laurdan dye in the mixed lipid (PC/cholesterol) vesicles having various amounts of cholesterol. The scale bar is 100 µm.

We have chosen 4-cyano-4'-pentylbiphenyl (5CB) LC, which shows a nematic phase at room temperature. It is well known that micrometre-thick LC films in contact with aqueous phosphate-buffered saline (PBS) show a bright optical appearance (planar alignment) under POM.[22] We observed that the addition of various concentrations (0.01-0.05 mg ml^{-1}) of PC vesicles at the LC-aqueous interface leads to a change in the optical appearance of the LC. A complete transition from a bright to a dark optical texture (leading to the homeotropic orientation of the LC molecules) was observed at 0.02 mg $ml^{-1,}$ as shown in Figure 2.2.1(a) (panel A).

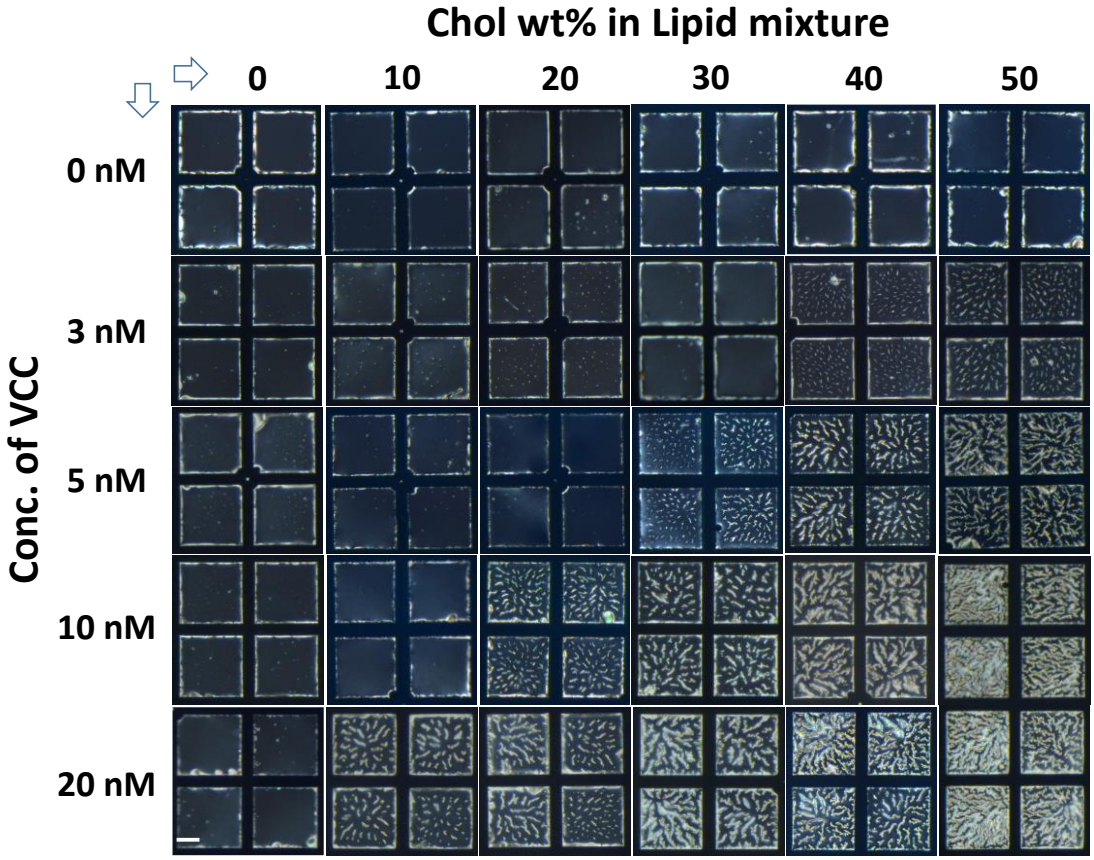

Figure 2.2.2 Polarized optical micrographs of the LC-aqueous interface captured after 20 min of addition of 0, 3, 5, 10, and 20 nM VCC onto the LC-aqueous interfaces decorated with 0.05 mg ml^{-1} of lipid mixture (PC embedded with 0-50 wt% cholesterol). The optical micrographs indicate the activity of VCC in the presence of various amounts of cholesterol with the evolution of bright dendritic textures. The scale bar is 100 µm.

This observation is consistent with the prior reports that follow an ordering transition of LCs from planar to homeotropic in the presence of lipid amphiphiles as they couple to the ordering of 5CB molecules through hydrophobic interactions.[20-24] Our second goal was to observe the ordering of 5CB in the presence of different levels (%weight) of cholesterol in PC (lipid mixture) for further investigation of VCC at the interface of a lipid mixture-decorated LC interface. We have used wt% of cholesterol by following the earlier literature report.[8] This goal was motivated by the fact that the presence of cholesterol is shown to be obligatory for the pore formation by VCC in the target membranes.[8] As shown in Figure 2.2.1(a) (panel B), when the cholesterol content in the lipid vesicles was 10% (w/w) of the total lipid mixture (PC/cholesterol), the ordering of LC remained the same as that of PC vesicles without having cholesterol (panel A, *vide supra*). However, a further increase in the cholesterol content in the lipid mixture (20-50 wt% of the cholesterol in PC) could trigger an ordering transition (homeotropic orientation) of LCs only at higher concentrations (Figure 2.2.1(a), panels C-F). Past studies have established that the homeotropic alignment of LCs upon the addition of lipid vesicles is due to the transfer of the lipid molecules to the LC-aqueous interface by vesicle fusion.[23, 24]

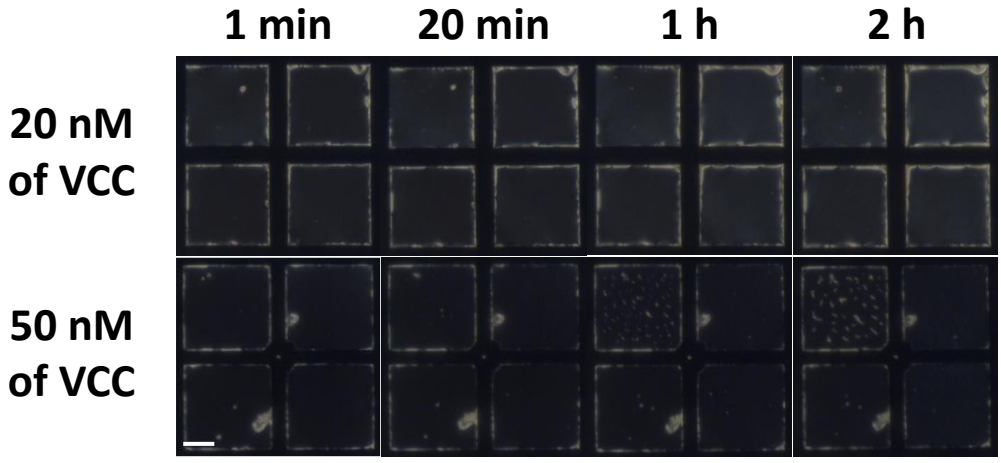

Figure 2.2.3 Optical images of PC-laden LC-aqueous interface upon addition of 20 and 50 nM VCC at different time points up to 2 h. The scale bar is 100 μm.

Then we asked the question, what drives the difference in the LC-reorientation at higher wt% (20-50 wt%) of cholesterol in the lipid mixture? We note that a high percentage of cholesterol in the mixed lipid vesicles promotes the conversion of the gel state of lipids into two coexisting liquid phases like the liquid crystalline (L_α) phase and liquid-ordered (L_o) state.[25] We anticipated that this (impedance in membrane fluidity of the mixed lipid vesicles) might lead to a low transferring rate of

the lipid to the LC-aqueous interface. To confirm this, we studied the fluorescence emission spectra of laurdan dye, a known reporter for phase transition of lipid vesicles having different amounts of cholesterol.[25-27] We make two observations from the fluorescence studies. First, an inspection of Figure 2.2.1(b) shows that in the absence of cholesterol, the emission spectrum of laurdan dye is centred at 490 nm, indicating that lipid molecules (PC) are in the disordered state. However, with an increase in the cholesterol amount in the lipid mixture, the emission maxima of the spectrum was observed around 440 nm, clearly establishing that the lipids are in a more packed phase. Second, quantification of the emission shift of the laurdan dye (as demonstrated through the generalized polarization (GP) factor) shows a continuous increase in GP with an increase in the cholesterol content of the lipid mixture (Figure 2.2.1(c)). Another possibility could be that the decrease in the density of PC lipid in the mixture might lead to the requirement of a high concentration of lipid to induce homeotropic alignment to LC. We have explored the second possibility in the context of protein interaction in the later section. Hence, the reduced extent of transfer of lipids from vesicles to the LC-aqueous interface might be the result of enhancement of the cholesterol content as well as the decreased density of PC lipid within the vesicles. As a result, the observed ordering transition of the LC from planar to homeotropic was evident only at higher concentrations of the lipid mixture (Figure 2.2.1(a), panels C-F).

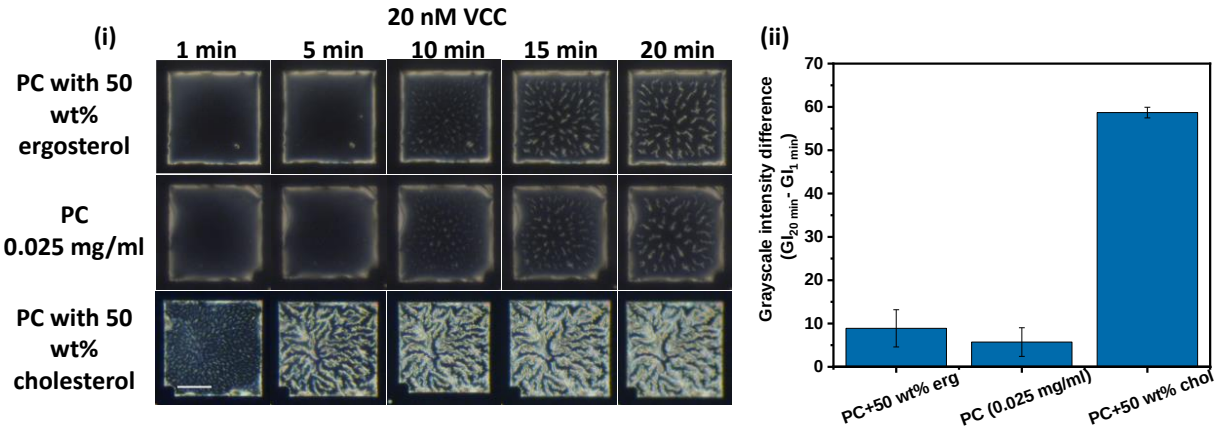

Figure 2.2.4 (i) Dynamic optical images of LC-aqueous interface laden with PC having 50 wt% ergosterol (erg), PC (0.025 mg/ml), and PC having 50 wt% cholesterol upon addition of 20 nM VCC. In all three experiments, the concentration of PC was 0.025 mg/ml. (ii) A plot showing the difference between final (measured at 20 min) and initial gray scale intensities (GI measured at 1 min), i.e., $GI_{20\ min}$- $GI_{1\ min}$ of different lipid-laden LC-aqueous interface in the presence of 20 nM VCC. The scale bar is 100 μm. One-way ANOVA was used to measure the level of statistical significance. $p = 2\times10^{-}$

^{3}<0.05 ($GI_{20\ min}$- $GI_{1\ min}$ for PC having 50 wt% erg), $p = 1\times10^{-2}$<0.05 ($GI_{20\ min}$- $GI_{1\ min}$ for PC (0.025 mg/ml), and $p = 2\times10^{-9}$<0. 05 ($GI_{20\ min}$- $GI_{1\ min}$ for PC having 50 wt% chol).

For example, in the case of 50 wt% cholesterol content in the lipid mixture, the complete dark optical appearance was visualized at 0.05 mg ml^{-1} (Figure 2.2.1, panel F). For the rest of our experiments with VCC, we kept the total concentration of lipid mixture (with various amounts of cholesterol) fixed at 0.05 mg ml^{-1} at the LC-aqueous interface. Our next experiment sought to determine if the lipid-laden aqueous interfaces of LC can report the binding of VCC at the physiologically relevant concentration (i.e., in the nM concentration range). Numerous reports have demonstrated that the insertion of proteins into the lipid layer in contact with the LC-aqueous films results in the reorientation of LCs.[20-24] The change in the optical response of LCs upon lipid-protein binding correlates with the secondary structure of the protein.[28] Proteins with a predominant β-sheet-rich secondary structure result in dendritic patterns of LCs, while α-helical proteins result in rounded or ellipsoidal bright domains.[29] With this idea kept in mind, and we monitored the optical appearance of LCs at the LC-aqueous interface decorated with the lipid mixtures (0-50 wt% cholesterol in PC) upon the addition of VCC. We note that the optical appearance of the mixed lipid-laden LC-aqueous interfaces was stable (Figure 2.2.2, first row) over the time periods for which we used those interfaces for further experiments. Inspection of Figure 2.2.2 reveals the emergence of bright LC domains after 20 min following the addition of 3 nM VCC to the aqueous solution in contact with the lipid-laden LC interface containing 40 and 50 wt% cholesterol in PC. With increasing concentrations of VCC to 5 and 10 nM, bright domains were observed in the presence of 30 and 20 wt% cholesterol in PC, respectively.

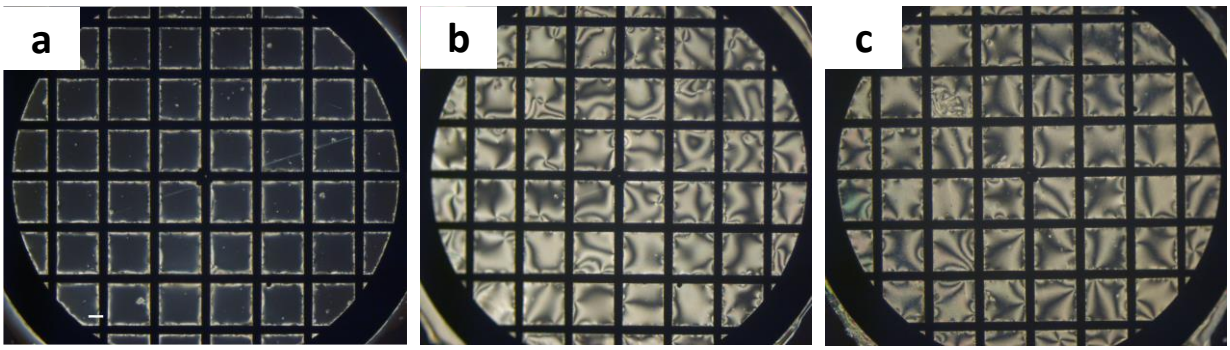

Figure 2.2.5 Optical appearance of (a) LC film encapsulated in gold grid supported over DMOAP coated glass slide at air interface; (b) LC-aqueous interface; (c) after 2 h incubation of 1 μM VCC at LC-aqueous interface in the absence of lipid. The scale bar is 100 μm.

With a further increase in the VCC concentration to 20 nM, elongated domains were seen at 10 wt% cholesterol/PC-decorated LC-aqueous interface. In any case, no change in the optical appearance (homeotropic alignment) of the LCs was noted in the PC-laden LC-aqueous interface (lacking any cholesterol in PC) as a function of the increasing VCC concentration. To further understand the role of cholesterol in mediating the LC response in the presence of VCC, we performed two control experiments. First, we prolonged the observation time for 20 nM of VCC at the PC-laden LC-aqueous interface.

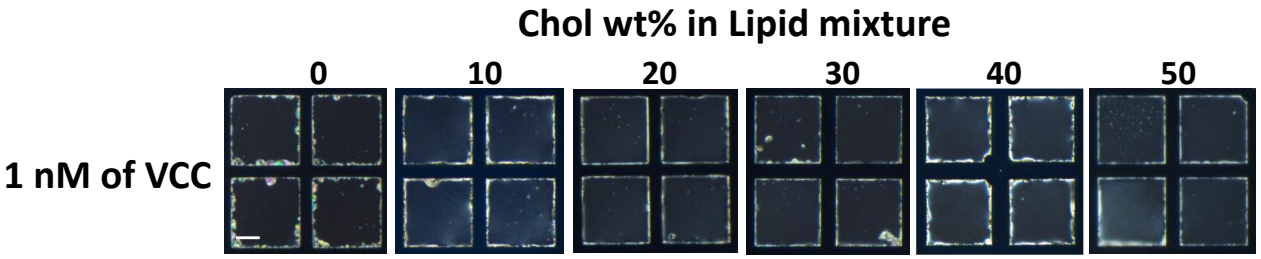

Figure 2.2.6 Optical appearance after incubating 1 nM of VCC with 0.05 mg/ml of lipid having 0-50 wt% of cholesterol for 20 min depicting no change in the LC ordering. The scale bar is 100 µm.

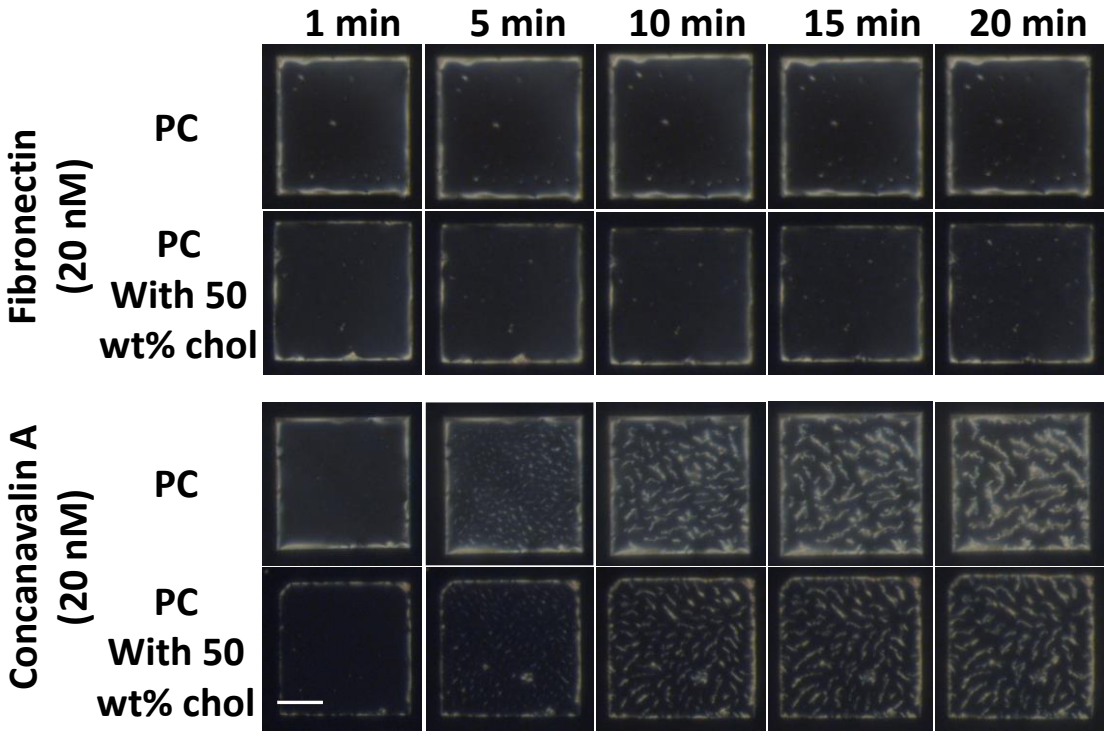

Figure 2.2.7 Optical images of PC and PC/cholesterol mixture laden LC-aqueous interface upon addition of 20 nM of fibronectin and Concanavalin A. Scale bar = 100 µm.

We did not observe any change in the optical appearance of the LCs up to 2 h upon the addition of 20 nM of VCC at these interfaces. Second, we increased the concentration of VCC up to 50 nM (i.e., 2.5 times of 20 nM) at the PC-laden LC-aqueous interface and observed the change in the optical view of the LCs. No considerable change in the optical appearance was observed up to 2 h in the presence of 50 nM of VCC at the lipid-laden aqueous-LC interface. Based on these experiments, we conclude that cholesterol plays a key role in mediating the LC response in the presence of VCC (Figure 2.2.3).

Next, we designed an experiment to comment on the effect of the impact of density, lateral heterogeneity, the concentration of PC lipid, and the importance of cholesterol in mediating lipid-VCC binding at aqueous-LC interfaces. We replaced cholesterol with ergosterol to see the dependence of the orientational response of LCs on various factors mentioned above. It is known that ergosterol behaves similarly to cholesterol with regard to phase transformations of the lipid but forms less ordered phases of the lipid than cholesterol.[30] Additionally, it is known that ergosterol has less interaction with VCC.[31] Hence, we hypothesized that if there is a change in the homeotropic ordering of LCs (in contact with ergosterol-PC lipid mixtures) upon the addition of VCC then the lower interfacial density of PC might also play a role in the LC reorientation.

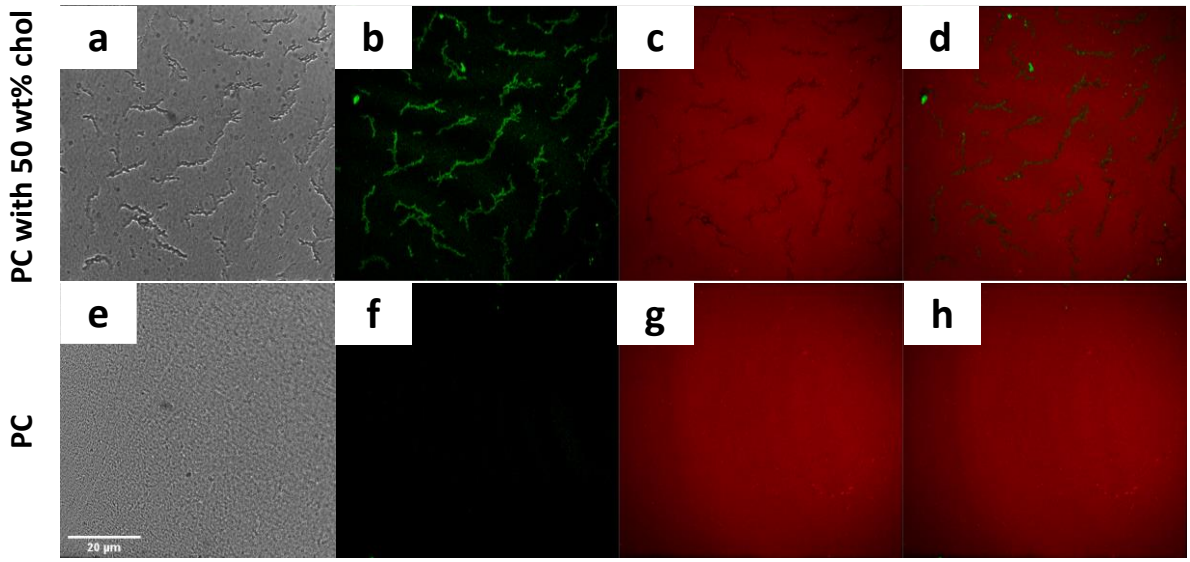

Figure 2.2.8 (a), (e) Bright field and (b–d), (f–h) confocal fluorescence images of 20 nM Alexa-488-labelled VCC incubated for 30 min with cy5 labelled PC containing (a–d) 50 wt% and (e–h) 0 wt% cholesterol-laden LC–aqueous interface, respectively. (d and h) The overlay of fluorescence images obtained with fluorescently labelled VCC and PC is shown in (b and c) and (f and g), respectively.

The concentrations of fluorescently labelled lipid and VCC are kept at 2.5 and 0.1%, respectively. Images (b–d) demonstrate the simultaneous localization of VCC- and lipid-rich regions at the LC–aqueous interface. The scale bar is 20 µm.

To investigate whether the dendritic domains are due to less areal density of lipid, we performed another control with a decreased concentration of PC lipid (the concentration of PC was kept the same as the concentration in the experiment with PC-50 wt% ergosterol/cholesterol mixture). First, we decorated the LC-aqueous interface with 0.05 mg ml^{-1} PC having 50 wt% ergosterol, added 20 nM VCC to this interface, and observed it for 20 min [Figure 2.2.4]. It should be noted that 0.05 mg ml^{-1} of lipid mixture (PC/50 wt% ergosterol) has 0.025 mg ml^{-1} of PC and ergosterol.

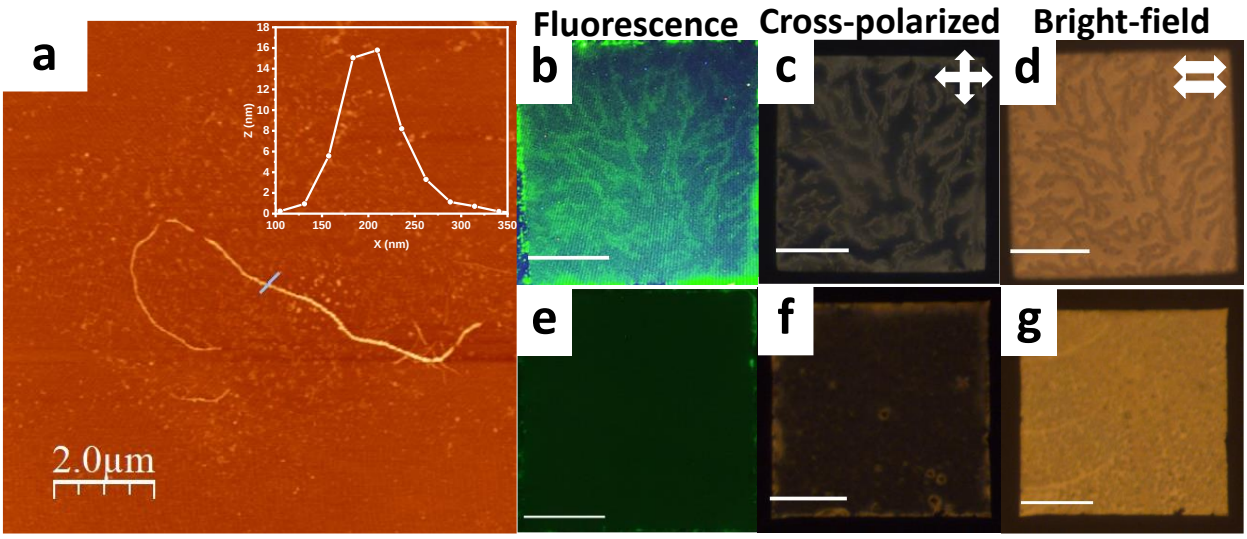

Figure 2.2.9 (a) AFM image of the aqueous layer at the LC–aqueous interface decorated with lipid mixture (PC with 50 wt% cholesterol) after 3 h of incubation with 20 nM VCC. The AFM micrograph shows the presence of fibril-like morphology. The inset of (a) shows the height profile of the fibril of ~15 nm. Epifluorescence [(b and e)], cross-polarized [(c) and (f)], and bright-field [(d and g)] images captured after 3 h of incubation of 20 nM VCC at the LC-aqueous interface decorated with PC containing (b–d) 50 wt% and (e–g) 0 wt% cholesterol in the presence of 5 µM of Th T added before imaging. The double-headed arrows on the top right sides of images (c) and (d) depict the orientation of polarizers. Scale bar = 100 µm.

To determine whether the response of LCs is either due to ergosterol or less lipid density over the interface, we performed another experiment with 20 nM of VCC added over a PC (0.025 mg ml^{-1})-decorated LC-aqueous interface. To enquire about the role of density, lateral heterogeneity,

concentration, and the importance of cholesterol, we performed another experiment with an LC-aqueous interface laden with PC having 50 wt% cholesterol and added 20 nM VCC to it and observed it for 20 min [Figure 2.2.4(i)]. As shown in Figure 2.2.4, we noted two observations: (i) PC with 50 wt% ergosterol shows the appearance of elongated domains upon the addition of VCC. The extent of LC reorientation was similar to that observed with 0.025 mg ml^{-1} of PC without ergosterol; (ii) in contrast with the observation as noted with PC/50 wt% cholesterol in the presence of VCC, the extent of LC reorientation is much less in PC with 50 wt% ergosterol as compared to PC with 50 wt% cholesterol. In addition, the difference in quantified gray scale intensities (measured at 1 and 20 min) is consistent with our above observations (Figure 2.2.4(ii)). Taken together, these observations suggested that the decrease in the areal density of PC lipid plays a role in the reorientation of LC upon the addition of VCC. However, the LC reorientation is markedly more pronounced in the case of PC with 50 wt% cholesterol, indicating that the presence of cholesterol plays a major role in dictating the LC response.

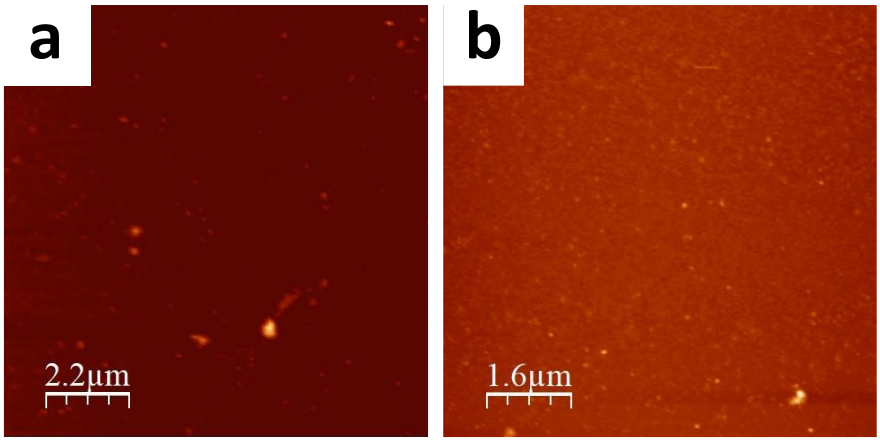

Figure 2.2.10 AFM imaging of samples collected after 3 h (a) from LC-aqueous interface having 20 nM of VCC without lipid; (b) from lipid-laden (PC with 50 wt% cholesterol) without VCC at LC-aqueous interface.

Thus, the overall impact of density is observed to be less in comparison to the specific binding of VCC with cholesterol at the LC-aqueous interface. We note several key observations from our experiments. First, the dendritic texture of the LCs observed as a result of the lipid-binding of VCC is suggestive of a β-sheet-rich secondary structure of the protein at the LC-aqueous interface consistent with the prior reports.[28, 29] Second, cholesterol is a requisite in the lipid composition to induce a reorientation of LCs for the interfacial interactions between VCC and the lipid mixture.

Third, for a particular concentration of VCC, the degree of LC ordering transition shows a linear correlation with the amount of cholesterol present, indicative of a continuous change in the orientation of the LCs at the aqueous interface. Fourth, at higher concentrations of VCC, the lipid-laden LC film shows elongated branched structures that get amplified by the LC medium even at lower cholesterol content in the lipid mixture. To confirm whether these branched structures (dendritic texture) are due to the interactions of the VCC with the lipid-laden LC-aqueous interface, we performed an additional control experiment. For this, we added 1 μM VCC at the LC-aqueous interface without a lipid/lipid mixture. It was observed that the addition of VCC without lipid results in no change in the optical appearance of the LCs, as shown in Figure 2.2.5. Next, to determine the sensitivity of the lipid-laden LC-aqueous interface towards VCC, we decreased the concentration of VCC to 1 nM and observed the optical response of LCs. Negligible change (remained homeotropic) in the optical appearance of the LC was observed at 1 nM at these interfaces (Figure 2.2.6). At this stage, we performed control experiments with two β-sheet rich proteins, i.e., fibronectin and concanavalin A (Figure 2.2.7). In the case of 20 nM fibronectin, we observed no change in the optical appearance of the aqueous-LC interface in PC with and without cholesterol.

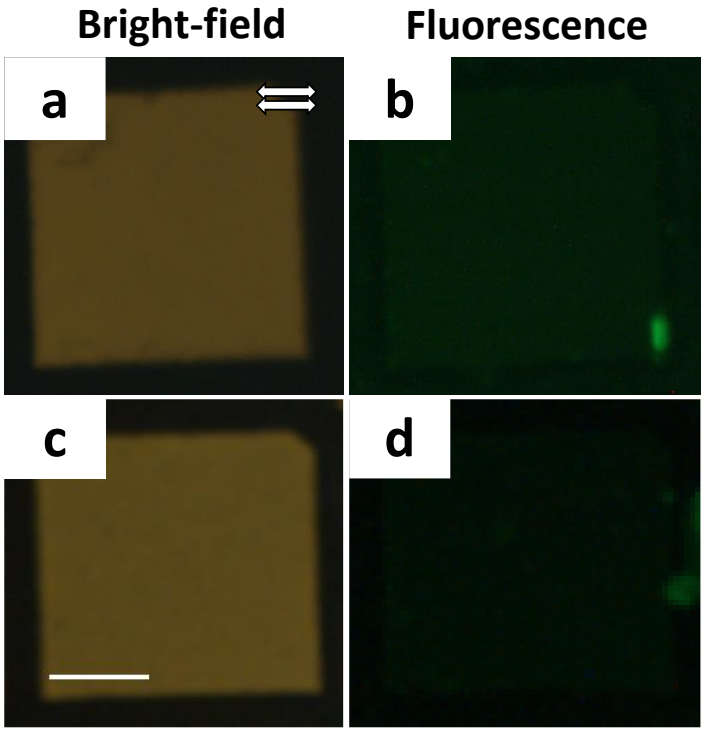

Figure 2.2.11 (a, c) Bright-field, (b, d) respective fluorescence images captured after 3 h incubation of 20 nM VCC without lipid and lipid mixture (PC with 50 wt% cholesterol) without VCC at LC-

aqueous interface in the presence of 5 µM ThT, added before the observation. The double-headed arrows on the top right of the image 'a' depict the orientation of polarizers. The scale bar is 100 µm.

However, with 20 nM concanavalin A, the LC responses were similar for PC with and without cholesterol. The interfacial behaviours of both the β-sheet-rich proteins were found to be different from that of VCC. To provide further insights into the dendritic patterns in contact with VCC at the lipid-laden LC-aqueous interface, we performed confocal fluorescence experiments. For this, LC-aqueous interfaces were decorated with a self-assembled layer of 0.05 mg ml^{-1} of 2.5% fluorescently labelled PC (Cy5 PC) containing 0 and 50 wt% cholesterol. To these, we added 20 nM of 0.1% of Alexa 488-labelled VCC and observed them under a confocal microscope.

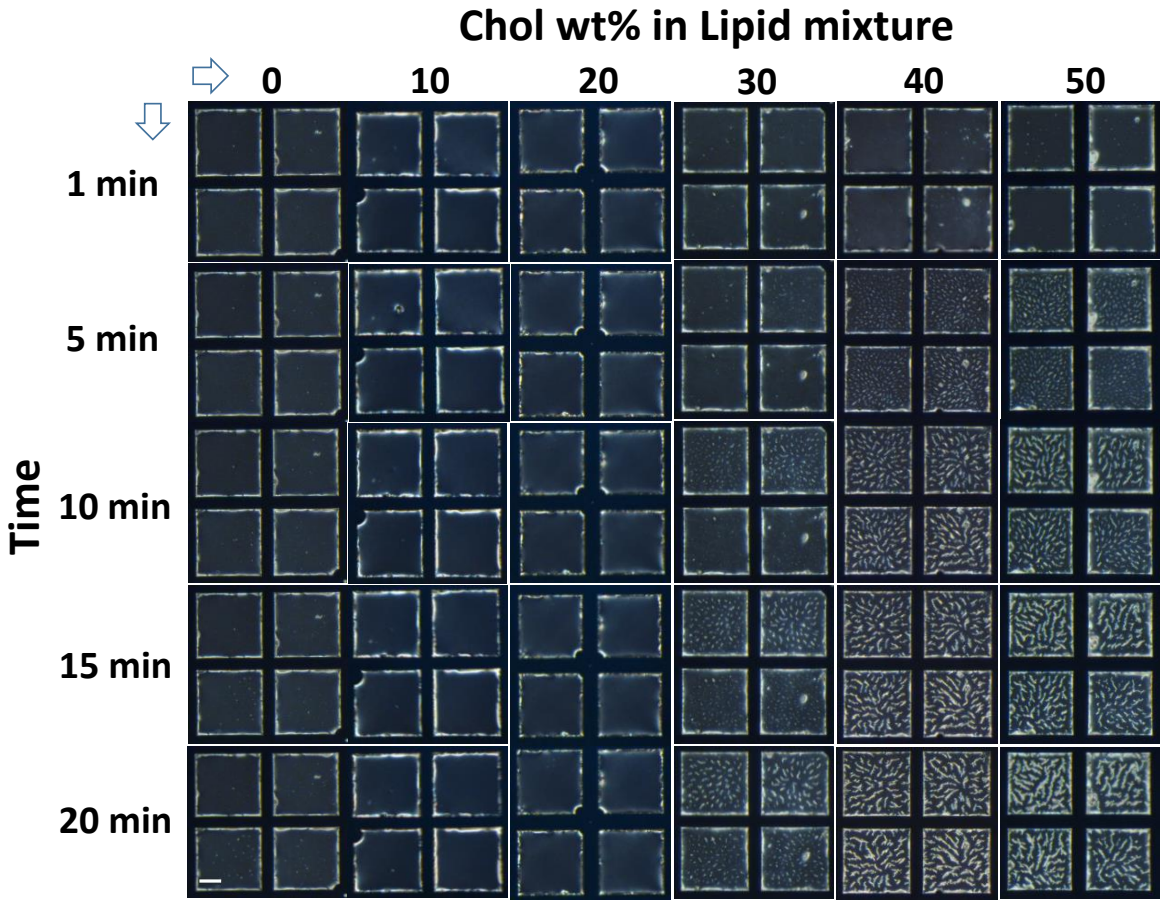

Figure 2.2.12 Time-lapse polarized light micrographs after the addition of 5 nM VCC on the LC-aqueous interface decorated with 0.05 mg ml^{-1} of lipid mixture (PC containing 0-50 wt% cholesterol). The optical micrographs demonstrate the activity of 5 nM VCC toward 30-50 wt% of cholesterol in the lipid mixture laden LC–aqueous interface, as evident from the bright dendritic textures. The scale bar is 100 µm.

The bright-field image (Figure 2.2.8(a)) clearly shows the dendritic patterns of LC. Figure 2.2.8(b) Inspection depicts the green-fluorescent dendritic patterns in the presence of PC having 50 wt% cholesterol. In contrast, no green fluorescence was observed in the absence of cholesterol in PC (Figure 2.2.8(f)). This suggests that these green domains correspond to regions where VCC protein interacts with the lipid mixture on the LC film. Similarly, as the lipid was doped with Cy5 PC, red fluorescence was observed in the LC film together with dark non-fluorescent regions that correspond to the dendritic structures as shown in Figure 2.2.8(c). The merged image clearly depicts the simultaneous VCC and lipid-rich regions (Figure 2.2.8(d)).

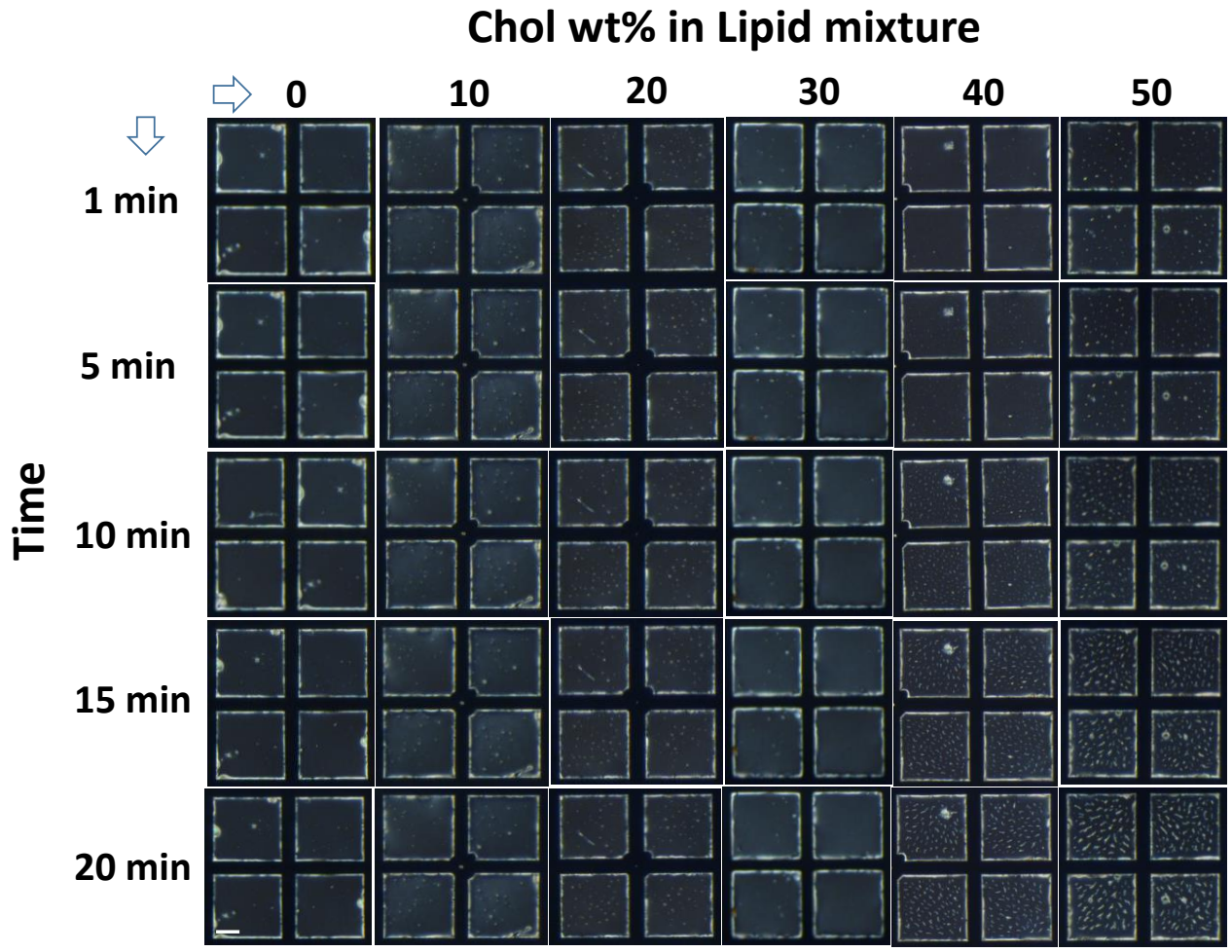

Figure 2.2.13 Dynamic LC response after the addition of 3 nM VCC with 0.05 mg/ml of PC embedded with 0-50 wt% cholesterol. The formation of bright domains was observed only in the case of 40 and 50 wt% of cholesterol. The optical micrographs at 20 min are also shown in Figure 2.2.2. The scale bar is 100 µm.

Overall, the results indicate that the green fluorescent and dark non-fluorescent regions are VCC-rich (lipid-lean), while the dark and red fluorescent regions are lipid-rich (VCC-lean), as clearly visible in Figure 2.2.8(b and c), respectively. However, we did not observe any VCC-rich domains in the case of the PC-adorned LC-aqueous interface lacking cholesterol (Figure 2.2.8(e-h)). In order to further characterize these elongated branch-like patterns in the presence of VCC at mixed lipid (PC/cholesterol)-laden LC-aqueous interfaces, we performed atomic force microscopy (AFM) experiments. The imaging was performed after incubation of VCC for 3 h at the mixed lipid-LC-decorated interfaces, followed by drying the extracted aqueous layer from those interfaces. A fibril-like morphology (Figure 2.2.9(a)) with a height of ~15 nm (inset of Figure 2.2.9(a)) was observed in AFM.

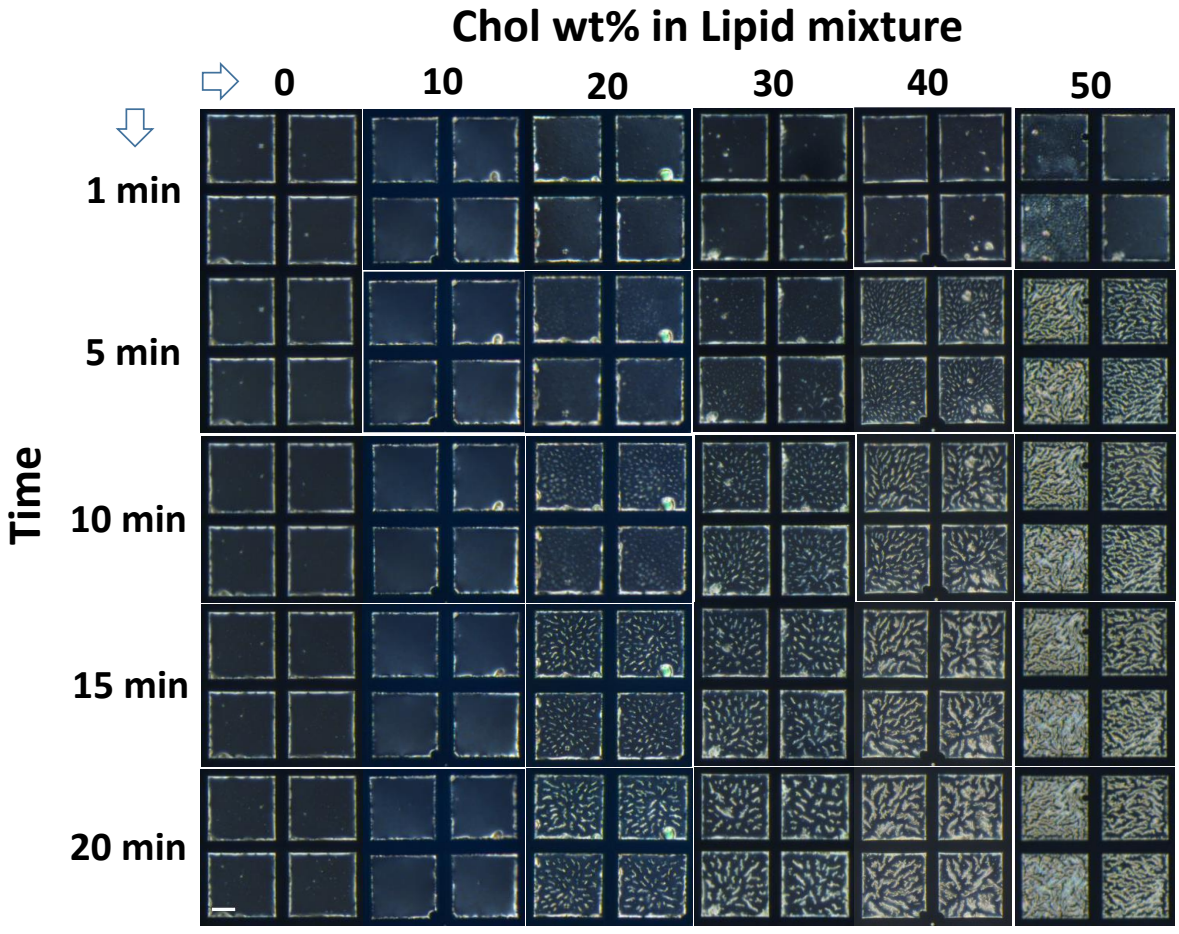

Figure 2.2.14 Dynamic LC response after the addition of 10 nM VCC with 0.05 mg/ml of PC embedded with 0-50 wt% cholesterol. The formation of bright domains was observed only in the case of 20-50 wt% cholesterol. The optical micrographs at 20 min are also shown in Figure 2.2.2. The scale bar is 100 µm.

To further characterize such fibrillar structures, we examined thioflavin T (Th T)-binding, if any, to these fibrils. Th T-binding is widely used to characterize amyloid-like fibrils and β-sheet protein structures.[32-35] In our study, we monitored the Th T fluorescence (added prior to the observation) of mixed lipid-laden LC-aqueous interfaces in contact with 20 nM VCC for 3 h. Inspection of Figure 2.2.9(b) shows a considerable Th T fluorescence in the fibrillar domains, which suggests that the branch-like domains are Th T active. The crossed polars and bright-field images of the same shown in Figure 2.2.9 (c and d) also indicate aggregated VCC structures at the interface. However, no such fluorescent domains were observed after incubation of 20 nM VCC and 5 µM Th T at the PC-laden LC-aqueous interface (0 wt% cholesterol) as shown in Figure 2.2.9 (e, f, and g).

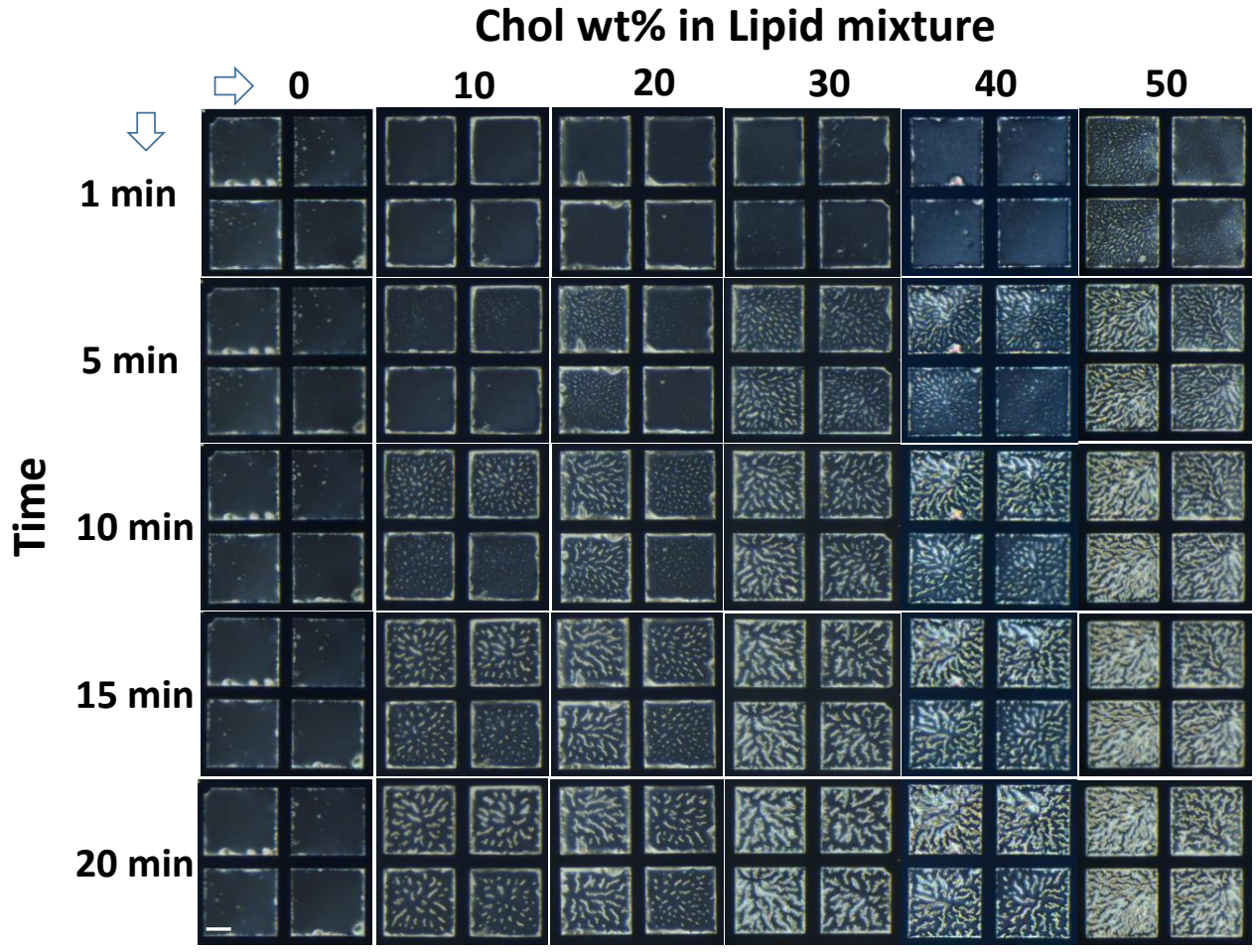

Figure 2.2.15 Dynamic LC response after the addition of 20 nM VCC with 0.05 mg/ml of PC embedded with 0-50 wt% cholesterol. The formation of bright domains was observed only in the case of 10-50 wt% cholesterol. The optical micrographs at 20 min are also shown in Figure 2.2.2. The scale bar is 100 µm.

We performed two additional control experiments to establish the role of cholesterol in the lipid mixture for the above-described response of the LC in the presence of VCC. First, we conducted AFM experiments of samples collected from (i) the LC-aqueous interface laden with lipid mixture (PC with 50 wt% cholesterol) without VCC and (ii) the LC-aqueous interface after incubation of VCC in the absence of lipid mixture. In both cases, we did not observe a fibrillar morphology in the AFM image, which further confirms that the interfacial lipid-protein interactions possibly led to the formation of fibril-like structures at the interface (Figure 2.2.10). Second, we performed Th T experiments upon incubation of 5 µM of Th T with 20 nM VCC at the LC-aqueous interface without lipid and the lipid mixture (PC with 50 wt% cholesterol)-laden interface without VCC (Figure 2.2.11). In any case, the addition of Th T did not lead to any fluorescence. Taken together, our data suggest that VCC interacts with the lipid mixture only in the presence of cholesterol, leading to the formation of the fibril-like domains at the LC-aqueous interface. It remains unclear at present how the cholesterol-containing lipid phase at the LC interface triggers the formation of such fibrillar structures by VCC, even at such lower protein concentrations.

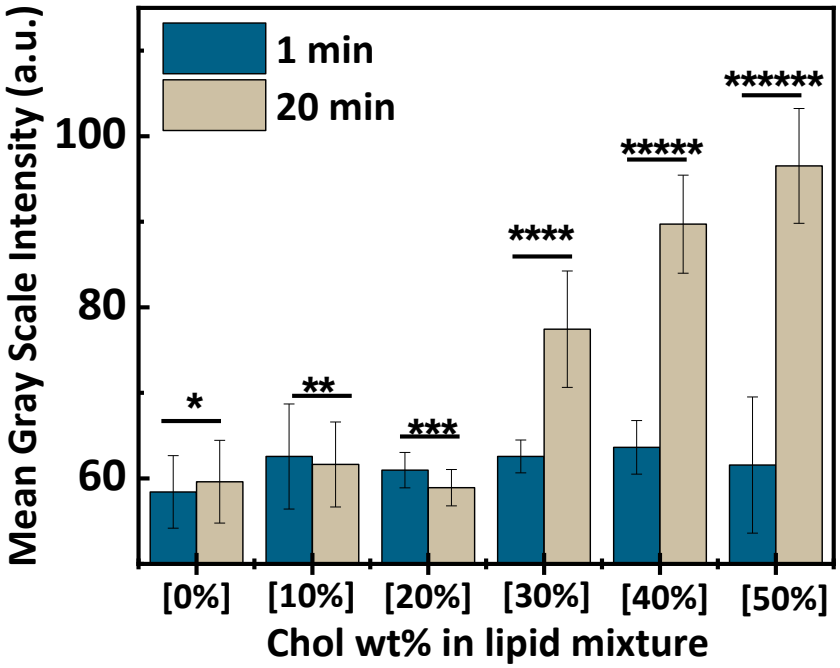

Figure 2.2.16 Comparison of the mean gray scale intensities of the polarized light micrographs captured after the addition of 5 nM VCC at 1 and 20 min on LC–aqueous interfaces decorated with PC containing various amounts of cholesterol in the lipid mixture. The indicated values correspond to the images shown in Figure 2.2.12. The plots show the average intensity of four grid squares for

each measurement. One-way ANOVA was used to measure the level of statistical significance. *p = 0.7>0.05, **p =0.8>0.05, ***p = 0.2>0. 05, ****p = 5×10^{-3}<0. 05, *****p = 2×10^{-4}<0. 05, ******p = 5×10^{-4}<0. 05.

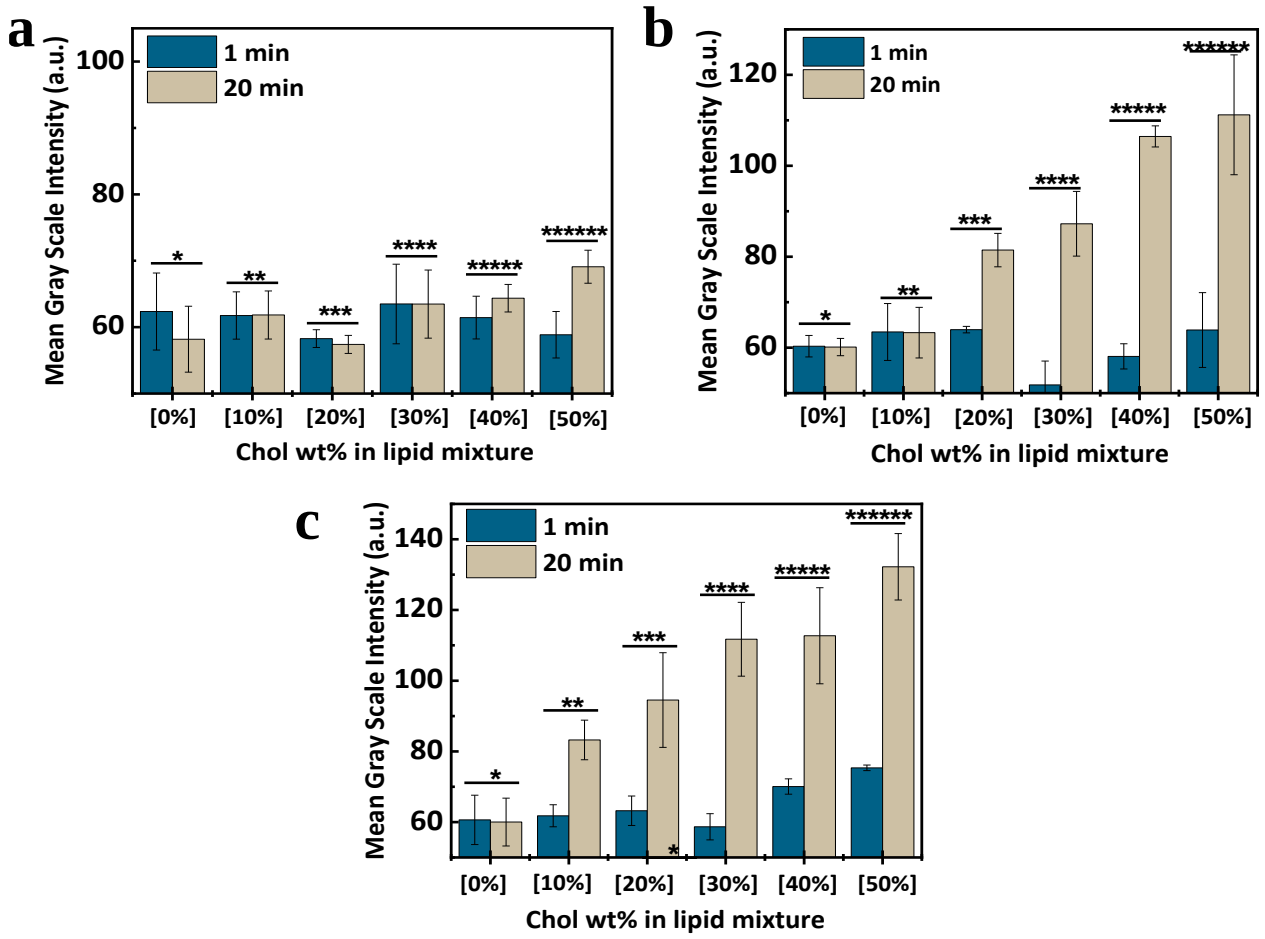

Figure 2.2.17 Comparison of mean gray scale intensities at 1 min and 20 min when PC lipid having variable amounts of cholesterol are exposed to (a) 3 nM, (b) 10 nM, (c) 20 nM amount of VCC protein. The mean gray scale intensities measurements shown in a, b, and c were performed for the optical micrographs in Figures 2.2.13, 2.2.14, and 2.2.15. The value indicated in the graph is the average of the mean gray scale intensity of four grid squares. One-way ANOVA was used to measure the level of statistical significance. a) *p = 0.3>0.05, **p = 0.9>0.05, ***p = 0.4>0. 05, ****p = 0.9 >0. 05, *****p = 0.2>0. 05, ******p = 3×10^{-3}<0. 05. b) *p = 0.9>0.05, **p = 0.9>0.05, ***p = 8×10^{-5}<0. 05, ****p = 2×10^{-4}<0. 05, *****p = 1×10^{-7}<0. 05, ******p = 8×10^{-4}<0. 05. c) *p = 0.9>0.05, **p = 5×10^{-4}<0.05, ***p = 4×10^{-3}<0. 05, ****p = 7×10^{-5}<0. 05, *****p = 8×10^{-4}<0. 05, ******p = 1×10^{-5}<0. 05.

It is possible that the cholesterol-containing PC phase at the LC interface provides a unique physicochemical environment that allows the formation of the fibrillar protein-lipid micro-domains, which in turn favour the formation of the observed fibrillar structures by VCC. Our next goal was to explore the dynamics of LC ordering transitions in response to the interfacial lipid-protein binding event. In this experiment, we first incubated the 5CB LC film against an aqueous solution of PC with various amounts of cholesterol, followed by the addition of VCC, and then captured the time-lapse polarized images. Inspection of Figure 2.2.12 reveals that following the addition of 5 nM of VCC at these interfaces, the optical appearance of the LC changed from dark to bright domains within 5 min in the presence of PC containing 40-50 wt% cholesterol (Figure 2.2.12, second row). We made three additional observations from the experiment. First, in the presence of PC with 30 wt% cholesterol at the LC interface, we observed the signature of the formation of bright domains only after 10 min of the addition of VCC.

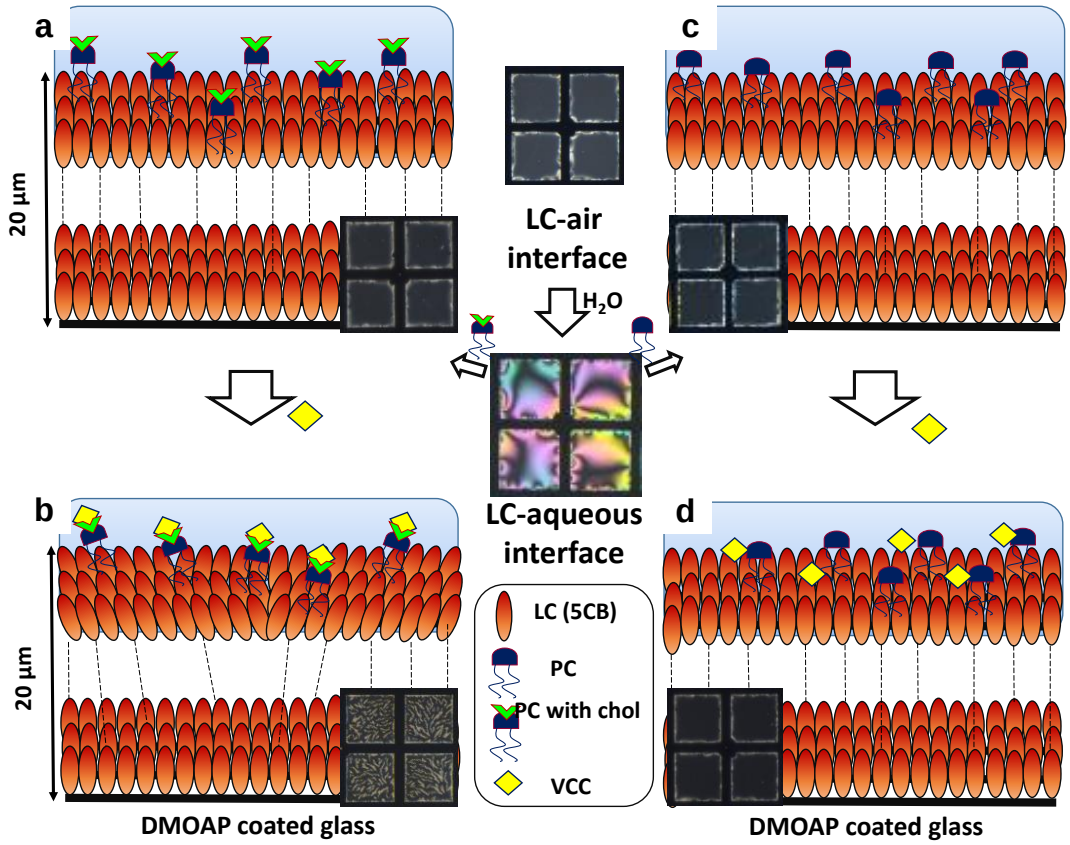

Figure 2.2.18 A schematic illustration to depict the changes triggered in the LC ordering by the addition of VCC to the lipid-laden LC–aqueous interface: (a and c) cartoons of LC film in contact

with buffer decorated with PC embedded (a) with and (c) without cholesterol. (b and d) Effect of addition of VCC on the LC–aqueous interface adorned (b) with and (d) without cholesterol.

Second, no change in the optical appearance (remained dark) was observed at 0-20 wt% cholesterol-containing lipid in the presence of 5 nM of VCC over the time periods we used in the experiments. These results support that a minimum of 30 wt% cholesterol in PC is required for the LC ordering transition at 5 nM VCC. This is consistent with the notion that the physiological membrane systems in general, contain ~30 % cholesterol.[36, 37] Therefore, the presence of ~30 % cholesterol in the biomembranes, appears to be the minimal optimal range that is essential to emulate the crosstalk between VCC and the membrane phospholipids in order to generate the membrane-damaging lesions by the toxins. To further understand the time-laps dynamics of the LC at various concentrations of VCC, we carefully analyzed the POM images after the addition of 3, 10 and 20 nM of VCC at mixed lipid-laden LC interfaces. The results shown in Figure 2.2.13 demonstrate that 3 nM of VCC can trigger an ordering transition of LCs (within 10 min) with a few dendritic patterns only in the presence of 40 and 50 wt% of cholesterol in PC. With a further increase in the VCC concentration to 10 and 20 nM, we observed the evolution of larger bright domains with a significantly faster rate at 20 and 10 wt% cholesterol in PC, respectively (Figures 2.2.14 and 2.2.15). In any case, VCC did not lead to an ordering transition of LC in the PC-decorated LC interface. Quantification of the light intensity transmitted through the LC-film in the presence of 5 nM VCC at various concentrations of cholesterol at the interface, as shown in Figure 2.2.16 reveals a significant increase in the gray scale brightness within 20 min for 30-50 wt% cholesterol in PC. The increase in gray scale brightness over time is consistent with stronger lipid-protein interaction at these interfaces. Also, we observed a significant increase in the difference of gray scale values measured at 1 and 20 min with an increase in the cholesterol content in the lipid mixture (PC/30-50 wt% cholesterol) after the addition of 5 nM VCC at the interface. The results support stronger lipid-protein interactions with an increase in cholesterol content in the lipid mixture (regardless of the impact of density as discussed in the initial section), consistent with our hypothesis. We also noted that gray scale intensity is significantly enhanced within the same time frame in the cases of 10 and 20 nM of VCC for 20-50 wt% and 10-50 wt% cholesterol in PC, respectively (Figure 2.2.17b and c). However, no substantial increase in grayscale brightness was observed in the case of 3 nM of VCC under similar experimental conditions (Figure 2.2.17a). A schematic illustration of the binding of VCC at the lipid mixture (PC with 0-50% cholesterol)-laden LC-aqueous interface is shown in Figure 2.2.18.

2.3. Conclusions

In summary, upon encountering the target membrane lipid bilayer, VCC monomers undergo irreversible structural reorganization to form stable oligomeric assemblies with defined stoichiometry.[38] In this process, defined pore-forming motifs of the toxin protomers are inserted into the membrane lipid bilayer to generate water-filled β-barrel pores.[9-12] Such a membrane pore formation process alters the selective permeability barrier functions of the biomembranes. In addition, transmembrane pore-formation in the membrane lipid bilayer can also generate membrane-damaging lesions that can result in drastic changes in the membrane architecture and integrity.[38] Consistent with such notions, we observed the formation of the elongated domains/defects in the cholesterol-containing lipid-laden LC-aqueous interface upon the addition of VCC. Interestingly, the effects of VCC on such lipid-decorated interfaces of LC show an obligatory requirement of cholesterol, similar to those observed for the physiological membranes. Furthermore, from epifluorescence and AFM imaging, we found that the interfacial binding of VCC with the cholesterol-containing lipid-decorated LC interface leads to the formation of fibrillar structures of VCC, that are possibly mixed with lipids. Consequently, the underlying LC is aligned along the fibrils of VCC at the interface, giving rise to a dendritic texture.

It is suggested that the β-sheet-rich proteins exhibit dendritic patterns and have strong interactions with lipids at the LC-aqueous interface.[28] This suggests that the interfacial environment of lipid-laden LC induces the conversion of the bound VCC into elongated fibrillar structures that are not documented in the conventional membrane lipid bilayer. It is remarkable to note here that the interaction of VCC with a thin layer of lipids assembled at the aqueous interface of LC can induce the formation of fibrillar structures even at a nM concentration range. Therefore, our work shows that the aqueous interfaces of LC can be used to elucidate the membrane-damaging action of β-PFTs that represent a unique class of protein toxins. Moreover, our study provides the opportunity to establish a robust platform to explore the details of the changes/defects generated in the membranes upon the action of membrane-interacting and membrane-damaging proteins, in general.

2.4. Experimental section

2.4.1. Materials

Required Fischer's Finest Premium Grade glass microscopic slides were bought from Fischer Scientific (Pittsburgh, PA). For washing the glass slides, Sulfuric acid, Hydrogen peroxide (30%

w/v), Chloroform (HPLC), and Sodium chloride (NaCl) were purchased from Merck. Ethanol was purchased from Jebsen & Jenssen GmbH and Co., Germany (S D fine-chem limited). 4-Cyano-4'-pentylbiphenyl (5CB) liquid crystal, PC (1-palmitoyl-2-oleoyl-*sn*-glycero-3-phosphocholine; 16:0/18:1), Cholesterol, PBS (Phosphate Buffered Saline; pH = 7.2), Tris buffer, thioflavin T (Th T), Dimethyloctadecyl [3-(trimethoxysilyl) propyl] ammonium chloride (DMOAP), Concanavalin A, Fibronectin, Trypsin, 1-(6-(dimethylamino)naphthalen2-yl)dodecan-1-one, 6-dodecanoyl-2-dimethylaminonaphthalene (Laurdan dye), 1,2-dioleoyl-*sn*-glycero-3-phosphocholine-N-(Cyanine 5) [Cy5 labelled PC], 3β-Hydroxy-5,7,22-ergostatriene (Ergoesterol) were purchased from Merck. Milli-Q water was obtained from the Millipore system (Bedford, MA). Coomassie brilliant blue dye and Luria Broth (LB media) were purchased from Himedia. Isopropyl-β-D-Thiogalactopyranoside (IPTG) was purchased from BR Biochem Life Sciences. Alexa Fluor 488 maleimide was purchased from Thermo Fischer Scientific. The precursor form of *Vibrio cholerae* cytolysin (VCC) i.e., Pro-VCC, was obtained by purification (detailed in methods). Gold Specimen grids (20 µm thick, 50 µm wide, 283 µm grid spacing) were obtained from Electron Microscopy Sciences (Fort Washington, PA).

2.4.2. Cleaning of Glass slides

The glass slides were placed in a glass jar, and then freshly prepared piranha solution (70:30 (v/v %) H_2SO_4:H_2O_2) was poured onto them. The whole system was immersed in a water bath whose temperature was maintained at 80 ℃. After 1 h, the glass slides were rinsed with an ample amount of Milli-Q water, dried with a stream of nitrogen gas, and kept in an oven at 100 ℃ for at least 3 h before use.[39]

Cleaned glass slides were then immersed in an aqueous solution containing 0.1 % (v/v) DMOAP solutions in DI water for 30 min at room temperature to form a hydrophobic coating over the glass slides. This was followed by washing to remove the excess DMOAP and drying using nitrogen purging. Further, for cross-linking to form a siloxane bond, these slides were put in the oven for 3-6 h.[22]

2.4.3. Preparation of LC-aqueous interfaces

The LC-aqueous interface preparation has already been reported in earlier reports.[22, 39] Briefly, DMOAP-coated glass slides were cut into small pieces, and gold grids were placed over them. Grids were then filled with approximately 0.2 µl of 5CB, and the excess of 5CB was taken out with a

syringe to form a uniform film of LC. For the generation of the LC-aqueous interface, the prepared system was placed in an optical well containing a PBS buffer (10 mM, 2 ml).

2.4.4. Preparation of PC vesicles with varying amounts of cholesterol (chol)

PC vesicles or liposomes embedded with different amounts of cholesterol (0%, 10%, 20%, 30%, 40%, and 50% by weight of total lipid) were prepared.[8] For this, the calculated amount of lipid was taken and dissolved in chloroform to make a suspension in a round bottom flask. A required amount of cholesterol (0-50% of cholesterol by weight) was added and then dried under a high vacuum for 3 h at room temperature. After 3 h, PBS buffer was added to the dried lipid, and then freeze-thaw cycles were carried out to prepare large lipid vesicles. Probe sonication of the aqueous lipid dispersion for 30 min resulted in small unilamellar vesicles. All lipid solutions so prepared were used within 24 h.

Table 1. Correlating the weight percentage used with the mole percentages.

S.no.	Weight %	Mole %
1	10	18
2	20	33
3	30	46
4	40	56
5	50	66

The earlier report by Huang et al. has described the maximum solubility of cholesterol in PC lipid is ~66 (±1) mol%.[40] The study has also demonstrated that in any lipid bilayer membrane, there is an upper limit on the cholesterol concentration that can be accommodated within the bilayer structure; excess cholesterol will precipitate as crystals of pure cholesterol monohydrate. In our experiments, we have also used 50 wt% as the maximum percentage of cholesterol (corresponding mole% in Table 1).

2.4.5. Purification of VCC

The purification of VCC has been done by Anish K. Mondal, a group member of our collaborator Dr. Kausik Chattopadhyay's lab (IISER Mohali). We have used it as a reagent for our study, which the collaborator has kindly provided. The work of the collaborator has been acknowledged and well respected.

Vibrio cholerae cytolysin (VCC) was recombinantly expressed and purified following the method described in the earlier studies.[11, 41] Protein concentration was calculated by measuring absorbance at 280 nm, using the theoretical extinction coefficient determined from the primary protein sequence.

The details are also provided in the following reference.

Gupta, T.; Mondal, A. K.; Pani, I.; Chattopadhyay, K.; Pal, S. K. Elucidating liquid crystal-aqueous interface for the study of cholesterol-mediated action of a β-barrel pore forming toxin. *Soft Matter* **2022**, *18*, 5293-5301.

2.4.6. Preparation of lipid-laden LC-aqueous interface

The formed vesicles of lipids were then added to the LC-aqueous interface to form lipid layers over the LC-aqueous interface and incubated for 30 min. After the equilibration period, excess lipids in the solution were removed by washing with a PBS buffer (10 mM, pH = 7.2) thrice. Rinsing was performed with high caution so that the lipid assembly and the LC film were not disturbed. Further, to understand protein interactions with the lipid-laden LC-aqueous interface, the buffer was replaced with varying concentrations of the protein, and the optical response of LC was observed under a polarizing optical microscope (POM). The dispersion of a variable amount of protein was carried out slowly from the walls of the optical well to ensure no turbulence in the aligned layer of lipid.

2.4.7. Optical Characterization of LC films

The optical characterization has also been reported in prior reports.[22, 29] Briefly, the optical response of LC was observed with a POM (Zeiss Scope.A1) in the transmission mode. The optical cell containing the 5CB film was placed on a rotating platform, and each image was focused and captured with a Q-imaging digital camera attached to the POM with an exposure time of 80 ms. Orthoscopic examinations of the orientation of 5CB were done. In all the experiments, images were captured, keeping the source intensity about 40% that of the full brightness.

2.4.8. Emission fluorescence spectra of Laurdan Dye

PC lipid with a variable amount of cholesterol and 0.5 mole % of Laurdan dye was dissolved in an HPLC chloroform solution, and then its vesicles were prepared using the aforementioned method. For recording the emission fluorescence spectra, the dye was excited at 360 nm wavelength with an exciting slit width of 1.5 nm, and the emission bandwidth was 3 nm. The spectra were recorded within the range of 375 to 650 nm using LabSolutions RF software. Generalized Polarization factor was calculated by using the formula "GP = Generalized Polarization = $(I_{440} - I_{490}) / (I_{440} + I_{490})$", where I_{440} and I_{490} refer to emission intensities at 440 nm and 490 nm, respectively.[42]

2.4.9. Labelling of VCC

The labelling of VCC has been done by Anish K. Mondal, a group member of our collaborator Dr. Kausik Chattopadhyay's lab (IISER Mohali). We have used it as a reagent for our study, which the collaborator has kindly provided. The work of the collaborator has been acknowledged and well respected.

VCC was labelled with Alexa Fluor 488-maleimide using the protocol recommended in the manufacturer's kit.[41] The details are provided in the following reference.

Gupta, T.; Mondal, A. K.; Pani, I.; Chattopadhyay, K.; Pal, S. K. Elucidating liquid crystal-aqueous interface for the study of cholesterol-mediated action of a β-barrel pore forming toxin. *Soft Matter* **2022**, *18*, 5293-5301.

2.4.10. Confocal Microscope Imaging

To visualize the localization of fluorescently labelled lipid and protein, we have done confocal microscope imaging. Samples were prepared by incubating 20 nM 0.1% Alexa-488 fluorescently labelled VCC with a 2.5% Cy5 fluorescently labelled PC lipid mixed with 0 and 50 wt% cholesterol. For imaging of the sample, a 63-long-distance water-immersed lens with hybrid detectors was used. The scanning speed was 400 Hz, and the image acquisition was set to 1,024×1,024 pixels. Cy5 and Alexa-488 fluorescent dyes were excited with 10% argon laser power, and laser gain was maintained constant at 5%.

A 488 nm laser line was employed for the excitation of Alexa-488 labelled VCC, whereas a laser of 650 nm was used for Cy5 excitation. SP8 upright confocal microscope was used to acquire confocal image stacks.

2.4.11. Atomic Force Microscopy (AFM) imaging

For AFM imaging, 20 nM VCC was incubated with the LC film decorated with lipid (PC and 50 wt% cholesterol) for 3 h. After the incubation, the glass slide was taken out, and about 100 µl of PBS buffer (10 mM, pH = 7.2) was poured over the grid to collect the sample in contact with the LC film.

Approximately 30 µl of the sample was placed over a cleaned Silicon (Si) wafer and air-dried. After drying, the sample deposited on the Si wafer was flushed with 100 µl of milli-Q water and dried by nitrogen purging for 15 min. The AFM images were taken under tapping mode by Innova Bruker AFM using an antimony-coated silicon tip with an 8 nm radius, and the images were processed using WSxM software.[43]

2.4.12. Epifluorescence Imaging of Aqueous-5CB interfaces

Fluorescence imaging was performed using a Zeiss (Scope A1) fluorescence microscope as documented earlier.[29] For ThT experiments, the LC-aqueous interface was incubated with a lipid having 50 wt% cholesterol for 30 min. Excess lipid was flushed out, followed by the addition of 20 nM VCC and incubated for 3 h. 5 µM of Th T was added in the end and incubated up to 20 min before imaging.

2.4.13. Quantitative response

The LC optical response at different time points and concentrations was quantified in terms of the gray scale intensity of the optical micrographs. The average gray scale intensity was measured using ImageJ software. The gray scale intensity was averaged for four grid squares of each micrograph to calculate the mean grayscale intensity. A 0.5-15% variation was observed in the gray scale over different sets of experiments.

2.4.14. Statistics

The data are reported as means ± standard error of the mean. A multifactorial repeated measures ANOVA was employed,[44, 45] to examine variations in the mean grayscale intensities of LC-aqueous interfaces laden with PC containing different weight% of cholesterol in the presence of VCC. Subsequently, Tukey's post-hoc analysis was conducted to delve deeper into the findings. Statistical significance was determined at $p < 0.05$.

2.5. Author Contributions

SKP, IP and TG collaborated with Dr. Kausik Chattopadhyay's lab (Department of Biological Sciences, IISER Mohali) to conceptualize and devise the framework for the project. TG meticulously executed all experimental procedures and thoroughly analysed the resulting data. Anish K. Mondal has purified the protein. The labelling of VCC has been done by Anish K. Mondal, a group member of our collaborator Dr. Kausik Chattopadhyay's lab (IISER Mohali). We have used it as a reagent for our study, which the collaborator has kindly provided. SKP and KC did overall project administration.

2.6. Acknowledgements

S. K. P. acknowledges the MoE-STARS grant (File no. STARS/ APR2019/CS/284/FS). T. G. thanks CSIR (09/947/(0223)/2019EMR-1) for a fellowship. T.G. acknowledges powerpoint and chemdraw, tools for various cartoons used in the table of contents (TOC) graphics and schematics. T.G. is grateful to the Royal Society of Chemistry for giving the permission to reuse/reproduce the whole article in my thesis which is well acknowledged and respected. The links of the article are https://pubs.rsc.org/en/content/articlelanding/2022/sm/d2sm00447j ; https://doi.org/10.1039/D2SM00447J.

References

1. Gouaux, E., Channel-forming toxins: tales of transformation. *Curr. Opin. Struct. Biol.* **1997,** *7* (4), 566-73.

2. Parker, M. W.; Feil, S. C., Pore-forming protein toxins: from structure to function. *Prog. Biophys. Mol. Biol.* **2005,** *88* (1), 91-142.

3. Valeva, A.; Walev, I.; Boukhallouk, F.; Wassenaar, T. M.; Heinz, N.; Hedderich, J.; Lautwein, S.; Möcking, M.; Weis, S.; Zitzer, A., Identification of the membrane penetrating domain of Vibrio cholerae cytolysin as a β-barrel structure. *Mol. Microbiol.* **2005,** *57* (1), 124-131.

4. Olson, R.; Gouaux, E., Vibrio cholerae cytolysin is composed of an alpha-hemolysin-like core. *Protein Sci.* **2003,** *12* (2), 379-83.

5. De, S.; Olson, R., Crystal structure of the *Vibrio cholerae* cytolysin heptamer reveals common features among disparate pore-forming toxins. *Proc. Natl. Acad. Sci. U. S. A.* **2011,** *108* (18), 7385-90.

6. Olson, R.; Gouaux, E., Crystal structure of the *Vibrio cholerae* cytolysin (VCC) pro-toxin and its assembly into a heptameric transmembrane pore. *J. Mol. Biol.* **2005,** *350* (5), 997-1016.

7. Chattopadhyay, K.; Banerjee, K. K., Unfolding of Vibrio cholerae hemolysin induces oligomerization of the toxin monomer. *J. Biol. Chem.* **2003,** *278* (40), 38470-5.

8. Kathuria, R.; Mondal, A. K.; Sharma, R.; Bhattacharyya, S.; Chattopadhyay, K., Revisiting the role of cholesterol in regulating the pore-formation mechanism of *Vibrio cholerae* cytolysin, a membrane-damaging β-barrel pore-forming toxin. *Biochem. J.* **2018,** *475* (19), 3039-3055.

9. Zitzer, A.; Zitzer, O.; Bhakdi, S.; Palmer, M., Oligomerization of *Vibrio cholerae* cytolysin yields a pentameric pore and has a dual specificity for cholesterol and sphingolipids in the target membrane. *J. Biol. Chem.* **1999,** *274* (3), 1375-80.

10. Ikigai, H.; Otsuru, H.; Yamamoto, K.; Shimamura, T., Structural requirements of cholesterol for binding to Vibrio cholerae hemolysin. *Microbiol. Immunol.* **2006,** *50* (10), 751-7.

11. Paul, K.; Chattopadhyay, K., Single point mutation in Vibrio cholerae cytolysin compromises the membrane pore-formation mechanism of the toxin. *FEBS J.* **2012,** *279* (21), 4039-51.

12. Rai, A. K.; Chattopadhyay, K., Trapping of *Vibrio cholerae* cytolysin in the membrane-bound monomeric state blocks membrane insertion and functional pore formation by the toxin. *J. Biol. Chem.* **2014,** *289* (24), 16978-87.

13. Lata, K.; Singh, M.; Chatterjee, S.; Chattopadhyay, K., Membrane Dynamics and Remodelling in Response to the Action of the Membrane-Damaging Pore-Forming Toxins. *J. Membr. Biol.* **2022,** *255* (2-3), 161-173.

14. Gupta, V. K.; Skaife, J. J.; Dubrovsky, T. B.; Abbott, N. L., Optical amplification of ligand-receptor binding using liquid crystals. *Science (New York, N.Y.)* **1998,** *279* (5359), 2077-80.

15. Lowe, A. M.; Abbott, N. L., Liquid Crystalline Materials for Biological Applications. *Chem. Mater.* **2012,** *24* (5), 746-758.

16. Lin, I. H.; Miller, D. S.; Bertics, P. J.; Murphy, C. J.; de Pablo, J. J.; Abbott, N. L., Endotoxin-induced structural transformations in liquid crystalline droplets. *Science (New York, N.Y.)* **2011,** *332* (6035), 1297-300.

17. Park, J. S.; Abbott, N. L., Ordering Transitions in Thermotropic Liquid Crystals Induced by the Interfacial Assembly and Enzymatic Processing of Oligopeptide Amphiphiles. *Adv. Mater.* **2008,** *20* (6), 1185-1190.

18. Tan, L. N.; Orler, V. J.; Abbott, N. L., Ordering transitions triggered by specific binding of vesicles to protein-decorated interfaces of thermotropic liquid crystals. *Langmuir* **2012,** *28* (15), 6364-76.

19. Woltman, S. J.; Jay, G. D.; Crawford, G. P., Liquid-crystal materials find a new order in biomedical applications. *Nat. Mater.* **2007,** *6* (12), 929-38.

20. Brake, J. M.; Abbott, N. L., Coupling of the orientations of thermotropic liquid crystals to protein binding events at lipid-decorated interfaces. *Langmuir* **2007,** *23* (16), 8497-507.

21. Das, D.; Sidiq, S.; Pal, S. K., Design of bio-molecular interfaces using liquid crystals demonstrating endotoxin interactions with bacterial cell wall components. *RSC Adv.* **2015,** *5* (81), 66476-66486.

22. Das, D.; Pal, S. K., Liquid Crystal Unveiled Interactions between Melittin and Phospholipids at Aqueous-Liquid Crystal Interface. *ChemistrySelect* **2017,** *2* (17), 4779-4786.

23. Lockwood, N.; Gupta, J.; Abbott, N., Self-assembly of amphiphiles, polymers and proteins at interfaces between thermotropic liquid crystals and aqueous phases. *Surf. Sci. Rep.* **2008,** *63* (6), 255-293.

24. Carlton, R. J.; Hunter, J. T.; Miller, D. S.; Abbasi, R.; Mushenheim, P. C.; Tan, L. N.; Abbott, N. L., Chemical and biological sensing using liquid crystals. *Liq. Cryst. Rev.* **2013,** *1* (1), 29-51.

25. M'Baye, G.; Mely, Y.; Duportail, G.; Klymchenko, A. S., Liquid ordered and gel phases of lipid bilayers: fluorescent probes reveal close fluidity but different hydration. *Biophys. J.* **2008,** *95* (3), 1217-25.

26. Shrivastava, S.; Cleveland, R. O.; Schneider, M. F., On measuring the acoustic state changes in lipid membranes using fluorescent probes. *Soft Matter* **2018,** *14* (47), 9702-9712.

27. Zhang, Y. L.; Frangos, J. A.; Chachisvilis, M., Laurdan fluorescence senses mechanical strain in the lipid bilayer membrane. *Biochem. Biophys. Res. Commun.* **2006,** *347* (3), 838-41.

28. Sadati, M.; Apik, A. I.; Armas-Perez, J. C.; Martinez-Gonzalez, J.; Hernandez-Ortiz, J. P.; Abbott, N. L.; de Pablo, J. J., Liquid Crystal Enabled Early Stage Detection of Beta Amyloid Formation on Lipid Monolayers. *Adv. Funct. Mater.* **2015,** *25* (38), 6050-6060.

29. Verma, I.; Selvakumar, S. L. V.; Pal, S. K., Surfactin-Laden Aqueous–Liquid Crystal Interface Enabled Identification of Secondary Structure of Proteins. *J. Phys. Chem. C* **2019,** *124* (1), 780-788.

30. Luchini, A.; Delhom, R.; Cristiglio, V.; Knecht, W.; Wacklin-Knecht, H.; Fragneto, G., Effect of ergosterol on the interlamellar spacing of deuterated yeast phospholipid multilayers. *Chem. Phys. Lipids* **2020,** *227*, 104873.

31. Harris, J. R.; Bhakdi, S.; Meissner, U.; Scheffler, D.; Bittman, R.; Li, G.; Zitzer, A.; Palmer, M., Interaction of the *Vibrio cholerae* cytolysin (VCC) with cholesterol, some cholesterol esters, and cholesterol derivatives: a TEM study. *J. Struct. Biol.* **2002,** *139* (2), 122-135.

32. Wang, X.; Yang, P.; Mondiot, F.; Li, Y.; Miller, D. S.; Chen, Z.; Abbott, N. L., Interfacial ordering of thermotropic liquid crystals triggered by the secondary structures of oligopeptides. *Chem. Commun.* **2015,** *51* (94), 16844-7.

33. Groenning, M., Binding mode of Thioflavin T and other molecular probes in the context of amyloid fibrils-current status. *J. Chem. Biol.* **2010,** *3* (1), 1-18.

34. Zhao, D. S.; Chen, Y. X.; Liu, Q.; Zhao, Y. F.; Li, Y. M., Exploring the binding mechanism of thioflavin-T to the β-amyloid peptide by blind docking method. *Sci. China: Chem.* **2012,** *55*, 112-117.

35. Xue, C.; Lin, Y. T.; Chang, D.; Guo, Z., Thioflavin T as an amyloid dye: fibril quantification, optimal concentration and effect on aggregation. *R. Soc. Open Sci.* **2017**, *4, 160696.*

36. Zhang, J.; Li, Q.; Wu, Y.; Wang, D.; Xu, L.; Zhang, Y.; Wang, S.; Wang, T.; Liu, F.; Zaky, M. Y.; Hou, S.; Liu, S.; Zou, K.; Lei, H.; Zou, L.; Zhang, Y.; Liu, H., Cholesterol content in cell membrane maintains surface levels of ErbB2 and confers a therapeutic vulnerability in ErbB2-positive breast cancer. *Cell Commun. Signal* **2019**, *17*, 15.

37. Yang, S. T.; Kreutzberger, A. J. B.; Lee J.; Kiessling V.; Tamm, L. K., The Role of Cholesterol in Membrane Fusion. *Chem. Phys. Lipids* **2016**, *199*, 136–143.

38. Mondal, A. K.; Chattopadhyay, K., Taking Toll on Membranes: Curious Cases of Bacterial beta-Barrel Pore-Forming Toxins. *Biochemistry* **2020,** *59* (2), 163-170.

39. Brake, J. M.; Abbott, N. L., An Experimental System for Imaging the Reversible Adsorption of Amphiphiles at Aqueous-Liquid Crystal Interfaces. *Langmuir* **2002,** *18* (16), 6101-6109.

40. Huang, J.; Buboltz, J. T.; Feigenson, G. W.; Maximum solubility of cholesterol in phosphatidylcholine and phosphatidylethanolamine bilayers. *Biochim. Biophys. Acta - Biomembr.* **1999**, *1417*(1), 89-100.

41. Mondal, A. K.; Verma, P.; Sengupta, N.; Dutta, S.; Bhushan Pandit, S.; Chattopadhyay, K., Tyrosine in the hinge region of the pore-forming motif regulates oligomeric β-barrel pore formation by *Vibrio cholerae* cytolysin. *Mol. Microbiol.* **2021,** *115* (4), 508-525.

42. Sanchez, S. A.; Tricerri, M. A.; Gratton, E., Laurdan generalized polarization fluctuations measures membrane packing micro-heterogeneity in vivo. *Proc. Natl. Acad. Sci. U. S. A.* **2012,** *109* (19), 7314-9.

43. Horcas, I.; Fernandez, R.; Gomez-Rodriguez, J. M.; Colchero, J.; Gomez-Herrero, J.; Baro, A. M., WSXM: a software for scanning probe microscopy and a tool for nanotechnology. *Rev. Sci. Instrum.* **2007,** *78* (1), 013705.

44. Gehlert, S.; Bungartz, G.; Willkomm, L.; Korkmaz, Y.; Pfannkuche, K.; Schiffer, T.; Bloch, W.; Suhr, F., Intense resistance exercise induces early and transient increases in ryanodine receptor 1 phosphorylation in human skeletal muscle. *PLoS One* **2012**, *7*(11), 49326.

45. O'Leary, B. M.; Lee, C. P.; Atkin, O. K.; Cheng, R.; Brown, T. B.; Millar, A. H., Variation in leaf respiration rates at night correlates with carbohydrate and amino acid supply. *Plant physiol.* **2017**, *174*(4), 2261-2273.

Chapter 3

Investigating Mutation and Membrane Guided Action of Listeriolysin O at Aqueous-Liquid Crystal Interface

Listeriolysin O (LLO) is a crucial cholesterol-dependent cytolysin secreted by *Listeria monocytogenes*. LLO lyse the phagosomal membrane via pore-formation, resulting in pathogenesis.[1, 2] Cholesterol-dependent cytolysin's ability to recognize and bind to membrane cholesterol is a hallmark in the pathogenesis of these pore-forming toxins, distinguishing them from other toxins.[3] Conservation of cholesterol-recognition motif (CRM) has been discovered to be one of the prerequisites for the membrane binding of some cholesterol-dependent cytolysins, but the role of CRM for LLO binding and pore-formation is still unclear.[4]

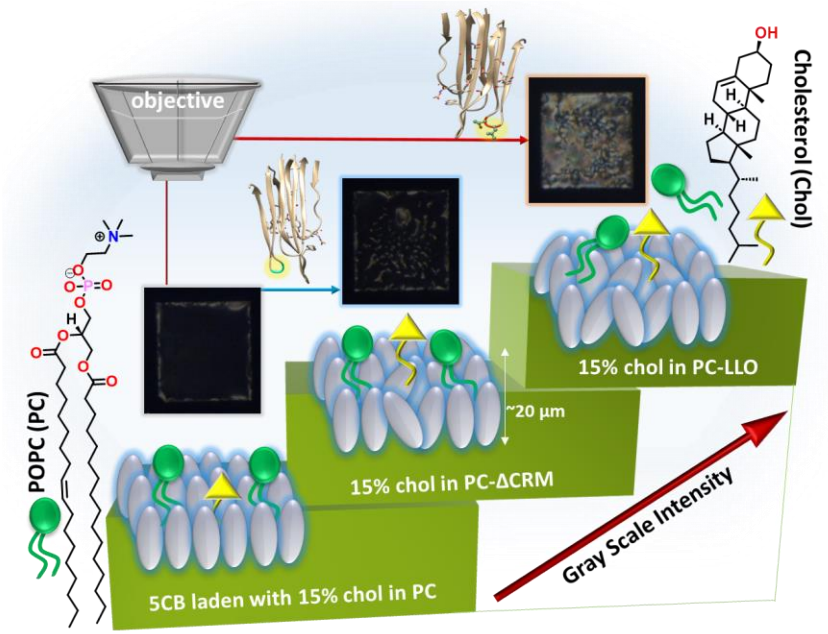

Hereby, we intend to investigate LLO-mediated lipid remodelling at physiological concentration using interfacial properties of biomimetic liquid crystal (LC)-aqueous interface. The examination addresses the significance of CRM in protein structure and membrane organizations for the cholesterol-mediated binding of LLO. We report that CRM assists in binding LLO to a unique amphipathic environment, especially at low cholesterol levels. However, eliminating or substituting CRM from LLO would significantly alter the threshold cholesterol level required for its activity. The study also revealed the effect of cholesterol-dependent membrane dynamics in the association and activity of LLO. Overall, our findings suggest a novel paradigm that opens an array of possibilities for discovering sequential mutations and delineating the molecular mechanisms of cholesterol-dependent cytolysins in nanomolar concentration regimes.

Gupta,T.; Lata, K., Chattopadhyay, K.; Pal, S. K., Investigating mutation and membrane guided action of Listeriolysin O at aqueous-Liquid Crystal Interface (*Manuscript uder revision in J. Mater. Chem. B*)

3.1. Introduction

Cholesterol-dependent cytolysins represent a widely disseminated family of pore-forming toxins (PFTs) employed mostly by Gram-positive bacteria, including *Bacillus*, *Streptococcus*, *Clostridium*, and *Listeria*, which are human pathogens.[1, 2] The cholesterol-dependent cytolysins assist in pathogenesis majorly by disrupting the host epithelial cells lining of the gastrointestinal tract and placenta through pore-formation and modulating the host immune system.[1-4] All cholesterol-dependent cytolysins share a four-domain tertiary structure and exhibit a cholesterol-dependent pore-forming and cytotoxic activity.[3] The presence of cholesterol in the target membrane is a prerequisite for the activity of cholesterol-dependent cytolysins.[1-4] Interestingly, studies have demonstrated that cholesterol is not necessarily required for the binding but for the further steps of pore-formation. For almost thirty years, identifying the cholesterol-dependent cytolysins cholesterol recognition/binding motif (CRM) has posed a challenge.[5-8] Numerous investigations have highlighted how specific regions and residues within domain 4 of the cholesterol-dependent cytolysins structure influence the binding of cholesterol-dependent cytolysins to the membrane.[5-7] A research has made progress in pinpointing the areas within domain 4 that interact with the membrane, focusing particularly on the undecapeptide.[8] Recently, it has been found that the primary interaction of cholesterol-dependent cytolysins with cholesterol has been mapped to a pair of threonine and leucine (Thr-Leu) in the loop (L1) of domain 4, designated as cholesterol recognition/binding motif (CRM).[9-12] The investigation (in reference 9) has shown that mutation of this Thr-Leu residue pair blocks cholesterol-dependent cytolysin-cholesterol interactions.[9] These investigations have characterized cholesterol-recognition motif (CRM) for a few cholesterol-dependent cytolysins like perfringolysin O (PFO), pneumolysin (PLY), and intermedilysin (ILY).[9] In the present study, we have explored the cholesterol-dependent interaction of a prominent member of the family, Listeriolysin O (LLO).

LLO is the major virulence factor secreted by the *L. monocytogenes*, a food-borne intracellular pathogen. One notable distinction of LLO among other cholesterol-dependent cytolysins is its crucial role in aiding pathogens in their intracellular journey and to remain within the host cells.[9, 13-15] The high immunogenicity of LLO gives it exceptional medicinal importance, highlighting the significance of its research. Yet, the structural motif and role of cholesterol in mediating the highly specific interaction of LLO are still elusive.[16] However, it

has been understood that it binds to the cholesterol-containing phagosomal membrane, which aids the pathogen's egress from the phagosome to the cytosol through transmembrane β-barrel pores of size up to 50 nm.[16] Certainly, the cholesterol-recognition motif in LLO conducts the binding of these cholesterol-dependent cytolysins to lipid membranes with cholesterol, but it is still unclear if the lipid serves to help in the binding of the protein or not.[16] We propose that some concurrent alterations in membrane dynamics, such as lipid mixing, lipid flipping, or lipid domain reorganizations, may be beneficial in regulating this pore-formation mechanism and need to be acknowledged. Unambiguously, cholesterol is indispensable for the activity of LLO, but the molecular implication of cholesterol in the mechanism of pore-formation is obscure.[16] Past studies have identified liquid crystals (LC) as stimulus-responsive materials due to the combination of fluidity and orientational order that enable dynamic self-organization.[17-25] The interfaces generated between thermotropic LCs and aqueous phases are especially interesting for reporting interactions involving biological organisms because of three major reasons: (i) to observe biomolecular binding events without any fluorescent labelling, (ii) interfaces are dynamic and species can be reorganized laterally in ways that resemble biomolecular interactions at biological membranes, (iii) the experimental setup is straightforward, it may apply to the creation of diagnostics for usage in resource-constrained settings. Hence, LCs-based transduction has been widely exploited to amplify the presence of a range of chemical and biological species (lipids, proteins, DNA, and mammalian and bacterial cells) at interfaces into optical signals.[18-36] Inspired by this, our previous research sought to establish that LC-aqueous interfaces have the potential to replicate the cholesterol-mediated membrane interactions of *Vibrio cholerae* cytolysin (VCC) at physiological concentrations.[37] Advancing our study herein, we ask if a biomimetic LC-aqueous interface could capture the LLO-mediated modulations to the unique amphipathic environment. In addition, the present study focuses on understanding the LLO-cholesterol interaction mediated by the cholesterol-recognition motif (CRM), which aids the membrane binding and activity. The CRM motif in LLO was substituted with a pair of glycine to generate the ΔCRM form of LLO and analyse the cholesterol-dependent membrane interactions and modulations by LLO.

We report that the mutation of the CRM region significantly affected the ability of LLO to interact with cholesterol. However, the binding ability was reduced only when there was a low amount of cholesterol in the membranes, suggesting the effect of cholesterol and

membrane dynamics on the activity of LLO. Also, cholesterol can be the key player in modulating the phase heterogeneity, packing, and hydrophobicity of lipids in the membranes.[38] The study scrutinized the potential of the LC interface to recognize the consecutive tempering of two amino acids based solely on LC optical responses under physiological environments. As a result, the LC-based method might be endorsed as the easiest assay to examine the structural basis and cholesterol-dependent pathogenicity of proteins produced by bacteria.

Overall, our research aims to comprehend the lipid-protein interactions occurring at the aqueous interface of LC at the nanoscale, which cannot be accessed by conventional measurement tools. However, there is still scope for further research on the interaction between membrane dynamics and LLO activity.

3.1.1. Objectives

Liquid crystal (LC)-aqueous interfaces represent a powerful tool for enhancing the exploration of diverse biomolecular interactions.[17-25] Considering this, the current investigation endeavours to present a straightforward yet robust design based on the utilization of differential lipid mixtures within a liquid crystal (LC)-aqueous interface. This design aims to mimic a biomimetic system, offering insights into the cholesterol-dependent interfacial actions and membrane-mediated binding mechanisms of Listeriolysin O (LLO). LLO is a prominent member of the cholesterol-dependent cytolysin family, instrumental in pathogen egress through the formation of pores in the phagosomal membrane, a process crucial to pathogenesis.[1-4] The distinctive ability of these pore-forming cholesterol-dependent cytolysins to recognize and bind to cholesterol sets them apart from other toxins. LLO, specifically, distinguishes itself by facilitating the intracellular survival of *Listeria monocytogenes* within host cells, rendering it a captivating target for their intracellular journey.[9] While the conservation of the cholesterol recognition motif (CRM) has been implicated in the activity of some cholesterol-dependent cytolysins, its role in LLO binding and pore formation remains obscure.[9, 16]

Consequently, this study aims to investigate the influence of LLO on lipid reorganization at physiological concentrations using the interfacial properties of a biomimetic liquid crystal (LC)-aqueous interface. The investigation also delves into the significance of CRM in protein

structure and its influence on membrane characteristics in the context of cholesterol-mediated LLO binding. Moreover, this research underscores the efficacy of LC-based methodology as an efficient strategy for gaining mechanistic insights at physiological concentrations, contributing to our understanding of the genesis and progression of cholesterol-dependent cytolysin-related diseases.

3.2. Result and Discussion

For *in vitro* insights into LLO actions towards the membrane, we first mimic an amphipathic membrane environment by self-assembling 1-palmitoyl-2-oleoyl-*sn*-glycero-3-phosphocholine (PC) at a thermotropic liquid crystal (LC) 5CB (4'-pentyl-4-biphenylcarbonitrile)-aqueous interface. For our initial set of experiments, we began by encapsulating 5CB using a TEM-gold grid supported on a glass substrate coated with Dimethyloctadecyl [3-(trimethoxysilyl) propyl] ammonium chloride (DMOAP) under phosphate-buffered saline (PBS).

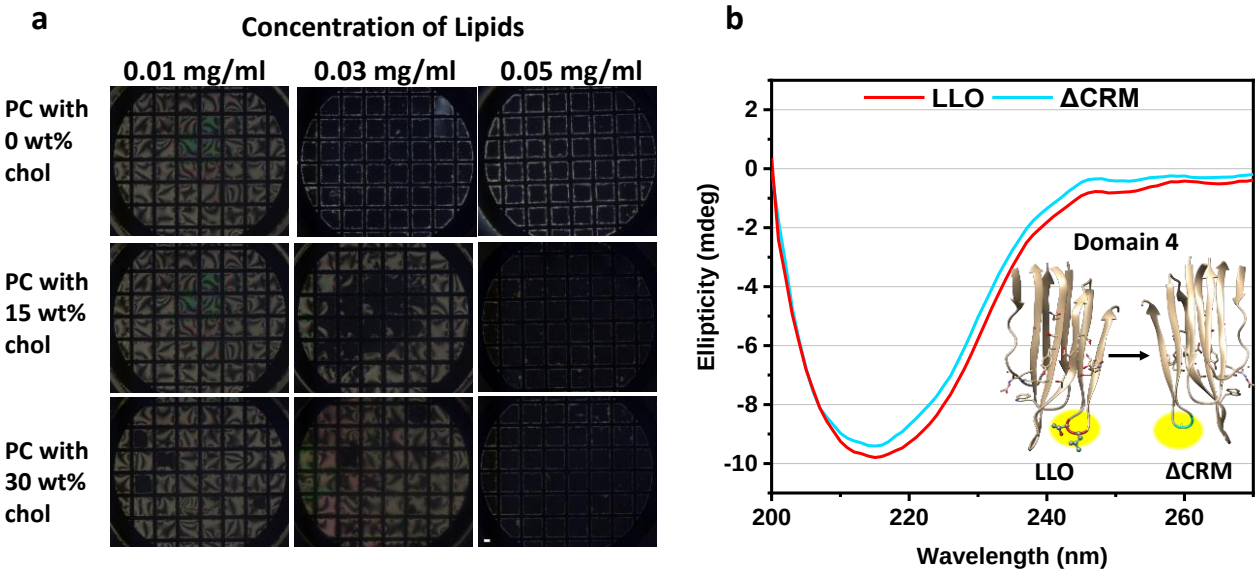

Figure 3.2.1 Polarized optical photomicrographs of LC-aqueous interface in (a) depicts LC response after 30 min incubation with 0, 15, and 30 wt% cholesterol in PC. The optical views displayed a uniformly dark appearance of LC at 0.03 mg/ml PC and 0.05 mg/ml lipid mixture (PC having 15 or 30 wt% cholesterol). Scale bar = 100 μm. The data is consistent with the findings of the previous study (chapter 2) and has been reperformed for further investigation.[37] The CD spectra in (b) illustrate the β-sheet rich nature of both LLO and its

mutant ΔCRM. The structure of domain 4 of LLO and ΔCRM is shown in the inset of (b) (PDB ID 4CDB, image generated in Chimera).

We observed that the thin films of 5CB exhibited a bright optical appearance under the PBS due to their ordering transitions, which is concordant with previous reports.[26, 27, 37] Subsequently, we sought to investigate the orientational behaviour of 5CB in various concentrations of PC. We observed that on the introduction of 0.01 mg/ml of PC, the appearance of 5CB remained unchanged for a period of 30 min (Figure 3.2.1a, first row). However, upon increasing the PC concentration to 0.03 mg/ml, we observed a completely dark appearance under a polarizing optical microscope (POM), as depicted in Figure 3.2.1a. As expected, the dark optical view remained intact with the further increase in PC concentration to 0.05 mg/ml. This dark appearance is a consequence of the homeotropic alignment of the 5CB and can be attributed to the anchoring of 5CB through hydrophobic interactions with the chains of biological lipids, which is consistent with earlier reports.[26-29] Our second goal was to gain insights into the interactions between LLO and the distinctive membrane environments formed by lipid mixtures of cholesterol and PC. For this, we conducted a second set of experiments to analyse the ordering pattern of 5CB in the presence of PC vesicles containing 15 and 30 weight % cholesterol. The rationale behind this objective was rooted in the observation that cholesterol plays a vital role in enabling LLO to form pores in target membranes.[1-4] We first did experiments with 0.01 and 0.03 mg/ml of lipid mixtures (15 or 30 wt% cholesterol into PC vesicles). Interestingly, we observed that the added lipid mixture did not result in a completely dark optical appearance of LC within 30 min (Figure 3.2.1a, second and third row). However, when the concentration of the lipid mixture was increased to 0.05 mg/ml, a completely dark optical appearance of the LC was observed. The variation in the ordering pattern of 5CB depending on the wt% of cholesterol in PC is consistent with our previous findings that suggest that the rigidity imposed by cholesterol and the reduction in PC density within the vesicles are likely contributing factors to this phenomenon.[37] Next, we sought to observe the role of CRM in LLO for its activity towards lipid membranes having 15 and 30 wt% cholesterol. To monitor this, we have designed an LLO mutant by substituting two amino residues, i.e., Thr-Leu, in LLO with a pair of glycine (Gly-Gly). The mutant is designated as ΔCRM.

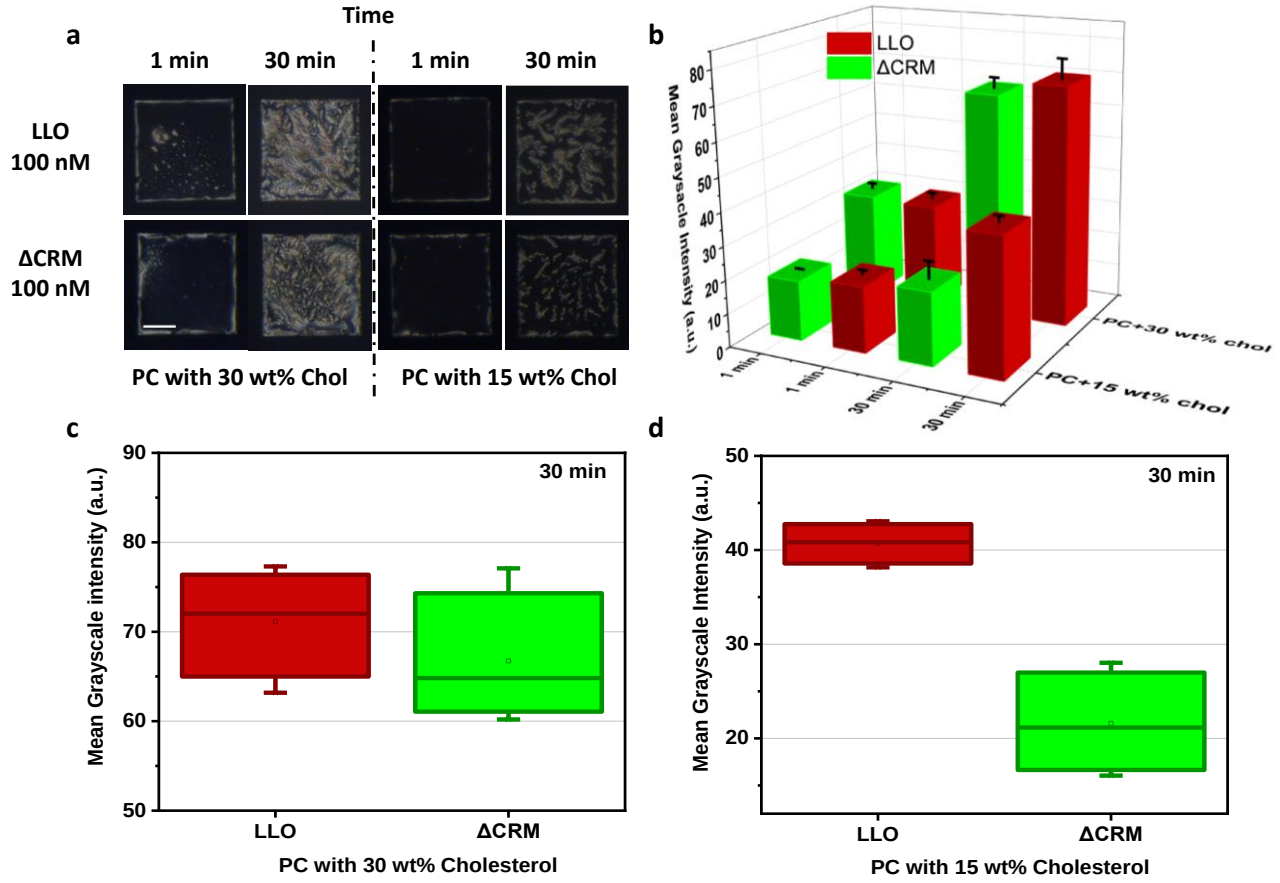

Figure 3.2.2. Polarized photomicrographs in (a) depict differential densities of optical domains at 1- and 30-min incubation of 100 nM LLO and its mutant ΔCRM with 30 and 15 wt% cholesterol in PC-laden at LC-aqueous interface. Scale bar = 100 μm. The bar graph (b) illustrates average mean grayscale intensities (four grid squares) at 1- and 30-min incubation of LLO and ΔCRM at the designed interfaces. The box plot in (c & d) illustrates the distribution of mean grayscale intensities for LLO and its mutant after 30 min incubation with PC containing 30 wt% and 15 wt% cholesterol, respectively, present at the LC-aqueous interface. (c) No significant differences (p =0.4>0.05; Anova) were observed in LLO and ΔCRM interactions with PC/30 wt% cholesterol after 30 min of incubation. (d) A significant difference (p=5×10^{-4}< 0.05; Anova) were observed in LLO and ΔCRM interactions with PC/15 wt% cholesterol after 30 min of incubation.

Before analysing their behaviour at the LC-aqueous interface in the presence of lipid mixtures, we first investigated the structures of both proteins by recording far-UV Circular Dichroism (CD) spectra. The spectra in Figure 3.2.1b illustrate the β-sheet rich nature of LLO, which is preserved after substituting glycine. Additionally, almost identical ellipticities of both proteins showed similar structural disposition of LLO and its mutant. Based on the above information, we sought to monitor the activity of LLO and its mutant ΔCRM at an LC-

aqueous interface laden with lipid mixtures. Subsequently, we incubated 100 nM of LLO and ΔCRM at lipid mixture (PC containing 15 wt% and 30 wt% cholesterol) decorated LC-aqueous interface. We made three observations based on the optical images presented in Figure 3.2.2a, captured at 1 and 30 min upon the addition of 100 nM proteins at those interfaces. First, we observed the emergence of bright optical domains shortly after 1 min of addition of LLO and ΔCRM to the lipid mixture decorated interface. Interestingly, this emergence of bright domains was more pronounced in the lipid mixture (30 wt% cholesterol in PC) than in the mixture with 15 wt% cholesterol in PC. Second, we observed the transformation of initially uniformly dark areas into completely bright appearances after 30 min of the addition of proteins to the 30 wt% cholesterol/PC lipid mixture laden at the LC-aqueous interface. This change indicated a significant alteration in the optical properties of the LC over time. The third observation revealed that dendritic domains were more pronounced when LLO was added to the lipid mixture containing 15wt% cholesterol in PC, as compared to its mutant variant ΔCRM, at the LC-aqueous interface. This suggests that LLO has a stronger influence on the formation and growth of dendritic structures in this particular lipid composition.

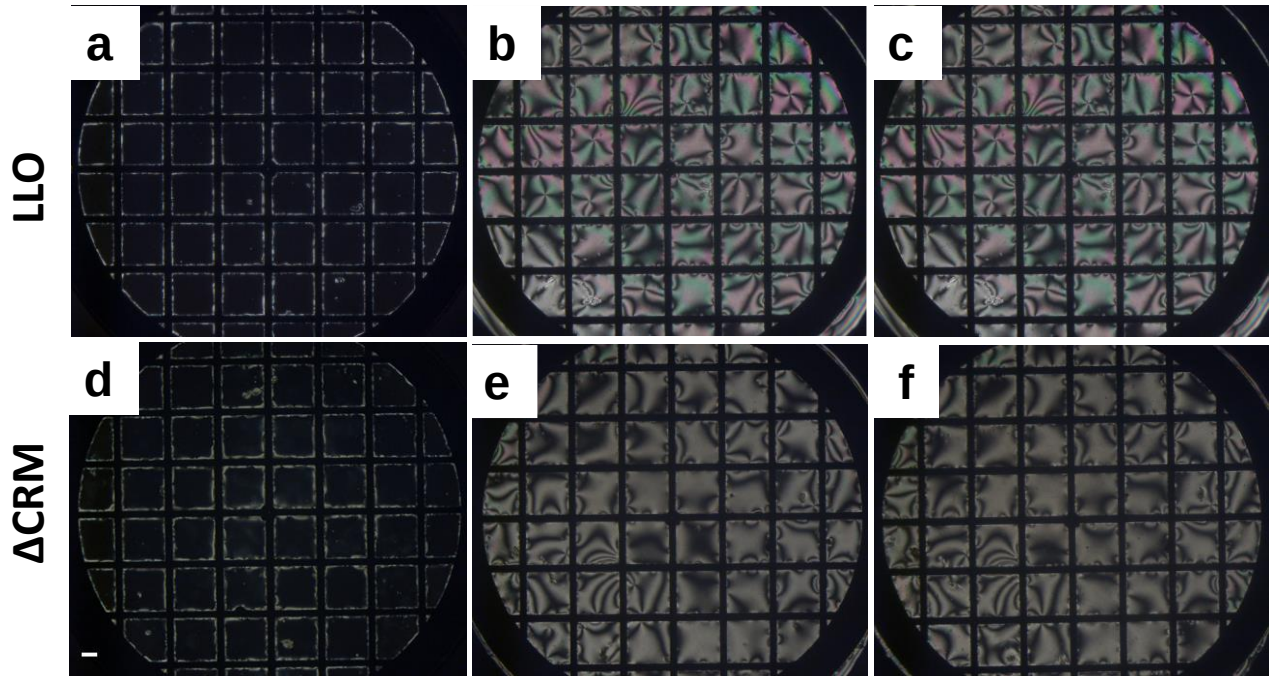

Figure 3.2.3 Optical images in (a, d) depict the LC-air interface under crossed polarizers POM. Photomicrographs in (b, e) displayed the same LC-film view under POM on immersion

in PBS buffer containing 200 nM LLO and ΔCRM. The consistency of view in images (c, f) captured after 2 h demonstrates no direct interactions of the protein with LC. Scale bar = 100 μm.

To further provide insights into the variations in the extent of the formation of optical domains, we conducted quantitative measurements. We calculated the mean grayscale intensities of the LC interface laden with different lipid mixtures (PC/30 & 15 wt% cholesterol) in the presence of LLO and ΔCRM (Fig. 3.2.2b). The box graphs displayed a significant difference in the mean grayscale intensities of 15 wt% cholesterol in PC (Fig. 3.2.2d) than 30 wt% in the PC (Fig. 3.2.2c) laden LC-aqueous interface in the presence of LLO and ΔCRM. This observation indicates the prominent binding of LLO with 15 wt% cholesterol in PC than ΔCRM.

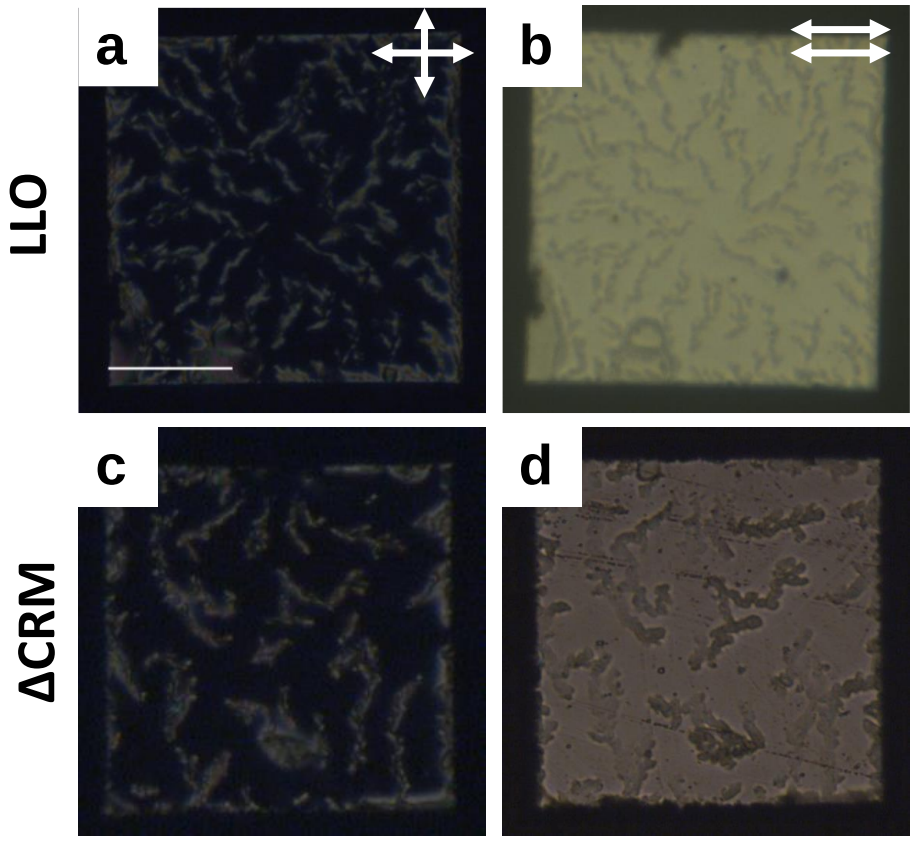

Figure 3.2.4 Polarized optical images in (a, c) depict respective LC's response of 100 nM LLO and ΔCRM upon incubation with 15 wt% cholesterol in a PC-laden aqueous interface of LC. Optical images (b, d) corresponding to (a, c) displayed similar dendritic patterns after

the removal of the analyser. The arrows on the top left of images (a) and (b) show the orientations of the polarizer and analyser during imaging. Scale bar = 100 μm.

In order to verify that the emerged dendritic domains are the result of LLO and ΔCRM-lipid interactions at the aqueous interfaces of LC, we performed two additional control experiments. First, we incubated 200 nM LLO and ΔCRM at the LC-aqueous interface without any lipid. Notably, no change in the optical appearance was observed over a prolonged time, and it did not form any branched domains (Figure 3.2.3). Second, we incubated 100 nM of LLO at the lipid mixture (15 wt% cholesterol in PC)-laden LC-aqueous interface. We observed the formation of the bright dendritic domains under POM, which were also visible after the removal of analysers, indicating modulations in lipid density due to protein interactions at those interfaces (Figure 3.2.4). These data sets confirmed the evolution of brush-like patterns is the result of the transduction of lipid-protein interactions to the LC.

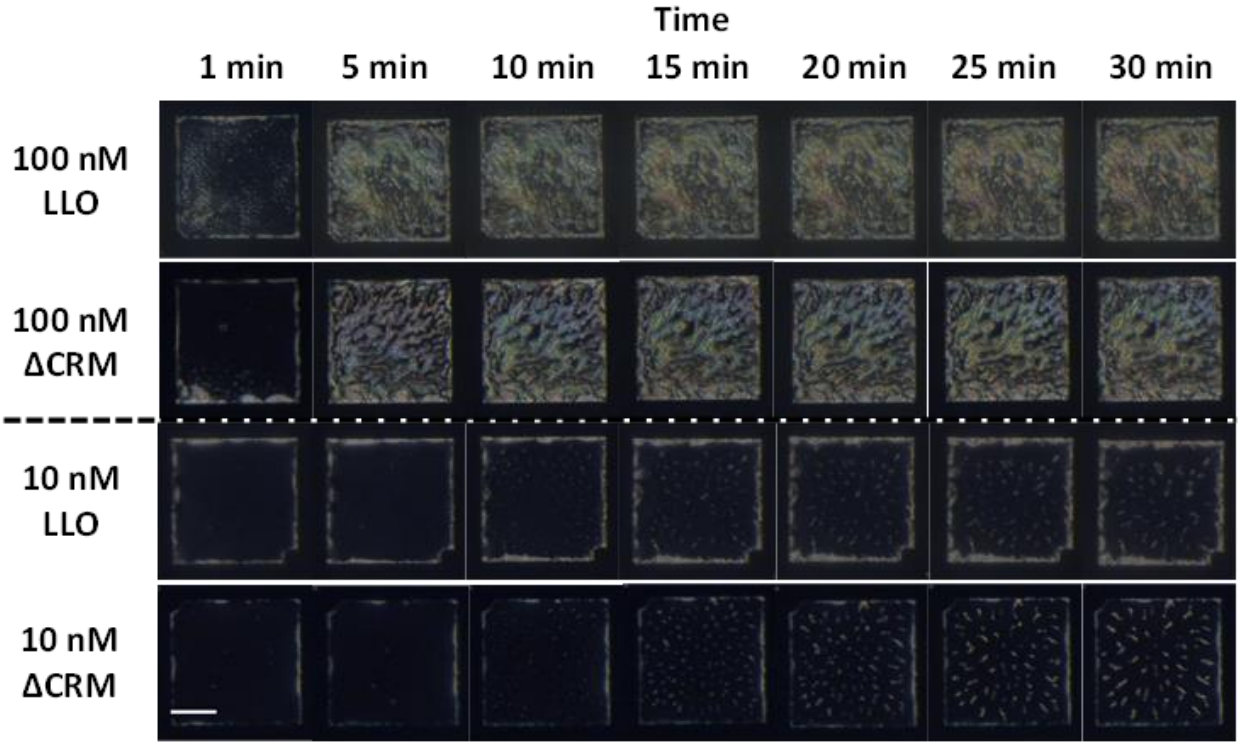

Figure 3.2.5 Time-lapsed images of LC response in the presence of 100 and 10 nM proteins added on interfaces laden with 30 wt% cholesterol. The images depict the similar activity of both proteins, indicating no difference in the binding of proteins even in the presence of CRM. Scale bar = 100 μm.

Our next goal was to gain insight into the progression of events over time and to understand the initial rate of interactions of proteins with different cholesterol concentrations. In this regard, we investigated the time-lapsed behaviour of both LLO and its mutant variant ΔCRM in the presence of lipid mixtures containing 30 wt% and 15 wt% cholesterol in PC at the LC-aqueous interface. First, we monitored the LC response laden with PC having a 30 wt% cholesterol when placed in contact with LLO and ΔCRM. Figure 3.2.5 revealed an almost similar rate of LLO and ΔCRM activity with 30% cholesterol in PC at higher (100 nM) as well as at lower concentrations (10 nM). The outcome suggests that the ability of LLO to bind to a mixture of 30 wt% cholesterol and PC lipids is uncurbed by the existence of CRM in the protein.

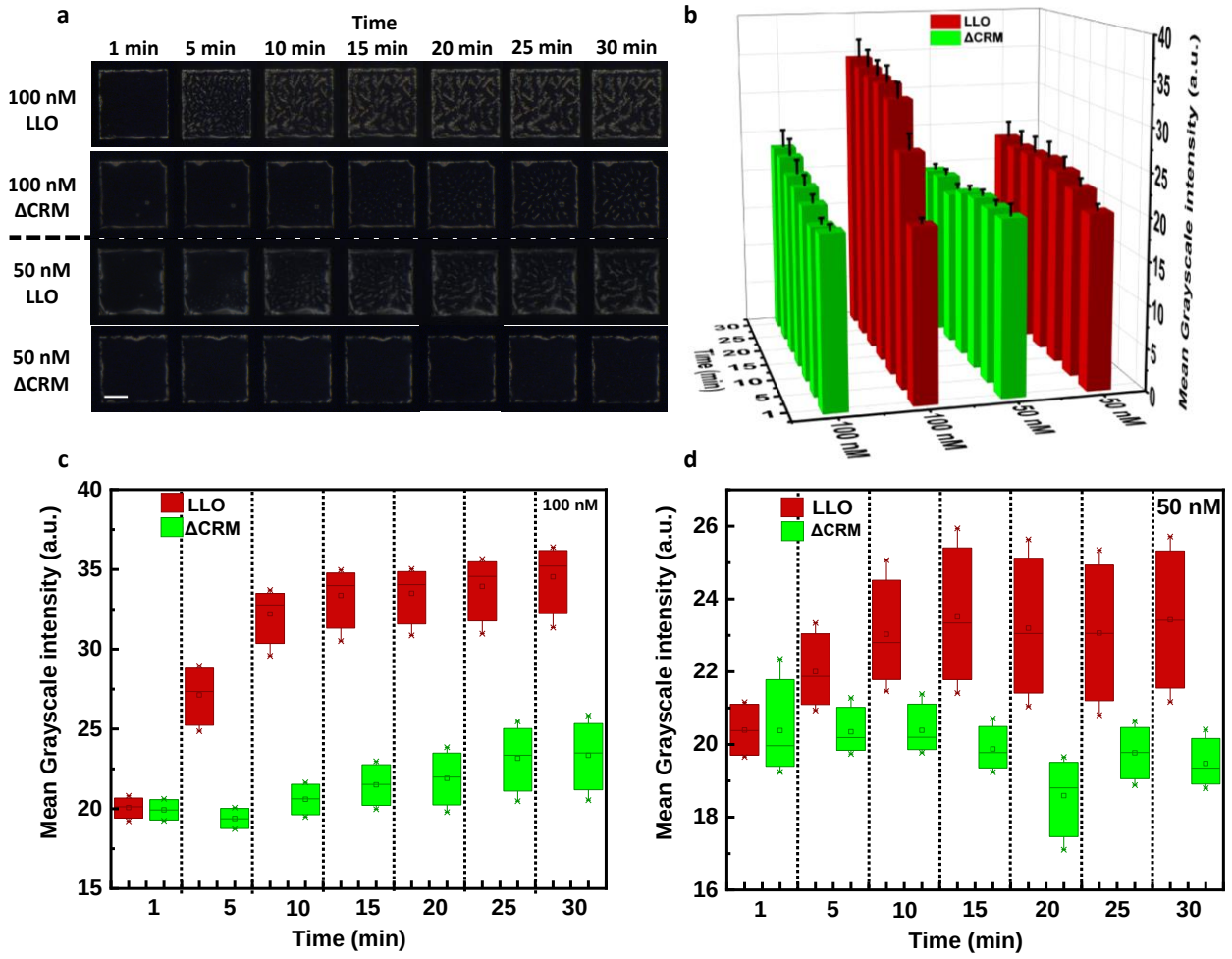

Figure 3.2.6 The optical images in (a) illustrate the time-dependent LC response encased with 15 wt% cholesterol in PC upon contact with 100 and 50 nM proteins (LLO and ΔCRM). The images indicate substantial differences in the activity of both proteins through differential emerging rates of domains. Scale bar = 100 µm. The bar graph in (b) showed the mean

grayscale intensities of PC/15 wt% cholesterol-laden LC-aqueous interfaces at different time points in the presence of LLO and ΔCRM. The box plot in (c & d) illustrates the distribution of mean grayscale intensities of PC/15 wt% cholesterol-laden LC-aqueous interface from 1 to 30 min in the presence of (c) 100 nM & (d) 50 nM of LLO and its mutant. One-way ANOVA was used to measure the level of statistical significance. c) p = 0.8>0.05(1 min), p = 2×10^{-4} (5 min), p = 2×10^{-5} (10 min), p = 5×10^{-5} (15 min), p=8×10^{-5} (20 min), p = 3×10^{-4} (25 min) and p=3×10^{-4} (30 min). d) p = 0.9 (1 min), p = 3×10^{-2} (5 min), p = 1×10^{-2} (10 min), p = 1×10^{-2} (15 min), p=5×10^{-3} (20 min), p = 1×10^{-2} (25 min) and p=8×10^{-3} (30 min).

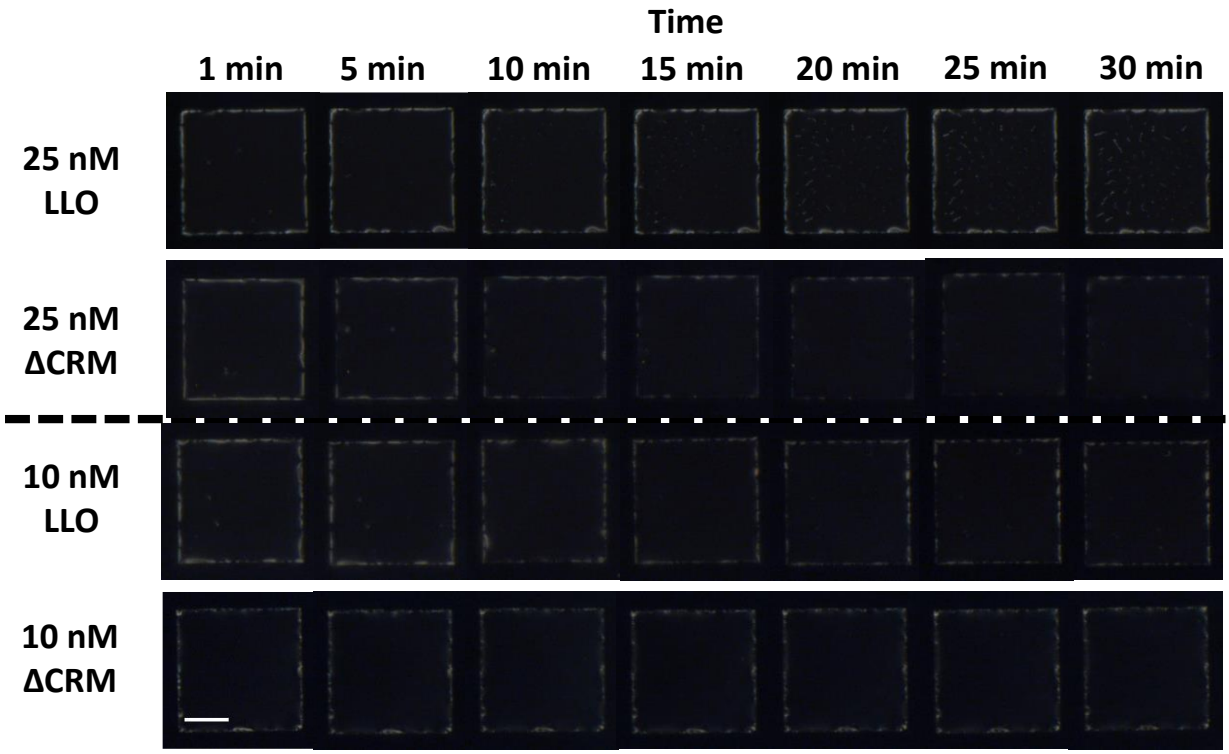

Figure 3.2.7 Time-lapsed polarized optical images of LC response in contact with 25 and 10 nM proteins at 15 wt% cholesterol in PC lipid-laden LC-aqueous interface. The data demonstrates 25 nM as the minimum concentration of LLO required to study LC responses in 15 wt% cholesterol/PC-laden LC. Scale bar = 100 μm.

Then, we analysed the activity of proteins with a lipid mixture of 15 wt% cholesterol in PC. The time-lapsed images of 100 and 50 nM LLO and ΔCRM displayed considerable differences in the activity of the proteins. The emergence of dendritic domains was found to

be much faster for LLO than ΔCRM (Figure 3.2.6a). Further, the quantification of interactions through the mean grayscale intensities difference supports our preposition of LLO pronounced binding with PC having 15 wt% cholesterol compared to its mutant ΔCRM (Fig. 3.2.6b-d). This observation also holds at lower concentrations of proteins, i.e., at 25 nM (Figure 3.2.7). However, after further decreasing the concentration to 10 nM, no changes in LC ordering were observed, suggesting that the sensitivity of the designed system was up to 25 nM (Figure 3.2.7).

Subsequently, we sought to determine the relationship between the spatial patterns of LC and the lateral distribution of lipids and proteins at those interfaces. To comprehend this, we performed confocal fluorescence microscopy to enquire about the localization of lipids and proteins at the aqueous-LC interface. The 15 wt% cholesterol in PC doped with 2.5% fluorescently labelled PC (Cy5 PC) was self-assembled at LC-aqueous interface and incubated with Alexa 488-labelled LLO and ΔCRM up to 30 min. As in our observation above, we noticed the growth of dendritic patterns visible under the bright field of the confocal microscope (Figure 3.2.8a, d). In addition, the fluorescence images illustrated green-fluorescent protein accumulated in the form of dendritic patterns (Figure 3.2.8b, e) and surrounding them is red in fluorescence (Figure 3.2.8c, f). This suggests the lateral distribution of protein- and lipid-rich regions, where dendritic patterns are protein-rich. Thus, our data indicate the phase segregations of lipids and proteins at the designed interfaces. Overall, the key findings from our observations are: (i) β-sheet rich nature of LLO and ΔCRM, as observed from emerging dendritic patterns[39-43] for both the proteins at the interface, which is also evident from CD spectra; (ii) CRM substitution lowers the activity of LLO at lower cholesterol content in the membrane. This indicates that Thr-Leu dipeptide binds cholesterol more strongly than a pair of Gly-Gly amino acids.

Next, to comprehensively examine and assess the energy interactions at the molecular level, we conducted atomistic computational calculations using density functional theory (DFT) in the gas phase. This approach allows us to delve into the intricate details of molecular systems and analyse the interplay of energies involved in their interactions. By employing DFT, we aim to investigate molecular properties and gain insights into the underlying energetic contributions within the system. The graph in Figure 3.2.9a illustrates interaction energy variations as a function of the distance between modelled dipeptide (similar configuration to that of protein) and cholesterol. The plotted graph was found to be like a simple potential

energy curve. The key observations drawn from the graph were: (i) deep potential well in Thr-Leu with cholesterol compared to a pair of Gly with cholesterol; (ii) the lowering energy at much longer distances in case of cholesterol approaching Thr-Leu than Gly-Gly. The depth of the well accounts for the minimum binding energy (E_o) required to separate two atoms from their equilibrium spacing to an infinite distance apart.[44] Furthermore, the lowering of interaction energy demonstrates the appearance of attractive forces between the molecules. Although, the study undertaken herein has provided a comprehensive analysis of energy interactions occurring at the molecular level, particularly within the gaseous phase. The inclusion of solvent molecules in computational studies enhances both the relevance and accuracy of analyses. However, this approach presents many challenges, primarily associated with increased computational expenses and time requirements. Incorporating solvent molecules increases the complexity of simulations, necessitating enhanced computational resources such as high-performance computing clusters, expanded memory capacities, and heightened processing power, consequently leading to prolonged simulation durations.[45-47] Nonetheless, we acknowledge the potential for future research to explore more sophisticated modelling techniques to reflect the intricacies of fully hydrated systems accurately.

Taken together, our data suggest that the attractive forces come into the picture at much higher distances and are quite large for Thr-Leu complexation with cholesterol, contrary to the Gly-Gly/cholesterol complex. Moreover, the shallow potential well in Gly-Gly with cholesterol indicates lower dissociation energy. Hence, these observations emphasize more interactions and larger stability of the Thr-Leu complex with cholesterol, contrary to the Gly-Gly/cholesterol complex. Additionally, if the protein approach to cholesterol, the CRM motif helps attain more stable bindings even at longer distances. However, in the real system, the protein may rearrange to decrease the bond length further and thus increase the interactions.

We also analysed the electrostatic potential (ESP) map assigned electron density of minimum energy complexes for better understanding. A large electrostatic potential exists on the stabilized Gly-Gly-cholesterol complex than the Thr-Leu-cholesterol complex (Figure 3.2.9b). This revealed greater charge separation in the Gly-Gly-cholesterol complex, demonstrating high reactivity and, in another sense, less complex stability. Thus, the results and experimental findings strongly suggest the superior binding of Thr-Leu with cholesterol compared to Gly-Gly.

Next, we aimed to investigate the factors contributing to both the similar and differential responses of LLO and ΔCRM proteins under high and low cholesterol content conditions. The experiment aimed to address two primary goals. First, we sought to investigate whether the observed results of the superior binding of LLO with cholesterol in comparison to its mutant were solely due to unique interactions between cholesterol and proteins. Second, to find whether these results were a consequence of cholesterol-induced impacts on the lipid assemblies at the interface.

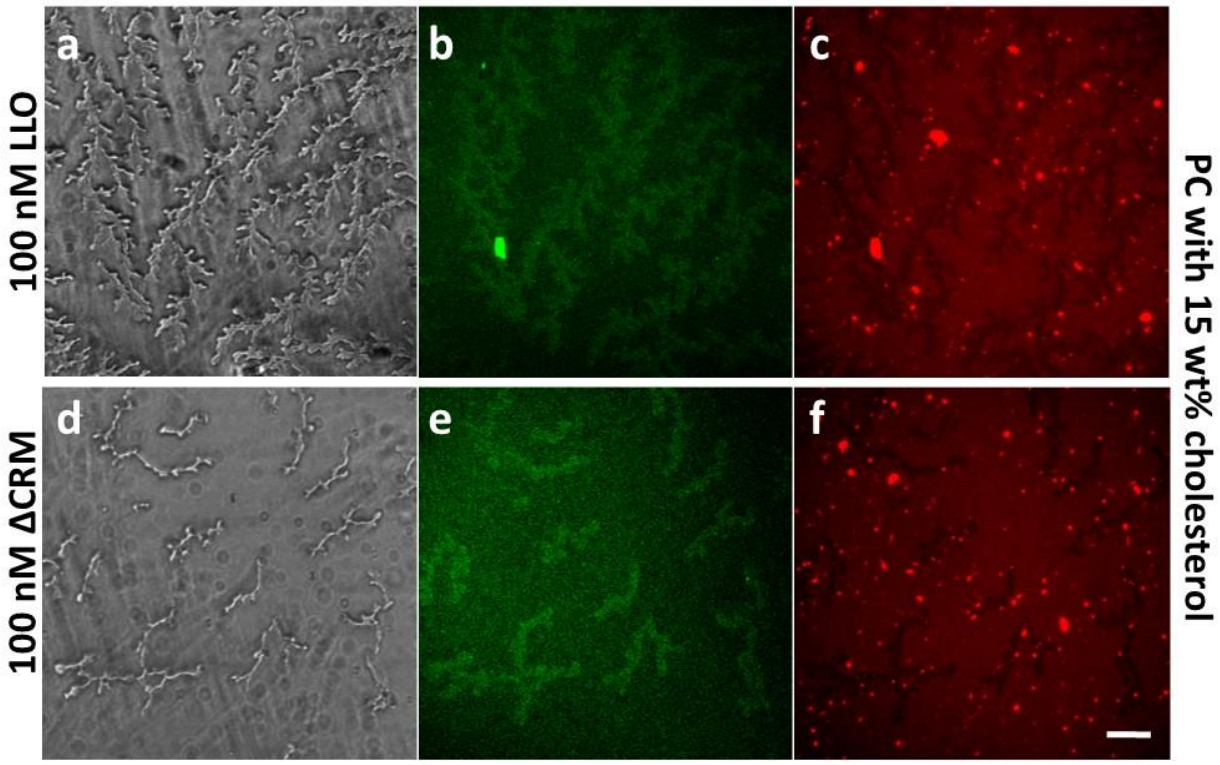

Figure 3.2.8 (a, d) Bright-field and (b, c, e, f) confocal fluorescence images of Alexa-488-labelled LLO and ΔCRM after 30 min incubation with 2.5% cy5 labelled PC dopped in PC having 15 wt% cholesterol lipid mixture decorated LC-aqueous interface. Green fluorescent in (b, e) and dark branched domains in (c, f) depict protein-rich domains, and surrounding them is a lipid-rich region. Scale bar = 20 µm.

To address these questions, we performed a control experiment wherein 100 nM proteins were added to the LC-laden with a lipid mixture of 15 wt% ergosterol in PC. We then observed the system for a duration of up to 30 min following the addition of 100 nM LLO and ΔCRM proteins. This control experiment allowed us to assess the role of ergosterol in influencing the observed results and to gain insights into the specific effects of cholesterol on

the lipid assemblies at the interface. The optical images in Figure 3.2.10 illustrate a similar response of both proteins at the lipid-mixture (PC/15 wt% ergosterol)-laden LC-aqueous interface. This observation suggests the implication of CRM in the specific recognition of cholesterol. Based on our findings, we can make two fundamental statements about the bindings of both proteins. First, at low cholesterol concentrations, LCs laden with lipid mixture exhibit a distinctive response when exposed to both LLO and ΔCRM, which differs from their response at higher cholesterol concentrations. Second, substituting the lower amount of cholesterol with ergosterol leads to the elimination of the disparity in the activity of both proteins.

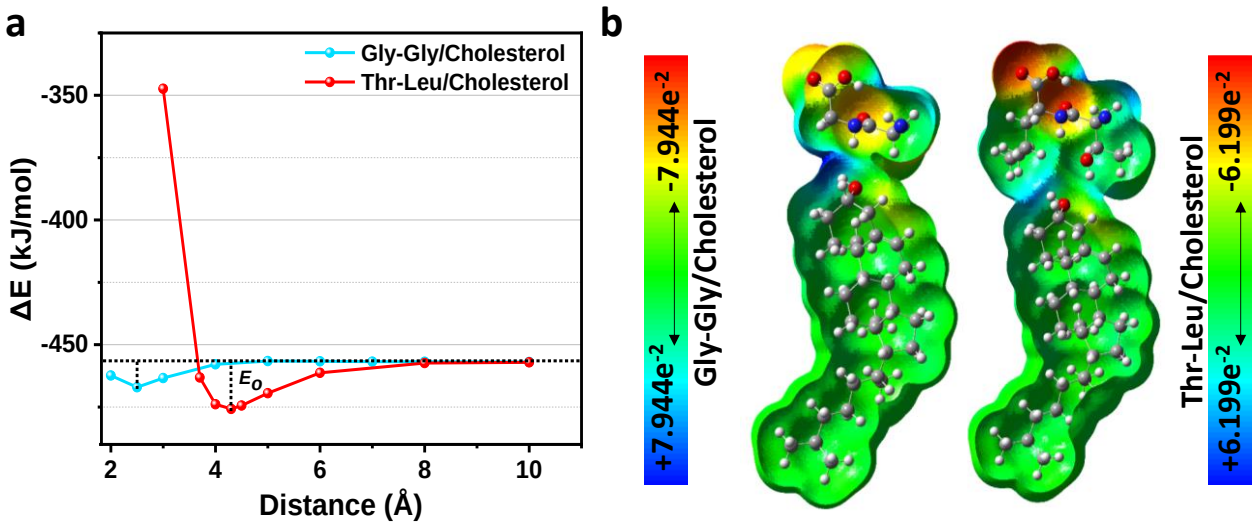

Figure 3.2.9 The graph in (a) displayed the total interaction energies (kJ/mol) of dipeptides (two amino acids) with cholesterol as a function of distance determined by B3LYP/6-311G (d, p) calculations. (b) Mapping molecular electrostatic potential surface assigned to the electron density from total SCF B3LYP density (isoval = 0.0004; mapped with ESP). The data set collectively demonstrates the more stable interactions of Thr-Leu with cholesterol in comparison to a pair of Gly with cholesterol.

These observations suggest that when cholesterol is abundant, LLO can be associated with lipids even without CRM-mediated cholesterol interaction. However, CRM-mediated cholesterol interactions are necessary to associate LLO in the presence of a nominal amount of cholesterol. This could be explained by the fact that some additional parameters may support the binding of LLO in the absence of CRM, with the lipid membranes having a high concentration of cholesterol. It has already been established that a high amount of cholesterol

would increase the hydrophobicity, ordered-ness, and heterogeneity in the membrane, leading to distinct dynamics of the lipid layer.[37] These changes in the lipid environment may intensify non-covalent hydrophobic interactions of proteins with the lipid membranes and their partitioning into distinct lipid phases of the membranes, which can account for the similar responses of LLO with and without CRM. However, at low concentrations of cholesterol, not much impact is known on lipid organizations. Therefore, CRM importance increases for the activity of LLO. This proposition is also supported by a control experiment with 15 wt% ergosterol. At 15wt% ergosterol PC mixture, the similar response of LC in the presence of proteins indicates the importance and specificity of cholesterol in the binding of LLO with the lipid membranes.

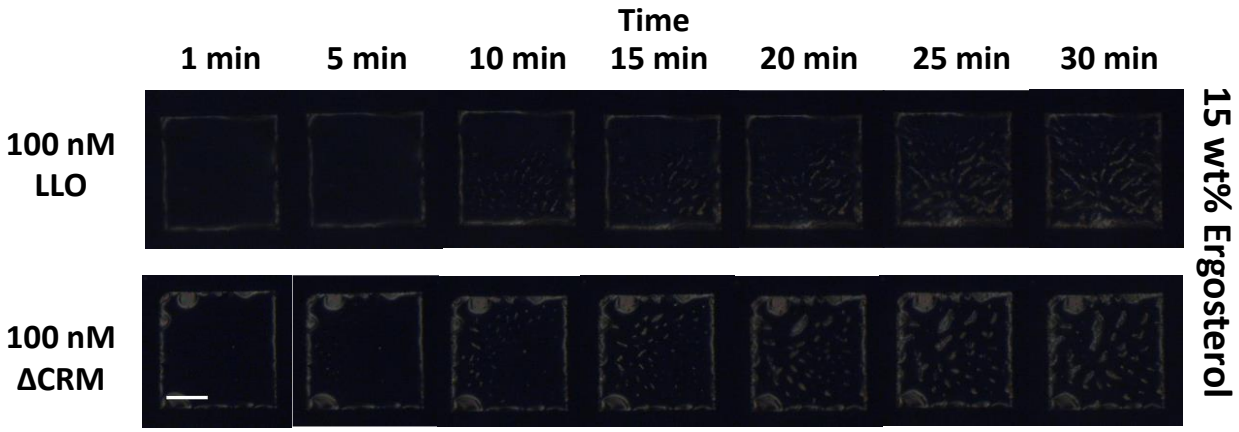

Figure 3.2.10 Time-lapsed polarized optical images of LC response in contact with 100 nM proteins at 15 wt% ergosterol in PC lipid-laden LC-aqueous interface. The data demonstrates the negligible difference in LC responses upon incubation of 100 nM LLO and ΔCRM with 15 wt% ergosterol/PC-laden LC. Scale bar = 100 μm.

Overall, our findings indicate the interplay of lipid membrane dynamism and cholesterol dependency in the binding of LLO. CRM's ability to assist in binding LLO to an amphipathic environment, especially at low cholesterol levels, indicates its critical role in the pathogenicity of *Listeria monocytogenes*. This study provides broader implications for understanding other cholesterol-dependent cytolysins and their roles in various infections, shedding light on common mechanisms that might be targeted in drug development.

3.3. Conclusions

In a nutshell, the study demonstrated the sophisticated mechanism of LLO for its binding towards various membranes through the simplest method of LC-aqueous interface as a potent hosting platform. The work displayed the varied membrane-bindings abilities of LLO and its mutant ΔCRM on lipid membranes hosted on LCs, highlighting the crucial function of CRM in the binding of LLO. The results indicated the remodelling of lipid membranes having 30 wt%-15 wt% cholesterol in zwitterionic lipids-PC to dendritic domains indicative of the β-sheet rich nature of LLO. A comparison of evolution rates of dendritic domains revealed the interplay of membrane dynamism and the role of CRM in the modulation of LLO binding to lipid membranes. At lower concentrations of cholesterol, CRM mutations render the low activity of LLO, which is in contrast with high cholesterol levels. The presence of high cholesterol in lipid membranes would support LLO by modulating the lipid nature, thus decreasing the impact of CRM mutation in the LLO. Thus, the study could help to get insights into the processes used by LLO to enable *Listeria* to elicit a variety of host cell responses during infection at physiological concentrations. Altogether, our research embraces the LC-aqueous interface as an augmentative tool to detect differences in the activity of protein on mutations of just two amino acids. In general, our study substantially strengthens the understanding of PFT binding behaviour.

3.4. Experimental Procedures

3.4.1. Materials

Required Glass microscopic slides of Fischer's Finest Premium Grade brand were bought from Fischer Scientific in Pittsburgh, Pennsylvania. These glass slides are piranha cleaned by using Sulfuric acid (H_2SO_4), Hydrogen peroxide (H_2O_2, 30% w/v) bought from Merck, and to neutralize it, Sodium chloride (NaCl) was also purchased from Merck. Chloroform (HPLC), 4′-pentyl-4-biphenylcarbonitrile (5CB), dimethyloctadecyl[3-(trimethoxysilyl)propyl]-ammonium chloride (DMOAP) were supplied by Sigma Aldrich. Required lipids, i.e., 1-palmitoyl-2-oleoyl-glycero-3-phosphocholine (POPC) and cholesterol, were bought from Avanti Polar Lipids, Inc (Alabaster, AL). Ethanol was supplied by Jebsen & Jenssen GmbH and Co., Germany (S D fine-chem Limited). 1,2-dioleoyl-*sn*-glycero-3-phosphocholine-N-(Cyanine 5) [Cy5 labelled POPC], 3β-Hydroxy-5,7,22ergostatriene (Ergoesterol) were ordered from Merck. Alexa Fluor 488 maleimide was purchased from Thermo Fischer Scientific to label LLO and its mutant. Gold grids of 20 μm thickness

(50 µm wide, 283 µm grid spacing) were bought from Electron Microscopy Sciences (Fort Washington, PA). We bought Luria Broth (LB media) and Coomassie bright blue dye from Himedia. IPTG (isopropyl-D-thiogalactopyranoside) was obtained from BR Biochem Life Sciences. All buffers were prepared using Milli-Q water, and the required pH was adjusted using a Metrohm 827 lab pH meter at room temperature (~25 °C). The Millipore technology (Bedford, MA) was used to obtain Milli-Q water.

3.4.2. Piranha Cleaning and Coating of Glass slides

Glass slides were cleaned with piranha solution (H_2SO_4:H_2O_2 (v/v) = 70:30) in accordance with accepted procedures.[48] Briefly, the freshly prepared piranha solution was added to the glass slides in a glass jar and then placed in a water bath at 80°C for one hour. After that, the slides were rinsed with ethanol and deionized water. The slides were dried using nitrogen gas purging and maintained in an oven set at 100 °C for at least 3 h. To coat them with a hydrophobic medium, these slides were then submerged in a 0.1% (v/v) DMOAP aqueous solution in DI water for 30 min at room temperature. After that, washing was done to get rid of the excess DMOAP before nitrogen drying. These slides were also heated in the oven for 3-6 h to promote cross-linking and the formation of a siloxane bond. The octadecyl chains of the DMOAP and the alkyl tails of 5CB molecules interact hydrophobically.

3.4.3. Preparation of vesicles of PC with varying amounts of cholesterol

The vesicles are prepared by earlier known method.[37] Briefly, to prepare mixed lipid vesicles, different amounts of cholesterol (0%, 15% and 30% by weight of total lipid) were incorporated in PC vesicles. For this, the predetermined amount of lipid was obtained and suspended in chloroform in a round bottom flask. The necessary amount of cholesterol (0, 15 and 30% of cholesterol by weight) was added, and the mixture was then dried for 3 h at room temperature under a vacuum. The dried lipid was rehydrated with PBS buffer after 3 h, and then freeze-thaw cycles were performed to create lipid vesicles. Small unilamellar vesicles were produced during probe sonication of the aqueous lipid dispersion for 30 min. Within 24 h, all the produced lipid solutions were utilised.

3.4.4. Purification of recombinant LLO and its mutant (ΔCRM)

The purification and mutation have been done by Kusum Lata, a group member of our collaborator Dr. Kausik Chattopadhyay's lab (IISER Mohali). We have used it as a reagent for our study, which

the collaborator has kindly provided. The work of the collaborator has been acknowledged and well respected.

3.4.5. Circular dichroism (CD) measurements

A Chirascan spectrophotometer (Applied Photophysics, U.K.) with a scan range of 200–260 nm and a step size of 1 nm was used for the far-UV CD studies. The solution of interest was kept in a quartz cell with a 1 mm path length. Freshly made aqueous solutions of 2 μM LLO and ΔCRM in 10 mM PBS (pH 7.4) were used. Using the ProData software that came with the CD instrument, the spectra for each sample were averaged over 5 scans and adjusted against the buffer signal.

3.4.6. Preparation of LC aqueous interface

The preparation of the LC-aqueous interface has already been described in earlier reports. In short, DMOAP-coated glass slides were broken up into tiny bits and overlaid with gold grids.[49] After adding roughly 0.2 μl of 5CB to the grids, the extra 5CB was syringed out to create a consistent film of LC. The constructed system was placed in an optical well containing a PBS buffer (10 mM, 2 ml) in order to create the LC-aqueous interface.

3.4.7. Decoration of lipid at LC-aqueous interface

The LC-aqueous interface was encased in lipid layers composed of the produced lipid vesicles, which were subsequently incubated for 30 min. Following the interval of equilibration, excess lipid in the solution was eliminated by three washes in PBS buffer (10 mM, pH = 7.2). Rinsing was done carefully to avoid disrupting the lipid assembly or the LC film. Further, the buffer was replaced with various concentrations of the protein, and the optical response of LC was studied under a polarizing optical microscope (POM) to better understand protein interactions with the lipid-rich LC-aqueous interface. To prevent turbulence in the aligned layer of lipid, a variable amount of protein was dispersed slowly and from the optical well's walls.

3.4.8. Optical Characterization of LC films

In earlier papers, optical characterisation has already been mentioned.[49-52] Briefly stated, a POM (Zeiss Scope.A1) in transmission mode was used to observe the optical response of LC. Each image was focussed and taken using a Q-imaging digital camera coupled to the POM with an exposure time of 80 ms. The optical well housing the 5CB film was placed on a revolving platform. The

orientation of 5CB was examined by the orthogonal orientation of the polarizer and analyser. In each trial, pictures were taken while maintaining a source intensity that was roughly 40% of the brightness.

3.4.9. Quantification of optical responses

The grayscale intensity of the optical micrographs was used to quantify the LC optical response at different intervals and concentrations. Using ImageJ software, the average grayscale intensity was calculated.[37] To get the mean grayscale intensity, the grayscale intensity was averaged over four grid squares on each micrograph.

3.4.10. Labelling of LLO and its mutant (ΔCRM)

The labelling of LLO and its mutant has been done by Kusum Lata, a group member of our collaborator Dr. Kausik Chattopadhyay's lab (IISER Mohali). We have used it as a reagent for our study, which the collaborator has kindly provided. The work of the collaborator has been acknowledged and well respected.

3.4.11. Confocal Fluorescence Microscope Imaging

We performed confocal microscopic imaging to observe the localisation of fluorescently labelled lipid PC and protein. A 2.5% Cy5 fluorescently labelled PC lipid combined with 15 wt% of cholesterol was incubated with 100 nM Alexa-488 fluorescently labelled LLO and mutant (ΔCRM) to create the samples. A lens of 63x and hybrid detectors were employed to image the sample. Image acquisition was set to 512×512 pixels with a 400 Hz scanning rate. 10% of the argon laser power was used to excite Cy5 and Alexa-488 fluorescent dyes while keeping laser gain constant at 5%. For the excitation of Alexa-488-labeled LLO and its mutant (ΔCRM), a 488 nm laser line was used, whereas a 650 nm laser was used for the excitation of Cy5. Stacks of confocal images were captured using an SP8 upright confocal microscope.

3.4.12. DFT calculations

DFT calculations were performed with the use of *Gaussian 09* suite of packages.[53] The Becke3-Lee-Yang-Parr hybrid functional (B3LYP) is exchange-correlation functional, and the 6-311G (d, p) basis set was used to do the DFT calculations within the context of the generalised gradient approximation (GGA).[54] Due to its effective application for bigger organic compounds as well as hydrogen-bonded systems in the past, B3LYP functional with the standard basis set 6-311G were used.[55]

3.4.13. Statistics

The data are reported as means ± standard error of the mean. A multifactorial repeated measures ANOVA was employed,[56, 57] to examine variations in the mean grayscale intensities of LLO and its mutant during interaction with PC containing 30 wt% and 15 wt% cholesterol at the LC-aqueous interface after 30 min of incubation. Subsequently, Tukey's post-hoc analysis was conducted to delve deeper into the findings. Statistical significance was determined at $p < 0.05$.

3.5. Author Contributions

TG and KL collaborated to conceptualize and devise the framework for the project. Kusum Lata has purified, mutated and labelled the protein. The labelling of LLO and its mutant has been done by Kusum Lata, a group member of our collaborator Dr. Kausik Chattopadhyay's lab (IISER Mohali). We have used it as a reagent for our study, which the collaborator has kindly provided. TG meticulously executed all experimental procedures and thoroughly analysed the resulting data. SKP and KC did the overall project administration.

3.6. Acknowledgements

S.K.P. acknowledge MOE/STARS1/284. T.G. thanks CSIR (09/947/(0223)/2019EMR-1) for the fellowship. T.G. acknowledges powerpoint, chemdraw, pymol and chimera tools for various cartoons and protein structures used in the table of contents (TOC) graphics.

References

1. a) Kayal, S.; Charbit, A., Listeriolysin O: a key protein of *Listeria monocytogenes* with multiple functions. *FEMS Microbiol. Rev.* **2006**, *30*, 514–529; b) Vázquez-Boland, J. A.; Kuhn, M.; Berche, P.; Chakraborty, T.; Domínguez-Bernal, G.; Goebel, W.; González-Zorn, B.; Wehland, J.; Kreft, J., Listeria pathogenesis and molecular virulence determinants. *Clin. Microbiol. Rev.* **2001**, *14(3)*, 584-640.

2. a) Koster, S.; Van Pee, K.; Hudel, M.; Leustik, M.; Rhinow, D.; Kuhlbrandt, W.; Chakraborty, T.; Yildiz, O., Crystal structure of listeriolysin O reveals molecular details of oligomerization and pore formation. *Nat. Commun.* **2014,** *5* (1), 3690; b) Gaillard, J. L.; Berche, P.; Mounier, J.; Richard, S.; Sansonetti, P., In vitro model of penetration and intracellular growth of Listeria monocytogenes in the human enterocyte-like cell line Caco-2. *Infect. Immun.* **1987**, *55(11)*, 2822-2829.

3. a) Tweten, R. K., Cholesterol-Dependent Cytolysins, a Family of Versatile Pore-Forming Toxins. *Infect. Immun.* **2005**, *73*, 6199–6209; b) Robbins, J. R.; Skrzypczynska, K. M.; Zeldovich, V. B.; Kapidzic, M.; Bakardjiev, A. I., Placental syncytiotrophoblast constitutes a major barrier to vertical transmission of Listeria monocytogenes. *PLoS Pathog.* **2010**, *6(1),* e1000732.

4. Alouf, J. E., Pore-forming bacterial protein toxins: an overview. *Curr. Top. Microbiol. Immunol.* **2001,** *257*, 1-14.

5. Nakamura, M.; Sekino, N.; Iwamoto, M.; Ohno-Iwashita, Y., Interaction of. theta.-toxin (perfringolysin O), a cholesterol-binding cytolysin, with liposomal membranes: change in the aromatic side chains upon binding and insertion. *Biochemistry* **1995**, *34*(19), 6513-6520.

6. Iwamoto, M.; Ohno-Iwashita, Y.; Ando, S., Role of the essential thiol group in the thiol-activated cytolysin from Clostridium perfringens. *Eur. J. Biochem.* **1987**, *167*(3), 425-430.

7. Shimada, Y.; Nakamura, M.; Naito, Y.; Nomura, K.; Ohno-Iwashita, Y., C-terminal amino acid residues are required for the folding and cholesterol binding property of perfringolysin O, a pore-forming cytolysin. *J. Biol. Chem*. **1999**, *274*(26), 18536-18542.

8. Heuck, A. P.; Tweten, R. K.; Johnson, A. E., Assembly and topography of the prepore complex in cholesterol-dependent cytolysins. *J. Biol. Chem*. **2003**, *278*(33), 31218-31225.

9. Farrand, A. J.; LaChapelle, S.; Hotze, E. M.; Johnson, A. E.; Tweten, R. K., Only two amino acids are essential for cytolytic toxin recognition of cholesterol at the membrane surface. *Proc. Natl Acad. Sci. U. S. A.* **2010,** *107* (9), 4341-6.

10. Morton, C. J.; Sani, M. A.; Parker, M. W.; Separovic, F., Cholesterol-dependent cytolysins: membrane and protein structural requirements for pore formation: Focus review. *Chem. Rev.* **2019**, 119, *13*, 7721–7736.

11. Hotze, E. M.; Tweten, R. K., Membrane assembly of the cholesterol-dependent cytolysin pore complex. *Biochim. Biophys. Acta - Biomembr.* **2012**, 1818, 1028-1038.

12. Christie, M. P.; Johnstone, B. A.; Tweten, R. K.; Parker, M. W.; Morton, C. J., Cholesterol-dependent cytolysins: from water-soluble state to membrane pore. *Biophys. Rev.* **2018,** *10*, 1337–1348.

13. Le, D. T.; Wang-Gillam, A.; Picozzi, V.; Greten, T. F.; Crocenzi, T.; Springett, G.; Morse, M.; Zeh, H.; Cohen, D.; Fine, R. L.; Onners, B., Safety and survival with GVAX pancreas prime and Listeria monocytogenes–expressing mesothelin (CRS-207) boost vaccines for metastatic pancreatic cancer. *J. Clin. Oncol.* **2015**, *33(12),*1325.

14. Xu, G.; Feng, D.; Yao, Y.; Li, P.; Sun, H.; Yang, H.; Li, C.; Jiang, R.; Sun, B.; Chen, Y., Listeria-based hepatocellular carcinoma vaccine facilitates anti-PD-1 therapy by regulating macrophage polarization. *Oncogene* **2020**, *39(7),* 1429-44.

15. Vassaux, G.; Nitcheu, J.; Jezzard, S.; Lemoine, N. R., Bacterial gene therapy strategies. *J. Pathol.* ***2006****, 208(2), 290-8.*

16. Lata, K.; Singh, M.; Chatterjee, S.; Chattopadhyay, K., Membrane Dynamics and Remodelling in Response to the Action of the Membrane-Damaging Pore-Forming Toxins. *J. Membr. Biol.* **2022,** *255* (2-3), 161-173.

17. Gupta, V. K.; Skaife, J. J.; Dubrovsky, T. B.; Abbott, N. L., Optical amplification of ligand-receptor binding using liquid crystals. *Science (New York, N.Y.)* **1998,** *279* (5359), 2077-80.

18. Lowe, A. M.; Abbott, N. L., Liquid Crystalline Materials for Biological Applications. *Chem. Mater.* **2012,** *24* (5), 746-758.

19. Lin, I. H.; Miller, D. S.; Bertics, P. J.; Murphy, C. J.; de Pablo, J. J.; Abbott, N. L., Endotoxin-induced structural transformations in liquid crystalline droplets. *Science (New York, N.Y.)* **2011,** *332* (6035), 1297-300.

20. Naveenkumar, P. M.; Mann, S.; Sharma, K. P., Spontaneous Sequestration of Proteins into Liquid Crystalline Microdroplets. *Adv. Mater. Interfaces* **2018,** *6* (3), 1801593.

21. Aery, S.; Parry, A.; Araiza-Calahorra, A.; Evans, S. D.; Gleeson, H. F.; Dan, A.; Sarkar, A., Ultra-stable liquid crystal droplets coated by sustainable plant-based materials for optical sensing of chemical and biological analytes. *J. Mater. Chem. C* **2023,** *11* (17), 5831-5845.

22. Nguyen, D. K.; Jang, C. H., Label-free liquid crystal-based detection of As(III) ions using ssDNA as a recognition probe. *Microchem. J.* **2020,** *156*, 104834.

23. Yang, X.; Tian, Y.; Li, F.; Yu, Q.; Tan, S. F.; Chen, Y.; Yang, Z., Investigation of the Assembly Behavior of an Amphiphilic Lipopeptide at the Liquid Crystal-Aqueous Interface. *Langmuir* **2019,** *35* (7), 2490-2497.

24. Yang, X.; Zhao, X.; Liu, F.; Li, H.; Zhang, C. X.; Yang, Z., Simple, rapid and sensitive detection of Parkinson's disease related alpha-synuclein using a DNA aptamer assisted liquid crystal biosensor. *Soft Matter* **2021,** *17* (18), 4842-4847.

25. Yang, X.; Yang, Z., Simple and rapid detection of ibuprofen─ a typical pharmaceuticals and personal care products─ by a liquid crystal aptasensor. *Langmuir* **2021,** *38* (1), 282-288.

26. Park, J. S.; Abbott, N. L., Ordering Transitions in Thermotropic Liquid Crystals Induced by the Interfacial Assembly and Enzymatic Processing of Oligopeptide Amphiphiles. *Adv. Mater.* **2008,** *20* (6), 1185-1190.

27. Perera, K.; Dassanayake, T. M.; Jeewanthi, M.; Haputhanthrige, N. P.; Huang, S. D.; Kooijman, E.; Mann, E.; Jákli, A., Liquid Crystal-Based Detection of Antigens with ELISA Sensitivity. *Adv. Mater. Interfaces* **2022,** *9* (25), 2200891.

28. Noonan, P. S.; Mohan, P.; Goodwin, A. P.; Schwartz, D. K., DNA Hybridization-Mediated Liposome Fusion at the Aqueous Liquid Crystal Interface. *Adv. Funct. Mater.* **2014,** *24* (21), 3206-3212.

29. Yang, X.; Li, H.; Zhao, X.; Liao, W.; Zhang, C. X.; Yang, Z., A novel, label-free liquid crystal biosensor for Parkinson's disease related alpha-synuclein. *Chem. Commun.* **2020,** *56* (40), 5441-5444.

30. Borbora, A.; Manna, U., Design of a Super-Liquid Crystal-Phobic Coating for Immobilizing Liquid Crystal μ-Droplets─ Without Affecting Their Sensitivity. *Langmuir* **2022,** *38* (30), 9221-9228.

31. Yang, X.; Zhao, X.; Zhao, H.; Liu, F.; Zhang, S.; Zhang, C. X.; Yang, Z., Combination of liquid crystal and deep learning reveals distinct signatures of Parkinson's disease-related wild-type α-synuclein and six pathogenic mutants. *Chem. Asian J.* **2022,** *17* (2), e202101251.

32. Manna, U.; Zayas-Gonzalez, Y. M.; Carlton, R. J.; Caruso, F.; Abbott, N. L.; Lynn, D. M., Liquid crystal chemical sensors that cells can wear. *Angew. Chem. Int. Ed.* **2013,** *52* (52), 14011-14015.

33. Yang, L.; Khan, M.; Park, S. Y., Liquid crystal droplets functionalized with charged surfactant and polyelectrolyte for non-specific protein detection. *RSC Adv.* **2015,** *5* (118), 97264-97271.

34. Tan, L. N.; Orler, V. J.; Abbott, N. L., Ordering transitions triggered by specific binding of vesicles to protein-decorated interfaces of thermotropic liquid crystals. *Langmuir* **2012,** *28* (15), 6364-76.

35. Woltman, S. J.; Jay, G. D.; Crawford, G. P., Liquid-crystal materials find a new order in biomedical applications. *Nat. Mater.* **2007,** *6* (12), 929-38.

36. Das, D.; Sidiq, S.; Pal, S. K., Design of bio-molecular interfaces using liquid crystals demonstrating endotoxin interactions with bacterial cell wall components. *RSC Adv.* **2015,** *5* (81), 66476-66486.

37. Gupta, T.; Mondal, A. K.; Pani, I.; Chattopadhyay, K.; Pal, S. K., Elucidating liquid crystal-aqueous interface for the study of cholesterol-mediated action of a β-barrel pore forming toxin. *Soft Matter* **2022,** *18* (28), 5293-5301.

38. Sunshine, H.; Iruela-Arispe, M. L., Membrane lipids and cell signaling. *Curr. Opin. Lipidol.* **2017,** *28* (5), 408-413.

39. Wang, X.; Yang, P.; Mondiot, F.; Li, Y.; Miller, D. S.; Chen, Z.; Abbott, N. L., Interfacial ordering of thermotropic liquid crystals triggered by the secondary structures of oligopeptides. *Chem. Commun.* **2015,** *51* (94), 16844-7.

40. Sadati, M.; Apik, A. I.; Armas-Perez, J. C.; Martinez-Gonzalez, J.; Hernandez-Ortiz, J. P.; Abbott, N. L.; de Pablo, J. J., Liquid Crystal Enabled Early Stage Detection of Beta Amyloid Formation on Lipid Monolayers. *Adv. Funct. Mater.* **2015,** *25* (38), 6050-6060.

41. Brake, J. M.; Abbott, N. L., Coupling of the orientations of thermotropic liquid crystals to protein binding events at lipid-decorated interfaces. *Langmuir* **2007,** *23* (16), 8497-507.

42. Pani, I.; Madhu, P.; Najiya, N.; Aayush, A.; Mukhopadhyay, S.; Pal, S. K., Differentiating Conformationally Distinct Alzheimer's Amyloid-β Oligomers Using Liquid Crystals. *J. Phys. Chem. Lett.* **2020,** *11* (21), 9012-9018.

43. Verma, I.; Selvakumar, S. L. V.; Pal, S. K., Surfactin-Laden Aqueous–Liquid Crystal Interface Enabled Identification of Secondary Structure of Proteins. *J. Phys. Chem. C* **2019,** *124* (1), 780-788.

44. Padmavathi, D. A., Potential Energy Curves & Material Properties. *Mater. sci. appl.* **2011,** *02* (02), 97-104.

45. Mardirossian, N.; Head-Gordon, M., Thirty years of density functional theory in computational chemistry: an overview and extensive assessment of 200 density functionals. *Mol. Phys.* **2017**, 115(19), 2315-2372.

46**.** Goerigk, L.; Grimme, S., A general database for main group thermochemistry, kinetics, and noncovalent interactions− assessment of common and reparameterized (meta-) GGA density functionals. *J. Chem. Theory Comput.* **2010,** *6(1),* 107-26.

47**.** Reimers, J. R.; Ford, M. J.; Goerigk, L., Problems, successes and challenges for the application of dispersion-corrected density-functional theory combined with dispersion-based implicit solvent models to large-scale hydrophobic self-assembly and polymorphism. *Mol. Simul.* **2016**, *42*, 494-510.

48**.** Brake, J. M.; Abbott, N. L., An Experimental System for Imaging the Reversible Adsorption of Amphiphiles at Aqueous-Liquid Crystal Interfaces. *Langmuir* **2002,** *18* (16), 6101-6109.

49. Das, D.; Pal, S. K., Liquid Crystal Unveiled Interactions between Melittin and Phospholipids at Aqueous-Liquid Crystal Interface. *ChemistrySelect* **2017,** *2* (17), 4779-4786.

50. Das, D.; Sidiq, S.; Pal, S. K., A Simple Quantitative Method to Study Protein-Lipopolysaccharide Interactions by Using Liquid Crystals. *ChemPhysChem* **2015**, *16*, 753-760.

51. Price, A. D.; Schwartz, D. K., DNA Hybridization-Induced Reorientation of Liquid Crystal Anchoring at the Nematic Liquid Crystal/Aqueous Interface. *J. Am. Chem. Soc.*, **2008**, *130*, 8188-8194.

52. Popov, P.; Honaker, L. W.; Kooijman, E. E.; Mann, E. K.; Jákli, A. I., A liquid crystal biosensor for specific detection of antigens. *Sens. Biosensing Res.*, **2016**, *8*, 31-35.

53. Frisch, M. J.; Trucks, G. W.; Cioslowski, J.; Fox, D. J. et al., Gaussian 09 (Revision C.01) Gaussian, Inc., Wallingford CT, 2010.

54. Prayogo, G. I.; Shin, H.; Benali, A.; Maezono, R.; Hongo, K., Importance of Van der Waals Interactions in Hydrogen Adsorption on a Silicon-carbide Nanotube Revisited with vdW-DFT and Quantum Monte Carlo. *ACS Omega* **2021,** *6* (38), 24630-24636.

55. March, N. H., Electron density theory of atoms and molecules. *J. Phys. Chem.* **1982,** *86* (12), 2262-2267.

56. Gehlert, S.; Bungartz, G.; Willkomm, L.; Korkmaz, Y.; Pfannkuche, K.; Schiffer, T.; Bloch, W.; Suhr, F., Intense resistance exercise induces early and transient increases in ryanodine receptor 1 phosphorylation in human skeletal muscle. *PLoS One* **2012**, *7*(11), 49326.

57. O'Leary, B. M.; Lee, C. P.; Atkin, O. K.; Cheng, R.; Brown, T. B.; Millar, A. H., Variation in leaf respiration rates at night correlates with carbohydrate and amino acid supply. *Plant physiol.* **2017**, *174*(4), 2261-2273.

Chapter 4

Ultrasensitive Detection of Lipid-Induced Misfolding of the Prion Protein at the Aqueous-Liquid Crystal Interface

The misfolding of the α-helical cellular prion protein into a self-propagating β-rich aggregated form is a key pathogenic event in fatal and transmissible neurodegenerative diseases collectively known as prion diseases.[1-4] Herein, we utilize the interfacial properties of liquid crystals (LCs) to monitor the lipid-membrane-induced conformational switching of prion protein (PrP) into β-rich amyloid fibrils. The lipid-induced conformational switching resulting in aggregation occurs at the nanomolar protein concentration and is primarily mediated by electrostatic interactions between PrP and lipid headgroups.

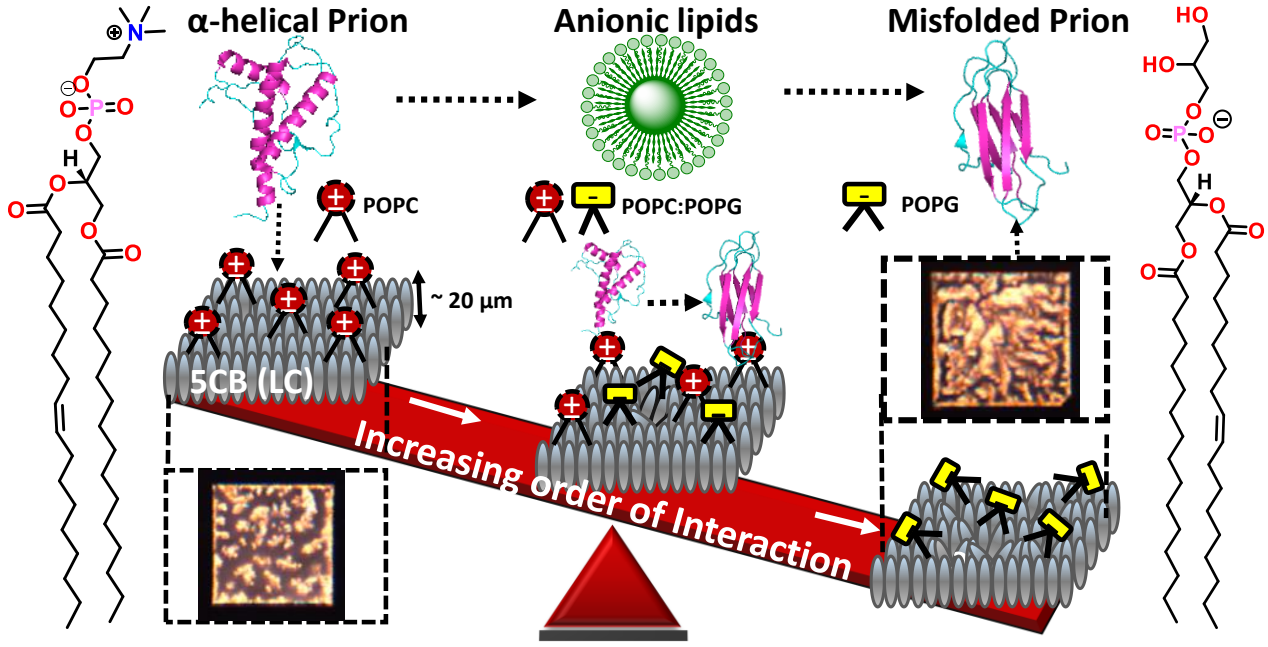

Our LC-based methodology offers a potent and sensitive tool to detect and delineate molecular mechanisms of PrP misfolding mediated by lipid-protein interactions at the aqueous interface under physiological conditions.

4.1. Introduction

Prion diseases represent a class of fatal neurodegenerative diseases that involve the misfolding and aggregation of prion protein (PrP).[1] The cellular prion protein is a glycosylphosphatidylinositol (GPI)-anchored protein primarily localized within lipid rafts and is most abundantly expressed within the central nervous system.[1] A crucial step in the pathophysiology of PrP is thought to include a dramatic conformational transformation of a primarily α-helical native protein into a β-rich misfolded form that assembles into protease-resistant amyloid-like aggregates. These aggregates are highly stable and resistant to degradation, causing a cascade of pathological events that lead to neuronal dysfunction, cell death, and characteristic symptoms associated with prion diseases. Also, the self-propagating nature of the misfolded β-rich aggregates enables them to induce further conformational changes in normal PrP, perpetuating the disease process. Past studies indicate that the interaction of PrP with lipid membranes influences its aggregation pathway.[2-4] However, utilizing sophisticated biophysical methods, like nuclear magnetic resonance (NMR), circular dichroism (CD), and Fourier transform infrared spectroscopy, to investigate the interaction between PrP and lipid necessitates a high protein and lipid concentration that is typically far from the physiological concentration regime.[5] Moreover, such techniques failed to capture the interactions of PrP with zwitterionic lipids.[6] Additionally, they are silent regarding membrane remodelling throughout the interactions. It is, therefore, imperative to study the lipid-membrane-mediated conformational conversion of PrP at a low-concentration regime for a better understanding of molecular mechanisms underlying prion diseases, thus necessitating the use of ultrasensitive methods. The liquid crystal (LC)-aqueous interface evolved as a valuable tool for understanding numerous atmospheric and biological phenomena.[7-17] LCs captured global interest as a result of their multiple enticing qualities, such as low surface-anchoring energy, communication, and self-responsiveness.[9, 10] Because of these properties, modest perturbations to macroscale responses are amplified through micrometre thin LC sheets.[9, 10] As a result of the high optical anisotropy and birefringence of LC, the molecular reorientation of LC can be captured using polarized optical microscopy (POM).[7-10] A line of evidence suggests that thin films of thermotropic nematic LC have proven to be excellent reporters of several binding events, such as lipid-protein interactions at aqueous interfaces.[7–9] Herein, we utilize LC-based biomimetic systems to understand

insights into the conformational changes of PrP, low- and high-level binding, and the remodelling of membranes during interactions at physiological concentrations associated with the underlying factors of neuropathology.

4.1.1. Objectives

The LC-aqueous interface presents an invaluable platform for the comprehensive exploration of diverse biomolecular interactions. Drawing inspiration from this, the present study embarks on a straightforward yet robust approach centred on differentially charged lipid monolayers incorporated into the LC-aqueous interface. This novel design aims to dissect the intricacies of interfacial binding and the conformational transitions of the PrP, a phenomenon intricately entwined with the etiology of fatal neurodegenerative disorders afflicting both humans and animals. The misfolding and aggregation of PrP, proteins that typically serve functional roles, underpin the pathology of these disorders.

Previous efforts to investigate PrP folding dynamics have harnessed advanced spectroscopic techniques such as circular dichroism (CD) and fluorescence, revealing the pivotal influence of specific lipid compositions in surmounting the energy barrier associated with PrP unfolding and aggregation.[1-5] However, despite accumulating evidence regarding the mechanisms governing PrP propagation, the precise forces orchestrating its conformational transitions have remained enigmatic.[2-5] Consequently, this study aims to shed light on three pivotal facets intrinsic to the fundamental determinants of neuropathology:

(i) The mediation of low and high-level PrP binding with lipids through ionic and non-covalent forces.

(ii) The role of multivalent interactions in shaping PrP conformational states.

(iii) The consequential membrane remodelling events that transpire during these interactions.

Furthermore, this innovative LC-based design has demonstrated the ability to discern the most subtle interactions of PrP with zwitterionic lipids, a feat unattainable with exceedingly complex spectroscopic approaches. The report underscores the substantial influence of electrostatic forces contingent on membrane interfacial properties in driving the initial binding of PrP, elevating the effective PrP concentration, and fostering short-range hydrophobic and protein-protein interactions. In essence, this research underscores the

efficacy of LC-based methodologies in providing mechanistic insights into the genesis and progression of prion diseases at physiologically relevant concentrations.

Our work integrates the experimental results from a myriad of techniques, including Langmuir-Blodgett (LB), polarizing optical microscopy (POM), atomic force microscopy (AFM), Zeta-potential analysis, fluorimetry, circular dichroism, confocal microscopy, and epifluorescence microscopy. These findings furnish a deeper understanding of interfacial biological phenomena and offer critical insights for designing and implementing bio-mimetic platforms utilizing LCs.

4.2. Results and Discussion

The current research elucidates the incorporation of a nematic thermotropic liquid crystal (5CB, 4'-pentyl-4-biphenylcarbonitrile) at biomolecular interfaces to gain insight into the behaviour of both Prion protein (PrP) and lipids during their interactions. Prior investigations involving lipid-coated LC-aqueous interfaces have uncovered similar lateral mobility characteristics between adsorbed phospholipids and biological membranes.[7-9] In addition, the study has also demonstrated the enhancement of interfacial interactions between lipids and proteins (at nanomolar concentrations) using optical readouts of the LC.[14, 15] Consistent with prior findings, when 5CB is confined within gold-grids on N, N-dimethyl-N-octadecyl-3 aminopropyltrimethoxysilyl chloride (DMOAP) coated glass slides, it exhibits a dark optical appearance indicative of homeotropic alignment under polarized optical microscopy (Figure 4.2.1a, e, i).[14-16] This optical appearance transitions to a bright one when the designed chip is immersed in an optical well containing a buffer (Figure 4.2.1b, f, j).

In the initial stages of our study, we utilized the Langmuir-Blodgett (LB) technique to prepare lipid monolayers at the LC-aqueous interface in a well-defined thermodynamic state and with specific densities. We chose two lipids with different charges, namely, zwitterionic 1-palmitoyl-2-oleoyl-*sn*-glycero-3-phosphocholine (POPC), anionic 1-palmitoyl-2-oleoyl-*sn*-glycero-3-phospho-1′-*rac*-glycerol (POPG), and a mixture of POPC:POPG (1:1 mole ratio) to investigate the influence of ionic forces on PrP. Careful examination of Figure 4.2.1m revealed that an areal density of 1.25 lipid molecules/nm² was suitable for achieving homeotropic alignment of the LC in the presence of lipids and lipid mixtures (Figure 4.2.1c, g, k). Furthermore, optical observations were conducted over 2 h to assess the system's stability during the experimental duration.

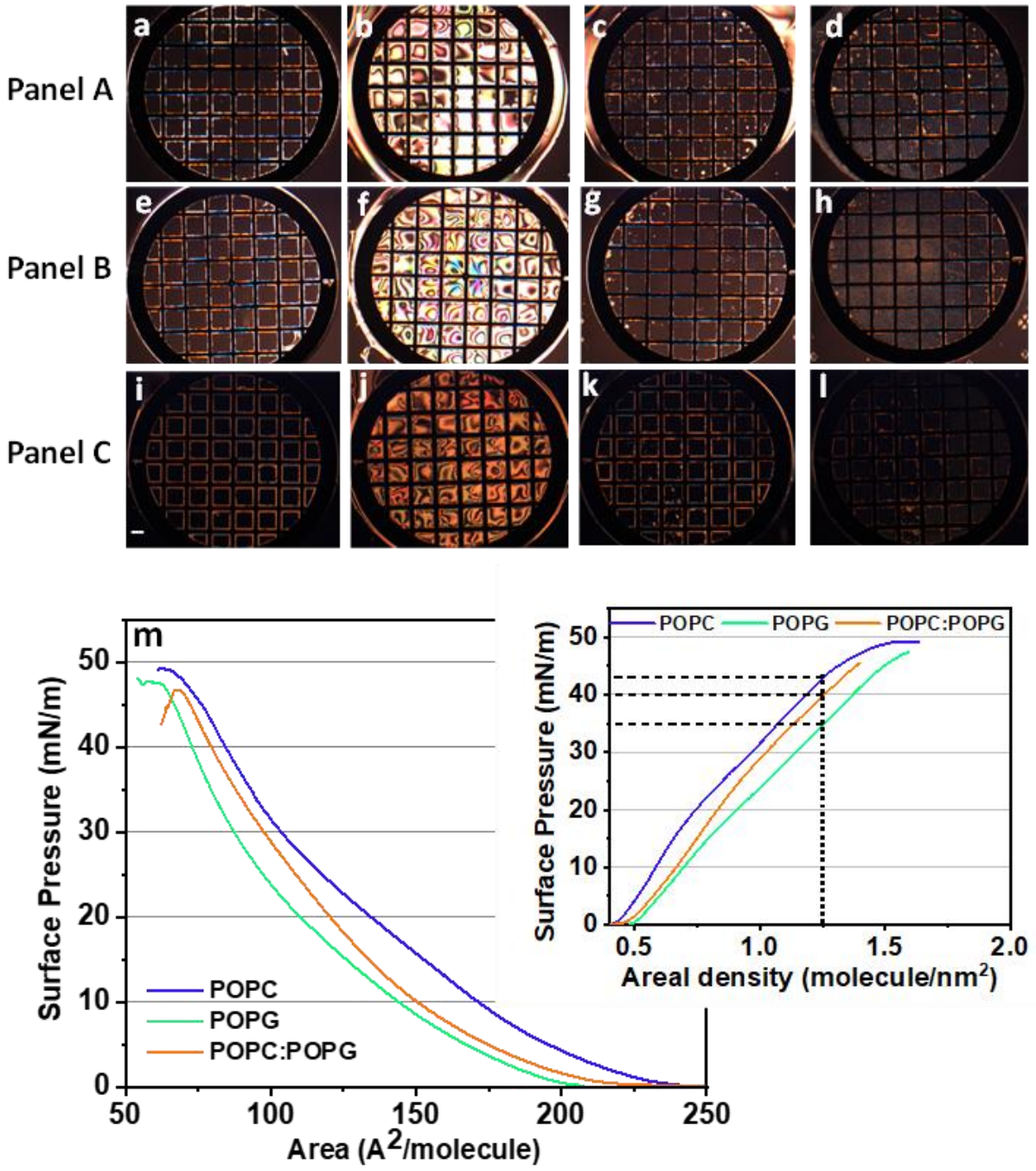

Figure 4.2.1 Captured polarized optical photomicrographs in (a, e, i) depict the LC-air interfaces giving a dark optical appearance, which changes to bright when placed in buffer (b, f, j). The bright optical appearance of LC-aqueous interfaces alters to dark after adsorption of (c) POPG, (g) POPC, and (k) POPC:POPG (1:1 mole ratio) lipid monolayers. Imaged lipid-laden LC-aqueous interfaces in (d, h, l) after 2 h indicate the stability of monolayers. Scale bar = 200 μm. Langmuir-Blodgett isotherms surface pressure versus mean molecular area shown in (m), indicate monolayers

formations of lipids POPG, POPC, and POPC:POPG at surface pressure ~ 35, 43 and 40 mN/m respectively, on sodium phosphate buffer as an aqueous sub-phase. The surface pressure is chosen to maintain the same lipid densities, i.e., 1.25 molecules/nm^2 for all lipids at the LC-aqueous interface.

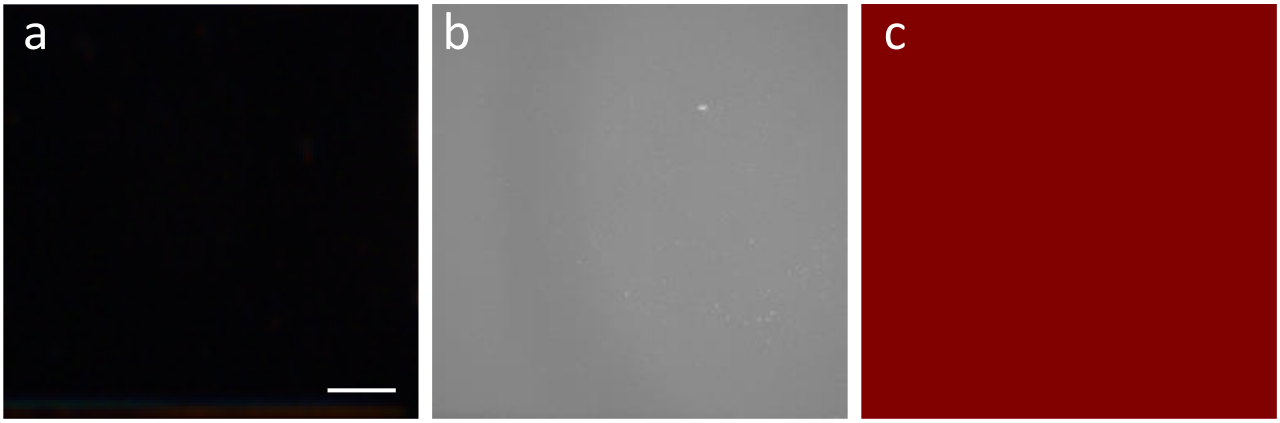

Figure 4.2.2 (a) Polarized optical (dark), (b) bright field, and (c) epifluorescence micrographs of the LC film in contact with 2.5% fluorescently labelled cy5 POPC transferred to 5CB LC using Langmuir-Blodgett technique. Scale bar = 20 µm.

The absence of any changes in the optical appearance (Figure 4.2.1d, h, l) indicates the stable assembly of lipids at the interface. Next, to confirm the complete coverage of the POPC monolayer at the interface, we employed confocal fluorescence microscopy. By incorporating 2.5% cy5-labeled POPC, the consistent red fluorescence in the microscopic image signifies uniform coverage at the interface (Figure 4.2.2).

Subsequently, we conducted an experimental investigation wherein a concentration of 150 nanomolar (nM) of PrP was subjected to interaction with distinct lipid-decorated LC-aqueous interfaces in order to assess PrP activity. Interestingly, the optical images captured after 30 min of incubation drew different observations for zwitterionic (POPC) and anionic (POPG and 1:1 POPC/POPG) lipid laden interfaces. The POPC-adorned 5CB optical response showed the emergence of small domains, whereas a completely bright image was obtained in POPG and POPC/POPG lipid laden 5CB (as shown in Figure 4.2.3a). These findings implied a lower affinity of PrP for POPC, resulting in minimal perturbation of the POPC assembly at the LC-aqueous interface when contrasted with the anionic POPG and the mixed POPC:POPG lipid compositions. Furthermore, to quantitatively evaluate these interactions, we assessed the mean grayscale intensities prior to and after the 30 min incubation period with PrP. Figure 4.2.3b illustrates the relative increase

in the intensity of transmitted light in the order of POPC < POPC:POPG < POPG. These results align with the aforementioned hypothesis, indicating minor alterations in the local areal density of POPC in contrast to POPG and the mixed lipid composition. Collectively, these observations provide valuable insights into the intricate interplay between PrP and lipid compositions at the LC-aqueous interface, underscoring the concentration-dependent effects of PrP on the structural characteristics of these interfaces.

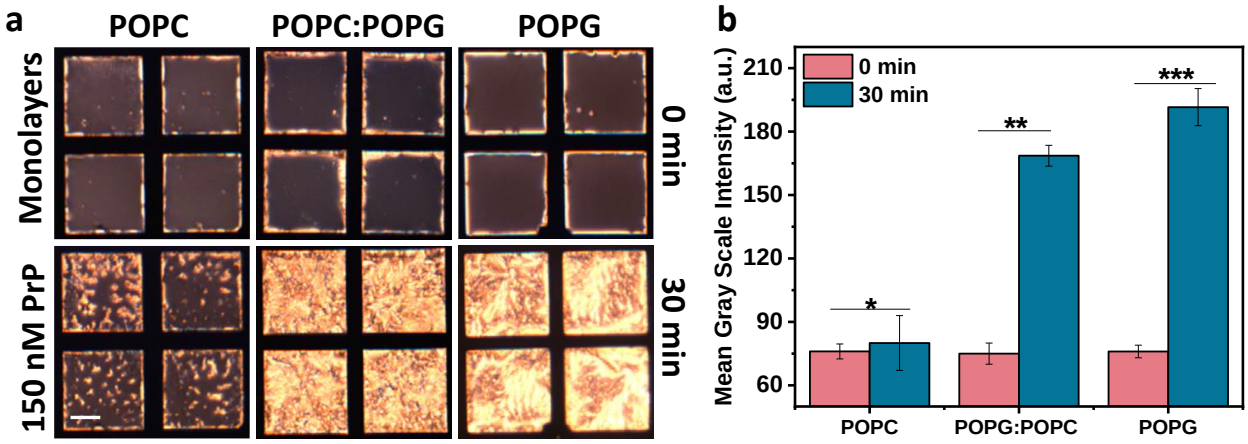

Figure 4.2.3 Polarized optical images in (a) represent the dark optical appearance, i.e. due to LC-aqueous interface laden with POPC, POPC:POPG (1:1 mole ratio), POPG lipid monolayers (row 1). Photomicrographs either with small brighter domains or having full brightness were obtained (row 2) on incubation of the interfaces with 150 nM PrP for 30 min. Scale bar = 100 µm. The bar graph in (b) demonstrates mean grayscale intensities comparisons of optical images in (a) captured before and after 30 min of addition of PrP on LC-aqueous interface laden with POPC, POPG:POPC (1:1 mole ratio) and POPG lipid monolayers. One-way ANOVA was used to measure the level of statistical significance. *p=0. 6>0.05, **p=1×10^{-7}< 0.05, and ***p =2×10^{-7}< 0. 05.

Taken together, these results suggest the profound interaction of PrP with negatively charged lipids and its membrane-induced conformation conversion into β-sheet rich structures. Subsequently, we inquired whether the bright domains that emerged were a consequence of interactions between PrP and the lipids integrated at the LC-aqueous interface. In this context, the presentation of a control experiment has been undertaken to provide supportive evidence. The rationale behind this investigation was driven by two primary objectives. Firstly, we aimed to establish that the observed domains resulted from specific interactions between PrP and the lipids assembled at the LC-aqueous interface, as opposed to random disturbances in lipid assembly. Secondly, our investigation aimed to

discern the potential existence of direct interactions between PrP and the LC 5CB that could induce their reorientation at the interface. To explore this, we subjected a 200 nM concentration of PrP to an LC-aqueous interface devoid of any lipid components for a duration of up to 2 h. The crossed-polar optical image captured after this 2 h incubation period, as depicted in Figure 4.2.4, revealed a negligible alteration in the optical characteristics. Consequently, based on the entirety of the aforementioned observations, we can draw the conclusion that the emergence of bright domains is a consequence of changes in the areal density of lipids induced by interactions between PrP and the lipids occurring at the LC-aqueous interface.

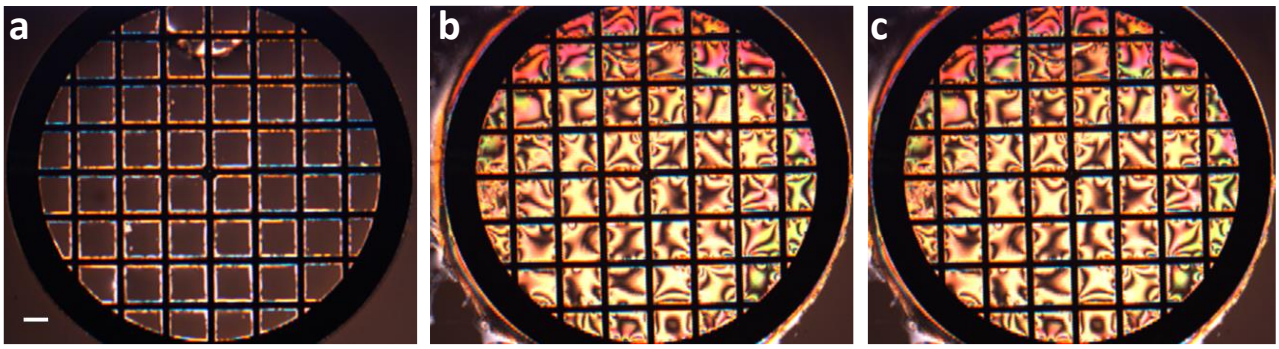

Figure 4.2.4 Imaged optical views of LC-interfaces transformations when placed in contact with (a) air, i.e., LC-air interface, (b) buffer, i.e., LC-aqueous interface, and (c) LC-aqueous interface in the presence of 200 nM prion protein after 2 h of incubation. Negligible change in the LC-aqueous interface depicts no direct interactions between prion protein and 5CB. Scale bar = 100 µm.

The aforementioned hypothesis has further been corroborated through an examination of the LC response at lower concentrations of PrP, ranging from 100 to 10 nM. Several significant observations have been documented as a result of this experiment: (i) Notably, when the LC-aqueous interface was enriched with POPC lipids, no discernible alterations in its optical appearance were observed following a 30 min incubation with PrP concentrations ranging from 100 to 10 nM, as illustrated in Figure 4.2.5. However, in stark contrast, the outcomes observed with LC interfaces doped with either 100% or 50% POPG lipids contradicted the findings associated with PrP-POPC interactions at lower concentrations. (ii) An intriguing pattern emerged in the case of anionic lipids, notably the appearance of extended dendritic structures. (iii) The optical domains were reduced with a decreasing PrP concentration, and no domains were observed at 10 nM PrP. Taken together, these results suggest the profound interaction of PrP with negatively charged lipids, leading to its membrane-induced conformation conversion into β-sheet-rich structures. The claim relies on an earlier study, which

demonstrates that dendritic patterns correlate with the β-sheet-rich conformation of the protein at the LC-aqueous interface.[17]

At this point, we conducted a Circular Dichroism (CD) analysis to substantiate the conformational metamorphosis of PrP induced by the presence of POPG lipid. The CD spectra obtained in our analysis substantiate our previous findings, clearly illustrating the transition from an α-helical conformation of PrP to a β-sheet-rich conformation when PrP is exposed to POPG lipid, as depicted in Figure 4.2.6. This CD analysis provides further compelling evidence of the conformational changes undergone by PrP in response to interactions with POPG lipids, which is consistent with our previous observations. Thus, these facts and earlier research backed up the notion of prominent electrostatic interactions between PrP and lipids.[2, 3] Additionally, our observation demonstrates the sensitivity of LC-aqueous interfaces to PrP up to 25 nM.

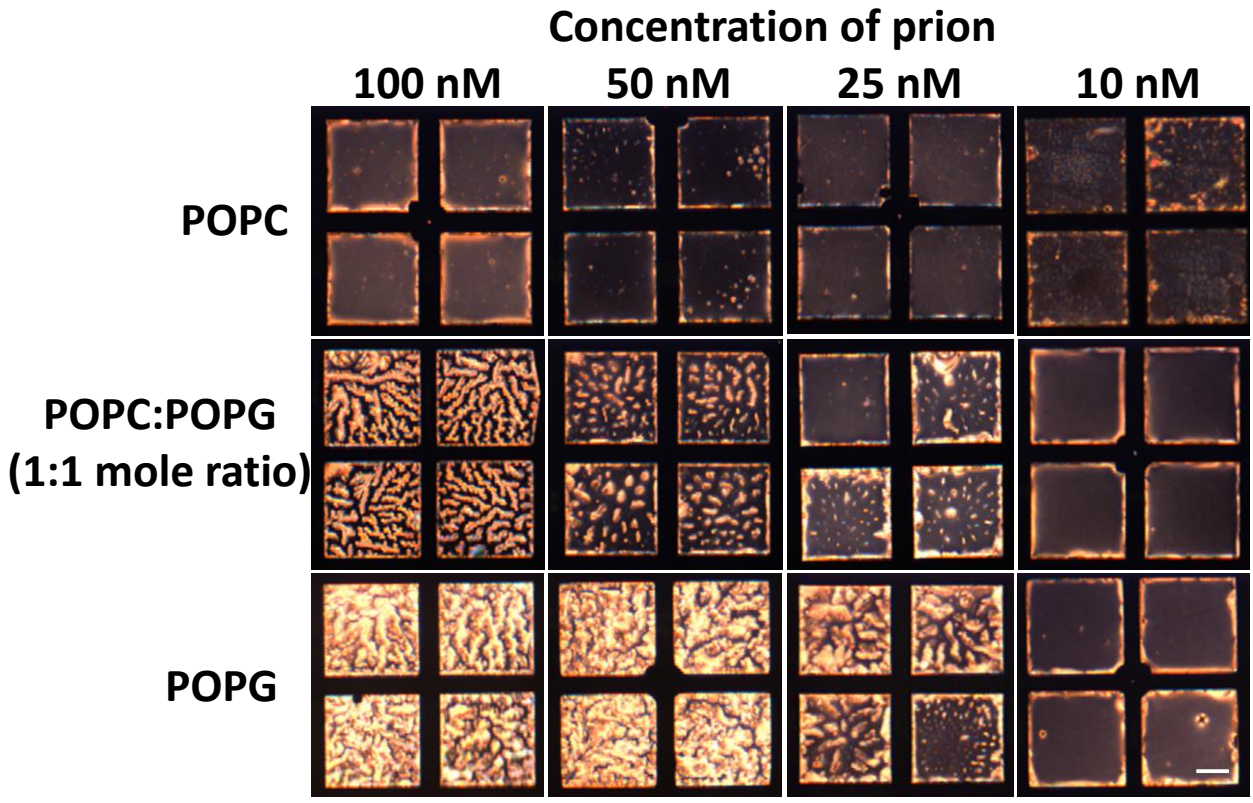

Figure 4.2.5 The photomicrographs of LC response in contact with 100-10 nM PrP, laden with zwitterionic POPC lipid, mixed lipid having 1:1 mole ratio of POPC and POPG lipid, anionic POPG lipid monolayers. Row 1 depicts no change in the optical appearance of the LC-aqueous interface laden with POPC lipid after 30 min incubation with 100-10 nM PrP. Images in row 2,3 show the

appearance of brighter elongated domains in the case of mixed lipid (POPC:POPG) and anionic POPG lipid monolayers laden LC-aqueous interface in the presence of 100-25 nM PrP, respectively. The view didn't change when 10 nM PrP was exposed to a mixed and anionic lipid-laden LC-aqueous interface. Scale bar = 100 µm.

Furthermore, in order to assess the specificity of our system, the response of POPC and POPG-laden-LC was observed in the presence of three control proteins (BSA, cytochrome c, and Lf). Interestingly, no considerable response of LC depicted the specificity of our designed system towards PrP (Figure 4.2.7). Next, to characterize the interaction of PrP with lipids, we performed zeta-potential measurements at LC droplets. During the analysis, the zeta-potential of PrP was found to be +5.6 ± 2.17 at physiological pH (7.4). Figure 4.2.8a depicts the slightest increase in the surface charges with 10 µM PrP exposure to POPC-laden LC droplets. However, a significant increase was noticed in POPC: POPG (1:1). Furthermore, the increase in zeta potential was even more pronounced for 100% POPG. The result corroborates the above observations.

Overall, a fundamental understanding of the findings reveals the significant contribution of the electrostatic interactions between PrP and lipids, which can be linked to the spatial redistribution of lipid assembly and LC reorientation. To further support this, we estimated the binding constant of PrP with different lipids using an intrinsic fluorescence assay. The data (Figure 4.2.9) pointed towards three main observations as outlined: (i) decrease in fluorescence intensity of 1 µM PrP with no drift in the spectra on titrating with POPC lipid, (ii) increase and blue-shift in the intrinsic fluorescence spectra of PrP on titrating with POPG lipid, and (iii) complex phenomenon being observed with initially no change and then slight blue-shifting with an increase in the intensity of intrinsic fluorescence spectra of PrP on titrating with POPC:POPG lipid. The key findings suggested the structural alterations in PrP led to more solvent exposure of tryptophan in the presence of POPG lipid. However, the slight decrease in the case of POPC can be attributed to the dilution of the PrP in the total solution. Additionally, the initial no drift and negligible intensity change in the intrinsic fluorescence spectra of PrP illustrated the counter effects of POPG and POPC lipid, but on further increasing the concentration, the effect of the presence of anionic POPG lipid could be seen in the spectra. The approximate estimation of the binding constant was done using a data set and double logarithmic plot [$\log(F_0\text{-}F/\ \Delta F_{max})$] vs. log [lipid] as reported in the literature.[18] Notably, for PrP, the binding constant with POPG lipid (K_b~$3.5*10^{-2}$ μM^{-1}) was found to be almost one order of magnitude higher than with POPC lipid (K_b~$1.89*10^{-3}$ μM^{-1}).

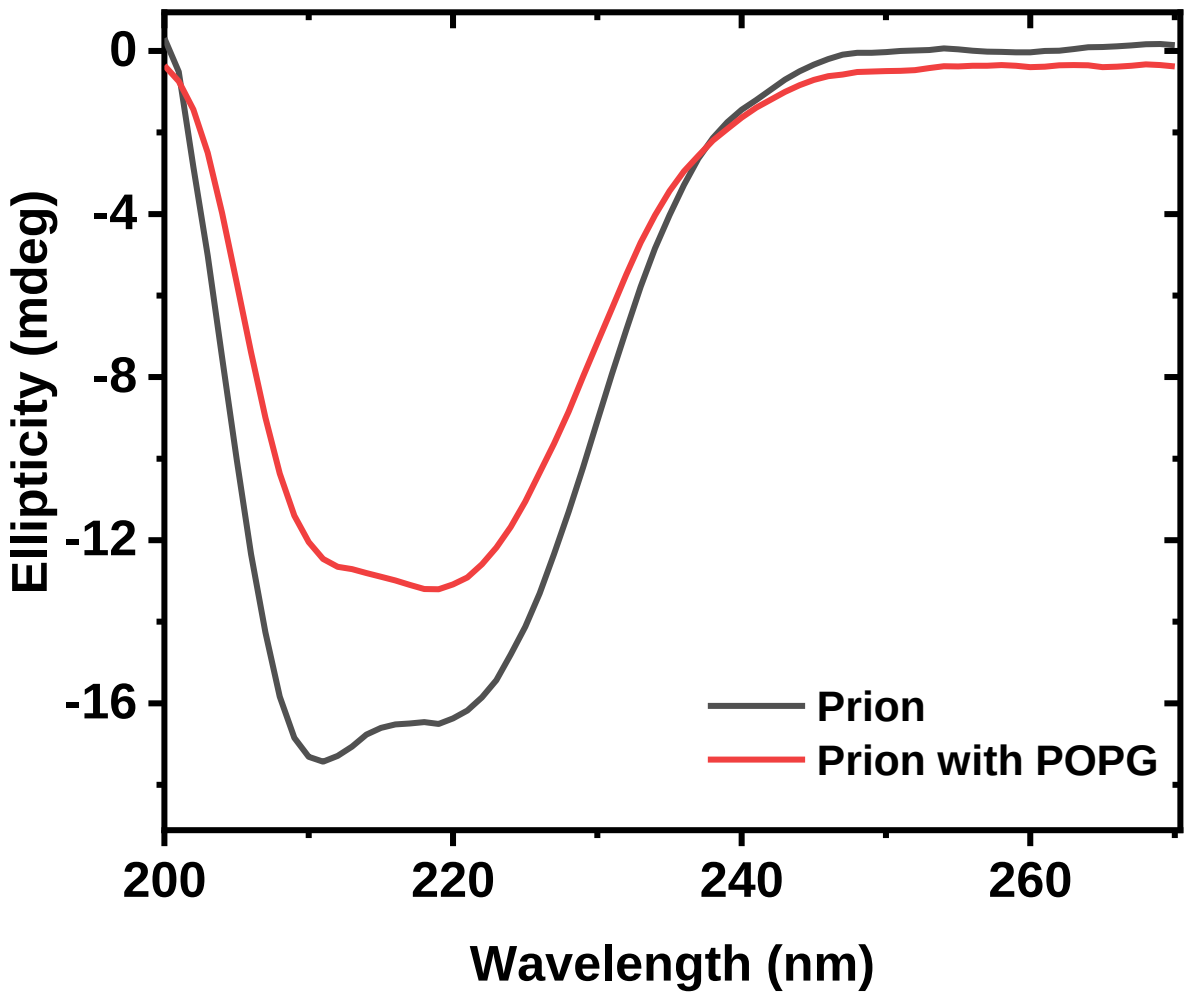

Figure 4.2.6 CD spectra of prion in the absence and presence of POPG lipid. The graph indicates the α-helical nature of PrP before exposure to POPG lipid.

Our next goal was to investigate the correlation between spatial distribution and lateral allocations of lipids and PrP at the interfaces. To comprehend this, we physically hybridized 2.5% lissamine rhodamine B 1,2-dihexadecanoyl-*sn*-glycero-3-phosphoethanolamine (Rhodamine-DHPE) with POPC:POPG and formed mixed lipid monolayer at similar lipid areal density. We anticipated that the rhodamine-DHPE doped lipid would exhibit red fluorescence in the lipid-rich regions. Consistent with our statement, we observed uniform red fluorescence with no spatial patterns (Figure 4.2.8b, c) without PrP. However, branched non-fluorescent patterns appeared when incubating the system with 150 nM PrP for 30 min on a mixed monolayer-laden LC-aqueous interface (Figure 4.2.8d, e).

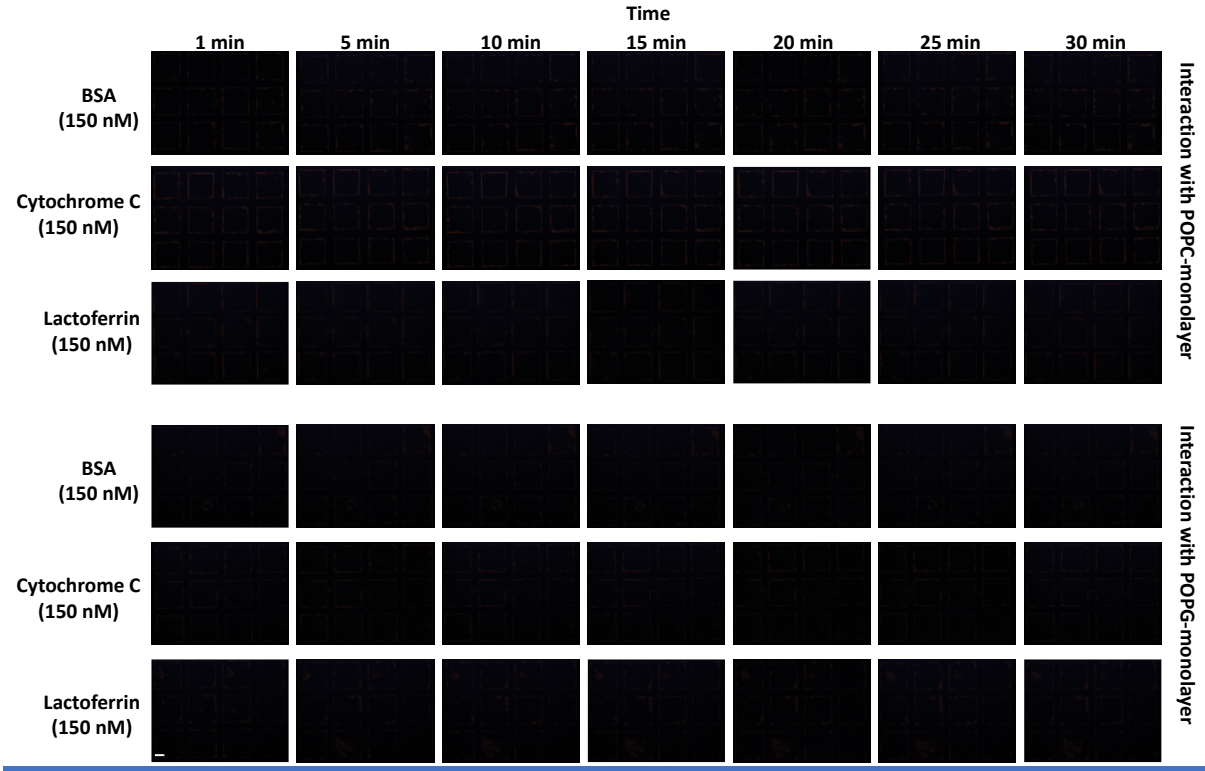

Protein	Isoelectric point	Charge at experimental pH	Molecular weight	Secondary structure
BSA	4.5	negative	66.4 KDa	α-helix
Cytochrome C	9.6	positive	12.3 KDa	α-helix
Lf	8.7	positive	80 KDa	β-sheet rich
PrP	9.57	positive	25 KDa	α-helix

Figure 4.2.7 The crossed-polarized images demonstrate the response of PC and PG laden-LC aqueous interface in the presence of different proteins, i.e., bovine serum albumin (BSA), cytochrome c, and lactoferrin (Lf). Scale bar=100 μm. The table illustrates the structural and physiological properties of proteins used in this report.

The results suggest interfacial phase segregations to PrP and lipid-rich domains where the dendritic branched domains correspond to PrP-rich regions. Also, the bright dendritic domains in PrP-incubated 5CB-aqueous interfaces under POM are composed primarily of protein. We next asked whether the β-rich aggregates formed on the PrP-lipid-LC-aqueous interface drive the dendritic patterns. To answer this, we then performed a thioflavin T (ThT) assay (amyloid marker).[19] ThT fluorescence in Figure 4.2.10b and f, respectively, illustrate green fluorescent branched domains emerging at POPC and POPC:POPG lipids laden LC-aqueous interface upon incubation with 150

nM PrP. This phenomenon is congruent with the observations presented in the bright field images in Figures 4.2.10a and e.

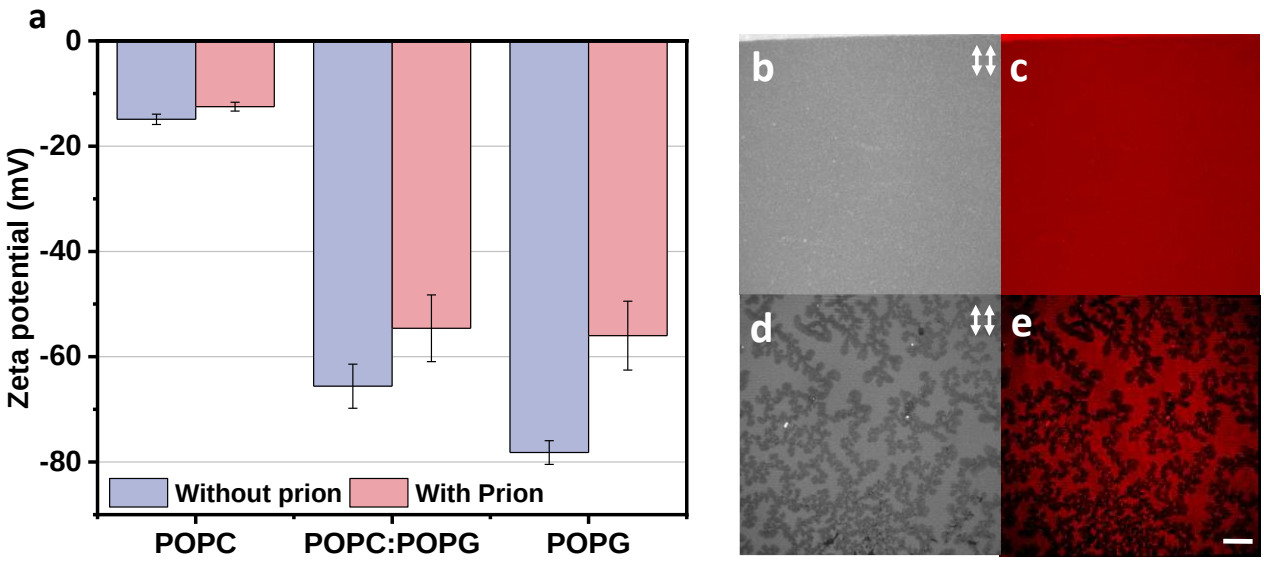

Figure 4.2.8 (a) Bar graph shows zeta-potential variations on 30 min incubation of 10 µM PrP with different lipids (POPC, 1:1 POPC:POPG and POPG) laden LC droplets. The minimum and maximum rise in surface charge potential was observed in POPC and POPG-laden LC-aqueous interfaces, respectively. Bright-field (b, d) and confocal fluorescence (c, e) images of LC-aqueous interface laden with POPC:POPG (1:1 mole ratio) and 2.5% rhodamine-DHPE mixed monolayer before (b, c) and after 30 min (d, e) addition of 150 nM PrP. Dark non-fluorescent regions in the image (e) correspond to lipid-lean or PrP-rich regions. The double-headed arrows on the top right of the image (b & d) represent the orientation of the polarizer and analyzer. Scale bar = 20 µm.

In the PrP-POPG-laden LC-aqueous interface, distinct domains were visible in the bright field image (Figure 4.2.10i). Conversely, the corresponding epifluorescence image (Figure 4.2.10j) exhibited a uniform green fluorescence without any domains. To further investigate if fluorescence appeared as a result of β-rich aggregates of PrP at the lipid interface and not because of the direct binding of ThT with the lipid monolayer, we incubated POPC, POPC/POPG, and POPG with 5 μM ThT for 15 min before imaging after 4 h (panels c, d, g, h, k and l of Figure 4.2.10). As expected, POPC and POPC/POPG did not show substantial ThT fluorescence (panels d and h of Figure 4.2.10), which is in contrast to that of the POPG-laden interface (Figure 4.2.10l). Thus, the complete green image with no fluorescent domains (Figure 4.2.10j) was attributed to the background noise due to the ThT binding with POPG lipid. Additionally, the ThT epifluorescence image of 150 nM PrP at the interface

(Figure 4.2.11) without lipid further confirmed our propositions. Overall, the results suggest lipids-induced conformational switching of PrP into β-rich structures at those interfaces.[20] Next, to visualize β-rich PrP morphology at various lipids-laden, we performed atomic force microscopy (AFM) at 30 min and a prolonged (4 h) time point. AFM scans after 30 min showed oligomers of ~30-40 nm (Figure 4.2.12) for all the samples. However, the AFM image of the sample from the POPC-laden LC-aqueous interface incubated with 150 nM PrP after 4 h depicts the formation of a random cluster and filaments of ~5-10 nm height (Figure 4.2.10m & p).

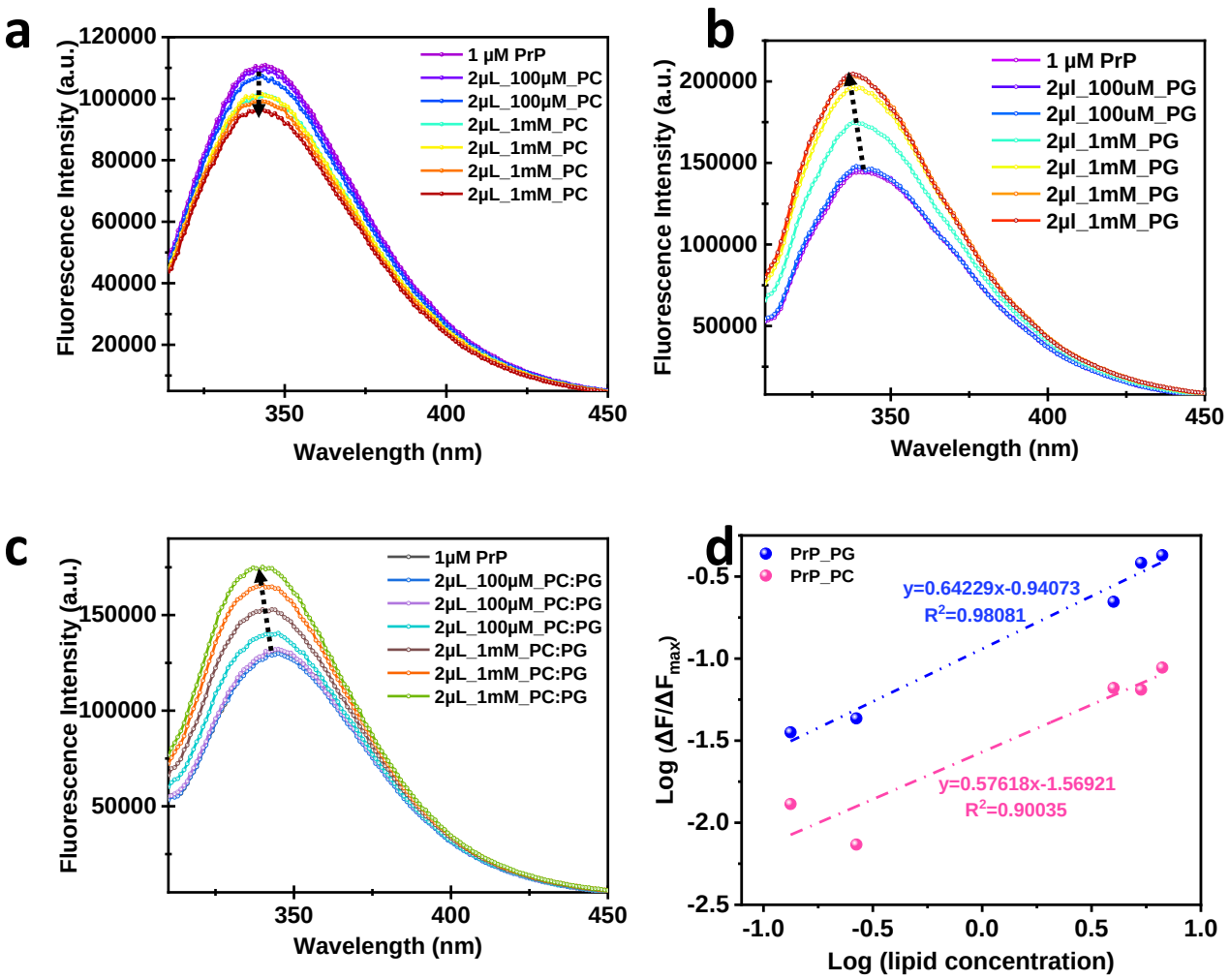

Figure 4.2.9 The fluorescence emission spectra in (a-d) depict the relative changes in 1 μM PrP tryptophan fluorescence intensity in the presence of different additions of (a) POPC, (b) POPG and (c) POPC:POPG. The plot in (d) is the double logarithmic plot between $\log(\Delta F/\Delta F_{max})$ vs log[lipids] for protein-lipid conjugations. Experimental conditions: [Sodium Phosphate buffer] = 10 mM, pH 7.4, T = 25 °C, Slit Width ex/em = 1.5/3 nm.

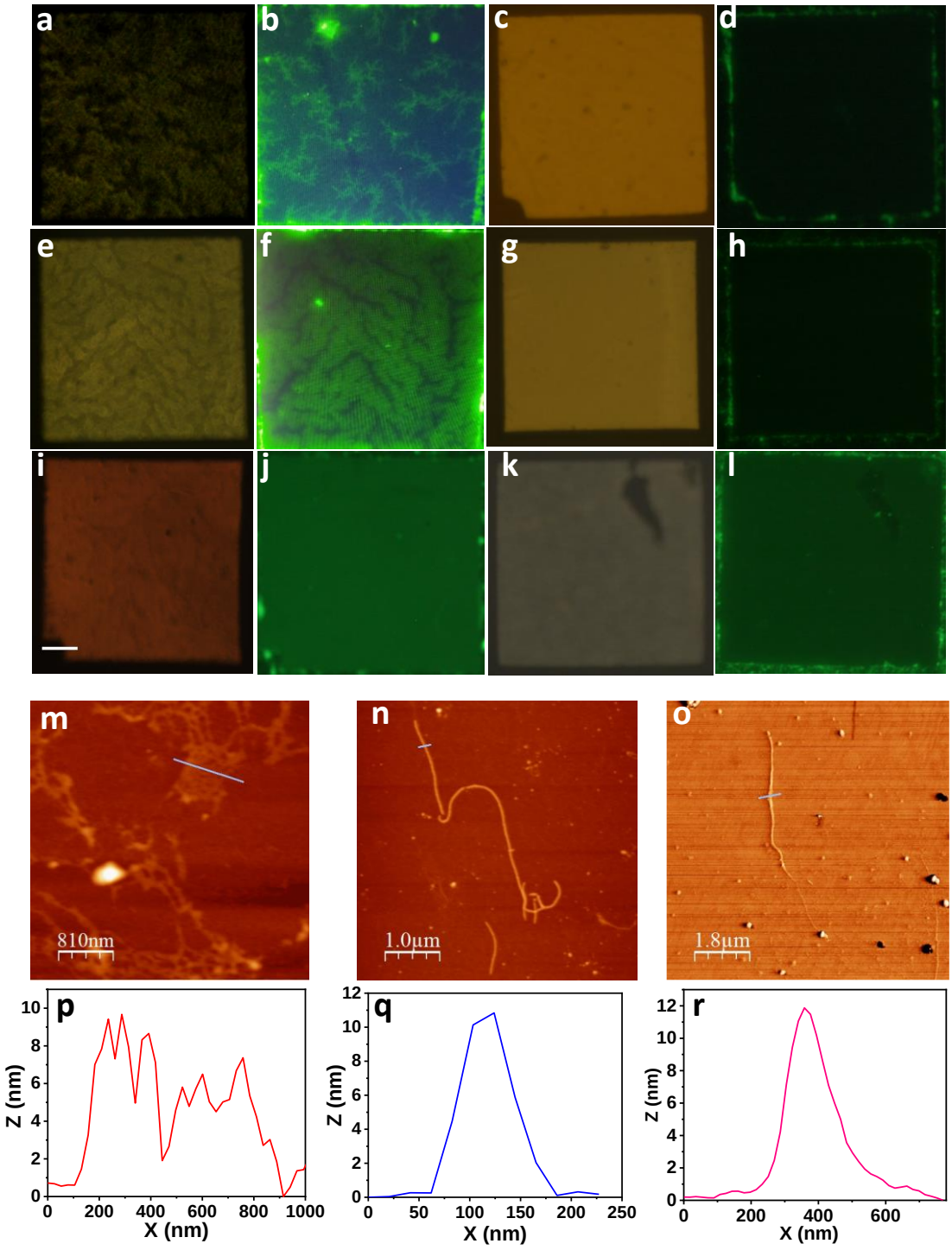

Figure 4.2.10 Bright-field images (a, e, i) captured after 4 h incubation of 150 nM PrP with (a) POPC, (e) 1:1 POPC:POPG and (i) POPG laden LC-aqueous interface. Corresponding epifluorescence images (b, f, j) pictured after 15 min incubation with 5 μM ThT. Control bright field images (c, g, k) of LC laden with (c) POPC, (g) 1:1 POPC:POPG, and (k) POPG in PrP absence. The

images depict no evolution of domains in the absence of PrP. Epifluorescence images (d, h, l) of these controlled bright-field images captured under similar fluorescent conditions demonstrate negligible fluorescence in POPC and 1:1 POPC:POPG. In contrast, green fluorescence was observed in image (l), indicating POPG direct interactions with ThT. Scale bar = 50 μm. AFM images (m, n, o) were obtained by extracting an aqueous layer from the grid decorated with m) POPC, n) 1:1 POPC:POPG, and o) POPG incubated with 150 nM PrP up to 4 h. The graphs p, q, and r represent the height profile of the cluster in the image (m) and fibrils in the image (n, o).

In summary, our findings provide strong evidence for the transformation of monomeric PrP into amyloidogenic clusters, filaments, or fibrils when in the presence of both zwitterionic and anionic lipids. Our investigations, employing AFM and ThT assays, yield consistent results, collectively indicating a conformational transition of PrP into β-rich aggregates at the selected lipid-enriched LC-aqueous interface. In addition, the sample from POPC:POPG and POPG-laden LC-aqueous interface incubated with PrP showed the formation of long amyloid fibrils with a height of ~10-12 nm (Figure 4n, q and Figure 4o, r).[21] To further validate the observation, we performed AFM of extract from lipids without PrP at LC-aqueous interface (Figure 4.2.13 a, b, c), and no fibrillar morphology was obtained.

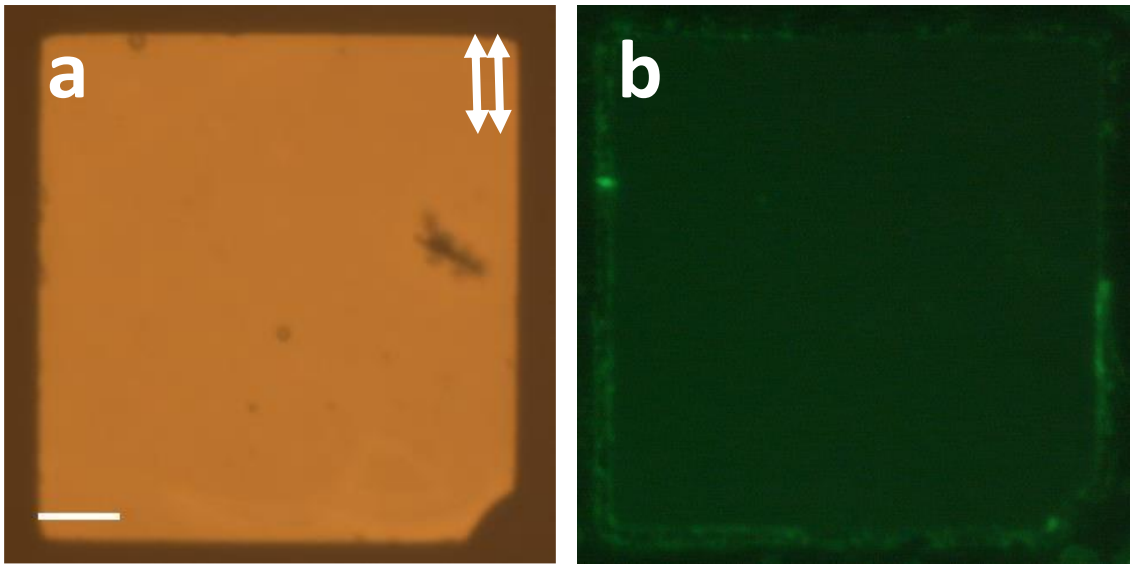

Figure 4.2.11 Bright-field (a) and epifluorescence micrographs (b) of LC-aqueous interface captured after 4 h incubation with 150 nM prion in the presence of 5 μM ThT (added 20 min before observation). The double-headed arrows on the right top of the image (a) depict the polarizer's and analyzer's relative orientations during imaging. Scale bar = 50 μm.

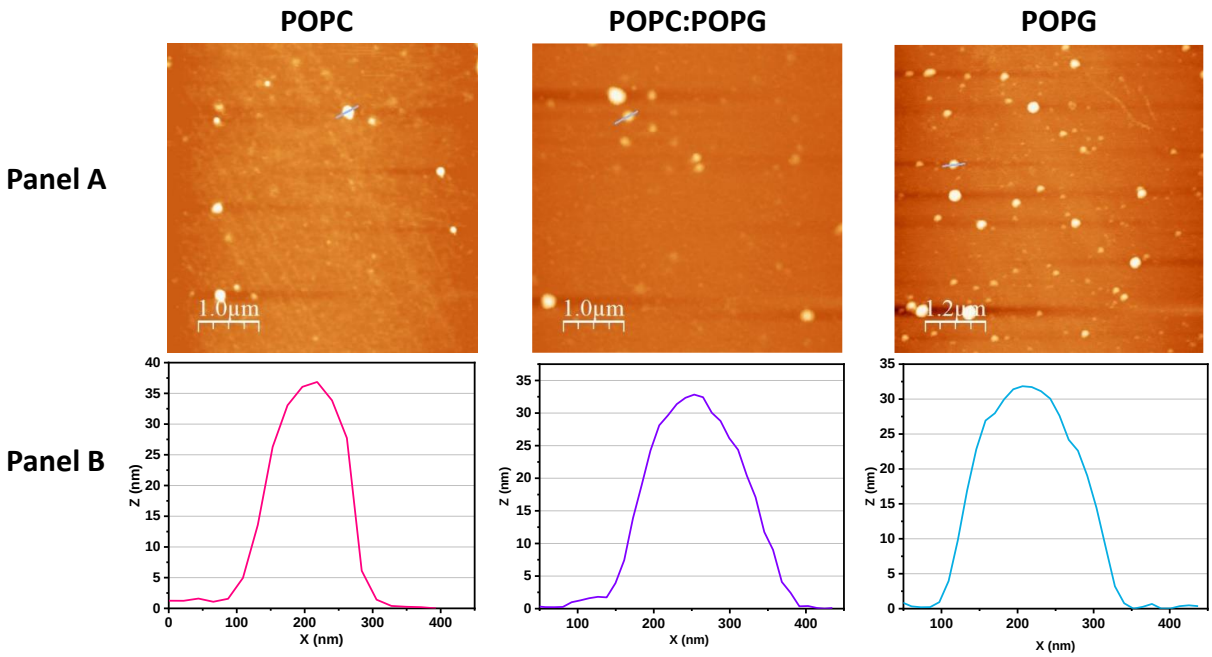

Figure 4.2.12 Panel A represents AFM imaging of extract from LC-aqueous interface laden with POPC, 1:1 POPC:POPG, and POPG after 30 min addition of prion protein. The plots in Panel B indicate the height profiles of blue-lined oligomers in Panel A.

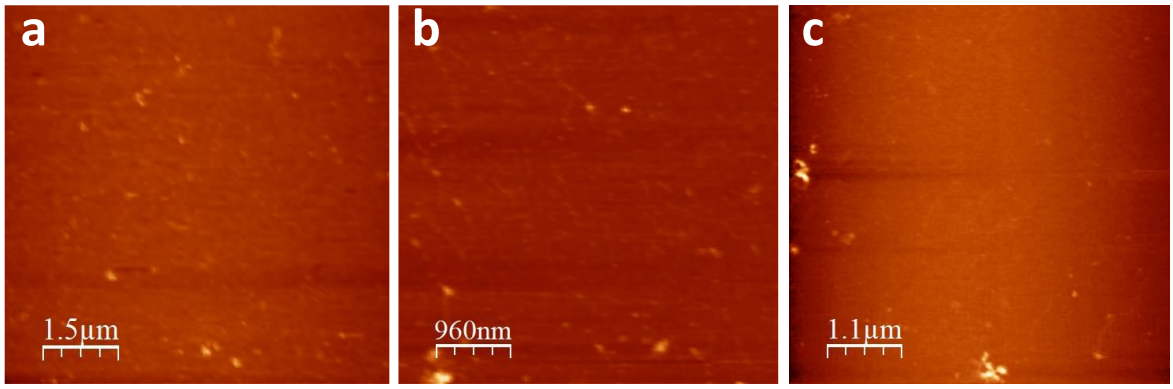

Figure 4.2.13 AFM images of extract from LC-aqueous interface after 4 h incubation in the presence of a) POPC, b) 1:1 POPC:POPG, and c) POPG lipids in the absence of prion protein. The images displayed the absence of any distinct morphological features at the interfaces.

However, a noteworthy observation pertains to the LC-aqueous interface adorned with POPC lipids, which deviates from the outcomes observed in previous bulk solution studies. These prior bulk solution studies indicated no such conformational modulations of PrP were observed upon exposure of PrP to zwitterionic POPC lipid.[2-5] The divergent behaviour in this context suggests that LC-

mediated mechanisms increase the exposure of the hydrophobic core of POPC lipids, subsequently reducing the energy barrier required for PrP unfolding. This unique behaviour underscores the significance of the LC-aqueous interface in modulating the conformational dynamics of PrP in the presence of lipid components.

4.3. Conclusions

Based on our comprehensive findings, we can conclude that electrostatic forces serve as pivotal determinants in orchestrating lipid-protein interactions during the initial binding phase. Consequently, the characteristics of the membrane interface exert a profound influence on PrP-lipid interactions, leading to a notable increase in the effective concentration of PrP at the interface. This, in turn, facilitates the establishment of short-range hydrophobic and protein-protein interactions. As a consequential outcome, the PrP molecule undergoes a process of misfolding driven by its hydrophobic interactions and assisted by the effective neutralization of electrostatic charges, ultimately resulting in enhanced aggregation into oligomers. Within the context of the LC-aqueous interface, these nanometer-sized oligomers effectively function as colloidal entities, and the specific aggregation patterns they assume are subject to modulation by chemoresponsive LCs, contingent on the densities of these oligomers at the interfaces. [22, 23]

In summary, our study introduces an efficacious LC-aqueous interfacial system for monitoring the cascade of lipid-induced conformational switching and aggregation of PrP. The devised platform exhibits exceptional sensitivity to the non-covalent forces that govern lipid-protein interactions. Our results further reveal the intriguing phenomenon of lipid membrane remodelling into dendritic domains during these interactions. Additionally, our research identifies the distinct membrane components that steer PrP either toward fibrillation or clustering at the LC-aqueous interface. It is worth noting that this is the pioneering study to investigate such aggregates at physiological concentrations, revealing two distinct growth outcomes hinging on the lipid composition of the interfacial membrane.

In conclusion, our study offers a straightforward strategy for investigating protein-lipid membrane interactions, even at sub-micromolar concentrations. Furthermore, we anticipate that our methodology holds promise for yielding valuable molecular insights into a spectrum of neurodegenerative diseases characterized by lipid-mediated protein misfolding and amyloid formation.

4.4. Experimental Procedures

4.4.1. Materials

Needed Fischer's Finest Premium Grade glass microscopic slides were purchased from Fischer Scientific (Pittsburgh, PA). For piranha cleaning of the glass slides, Sulfuric acid (H_2SO_4), Hydrogen peroxide (H_2O_2, 30% w/v), Chloroform (HPLC), and Sodium chloride (NaCl) were bought from Merck. 4′-pentyl-4-biphenylcarbonitrile (5CB), dimethyloctadecyl[3-(trimethoxysilyl)propyl]-ammonium chloride (DMOAP), thioflavin T (ThT) were purchased from Sigma Aldrich. Required lipids, i.e., 1-palmitoyl-2-oleoyl-*sn*-glycero-3-phospho-(1'-*rac*-glycerol) (sodium salt) (POPG) and 1-palmitoyl-2-oleoyl-glycero-3-phosphocholine (POPC) were bought from Avanti Polar Lipids, Inc (Alabaster, AL).

Lissamine rhodamine B 1,2-dihexadecanoyl-*sn*-glycero-3- phosphoethanolamine, triethylammonium salt (rhodamine DHPE) was purchased from Molecular Probe, Invitrogen. Guanidinium hydrochloride (GdmCl) used for purification was obtained from Amresco. All buffers were prepared using Milli-Q water, and the required pH was adjusted using a Metrohm 827 lab pH meter at room temperature (~25 °C). The Millipore technology (Bedford, MA) was used to obtain Milli-Q water. Gold grids of 20 μm thickness (50 μm wide, 283 μm grid spacing) were from Electron Microscopy Sciences (Fort Washington, PA).

4.4.2. Piranha Cleaning and Coating of Glass Slides

According to established protocols, glass slides were cleaned with piranha solution (H_2SO_4:H_2O_2 (v/v) = 70:30).[24] Concisely, the glass slides in a glass jar were submerged in the freshly prepared piranha solution and placed in a water bath at 80 ˚C for 1 h. After that, ethanol and deionized water were used to rinse the slides. Following this, the glass slides were dried by purging nitrogen gas and kept in the oven at 100 ˚C for at least 3 h.

In order to coat the cleaned glass slides with a hydrophobic medium, the glass slides were then immersed in 0.1 % (v/v) DMOAP aqueous solution in DI water for 30 min at room temperature. After that, washing was done to eliminate the surplus DMOAP before drying with nitrogen purging. Furthermore, these slides were heated in the oven for 3-6 hours to allow cross-linking to create a siloxane bond.[25]

The chemical modification of the glass slide's surface with a hydrophobic medium led to hydrophobic interactions between the octadecyl chains of the DMOAP and the alkyl tails of 5CB molecules, encouraging a perpendicular alignment of LC molecules to the substrate.

4.4.3. Preparation of lipids monolayers

Lipid Langmuir films were prepared using a Langmuir-Blodgett trough attached to the KSV Minimicro film balance and equipped with a filter paper Wilhelmy plate for surface pressure measurements.[26] The trough was filled with sodium phosphate buffer (pH ~ 7.4). Chloroform solution of the required lipid at a concentration of 1 mg/ml was gently dispersed at the air interface of the buffer. The chloroform solution was allowed to evaporate for 15 min by adding a known volume of the required lipid. Then, the barriers were symmetrically compressed at a 5 mm/min compression rate. KSV Nima software was used to compute the surface pressure against the area per molecule, plotted in Origin 9.65.

4.4.4. Expression and Purification of Prion

The expression and purification of Prion have been done by Lisha Arora, a group member of our collaborator Dr. Samrat Mukhopadhyay's lab (IISER Mohali). We have used it as a reagent for our study, which the collaborator has kindly provided. The work of the collaborator has been acknowledged and well respected. Briefly, recombinant full-length human prion protein (23−231) with N-terminal His-tag cloned in pRSET B vector was transformed in *E.coli* strain BL21(DE3) pLysS and was purified using previously published protocols.[21]

The details are also provided in the following reference.

Gupta, T.; Arora, L.; Mukhopadhyay, S.; Pal, S. K., Ultrasensitive Detection of Lipid-Induced Misfolding of the Prion Protein at the Aqueous-Liquid Crystal Interface. *J. Phys. Chem. Lett.* **2024**, *15*, 8, 2117–2122.

4.4.5. Preparation and optical characterization of lipid-laden, LC-Filled Specimen Grid

DMOAP-treated glass slides were cut into small square pieces and mounted with gold specimen grids. Using a blunt-tipped syringe, the grids were loaded with roughly 0.2 μL of 5CB such that the LC was distributed equally. In order to form a flat LC film with constant thickness, an excess of 5CB was removed using a Hamilton syringe.[26-36]

Grid inversion was possible without losing LCs from the grids as the capillary forces held the 5CB inside the grids. Further, to decorate LC films with the desired lipid, the LC-filled grids were brought into horizontal contact with the air-water interface using tweezers and then instantly dipped into the subphase.[26]

The procedure was followed after attaining a particular surface pressure of lipid corresponding to 1.25 molecule/ nm^2 lipid areal density. After this procedure, the glass slide was dipped into an optical well with 2 ml of sodium phosphate buffer (7.4 pH). Polarized light was used in transmission mode to accomplish optical imaging of the LC interfaces on the Olympus CX31 and Zeiss Axio Scope1 Polarizing Optical Microscope (POM). The relative orientation of LC is determined in polarized optical microscopy by measuring the amount of polarized light that passes through an LC sample using two polarizers. The required amount of prion protein was added to the buffer containing lipid-decorated LC films to further study prion interactions with the desired lipid. Again, the system was optically imaged under POM.

ImageJ was used to determine the average grayscale intensity of the polarized optical micrographs under a constant light source. All the experiments were repeated at least three times at room temperature.[25]

4.4.6. Confocal Microscope Imaging

Confocal microscopic imaging was done to visualize lipid-doped localization with 2.5% rhodamine DHPE fluorescent dye. Samples were prepared to form mixed lipids, i.e., 1:1 POPC:POPG (1 mg/ml) and doped DHPE monolayer at the LC interface. A 63 long-distance water-immersed objective with hybrid detectors was utilized to image the sample.

Image acquisition was set to 512×512 pixels with a 400 Hz scanning rate. A 561 nm diode-pumped solid-state (DPSS) laser source was used to excite rhodamine DHPE fluorescent dye. Confocal image stacks were captured using a photomultiplier tube (PMT) detector in SP8 upright confocal microscope.

4.4.7. LC droplets preparation and zeta potential Measurements

To measure zeta potential variations at the LC surface, we employed LC droplets by adding 1 µl 5CB into 100 µl of buffer or 1 mg/ml of lipids.[36] The dispersions were prepared by vortexing for 1 minute at 3,000 rpm, followed by 1 min homogenizer emulsification.

For the PrP studies, 10 µl of the PrP stock solution was added to the 40 µl of the lipids–5CB droplet emulsion to create a 10 µM concentration of PrP. After 15 min of incubation, the solution was diluted to 800 µl. Zetasizer Nano ZS90 instrument (Malvern Instruments Inc.) was used to measure the zeta potential at room temperature with a cell-driven voltage of 30 V.[27]

4.4.8. Intrinsic fluorescence of PrP with various lipids

Fluorescence studies were conducted on PrP using a concentration of 1 µM. The solution was titrated with different lipids in a quartz cuvette with a path length of 1 cm. The excitation wavelength was set at 280 nm, and the emission spectra were recorded in the range of 300 to 500 nm. Binding constants were determined by plotting a double logarithmic graph of $[\log(F_0\text{-}F/\Delta F_{max})]$ versus log [lipid].[18] The excitation and emission slit widths were 1.5 and 3 nm.

4.4.9. Epifluorescence microscopy

Using the green fluorescent protein (GFP) filter of the Zeiss (Scope A1) fluorescent microscope, ThT fluorescence imaging was performed, as previously reported. Samples were prepared by incubating 150 nM prion with desired lipid monolayer laden LC-aqueous interface up to 4 h. 5 µM ThT was added 20 min before imaging.[20]

4.4.10. Atomic force microscopy (AFM)

For AFM, 150 nM prion was incubated with a lipid-laden LC-aqueous interface up to the desired time point (i.e., 30 min or 4 h) and then extracted ~ 50 µl of buffer sample from the interface and placed on the Silicon wafer (Si). The sample was left undisturbed for air drying. After drying, the wafer was flushed with 100 µl milli-Q water and dried by purging nitrogen. The AFM images were captured by the Innova Bruker AFM in tapping mode using an antimony-coated silicon tip with an 8 nm radius. WSxM software was used to process the images.[36, 37]

4.4.11. Circular Dichroism (CD)

Far-UV circular dichroism (CD) investigations were carried out employing a Chirascan spectrophotometer, a product of Applied Photophysics in the United Kingdom. This high-precision instrument featured a scan range spanning from 200 to 280 nm, with incremental steps of 1 nm. The solution under scrutiny was enclosed within a quartz cell characterized by a path length of 1 mm.[38-41] For these experiments, freshly prepared aqueous solutions containing 10 µM concentrations of the PrP were employed. These solutions were meticulously prepared in a 10 mM buffer solution at a pH

of 7.4. In order to examine the conformational changes occurring in PrP during its interaction with POPG, a solution containing 10 μM of PrP was subjected to a one-hour incubation period with lipids at a concentration of 1 mg/ml.

The entire process of data acquisition and subsequent analysis was executed using the ProData software, which was supplied alongside the CD instrument. Each spectrum was constructed by averaging the results of 5 scans and subsequently adjusted against the buffer signal to ensure precise and reliable analysis.

4.4.12. Statistics

The data are reported as means ± standard error of the mean. A multifactorial repeated measures ANOVA was employed,[42-44] to examine variations in the mean grayscale intensities of LC-aqueous interfaces laden with various lipids in the presence of prion protein.

Subsequently, Tukey's post-hoc analysis was conducted to delve deeper into the findings. Statistical significance was determined at $p < 0.05$.

4.5. Author Contributions

TG has conceptualized and devised the framework for the project. TG meticulously executed all experimental procedures and conducted a thorough analysis of the resulting data. LA purified the Prion protein. The expression and purification of Prion have been done by Lisha Arora, a group member of our collaborator Dr. Samrat Mukhopadhyay's lab (IISER Mohali). We have used it as a reagent for our study, which the collaborator has kindly provided. SKP and SM did the overall project administration.

4.6. Acknowledgement

S.K.P. acknowledge MOE/STARS1/284. T.G. acknowledges CSIR (09/947/(0223)/2019-EMR-1) for a fellowship. T.G. acknowledges powerpoint, chemdraw, pymol and chimera tools for various cartoons and protein structures used in the table of contents (TOC) graphics. T.G. is grateful to the American Chemical Society for giving the permission to reuse/reproduce the whole article in my thesis which is well acknowledged and respected.

The links of the article are https://pubs.acs.org/doi/10.1021/acs.jpclett.3c02770 ; https://doi.org/10.1021/acs.jpclett.3c02770.

References

1. Prusiner, S. B., *Prion Biology and Diseases.* Gold Spring Harbour Laboratory Press: New York, 2017.

2. Baskakov, I. V.; Legname, G.; Prusiner, S. B.; Cohen, F. E., Folding of prion protein to its native α-helical conformation is under kinetic control. *J. Biol. Chem.* **2001,** *276* (23), 19687-90.

3. Agarwal, A.; Das, D.; Banerjee, T.; Mukhopadhyay, S., Energy migration captures membrane-induced oligomerization of the prion protein. *Biochim. Biophys. Acta. Proteins Proteom* **2020,** *1868* (2), 140324.

4. Wang, F.; Yang, F.; Hu, Y.; Wang, X.; Wang, X.; Jin, C.; Ma, J., Lipid interaction converts prion protein to a PrPSc-like proteinase K-resistant conformation under physiological conditions. *Biochemistry* **2007,** *46* (23), 7045-53.

5. Critchley, P.; Kazlauskaite, J.; Eason, R.; Pinheiro, T. J., Binding of prion proteins to lipid membranes. *Biochem. Biophys. Res. Commun.* **2004,** *313* (3), 559-67.

6. Robinson, P. J.; Pinheiro, T. J., Phospholipid composition of membranes directs prions down alternative aggregation pathways. *Biophys. J.* **2010,** *98* (8), 1520-8.

7. Brake, J. M.; Daschner, M. K.; Luk, Y. Y.; Abbott, N. L., Biomolecular interactions at phospholipid-decorated surfaces of liquid crystals. *Science* **2003,** *302* (5653), 2094-7.

8. Yang, X.; Li, H.; Zhao, X.; Liao, W.; Zhang, C. X.; Yang, Z., A novel, label-free liquid crystal biosensor for Parkinson's disease related α-synuclein. *Chem. Commun.* **2020,** *56* (40), 5441-5444.

9. Lockwood, N.; Gupta, J.; Abbott, N., Self-assembly of amphiphiles, polymers and proteins at interfaces between thermotropic liquid crystals and aqueous phases. *Surf. Sci. Rep.* **2008,** *63* (6), 255-293.

10. Carlton, R. J.; Hunter, J. T.; Miller, D. S.; Abbasi, R.; Mushenheim, P. C.; Tan, L. N.; Abbott, N. L., Chemical and biological sensing using liquid crystals. *Liq. Cryst. Rev.* **2013,** *1* (1), 29-51.

11. Manna, U.; Zayas-Gonzalez, Y. M.; Carlton, R. J.; Caruso, F.; Abbott, N. L.; Lynn, D. M., Liquid crystal chemical sensors that cells can wear. *Angew. Chem. Int. Ed.* **2013,** *52* (52), 14011-14015.

12. Tercero, M. D. D.; Abbott, N. L., Ordering transitions in liquid crystals permit imaging of spatial and temporal patterns formed by proteins penetrating into lipid-laden interfaces. *Chem. Eng. Commun.* **2008,** *196* (1-2), 234-251.

13. Tan, L. N.; Orler, V. J.; Abbott, N. L., Ordering transitions triggered by specific binding of vesicles to protein-decorated interfaces of thermotropic liquid crystals. *Langmuir* **2012,** *28* (15), 6364-76.

14. Perera, K.; Dassanayake, T. M.; Jeewanthi, M.; Haputhanthrige, N. P.; Huang, S. D.; Kooijman, E.; Mann, E.; Jákli, A., Liquid Crystal-Based Detection of Antigens with ELISA Sensitivity. *Adv. Mater. Interfaces* **2022,** *9* (25), 2200891.

15. Daschner De Tercero, M.; Abbott, N. L., Ordering Transitions in Liquid Crystals Permit Imaging of Spatial and Temporal Patterns Formed by Proteins Penetrating into Lipid-Laden Interfaces. *Chem. Eng. Commun.* **2008,** *196* (1-2), 234-251.

16. Brake, J. M.; Daschner, M. K.; Abbott, N. L., Formation and characterization of phospholipid monolayers spontaneously assembled at interfaces between aqueous phases and thermotropic liquid crystals. *Langmuir***,** *21* (6), 2218-2228.

17. Wang, X.; Yang, P.; Mondiot, F.; Li, Y.; Miller, D. S.; Chen, Z.; Abbott, N. L., Interfacial ordering of thermotropic liquid crystals triggered by the secondary structures of oligopeptides. *Chem. Commun.* **2015,** *51* (94), 16844-7.

18. Tedesco, A. C.; Oliveira, D. M.; Lacava, Z. G. M.; Azevedo, R. B.; Lima, E. C. D.; Gansau, C.; Buske, N.; Morais, P. C., Determination of binding constant K_b of biocompatible, ferrite-based magnetic fluids to serum albumin. *J. Appl. Phys.* **2003,** *93* (10), 6704-6706.

19. Xue, C.; Lin, T.; Chang, D.; Guo, Z., Thioflavin T as an amyloid dye: fibril quantification, optimal concentration and effect on aggregation. *R. Soc. Open Sci.* **2017**, 4, 16069615.

20. Sadati, M.; Apik, A. I.; Armas-Perez, J. C.; Martinez-Gonzalez, J.; Hernandez-Ortiz, J. P.; Abbott, N. L.; de Pablo, J. J., Liquid Crystal Enabled Early Stage Detection of Beta Amyloid Formation on Lipid Monolayers. *Adv. Funct. Mater.* **2015,** *25* (38), 6050-6060.

21. Pani, I.; Madhu, P.; Najiya, N.; Aayush, A.; Mukhopadhyay, S.; Pal, S. K., Differentiating Conformationally Distinct Alzheimer's Amyloid-β Oligomers Using Liquid Crystals. *J. Phys. Chem. Lett.* **2020,** *11* (21), 9012-9018.

22. Andrienko, D.; Tasinkevych, M.; Dietrich, S., Effective pair interactions between colloidal particles at a nematic-isotropic interface. *Europhys. Lett.* **2005,** *70* (1), 95-101.

23. Koenig, G. M., Jr.; Lin, I. H.; Abbott, N. L., Chemoresponsive assemblies of microparticles at liquid crystalline interfaces. *Proc. Natl. Acad. Sci. U. S. A.* **2010,** *107* (9), 3998-4003.

24. Brake, J. M.; Abbott, N. L., An Experimental System for Imaging the Reversible Adsorption of Amphiphiles at Aqueous−Liquid Crystal Interfaces. *Langmuir* **2002,** *18* (16), 6101-6109.

25. Gupta, T.; Mondal, A. K.; Pani, I.; Chattopadhyay, K.; Pal, S. K., Elucidating liquid crystal-aqueous interface for the study of cholesterol-mediated action of a β-barrel pore forming toxin. *Soft Matter* **2022,** *18* (28), 5293-5301.

26. Meli, M. V.; Lin, I. H.; Abbott, N. L., Preparation of microscopic and planar oil-water interfaces that are decorated with prescribed densities of insoluble amphiphiles. *J. Am. Chem. Soc.* **2008,** *130* (13), 4326-33.

27. Das, D.; Sidiq, S.; Pal, S. K. A Simple Quantitative Method to Study Protein-Lipopolysaccharide Interactions by Using Liquid Crystals. *ChemPhysChem* **2015**, *16*, 753−760.

28. Pani, I.; Swasthi, H. M.; Mukhopadhyay, S.; Pal, S. K. Design of aqueous-liquid crystal interfaces to monitor protein aggregation at nanomolar concentrations. *J. Phys. Chem. C* **2019**, *123*, 1305-1312.

29. Popov, P.; Honaker, L. W.; Kooijman, E. E.; Mann, E. K.; Jákli, A. I. A liquid crystal biosensor for specific detection of antigens. *Sens. Biosensing Res.* **2016**, *8*, 31-35.

30. Noonan, P. S.; Mohan, P.; Goodwin, A. P.; Schwartz, D. K., DNA Hybridization-Mediated Liposome Fusion at the Aqueous Liquid Crystal Interface. *Adv. Funct. Mater.* **2014**, *24*, 3206-3212.

31. Price, A. D.; Schwartz, D. K., DNA Hybridization-Induced Reorientation of Liquid Crystal Anchoring at the Nematic Liquid Crystal/Aqueous Interface. *J. Am. Chem. Soc.* **2008**, *130*, 8188-8194.

32. Park, C. S.; Iwabata, K.; Sridhar, U.; Tsuei, M.; Singh, K.; Kim, Y.-K.; Thayumanavan S.; Abbott, N. L., A New Strategy for Reporting Specific Protein Binding Events at Aqueous–Liquid Crystal Interfaces in the Presence of Non-Specific Proteins. *ACS Appl. Mater. Interfaces* **2020**, *12*, 7869-7878.

33. Eimura, H.; Miller, D. S.; Wang, X.; Abbott, N. L.; Kato, T., Self-Assembly of Bioconjugated Amphiphilic Mesogens Having Specific Binding Moieties at Aqueous–Liquid Crystal Interfaces. *Chem. Mater.* **2016**, *28*, 1170-1178.

34. Das, D.; Sidiq, S.; Pal, S. K., Design of bio-molecular interfaces using liquid crystals demonstrating endotoxin interactions with bacterial cell wall components. *RSC Adv.* **2015,** *5* (81), 66476-66486.

35. Das, D.; Pal, S. K., Liquid Crystal Unveiled Interactions between Melittin and Phospholipids at Aqueous-Liquid Crystal Interface. *ChemistrySelect* **2017,** *2* (17), 4779-4786.

36. Verma, I.; Sidiq, S.; Pal, S. K., Poly(l-lysine)-Coated Liquid Crystal Droplets for Sensitive Detection of DNA and Their Applications in Controlled Release of Drug Molecules. *ACS Omega* **2017,** *2* (11), 7936-7945.

37. Horcas, I.; Fernandez, R.; Gomez-Rodriguez, J. M.; Colchero, J.; Gomez-Herrero, J.; Baro, A. M., WSXM: a software for scanning probe microscopy and a tool for nanotechnology. *Rev. Sci. Instrum.* **2007,** *78* (1), 01370.

38. Ranjbar, B.; Gill, P., Circular dichroism techniques: biomolecular and nanostructural analyses-a review. *Chem. Biol. Drug* **2009**, *74*(2), 101-120.

39. Frank, B.; Yin, X.; Schäferling, M.; Zhao, J.; Hein, S. M.; Braun, P. V.; Giessen, H.; Large-area 3D chiral plasmonic structures. *ACS Nano* **2013**, *7*(7), 6321-6329.

40. Lubitz, I.; Zikich, D.; Kotlyar, A., Specific high-affinity binding of thiazole orange to triplex and G-quadruplex DNA. *Biochemistry* **2010**, *49*(17), 3567-3574.

41. Borovok, N.; Molotsky, T.; Ghabboun, J.; Porath, D.; Kotlyar, A., Efficient procedure of preparation and properties of long uniform G4–DNA nanowires. *Anal. Biochem.* **2008**, *374*(1), 71-78.

42. Gehlert, S.; Bungartz, G.; Willkomm, L.; Korkmaz, Y.; Pfannkuche, K.; Schiffer, T.; Bloch, W.; Suhr, F., Intense resistance exercise induces early and transient increases in ryanodine receptor 1 phosphorylation in human skeletal muscle. *PLoS One* **2012**, *7*(11), 49326.

43. O'Leary, B. M.; Lee, C. P.; Atkin, O. K.; Cheng, R.; Brown, T. B.; Millar, A. H., Variation in leaf respiration rates at night correlates with carbohydrate and amino acid supply. *Plant physiol.* **2017**, *174*(4), 2261-2273.

44. Ghosh, D. K.; Seth, R.; Shah, N. D., Use of control charts for conducting ANOVA study. *Int. J. Agricult. Stat. Sci.* **2019,** *15*(1), 375-384.

Chapter 5

Liquid Crystals-Aqueous Interfaces Render Selective Detection of Distinctive Mycobacterial Cell Envelope Responses

Antibiotic-resistant infectious tuberculosis, attributed to *Mycobacterium tuberculosis (Mtb)*, remains a significant global health concern.[1-4] Herein, we utilize the interfacial properties of liquid crystal (LC) to gain insight into the spatiotemporal modifications of *Mtb* envelopes.

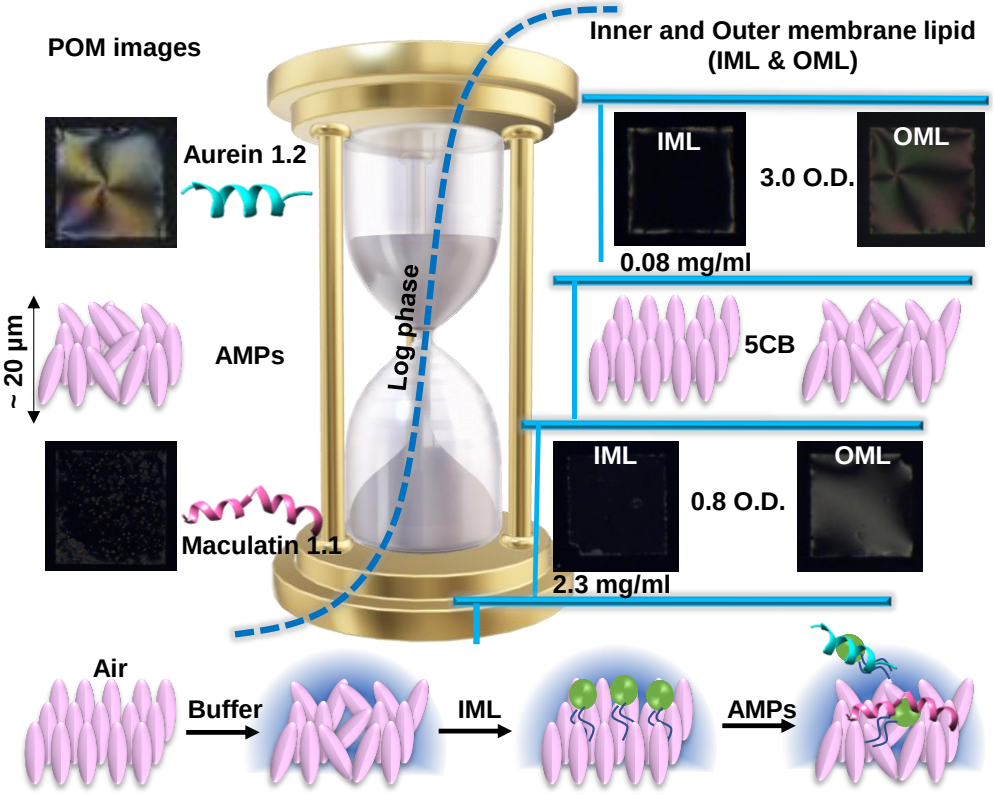

The optical responses of LC have revealed a disorganization of outer membrane lipids relative to inner membrane lipids, highlighting the adaptability of *Mtb*. This adaptability is characterized by significant evolutions in their spatial envelopes throughout their lifespan. The research underscores the capability of Austrian frog antimicrobial peptides (AMPs) to augment membrane permeability, thus facilitating the entry of drugs into bacterial cells. Thus, the LC-biointerface serves as a sensitive tool for elucidating the molecular mechanisms behind AMP-mediated antibiotic sensitization of bacterial membranes under physiological conditions.

Gupta, T.; Menon P A.; Kapoor S.; Pal, S. K., Liquid crystals-aqueous interfaces render selective detection of distinctive mycobacterial cell envelope responses. (*Manuscript submitted*)

5.1. Introduction

Antibiotic-resistant *Mycobacterium tuberculosis* (*Mtb*) stands as the causative agent responsible for tuberculosis, a global health concern.[1] The formidable challenge in combating *Mtb* arises from its complex lipid composition within the cell envelope, impeding the development of effective antibiotics.[2-4] Mycobacteria consist of unusual lipids such as long-chained (C60-C90) mycolic acids (MA), glycolipids such as GPLs (glycopeptidolipids), TDM (trehalose dimycolate) having MA chains and cyclopropane rings, PDIM (phthiocerol dimycocerosate) and sulfolipids (SLs) having methyl branches and hydroxylated kinks.[5] Furthermore, there is a correlation (albeit less explored) between mycobacterial lipidome during various stages of infection and differential sensitivity to different classes of antibiotics.[6] Thus, understanding these lipids is crucial for developing membrane-centric chemotypes and/or modifying existing routes for better drug uptake.[7] For the latter, antimicrobial peptides (AMPs) known for their membrane activity may spur drug uptake.[8, 9] Importantly, the growing trend of targeting mycobacterial membranes requires the development of sensitive, label-free screening systems for studying membrane properties in response to various conditions. To address this issue and enhance our arsenal against drug resistance, a profound understanding of *Mtb's* lipid structure becomes imperative. Liquid crystals (LCs) at their aqueous interface have emerged as valuable sensing tools due to their unique properties, such as low surface anchoring energy and responsiveness to disturbances.[10-17] Polarized optical microscopy (POM) of thermotropic nematic LC thin films can capture molecular reorientations, making them excellent indicators of biomolecular binding, membrane transitions and membrane-protein interactions at aqueous interfaces.[17-26]

In this work, using LC-based aqueous interface, we evaluated the conformational differences between the inner and outer membrane envelopes (IML & OML, respectively) of *Mycobacterium smegmatis* (*Msm,* a lab model for *Mtb)*[8] in response to distinct growth phases, which altered bacterial lipidome. Conformational attributes of these membrane layers underlined the sensitivity towards the LC interface. Next, we revealed distinct actions and sensitivities of two different AMPs, aurien and maculatin, on IML contingent upon growth states. Collectively, this work substantiates the use of LC-based optical detection to (a) correlate LC responses with mycobacterial lipid membrane organization and biophysical

properties governed by compositional differences and (b) to decipher the action of AMP and hence serve as an efficient screening avenue against membrane centric drugs/approaches.

5.1.1. Objectives

In the context of described investigation, our research endeavours are guided by several objectives. Firstly, our primary aim is to elucidate the distinctions inherent in the interfaces of the inner and outer membrane envelopes (IML & OML) of the bacterium under consideration. This involves a comprehensive exploration of the structural and compositional variances existing between these two membrane layers.

Secondly, we embark on an analysis of the impact of the growth phase of the bacterium on the aforementioned envelopes. By scrutinizing how the growth phase influences the characteristics and properties of the inner and outer membranes, we aim to discern any consequential alterations in their behaviours at the interfaces. This aspect of our study addresses the dynamic nature of bacterial membranes during different stages of growth, providing a nuanced understanding of the interplay between the growth phase and membrane behaviour.

Thirdly, our investigation delves into the nuanced examination of the specific actions undertaken by AMPs on membranes derived spatiotemporally from *Mtb*. This entails a meticulous exploration of the spatiotemporal variations in *Mtb's* membranes and the corresponding effects induced by the application of AMPs. Through this multifaceted approach, we aspire to uncover the intricacies characterizing the interactions between AMPs and *Mtb* membranes, aiming to contribute valuable insights into the underlying mechanistic processes. In summary, our study is designed to achieve a multifaceted understanding of the complex dynamics at play within the interfaces of the inner and outer membrane envelopes of the bacterium, with a focus on the influence of bacterial growth phases. Furthermore, the investigation extends to the detailed actions of AMPs on spatiotemporally derived *Mtb* membranes, with the overarching goal of unravelling the intricacies of the interactions between AMPs and *Mtb* membranes, thereby advancing our comprehension of the associated molecular mechanisms.

5.2. Result and Discussion

To achieve our goals, we introduced a novel approach involving the use of a nematic thermotropic liquid crystal, 5CB (4'-pentyl-4-biphenylcarbonitrile), at biomolecular interfaces. Our initial investigation aimed to explore potential differences within the IML & OML of *Mtb* by examining their interactions at the 5CB-aqueous interface. To do this, we prepared a thin 5CB film supported by a gold grid on a substrate coated with DMOAP and immersed it in a Tris buffer solution. Consistent with previous findings, we observed a planar alignment of 5CB due to its hybrid orientations at the aqueous interfaces.[18-20]

Next, we introduced lipid vesicles composed of spatially derived IML & OML extracted from *Mycobacterium smegmatis (Msm)* as a model for *Mtb*. These lipids were obtained from different *Msm* envelopes grown to various optical densities (O.D.), labelled as IML O.D. and OML O.D. It was noticed that the addition of 0.08 mg/ml of IML 3.0 resulted in the dark appearance of 5CB within 5 min (Figure 5.2.1a). In contrast, OML 3.0 failed to do so, even with a higher concentration of 4 mg/ml (Figure 5.2.1b). These findings imply some kind of variations in the spatially derived lipids of these bacteria.

Our next goal was to investigate whether different growth phases of the bacteria would result in distinct observations at these interfaces. To explore this, we extracted IML and OML during the early growth phase of the bacteria at 0.8 O.D. When different amounts of IML 0.8 were introduced to the 5CB-aqueous interface, we observed a consistent dark optical appearance of 5CB at 2.3 mg/ml (Figure 5.2.1c). In contrast, even 4 mg/ml of OML 0.8 did not induce the dark appearance of 5CB (Figure 5.2.1d). These collective observations suggest significant modifications in the spatially & temporally controlled extracted lipids from the bacteria. This implied that conformational variations within the IML and OML lipids impact their alignment at the interface. In fact, IML 3.0 is reported to have higher fluidity, leading to facile interaction with the LC interface.[27]

To elucidate the intricate relationship between molecular configurations of lipids and their behaviour at aqueous-5CB interfaces, we fabricated Langmuir-Blodgett (LB) monolayers and evaluated their characteristics at air-water interfaces. Four key insights emerge from the LB isotherms: (i) OML exhibits a lower collapse pressure (CP) compared to IML; (ii) lipids with lower O.D. display a lower CP; (iii) IML experiences a sharp increase in surface pressure at

a smaller molecular area compared to OML; (iv) IML attains a smaller molecular area at the CP compared to OML (Table 1).

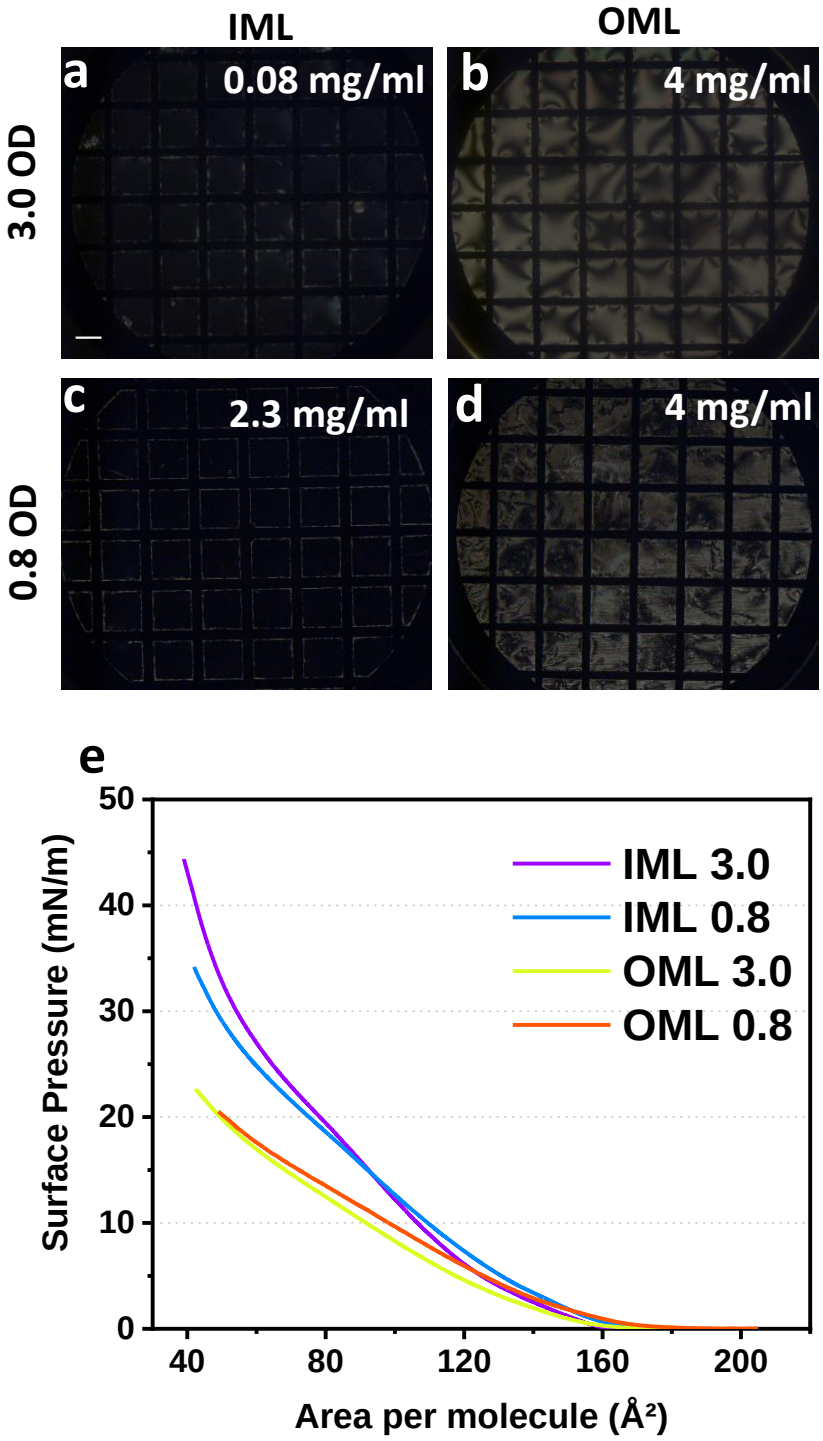

Figure 5.2.1. Polarized optical images (a-d) of the 5CB-aqueous interface were captured 10 min after the addition of (a) 0.08 mg/ml inner membrane lipid with an O.D. of 3.0 (IML 3.0); (b) 4 mg/ml outer membrane lipid with an O.D. of 3.0 (OML 3.0); (c) 2.3 mg/ml inner

membrane lipid with an O.D. of 0.8 (IML 0.8); and (d) 4 mg/ml outer membrane lipid with an O.D. of 0.8 (OML 0.8). Scale bar = 200 μm. The graph in (e) represents the surface pressure (π)−area density Langmuir-Blodgett (LB) monolayer isotherms of different spatiotemporally controlled extracted lipids from *Msm*.

Table 1. Comparison of the key parameters obtained from the LB isotherms for monolayers formed by spatiotemporally controlled extracted lipids.

Lipid Type	Optical density (O.D.)	surface pressure at the collapse ($mN\ m^{-1}$)	molecular area at collapse ($Å^2$)	onset of surface pressure ($Å^2$)
IML	0.8	34.182	41.97	171.25
IML	3.0	44.38	39.04	160.36
OML	0.8	20.532	49	184.69
OML	3.0	22.649	42.5	171.79

The sharp rise in collapse pressure, reduced molecular area at collapse, and higher collapse pressure observed in IML and high O.D. lipids indicate a consistent perpendicular alignment, densely packed, and well-organized assemblies within the compressed monolayer interface. Consequently, these LB isotherm findings highlight that OML lipids have a lower areal density and less organization, rendering them incapable of effectively aligning 5CB compared to IML. In summary, we can assert a stable arrangement of lipids in the order of IML 3.0 > IML 0.8 > OML 3.0 > OML 0.8. This implies the variations in the interfacial density of lipids can be discerned through the responsive behaviour of 5CB. Furthermore, these observations significantly contribute to establishing a link between the initial disorganization of bacterial lipids and their enhanced organization as they progress into more mature stages. Interestingly, these observations underscore the adaptability of *Mtb*, characterized by significant evolutions in their spatial envelopes throughout their lifespan.

Before delving into the examination of the influence of AMPs on the self-assembled IML at the interface, our initial investigation focused on the stability of these lipids at the interface. Notably, the lipid assembly remains stable for up to 2 h, even enduring washing (Figure

5.2.2). This suggests an irreversible binding of lipids at the interface. Given that IML lipids effectively aligned 5CB, our subsequent inquiry centred on investigating the impact of AMPs. We chose aurein and maculatin, which are recognized for their antimicrobial properties primarily through interactions with bacterial membranes, leading to membrane disruption and possibly cell death.[28]

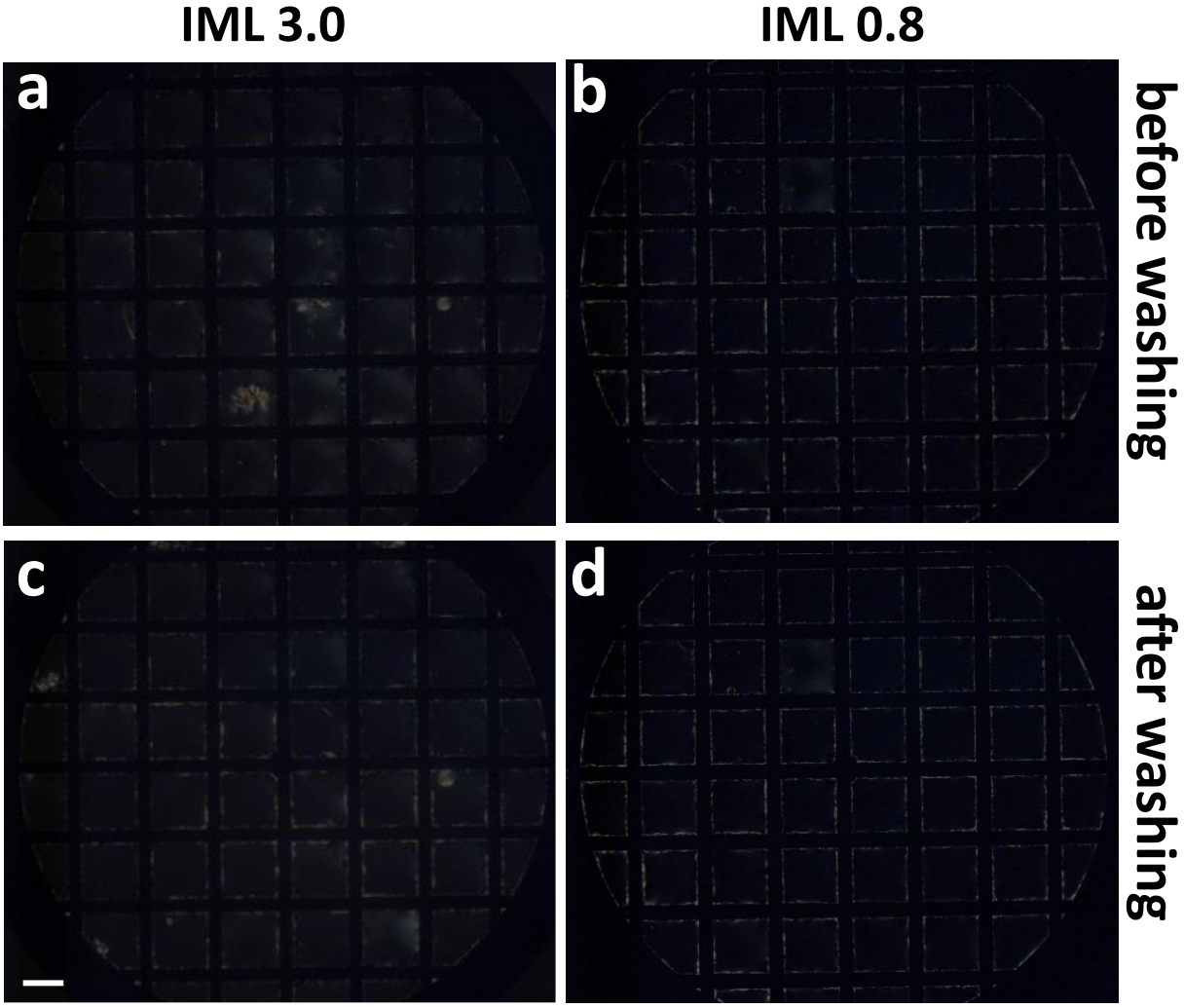

Figure 5.2.2. Optical observations of LC-aqueous interfaces decorated with (a, c) IML 3.0 and (b, d) IML 0.8. These observations encompassed assessments of the interfaces both (a, b) before and (c, d) after a washing procedure. Minimal alteration in the lipid-laden LC-aqueous interface underscores the platform's resilience to the effects of successive wash cycles, thereby affirming its inherent stability. Scale bar = 200 μm.

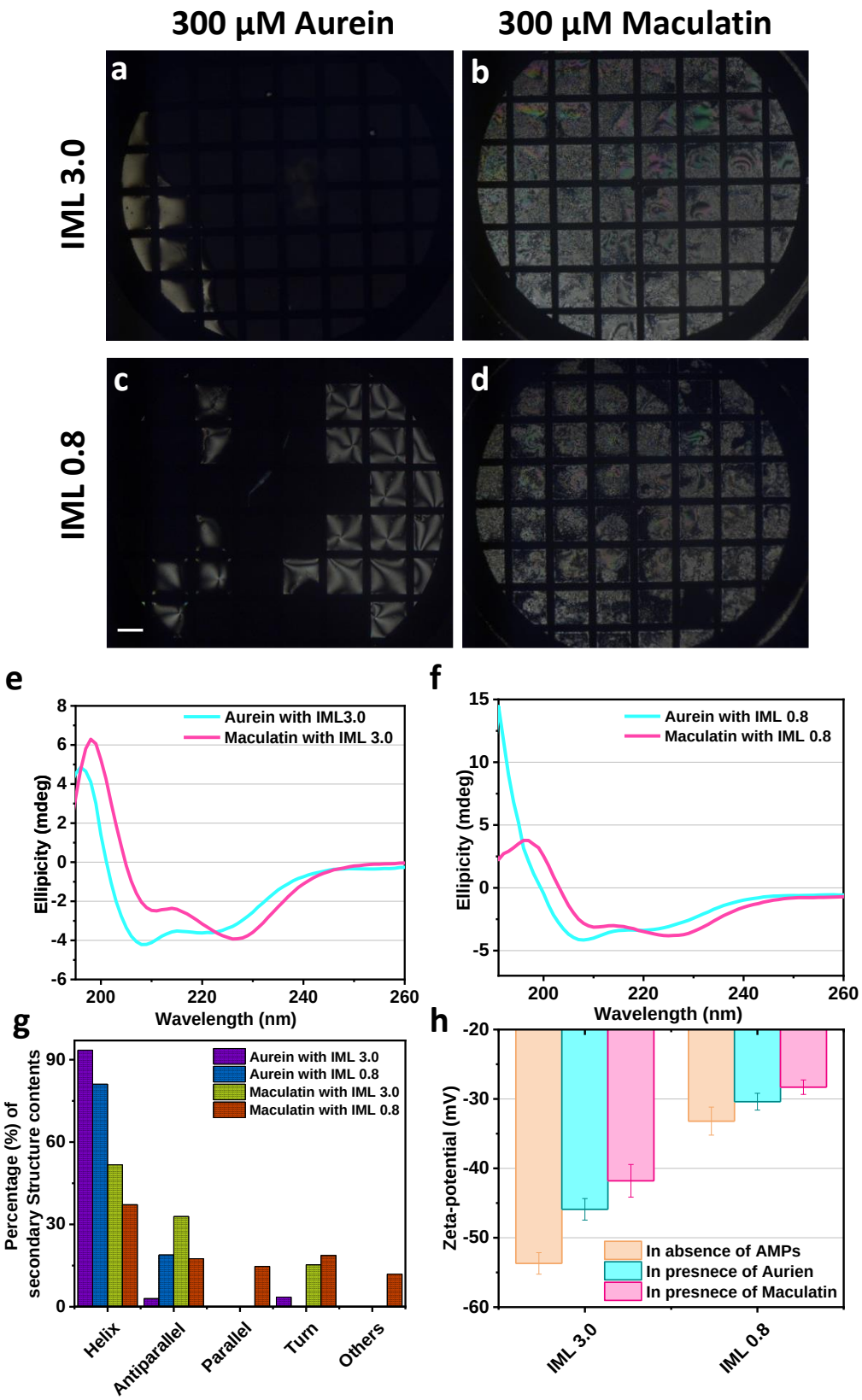

Figure 5.2.3. Polarized optical micrographs (a-d) of 5CB-aqueous interface laden with 0.08 mg/ml of IML 3.0 (a, b) and 2.3 mg/ml of IML 0.8 (c, d) after 20 min addition of 300 µM

aurein (a, c) and maculatin (b, d). Scale bar = 200 µm. Circular Dichroism (CD) spectra in (e and f) illustrate the conformational changes of aurein and maculatin when interacting with IML 3.0 and IML 0.8, respectively. The histogram in (g) represents the percentage (%) of secondary structure contents of AMPs on exposure to IML 3.0 and 0.8. The bar graph in (h) displays the variations in the zeta potential of the lipids in the presence of AMPs.

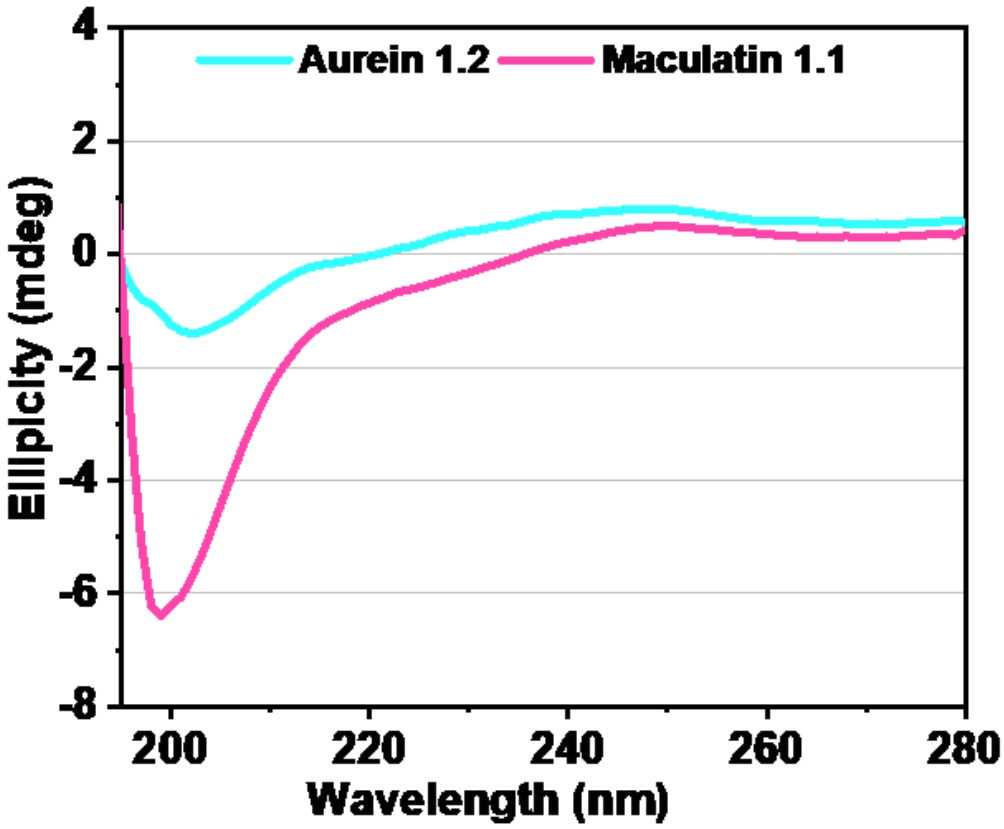

Figure 5.2.4. Circular dichrosim (CD) spectra of aurein and maculatin.

We incubated 300 µM aurein with 0.08 mg/ml of IML 3.0 deposited at the 5CB-aqueous interface. In certain grid squares, we observed a vivid optical appearance of 5CB, but in most of the grid squares, 5CB was absent (Figure 5.2.3a). In contrast, on incubating 300 µM maculatin with IML 3.0 at those interfaces, we observed a consistently bright optical appearance of 5CB (Figure 5.2.3b). However, the observed texture of 5CB in the case of maculatin was distinct from that induced by aurein. These intriguing observations prompted the question: why do such distinct 5CB responses emerge when interacting with AMPs derived from Australian frogs? This curiosity led us to explore whether these differences also manifest in the interactions of AMPs with IML 0.8. Upon exposing AMPs to 2.3 mg/ml IML

0.8-laden 5CB, we observed that the ensuing responses resembled those seen with IML 3.0 (Figure 5.2.3c & d).

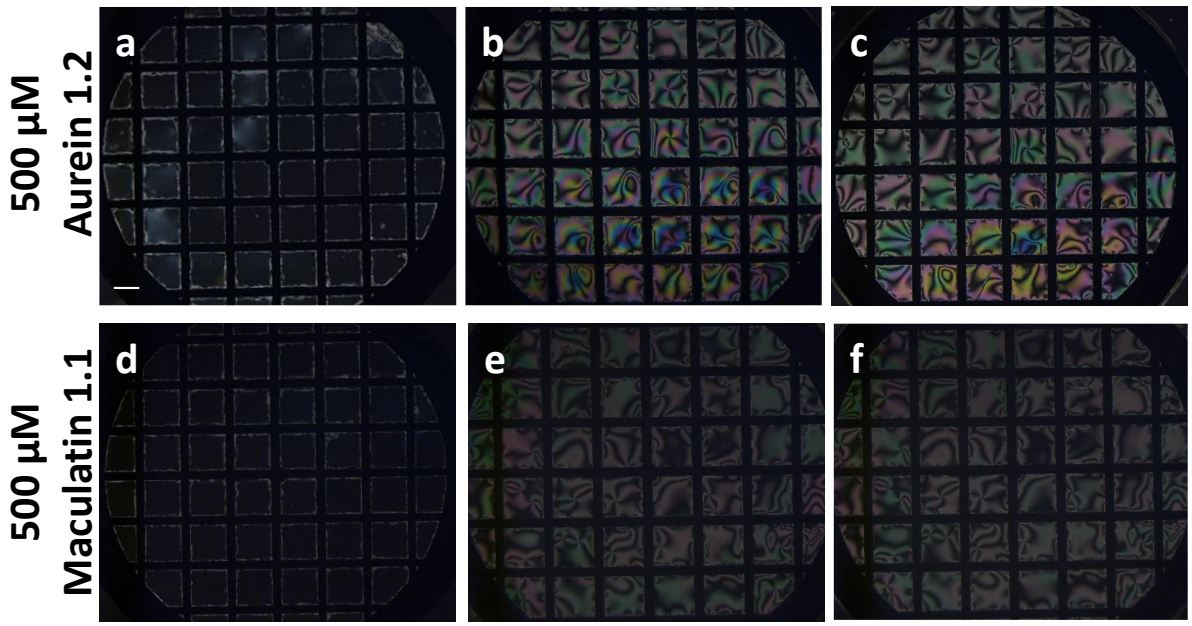

Figure 5.2.5. The photomicrographs of LC response in contact with (a, d) air; (b, e) Tris-buffer; (c) 500 µM of aurein 1.2 & (f) 500 µM of maculatin 1.1. The optical appearance remained unchanged in the presence and absence of AMPs in the solution, indicating no discernible interactions between the AMPs and LC. Scale bar = 200 µm.

However, the optical images also indicated that the responses of IML 0.8-laden 5CB to AMPs appeared to be less pronounced than those of IML 3.0-laden 5CB. We propose that the observed distinctions may arise from AMP-varied interactions with IML lipids at the 5CB-aqueous interface. Next, we conducted circular dichroism (CD) studies to investigate changes in AMP conformation, if any, upon exposure to IML. Figure 5.2.4 depicts the different CD spectra of AMPs, indicating their different conformations in solution. CD spectra in Figure 5.2.3e&f revealed alterations in the conformation of 10 µM AMPs when exposed to 1 mg/ml IML 3.0. Specifically, aurein displayed a maximal negative band at ~208 nm, while maculatin exhibited a peak at ~225 nm. These AMPs displayed similar peaks when exposed to IML 0.8 to that of IML 3.0 (Figure 5.5.3f). The examination of the secondary structure composition (Figure 5.2.3g) of AMPs subsequent to their interaction with IML revealed two principal observations: (i) a noteworthy predominance of α-helical structure in aurein and a marked

abundance of β-sheet conformation in maculatin; (ii) substantial variations in the secondary structure of AMPs following their interaction with IML 0.8 and 3.0. The acquiring of different conformations of AMPs with different lipids revealed lipidome differences to guide the lipid-peptide interactions.

Subsequently, we investigated the potential impact of electrostatic interactions on the interplay between AMPs and IML. Zeta potential measurements revealed a significant increase in the zeta potential of IML 3.0-laden 5CB droplets compared to those laden with IML 0.8 when exposed to cationic AMPs (Figure 5.2.3h). This underscores the crucial role of charges in the complex interactions between AMPs & membranes of *Msm*. Next, we aimed to assess the influence of μM concentrations of AMPs on 5CB in the absence of lipids. We observed no changes in the 5CB before and after the 2 h addition of 500 μM AMPs in the absence of any lipids (Figure 5.2.5). This observation supports the notion that the previously observed response of 5CB arises from the interactions between AMPs and the lipids at those interfaces.

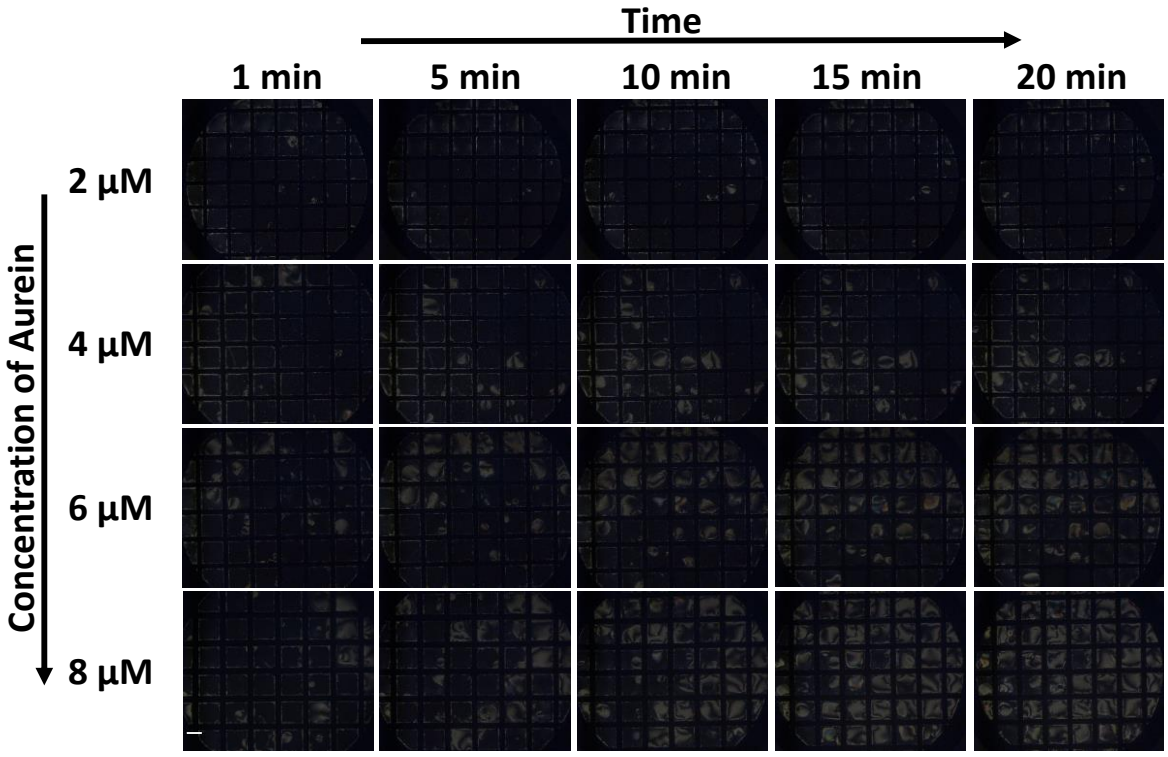

Figure 5.2.6. Crossed polar image of IML 3.0 laden LC-aqueous interface in the presence of 2-8 μM Aurein 1.2. The images depicted the emergence of bright, non-uniform domains at those interfaces. Scale bar = 200 μm.

To gain insight into the early-stage dynamics of AMPs, we examined their interactions with 5CB laden with IML 3.0 at various time intervals and concentrations. Upon introducing 2-8 μM aurein to that interface, we observed the appearance of bright optical domains at specific time points, persisting for up to 20 min (Figure 5.2.6). However, with an extended observation period, these domains gradually disappeared (Figure 5.2.7).

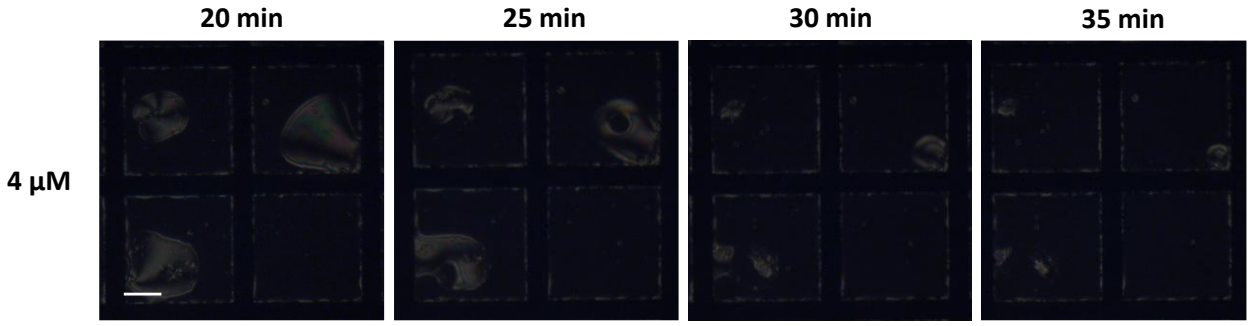

Figure 5.2.7. Polarized optical images of IML 3.0 laden LC-aqueous interface in the presence of 4 μM aurein at an extended observation period. The images illustrate the disappearance of domains with time, leading to a dark optical view of the LC. Scale bar = 100 μm.

Subsequently, by increasing the aurein concentration to 10 μM, we observed initial modest domain formation immediately after addition. However, at 5 min, we noticed a distinct secondary response characterized by sustained bright optical features. Remarkably, after 7 min, a return to the dark appearance due to the homeotropic alignment of 5CB was observed. Notably, this transition at 20 μM occurred more rapidly than at 10 μM (Figure 5.2.8). Furthermore, this homeotropic alignment appeared considerably darker than the previous alignment with lipid anchoring. We hypothesize that the binding of aurein to lipid-laden 5CB results in tilting & the removal of the upper lipid-laden 5CB layer. The tilting & exfoliation of the top layer exposes 5CB to the solution, causing a bright appearance. However, this brightness soon reverts as the free lipids in the solution and DMOAP influences the thinned film of 5CB.To confirm this hypothesis, we increased the aurein concentration to 50 μM, resulting in the noticeable removal of 5CB from the grid squares. These findings suggest that at higher concentrations, aurein interacts with IML 3.0, inducing a tilt in the membrane structure, reorienting 5CB, and subsequently causing their removal from the interface. We then focused on understanding the early-stage mechanisms of maculatin's action. To

investigate this, we exposed IML 3.0-laden 5CB to various concentrations of maculatin ranging from 2-8 μM and observed it for up to 20 min (Figure 5.2.9).

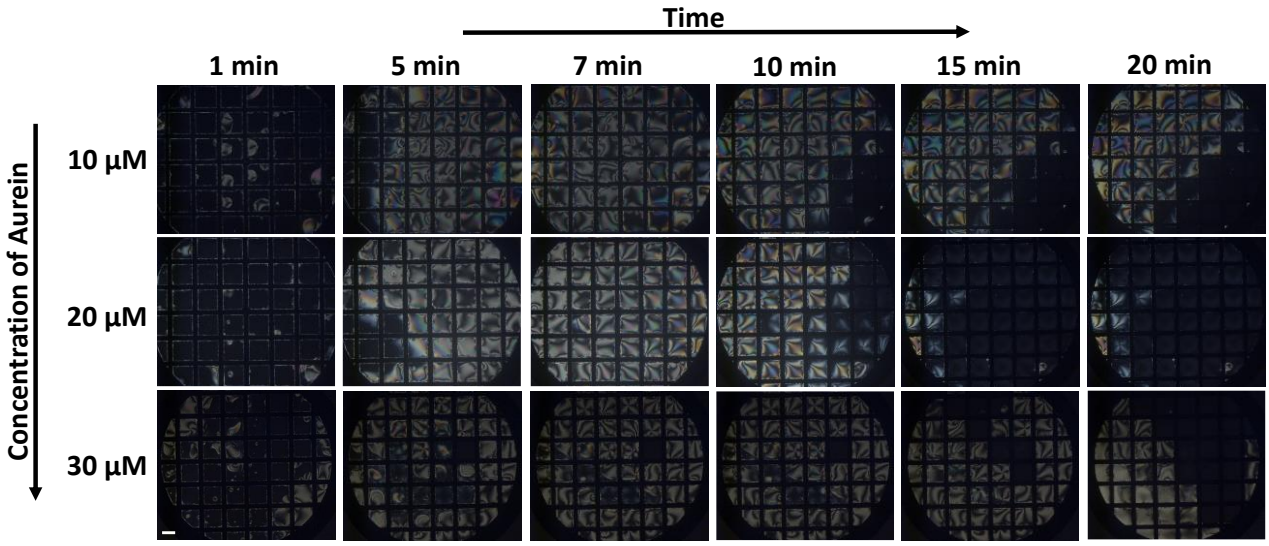

Figure 5.2.8. Polarized optical images of IML 3.0 laden LC-aqueous interface in the presence of 10-30 μM aurein. The images illustrate the uniform brightening of the optical images after 5 min, which reverts to dark in the case of 10 & 20 μM aurein. The removal of LC was observed at 30 μM of aurein. Scale bar = 200 μm.

Surprisingly, we observed almost no response of the 5CB in the presence of maculatin up to 8 μM. However, upon increasing the maculatin to 10 μM, we detected the emergence of faint, short-lived bright domains originating from the grid walls, which persisted for ~3-4 min (Figure 5.2.10). Remarkably, the presence of these domains remained consistent even at 100 μM maculatin. Further increasing to 150 μM maculatin, a secondary response was observed, characterized by the emergence of small dots that gradually evolved into branching domains (Figure 5.2.11).

This secondary response intensified with increasing concentration and time, eventually resulting in a complete brightening of the observed image. Notably, these results were observed at much higher concentrations than aurein. This suggests that small peptide aurein are significantly more effective at infiltrating the lipid domains within the bacterial membrane, indicating their enhanced ability to penetrate and interact with the bacterial membrane.

We categorized the initial, transient responses as "non-equilibrium responses" and identified the subsequent responses leading to permanent damage to our engineered interface as "equilibrium responses". We then examined whether these alterations remained observable even after removing the analyzer.

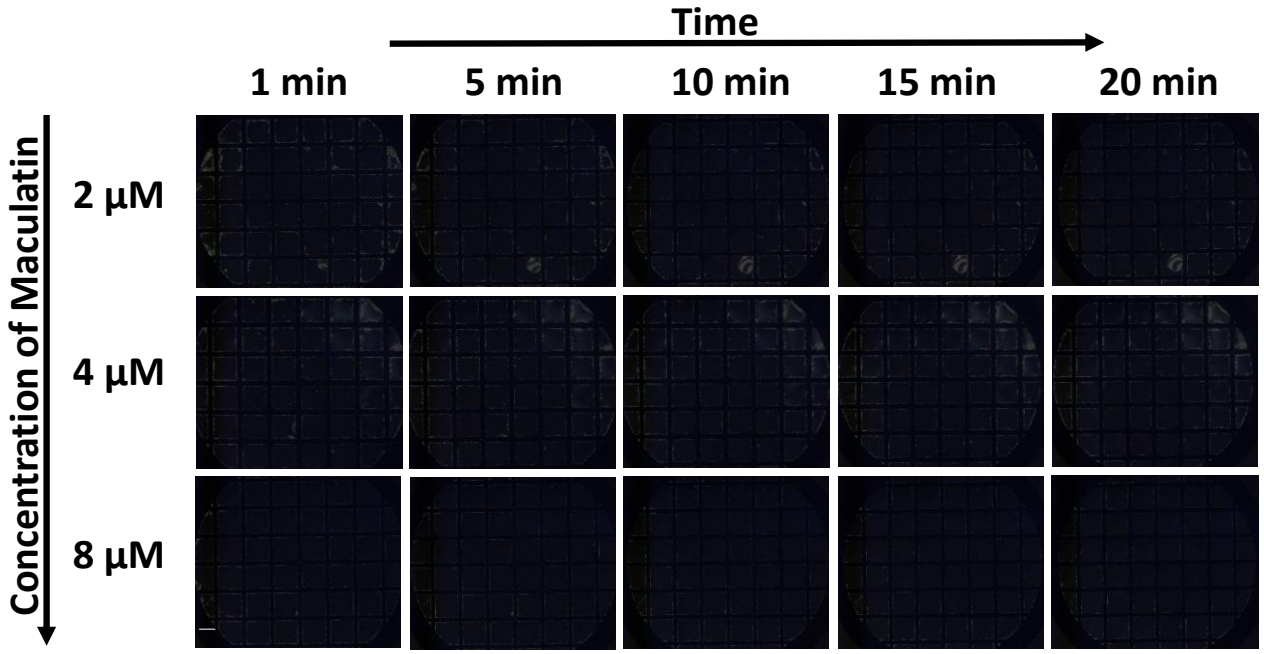

Figure 5.2.9. Polarized optical images of IML 3.0 laden LC-aqueous interface in the presence of 2-8 µM maculatin. The images illustrate the negligible change in the optical appearance of IML 3.0-laden LC in the presence of 2-8 µM maculatin. Scale bar = 200 µm.

The non-equilibrium responses induced by the AMPs aurein and maculatin were still discernible after analyzer removal, indicating modifications in the local areal densities of the molecules (Figure 5.2.12a-d). However, the equilibrium response induced by aurein was relatively uniform (Figure 5.2.12e, f) and became undetectable after analyzer removal in contrast to the equilibrium response by maculatin (Figure 5.2.12g, h). This signifies local areal density changes resulting from the binding of maculatin with IML. To investigate the potential aggregation of these AMPs at the interface, we subjected the IML 3.0-laden 5CB interface to a drying process while in the presence of working concentrations of both AMPs. The dried interface revealed a uniform dark optical appearance of 5CB in the presence of 10 and 100 µM aurein (Figure 5.2.13). Conversely, bright domains were observed at the dried IML 3.0-laden 5CB interface, which indicated the existence of aggregates at this interface.

We then considered whether there were changes in the response of 5CB in the presence of AMPs when laden with IML 0.8, extracted from the initial growth phase of *Msm*. Upon incubation of AMPs with IML 0.8-laden 5CB-aqueous interface, we observed responses of 5CB like those seen with IML 3.0 (Figure 5.2.14 & 5.2.15).

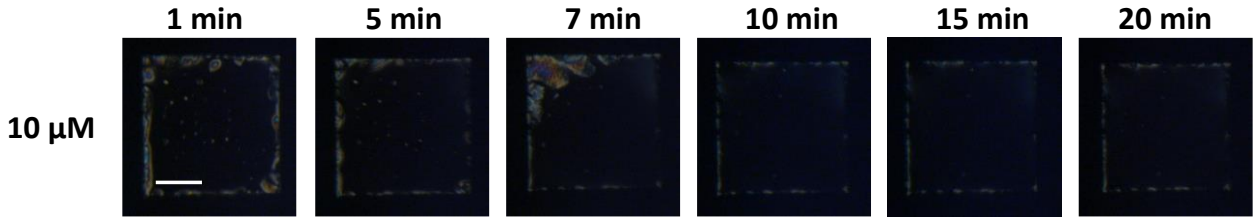

Figure 5.2.10. Polarized optical images of IML 3.0 laden LC-aqueous interface in the presence of 10 µM maculatin. The images illustrate the appearance of some unstable bright optical domains which revert to dark. Scale bar = 100 µm.

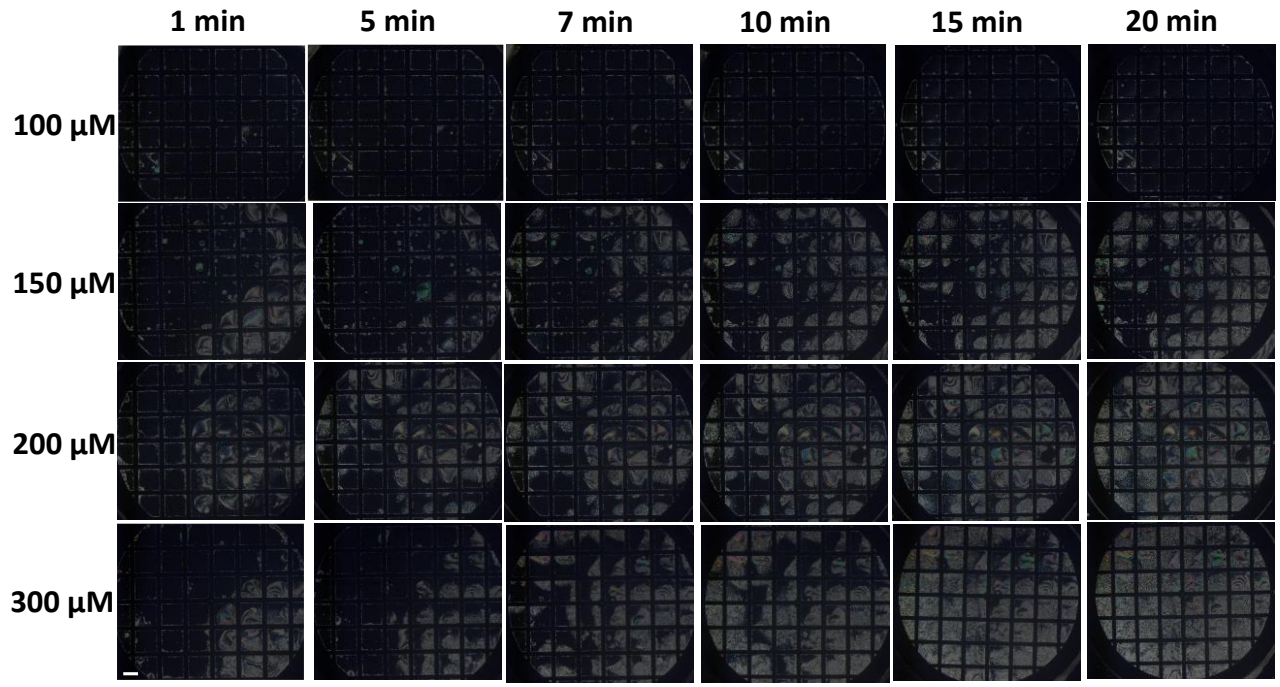

Figure 5.2.11. Polarized optical images of IML 3.0 laden LC-aqueous interface in the presence of 100-300 µM maculatin. The images illustrate the gradual emergence of bright domains that progressively encompass the entire interface. Scale bar = 200 µm.

However, these responses were less pronounced and required higher concentrations of AMPs. This suggests different actions of AMPs at earlier and later stages of *Mtb* growth. Next, we

explored how the emerging spatial patterns of 5CB correlate with the lateral distribution of IML and AMPs at the aqueous-5CB interface. To investigate this, we employed confocal fluorescence microscopy. We incorporated 2.5% of rhodamine DHPE (lissamine rhodamine B 1,2-dihexadecanoyl-*sn*-glycero-3-phosphoethanolamine) into the IML 3.0 and laden it at the 5CB-aqueous interface. Subsequently, we introduced 8 μM aurein, which included 1% FITC-labeled aurein, into the system for further analysis. The addition of rhodamine DHPE to the lipid resulted in anticipated red fluorescence signals in lipid-rich regions. Additionally, the FITC-labelled aurein was expected to emit green fluorescence in aurein-rich regions. Upon introducing 1% FITC-labelled aurein at a concentration of 8 μM, the initially uniform homeotropic alignment of the 5CB was disrupted, forming a distinct bright domain in the polarized field (Figure 5.2.16a). Notably, this domain exhibited green fluorescence (Figure 5.2.16c) and appeared non-fluorescent in red (Figure 5.2.16b) when examined using confocal fluorescence microscopy. Figure 5.2.16d illustrates the grayscale values in both the dark and bright regions of the red non-fluorescent and green-fluorescent areas, respectively.

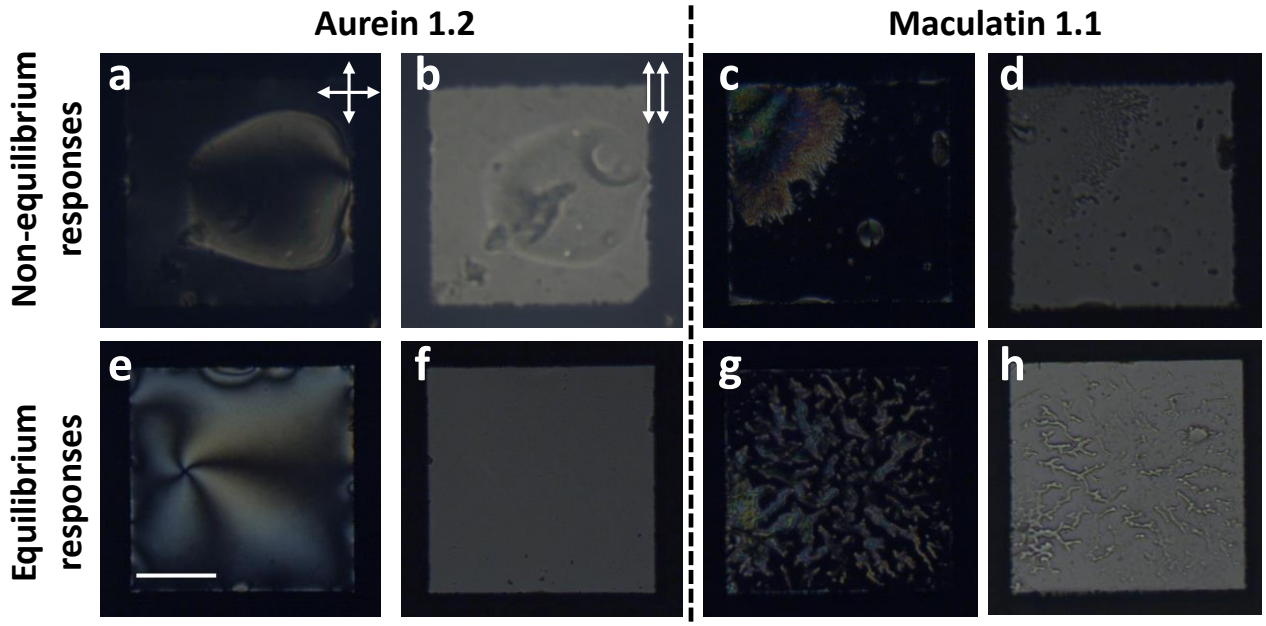

Figure 5.2.12. Polarized (a, c, e & g) and bright optical images (b, d, f & h) illustrate the optical response of IML-laden 5CB on exposure to AMPs. Images (a, b) & (c, d) show the non-equilibrium response of IML-laden 5CB when exposed to aurein & maculatin, respectively, at low and initial stages of high concentrations. Optical images (e, f) & (g, h) represent the equilibrium response of IML-decorated 5CB when exposed to aurein &

maculatin, respectively, at higher concentrations. Scale bar = 100 µm. The double-headed arrows at the top left of images a and b indicate the orientations of the analyzer and polarizer during imaging.

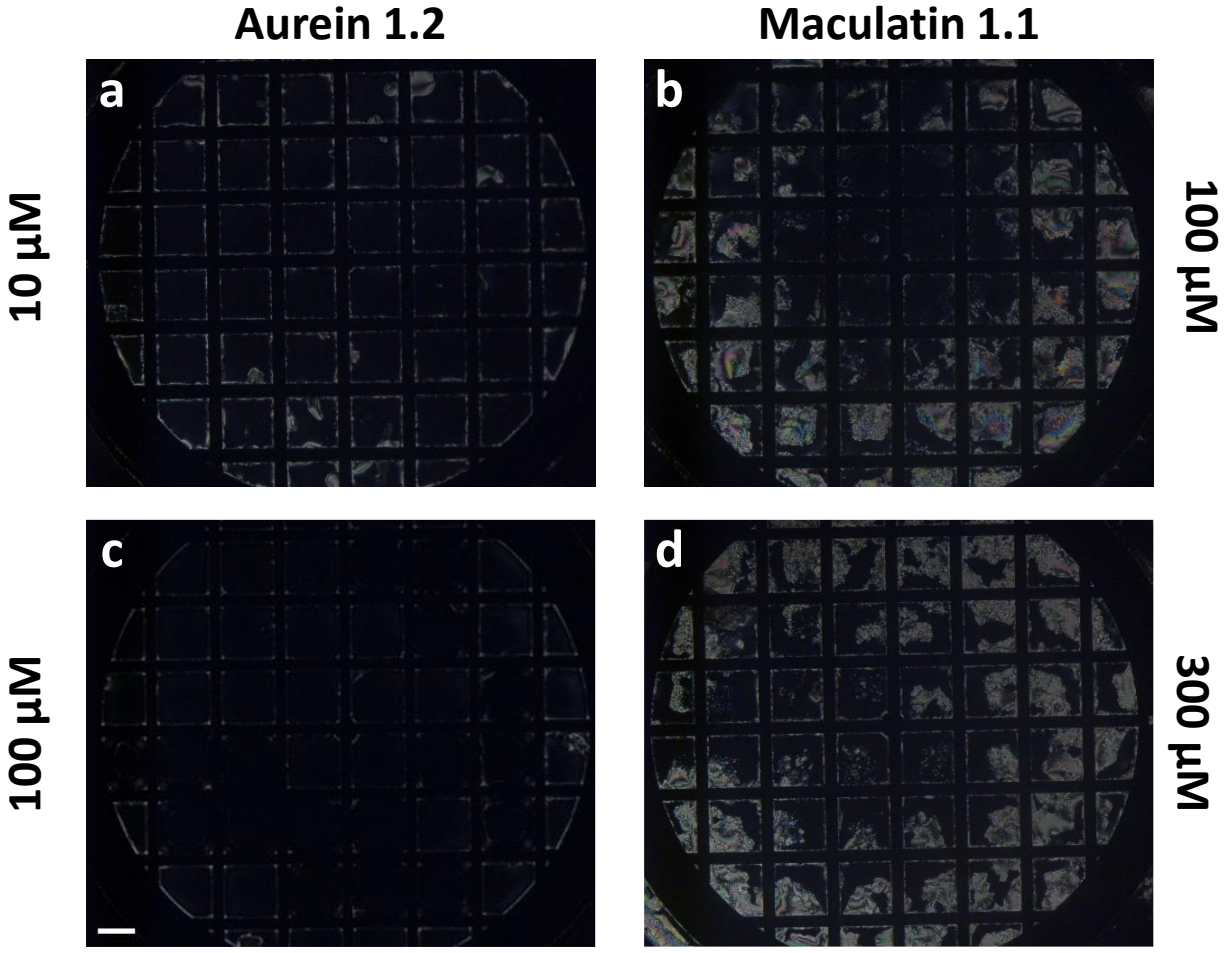

Figure 5.2.13. Polarized optical images of dried IML-laden LC-aqueous interface in the presence of working concentrations of AMPs. The images demonstrate a fully darkened interface in the presence of aurein, while in the case of maculatin, some aggregates were observed at the interface. Scale bar = 200 µm.

These collective observations indicate that the bright domain seen in POM images corresponds to regions rich in AMPs. The interaction of AMPs with IML-laden 5CB reveals several important findings. First, it delineates two distinct response patterns termed non-equilibrium and equilibrium responses. Second, the equilibrium response with aurein appears uniform, while maculatin induces branched 5CB domains, leading to phase separations at the

interface. Third, aurein imparts a dark optical appearance to 5CB without aggregate formations, unlike maculatin. Lastly, 5CB laden with IML 0.8 exhibits a diminished response compared to IML 3.0 in the presence of AMPs.

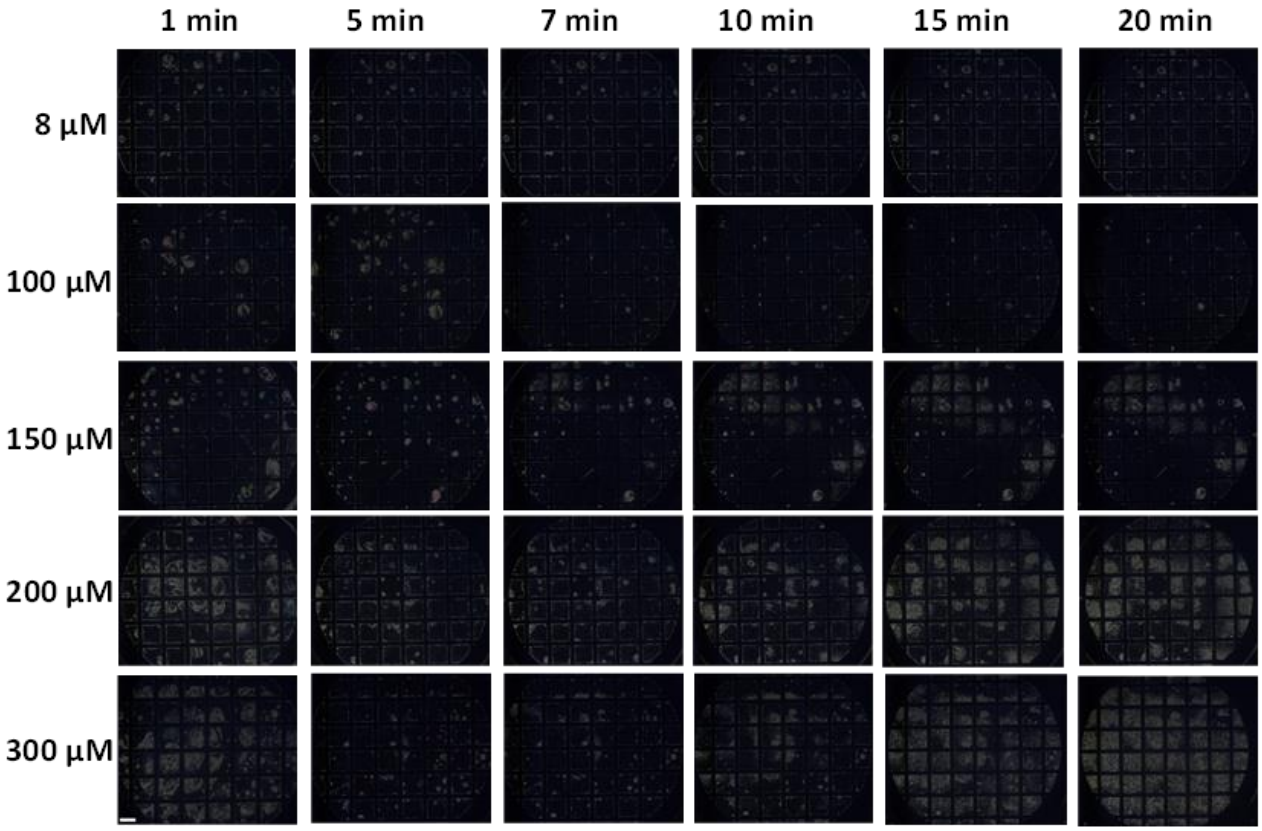

Figure 5.2.14. Polarized optical images of IML 0.8 laden LC-aqueous interface in the presence of 8-300 µM of maculatin. The images illustrate the gradual emergence of bright domains that progressively encompass the entire interface at 300 µM. Scale bar = 200 µm.

The first observation of non-equilibrium responses at lower AMP concentrations, especially at the initial stages of high concentrations, suggests two possible mechanisms. Firstly, lower concentrations may cause modest perturbations in long-chain lipids, allowing self-regeneration. Alternatively, small peptides may reorganize within membrane pockets, leading to 5CB realignment and a dark optical appearance. At higher concentrations, increased AMP surface coverage may result in irreversible membrane damage, primarily due to electrostatic interactions. These observations provide compelling evidence that a specific threshold quantity of AMPs is necessary to disrupt bacterial membranes effectively.

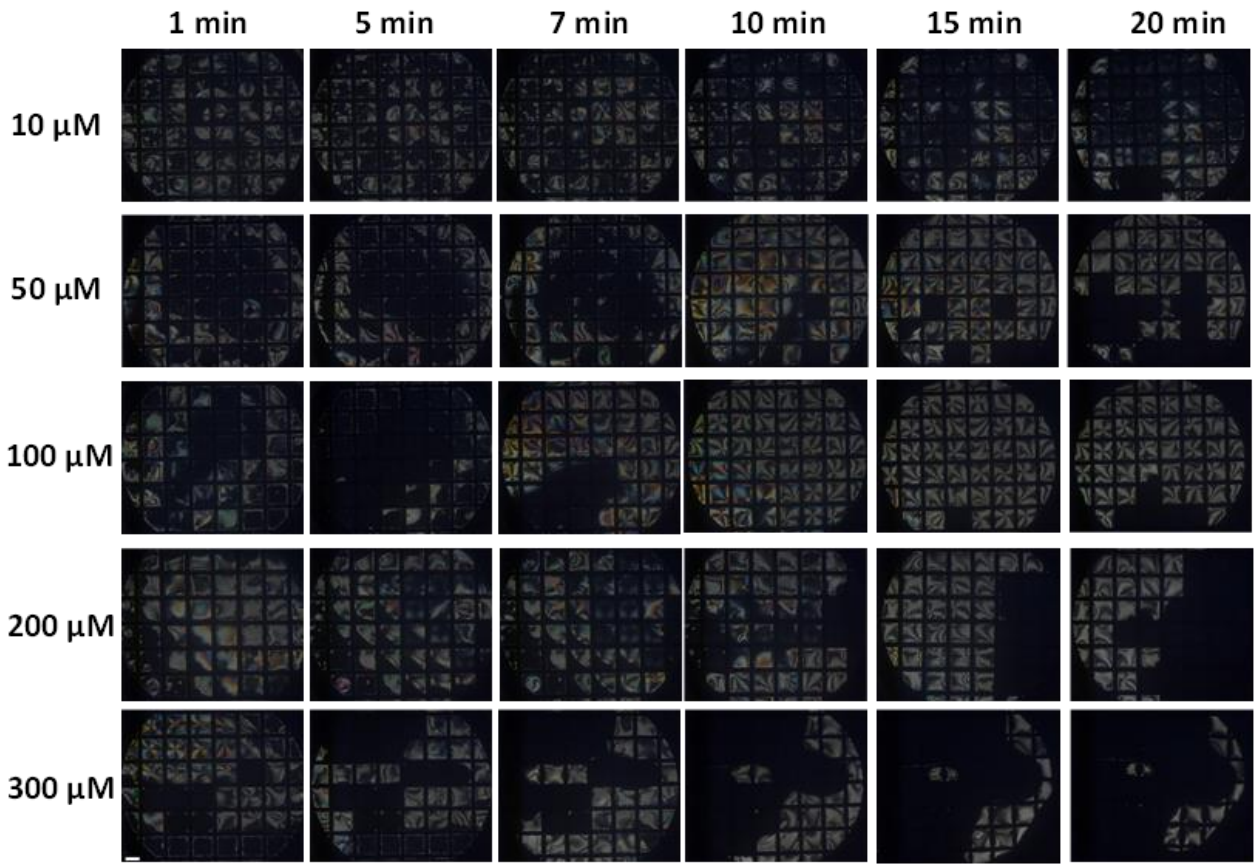

Figure 5.2.15. Polarized optical images of IML 0.8-laden LC-aqueous interface in the presence of 8-300 µM of maculatin. The images illustrate the gradual emergence of bright domains that progressively encompass the entire interface at 300 µM. Scale bar = 200 µm.

The second observation, concerning distinct responses of 5CB laden with IML in the presence of two AMPs, can be attributed to different interaction pathways. Aurein induces a bright optical appearance without discernible domains, eventually expelling IML from the interface. This suggests a detergent-like mechanism akin to the carpet model of AMP action.[28, 29] In contrast, maculatin interaction with IML at the 5CB interface leads to the emergence of branched dendritic domains, indicating a β-sheet-rich conformation.[30, 31]

The third observation of aggregation at the interface suggests the involvement of β-sheet strands and multimeric structures in membrane disintegration, resembling the barrel-stave model.[28]

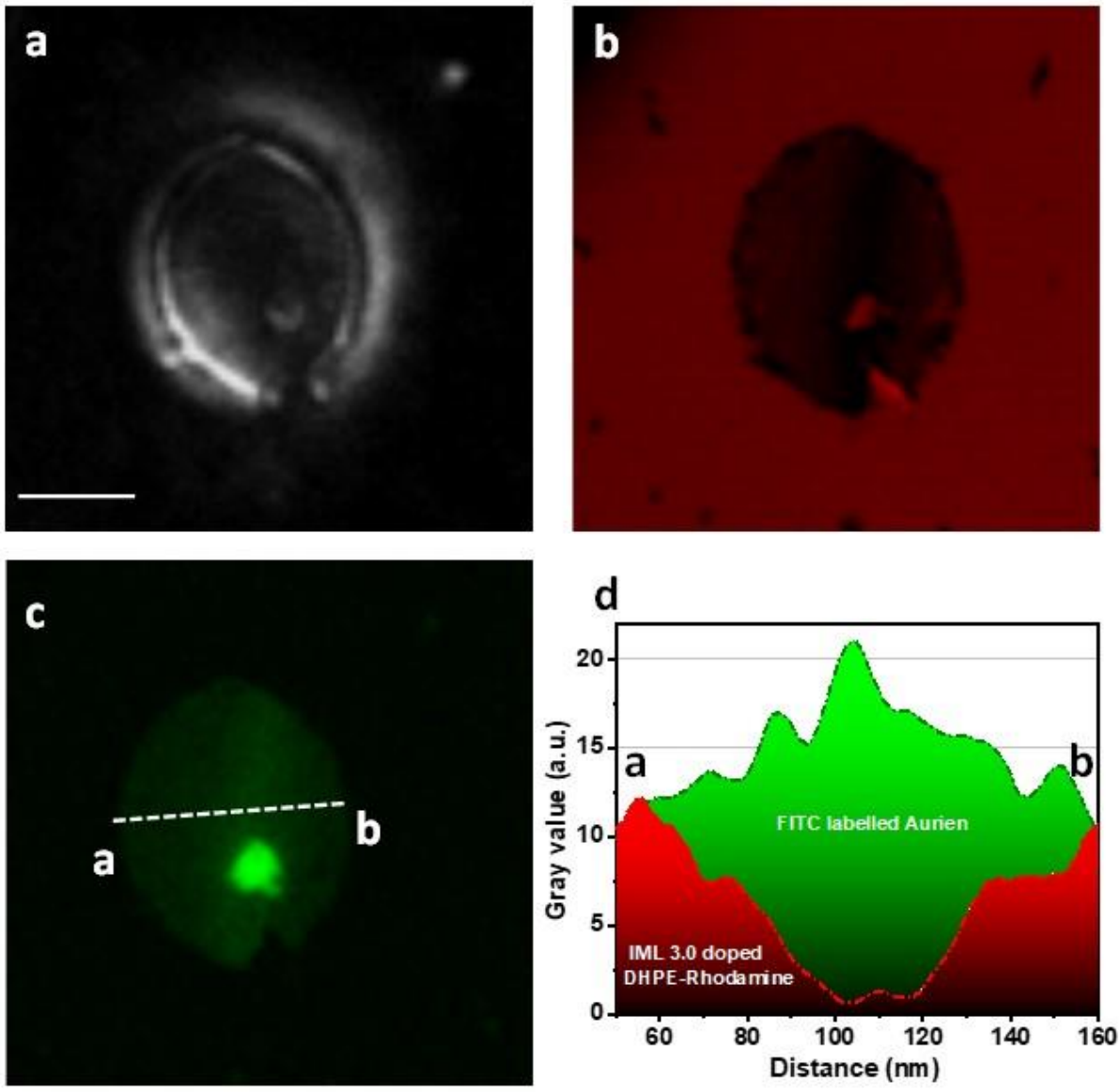

Figure 5.2.16. Crossed polars (a) and confocal fluorescence images (b, d) of LC-aqueous interface laden with IML 3.0 and 2.5% rhodamine-DHPE mixed lipid after addition of 8 μM of 1% of FITC-labelled aurein. The graph in (d) illustrates the grayscale values in both the dark and bright regions of the red non-fluorescent and green-fluorescent areas, respectively. Scale bar = 50 nm.

The final noteworthy observation of diminished responses of 5CB with IML 0.8 compared to IML 3.0 in the presence of AMPs may be explained by lipid density fluctuations and reduced electrostatic charges, accounting for the attenuated influence of AMPs during the initial growth phase of *Mtb*.

5.3. Conclusions

In summary, our research illuminates the adaptability of *Mtb* in dynamically modulating lipid compositions, resulting in fluctuating membrane densities and charge distributions across distinct growth phases. These adaptive lipid changes emerge as pivotal contributors to *Mtb's* resilience in challenging environmental conditions and its formidable resistance to drugs. Notably, our investigation unveils a consistently lower organizational structure in the outer membrane layer (OML) than the inner membrane layer (IML) throughout various growth phases, deepening our comprehension of Mtb's intricate membrane dynamics.

Furthermore, our study yields valuable insights into the distinct mechanisms employed by various antimicrobial peptides (AMPs) to disrupt bacterial membranes. Significantly, we observe that effective membrane disruption occurs only at concentrations surpassing a specific threshold. Intriguingly, during the early stages of bacterial growth, variations in membrane density and charge modulation appear to mitigate the impact of AMPs. This finding suggests a potential synergistic enhancement in the efficiency of dismantling bacterial envelopes when aurein and maculatin are combined.

While our investigation predominantly focuses on the well-organized inner membranes of bacteria, it serves as a foundational step towards establishing a robust platform for scrutinizing specific alterations and deficiencies induced in membranes by various antibiotics. This broader perspective contributes to the advancement of our understanding of bacterial membrane-based therapeutic approaches. In conclusion, our research provides a straightforward yet powerful approach for delving into bacterial lipid modulation and the effects of drugs. We anticipate that this strategy will serve as a valuable tool for gaining molecular insights into antibiotic potentiators, with promising applications in point-of-care diagnostics and therapeutic interventions.

5.4. Experimental Procedures

5.4.1. Materials

Fischer's Finest Premium Grade glass microscope slides were procured from Fischer Scientific located in Pittsburgh, Pennsylvania. These glass slides underwent a cleaning process using piranha solution, which consisted of Sulfuric acid (H_2SO_4) and Hydrogen peroxide (H_2O_2, 30% w/v) sourced from Merck. To neutralize the cleaning solution, Sodium chloride (NaCl) from Merck was utilized.

Additionally, the following chemical substances were obtained: Chloroform (HPLC), 4′-pentyl-4-biphenylcarbonitrile (5CB), Fluorescein 5-isothiocyanate (FITC), ammonium chloride, Sephadex G-25, dimethyl sulfoxide (DMSO) and dimethyloctadecyl[3-(trimethoxysilyl)propyl]-ammonium chloride (DMOAP) were supplied by Sigma Aldrich. Ethanol was sourced from Jebsen & Jenssen GmbH and Co., Germany (S D fine-chem Limited). Thermo Fischer Scientific. Gold grids, with a thickness of 20 μm and dimensions of 50 μm width and 283 μm grid spacing, were acquired from Electron Microscopy Sciences, headquartered in Fort Washington, PA. *Mycobacterium smegmatis* (Msm) MC2 155 was a humble gift Prof. Chopra (CDRI, Lucknow). Other chemicals were purchased from the following: MB7H9 (BD Difco, Fisher Scientific, UK), Dextrose (Sigma Aldrich, USA), BSA Fraction V (MP Biochemicals, USA), catalase from bovine liver (Sigma Aldrich, USA), glycerol (Merck), tylaxopol (Merck), MB7H10 (Himedia, India), Dioctyl sulfosuccinate sodium salt (AOT) (Sigma Aldrich, USA), heptane (EMPARTA, Merck, USA), chloroform (EMPARTA, Merck, USA), methanol (EMPARTA, Merck, USA), aluminium oxide basic (Sigma Aldrich, USA), ddH2O (MilliQ, Merck, USA), anthrone (Sigma Aldrich, USA), Aurein (Peptide 2.0, USA), maculatin (Peptide 2.0, USA). All required buffers were prepared using Milli-Q water, and pH adjustments were made using a Metrohm 827 lab pH meter, maintained at room temperature, approximately 25°C. Milli-Q water was obtained through Millipore Technology, located in Bedford, MA.

5.4.2. Piranha Cleaning and Coating of Glass slides

Following established protocols, the glass slides were meticulously cleaned using piranha solution (comprising H_2SO_4:H_2O_2 in a volumetric ratio of 70:30).[32] In brief, freshly prepared piranha solution was introduced to the glass slides within a glass container, subsequently immersing them in a water bath set at 80°C for a duration of 1 h. After this treatment, the slides were subjected to sequential rinses with ethanol and deionized water. A thorough drying process was then carried out using nitrogen gas purging, followed by an incubation period within an oven maintained at 100°C for a minimum of 3 h. To impart hydrophobic properties to the glass slides, they were immersed in a 0.1% (v/v) aqueous solution of DMOAP at room temperature for 30 min. Subsequently, a meticulous washing procedure was employed to remove excess DMOAP before subjecting the slides to nitrogen drying. Furthermore, these slides underwent an additional heating process spanning 3 to 6 h within the oven to facilitate cross-linking and the formation of siloxane bonds. The chemical modification of the glass slide surface with DMOAP substance resulted in the establishment of hydrophobic

interactions between the octadecyl chains of DMOAP and the alkyl tails of 5CB molecules. This modification encouraged the perpendicular alignment of LC molecules with respect to the substrate surface.

5.4.3. Bacterial Culture

Bacterial culture and their harvesting are being done by Anjana P. Menon, a group member of our collaborator Dr. Shobhna Kapoor's lab (IIT Bombay). The work by the collaborator has been acknowledged and well as respected. The method has been described in detail elsewhere.[33, 34, 35]

5.4.4. Extraction of lipid

Mycobacterial lipids were extracted using the methods reported previously.[36, 37] The extraction of lipids has been done by Anjana P. Menon, a group member of our collaborator Dr. Shobhna Kapoor's lab (IIT Bombay). The work by the collaborator has been acknowledged and well as respected. We have used them as reagents for our studies.

5.4.5. Liquid Chromatography, Mass Spectrometry & Data Processing and Analyses

All the characterization and purification of the lipids has been done by Anjana P. Menon, a group member of our collaborator Dr. Shobhna Kapoor's lab (IIT Bombay). The work by the collaborator has been acknowledged and well as respected. LC/MS data files were processed with the MassHunter Qualitative Analysis Software, version B.10.00, as reported previously[38] (Agilent Technologies; Santa Clara, CA).

5.4.8. Preparation of vesicles of Inner and Outer membrane lipid

The preparation of vesicles was conducted using a previously established method.[26] In brief, a predetermined quantity of lipid was obtained and introduced into a round-bottom flask, where it was suspended in chloroform. Subsequently, the required quantity of lipid was subjected to a drying process for a duration of 3 h at room temperature under vacuum conditions. Following this, the dried lipid was rehydrated with Tris buffer containing 5 mM of $MgCl_2$ after a 3 h period. Freeze-thaw cycles were then implemented to facilitate the formation of lipid vesicles. Small unilamellar vesicles were generated through probe sonication of the aqueous lipid dispersion, a process that lasted for 30 min. It is noteworthy that all prepared lipid solutions were utilized within a 24 h timeframe.

5.4.9. Preparation of LC aqueous interface

The establishment of the LC-aqueous interface was executed following established protocols, as previously detailed in the literature.[39] In brief, glass slides coated with DMOAP were fragmented into small fragments and subsequently overlaid with gold grids. Subsequently, approximately 0.2 µl of 5CB was dispensed onto the grids, and any excess 5CB was removed by aspiration, ensuring the formation of a uniform LC film. This assembled system was then positioned within an optical well, wherein a 10 mM buffer solution was introduced to generate the LC-aqueous interface.

5.4.10. Preparation of LC aqueous interface

The preparation of the LC-aqueous interface has already been described in earlier reports. In short, DMOAP-coated glass slides were broken up into tiny bits and overlaid with gold grids.[40-46] After adding roughly 0.2 µl of 5CB to the grids, the extra 5CB was syringed out to create a consistent film of LC.[41-43] The constructed system was placed in an optical well containing a PBS buffer (10 mM, 2 ml) in order to create the LC-aqueous interface.

5.4.11. Preparation and optical characterization of lipid-laden-LC-filled Specimen Grid

The LC-aqueous interface was enveloped within lipid layers comprised of lipid vesicles that were synthesized and subsequently allowed to incubate. Following the lipid encapsulation, the buffer solution was substituted with various concentrations of the AMPs of interest. Subsequently, the optical response of the LC system was examined using a polarizing optical microscope (POM) to gain insights into the interactions between the protein and the lipid-rich LC-aqueous interface. To maintain the alignment of the lipid layer and avoid turbulence, the AMPs were gently introduced from the walls of the optical well. As previously documented in earlier publications, optical characterization procedures have been outlined. In summary, optical characterization involved the use of a Zeiss Scope.A1 polarizing optical microscope (POM) in transmission mode to observe the optical behaviour of the LC system.[44-46] Each image capture was meticulously focused and acquired using a Q-imaging digital camera, which was integrated with the POM and set with an exposure time of 80 milliseconds.[21] The LC sample, enclosed within an optical well, was positioned on a rotating platform. The orientation of the LC material was assessed by ensuring the orthogonal alignment of the polarizer and analyzer. During each experimental trial, images were acquired while maintaining a source intensity level that approximately equated to 40% of the maximum brightness setting.

5.4.12. Circular dichroism measurements

Far-UV circular dichroism (CD) studies were conducted using a Chirascan spectrophotometer manufactured by Applied Photophysics in the United Kingdom. The instrument possessed a scan range spanning from 190 to 280 nm, with a step size of 1 nm. The solution under investigation was placed within a quartz cell featuring a 1 mm path length.[47-50]

Freshly prepared aqueous solutions containing 10 µM concentrations of aurein 1.2 and maculatin 1.1 were employed for the experiments. These solutions were prepared in a 10 mM Tris buffer at a pH of 7.4. To investigate conformational alterations in AMPs during their interaction with IML, a solution containing 10 µM of AMPs was subjected to a one-hour incubation period with lipids at a concentration of 1 mg/ml. Data acquisition and analysis were performed using the ProData software provided with the CD instrument. Each spectrum was generated by averaging the results of 5 scans and subsequently adjusted against the buffer signal for accurate analysis. The data pertaining to the AMPs' percentage secondary structure content was processed using the BestSel software.

5.4.13. LC droplets preparation and zeta potential Measurements

To investigate variations in zeta potential at the surface of the LC, we employed LC droplets through the addition of 1 µl of 5CB to either 100 µl of DI water or a lipid solution at a concentration of 1 mg/ml. The resulting dispersions were prepared via vortex mixing for 1 minute at a rate of 3,000 revolutions per minute (rpm), followed by 1-minute emulsification using a homogenizer. In the context of the AMP studies, we introduced 10 µl of the AMPs stock solution into a mixture containing 40 µl of the lipid-5CB droplet emulsion, thus achieving a final concentration of 10 µM for the AMPs. After a 15-minute incubation period, the solution was diluted to a final volume of 800 µl with DI water. The measurement of zeta potential under these experimental conditions was performed using the Zetasizer Nano ZS90 instrument manufactured by Malvern Instruments Inc., at room temperature, applying a cell-driven voltage of 30 V.

5.4.14. FITC-Labelling of Aurein 1.2 AMP

To fluorescently label Aurein 1.2 with FITC, a solution of 1 mg/ml FITC was prepared by dissolving FITC in dimethyl sulfoxide (DMSO). Subsequently, 100 µl of this FITC solution was mixed with 5 mg/ml of Aurein 1.2. The resulting mixture was then placed in a dark environment at a temperature of 4 ^{o}C for a duration of 5 to 6 h. Following this incubation period, the ongoing reaction of labelling

was halted by adding 50 mM of ammonium chloride, and the mixture was allowed to react for an additional 2 h. Subsequently, the reaction mixture was passed through a column made of Sephadex G-25 (gel filtration), and the formed conjugate was purified by elution through the column using a 10 mM Tris buffer (pH=7.4). The eluted samples were collected in separate vials for further analysis. UV absorption spectra were recorded for the collected samples, revealing absorption maxima at 280 nm for the FITC-Aurein conjugate and 495 nm for FITC alone. The concentration of the protein was determined based on the absorbance value at 280 nm.

5.4.15. Confocal Microscope Imaging

Confocal microscopic imaging was employed to visualize the localization of lipid-doped components, specifically utilizing a 2.5% concentration of rhodamine DHPE fluorescent dye. To prepare the samples, a mixture of lipids consisting of IML 3.0 and the doped DHPE fluorescent dye was created. This lipid mixture was dissolved in high-performance liquid chromatography (HPLC) chloroform to generate vesicles. These vesicles were subsequently combined with the liquid crystal (LC)-aqueous interface. For imaging purposes, a specialized setup was employed, which included a 63x long-distance water-immersed objective equipped with hybrid detectors. The image acquisition settings were configured to capture images at a resolution of 512x512 pixels, with a scanning rate of 400 Hz. A diode-pumped solid-state (DPSS) laser source emitting light at a wavelength of 561 nm was utilized to excite the rhodamine DHPE fluorescent dye. Confocal image stacks were acquired using a photomultiplier tube (PMT) detector within an SP8 upright confocal microscope system. This approach allowed for the precise visualization and examination of the lipid-doped localization within the samples.

5.5. Author Contributions

TG and APM collaborated to conceptualize and devise the framework for the project. APM purified the lipids from *Mtb*. The expression and purification of lipids have been done by Anjana Peethambaran Menon, a group member of our collaborator Dr. Shobhna Kapoor's lab (IIT Bombay). We have used it as a reagent for our study, which the collaborator has kindly provided. TG meticulously executed all experimental procedures and thoroughly analysed the resulting data. SKP and SK did the overall project administration.

5.6. Acknowledgements

S.K.P. acknowledge MOE/STARS1/284. T.G. thanks CSIR (09/947/(0223)/2019EMR-1) for the fellowship. T.G. acknowledges powerpoint, chemdraw, and pymol tools for various cartoons and protein structures used in the table of contents (TOC) graphics.

References

1. Singh, R.; Dwivedi, S. P.; Gaharwar, U. S.; Meena, R.; Rajamani, P.; Prasad,T., Recent updates on drug resistance in Mycobacterium tuberculosis. *J. Appl. Microbiol.* **2020**, *128*, 1547-1567.

2. Hawkes, D. J.; Mak, J., Lipid membrane; a novel target for viral and bacterial pathogens. *Curr. Drug Targets* **2006**, *7*, 1615-1621.

3. Mingeot-Leclercq, M. P.; Décout, J. L., Bacterial lipid membranes as promising targets to fight antimicrobial resistance, molecular foundations and illustration through the renewal of aminoglycoside antibiotics and emergence of amphiphilic aminoglycosides. *Med. Chem. Comm.* **2016**, *7*, 586-611.

4. Subedi, Y. P.; AlFindee, M. N.; Takemoto, J. Y.; Chang, C. T., Antifungal amphiphilic kanamycins: new life for an old drug. *Med. Chem. Comm.* **2018**, *9*, 909-919.

5. Jackson, M.; Stadthagen, G.; Gicquel, B., Long-chain multiple methyl-branched fatty acid-containing lipids of *Mycobacterium tuberculosis*: Biosynthesis, transport, regulation and biological activities. *Tuberculosis* **2007**, *87*, 78-86.

6. Brennan, P. J.; Nikaido, H., The envelope of mycobacteria. *Annu. Rev. Biochem.* **1995**, *64*, 29-63.

7. Pal, R.; Hameed, S.; Kumar, P.; Singh, S.; Fatima, Z., Comparative lipidomics of drug sensitive and resistant *Mycobacterium tuberculosis* reveals altered lipid imprints. *3 Biotech.* **2017**, *7*, 1-10.

8. Pizzolato-Cezar, L. R.; Okuda-Shinagawa, N. M.; Machini, M. T., Combinatory Therapy Antimicrobial Peptide-Antibiotic to Minimize the Ongoing Rise of Resistance. *Front. microbiol.* **2019**, *10*, 1703.

9. Sheard, D. E.; Simpson, N. M. O'B.; Wade, J. D.; Separovic F., Combating bacterial resistance by combination of antibiotics with antimicrobial peptides. *Pure Appl. Chem.* **2019,** *91,* 199-209.

10. Gupta, V. K.; Skaife, J. J.; Dubrovsky, T. B.; Abbott, N. L., Optical amplification of ligand-receptor binding using liquid crystals. *Science* **1998**, *279*, 2077-2080.

11. Lowe, A. M.; Abbott, N. L., Liquid Crystalline Materials for Biological Applications. *Chem. Mater*. **2012**, 24, 746-758.

12. Lin, I. H.; Miller, D. S.; Bertics, P. J.; Murphy, C. J.; de Pablo, J. J.; Abbott, N. L., Endotoxin-induced structural transformations in liquid crystalline droplets. *Science* **2011**, *332*, 1297-1300.

13. Naveenkumar, P. M.; Mann, S.; Sharma, K. P., Spontaneous Sequestration of Proteins into Liquid Crystalline Microdroplets. *Adv. Mater. Interfaces* **2019**, *6*, 1801593.

14. Aery, S.; Parry, A.; Calahorra, A. A.; Evans, S. D.; Gleeson, H. F.; Dan, A.; Sarkar, A., Ultra-stable liquid crystal droplets coated by sustainable plant-based materials for optical sensing of chemical and biological analytes. *J. Mater. Chem. C* **2023**, *11*, 5831-5845.

15. Yang, X.; Tian, Y.; Li, F.; Yu, Q.; Tan, S. F.; Chen, Y.; Yang, Z., Investigation of the Assembly Behavior of an Amphiphilic Lipopeptide at the Liquid Crystal–Aqueous Interface, *Langmuir* **2019**, *35*, 2490-2497.

16. Yang, X.; Zhao, X.; Liu, F.; Li, H.; Zhang, C. X.; Yang, Z., Simple, rapid and sensitive detection of Parkinson's disease related alpha-synuclein using a DNA aptamer assisted liquid crystal biosensor. *Soft Matter* **2021**, *17*, 4842-4847.

17. Yang, X.; Yang, Z.; Simple and Rapid Detection of Ibuprofen─A Typical Pharmaceuticals and Personal Care Products─by a Liquid Crystal Aptasensor. *Langmuir* **2022**, *38*, 282-288.

18. Park, J. S.; Abbott, N. L., Ordering Transitions in Thermotropic Liquid Crystals Induced by the Interfacial Assembly and Enzymatic Processing of Oligopeptide Amphiphiles. *Adv. Mater.* **2008**, *20*, 1185-1190.

19. Perera, K.; Dassanayake, T. M.; Jeewanthi, M.; Haputhanthrige, N. P.; Huang, S. D.; Kooijman, E.; Mann, E.; Jákli, A., Liquid Crystal-Based Detection of Antigens with ELISA Sensitivity. *Adv. Mater. Interfaces* **2022**, *9*, 2200891.

20. Noonan, P. S.; Mohan, P.; Goodwin, A. P.; Schwartz, D. K.; DNA Hybridization-Mediated Liposome Fusion at the Aqueous Liquid Crystal Interface. *Adv. Funct. Mater.* **2014**, *24*, 3206-3212.

21. Yang, X.; Li, H.; Zhao, X.; Liao, W.; Zhang, C. X.; Yang, Z.; A novel, label-free liquid crystal biosensor for Parkinson's disease related alpha-synuclein. *Chem. Commun.* **2020**, *56*, 5441-5444.

22. Borbora, A.; Manna, U., Design of a Super-Liquid Crystal-Phobic Coating for Immobilizing Liquid Crystal μ-Droplets─ Without Affecting Their Sensitivity. *Langmuir* **2022**, *38*, 9221-9228.

23. Yang, X.; Zhao, X.; Zhao, H.; Liu, F.; Zhang, S.; Zhang, C. X.; Yang, Z., Combination of liquid crystal and deep learning reveals distinct signatures of Parkinson's disease-related wild-type α-synuclein and six pathogenic mutants. *Chem. Asian J.* **2022**, *17*, e202101251.

24. Manna, U.; Zayas-Gonzalez, Y. M.; Carlton, R. J.; Caruso, F.; Abbott, N. L.; Lynn, D. M., Liquid crystal chemical sensors that cells can wear. *Angew. Chem. Int. Ed.* **2013**, *52*, 14011-14015.

25. Yang, L.; Khan, M.; Park, S. Y., Liquid crystal droplets functionalized with charged surfactant and polyelectrolyte for non-specific protein detection. *RSC Adv.* **2015**, *5*, 97264-97271.

26. Gupta, T.; Mondal, A. K.; Pani, I.; Chattopadhyay, K.; Pal, S. K., Elucidating liquid crystal-aqueous interface for the study of cholesterol-mediated action of a β-barrel pore forming toxin. *Soft Matter* **2022**, *18*, 5293-5301.

27. Adhyapak, P.; Srivatsav, A. T.; Mishra, M.; Singh, A.; Narayan, R.; Kapoor, S., Dynamical organization of compositionally distinct inner and outer membrane lipids of mycobacteria. *Biophys. J.* **2020**, *118*, 1279-1291.

28. Benfield, A. H.; Henriques, S. T., Mode-of-action of antimicrobial peptides: membrane disruption vs. intracellular mechanisms. *Front. Med. Technol.* **2020**, *2*, 610997.

29. Huan, Y.; Kong, Q.; Mou, H.; Yi, H., Antimicrobial peptides: classification, design, application and research progress in multiple fields. *Front. Microbiol.* **2020**, *11*, 582779.

30. Wang, X.; Yang, P.; Mondiot, F.; Li, Y.; Miller, D. S.; Chen, Z.; Abbott, N. L., Interfacial ordering of thermotropic liquid crystals triggered by the secondary structures of oligopeptides. *Chem. Comm.* **2015**, *51*, 16844-16847.

31. Sadati, M.; Apik, A. I.; Armas-Perez, J. C.; Martinez-Gonzalez, J.; Hernandez-Ortiz, J. P.; Abbott, N. L.; de Pablo, J. J., Liquid crystal enabled early stage detection of beta amyloid formation on lipid monolayers. *Adv. Funct. Mater.* **2015**, *25*, 6050-6060.

32. Brake, J. M.; Abbott, N. L., An Experimental System for Imaging the Reversible Adsorption of Amphiphiles at Aqueous-Liquid Crystal Interfaces. *Langmuir* **2002,** *18* (16), 6101-6109.

33. Lelovic N.; Mitachi K.; Yang J.; Lemieux M. R.; Ji Y.; Kurosu M., Application of Mycobacterium smegmatis as a surrogate to evaluate drug leads against Mycobacterium tuberculosis. *J. Antibiot.* **2020,** *73* (11), 780-789.

34. Belanger A. E.; Hatfull G. F., Exponential-Phase Glycogen Recycling Is Essential for Growth of *Mycobacterium smegmatis. J. Bacteriol.* **1999,** *181*(21), 6670-6678.

35. Smeulders M. J.; Keer J.; Speight R. A.; Williams H. D., Adaptation of Mycobacterium smegmatis to stationary phase. *J. Bacteriol.* **1999**, *181*(1), 270-83.

36. Bansal-Mutalik R.; Nikaido H.; Mycobacterial outer membrane is a lipid bilayer and the inner membrane is unusually rich in diacyl phosphatidylinositol dimannosides. *Proc. Natl. Acad. Sci. U. S. A.* **2014,** *111*(13), 4958-4963.

37. Adhyapak P.; Srivatsav A. T.; Mishra M.; Singh A.; Narayan R.; Kapoor S., Dynamical Organization of Compositionally Distinct Inner and Outer Membrane Lipids of Mycobacteria. *Biophys. J.* **2020,** *118*(6), 1279-1291.

38. Sartain M. J.; Dick D. L.; Rithner C. D.; Crick D. C.; Belisle J. T., Lipidomic analyses of *Mycobacterium tuberculosis* based on accurate mass measurements and the novel "*Mtb* LipidDB"[S]. *J. Lipid Res.*, **2011**, *52*(5), 861-872.

39. Meli, M. V.; Lin, I. H.; Abbott, N. L., Preparation of microscopic and planar oil-water interfaces that are decorated with prescribed densities of insoluble amphiphiles. *J. Am. Chem. Soc.* **2008,** *130* (13), 4326-4333.

40. Das, D.; Pal, S. K., Liquid Crystal Unveiled Interactions between Melittin and Phospholipids at Aqueous-Liquid Crystal Interface. *ChemistrySelect* **2017,** *2* (17), 4779-47.

41. Das, D.; Sidiq, S.; Pal, S. K., Design of bio-molecular interfaces using liquid crystals demonstrating endotoxin interactions with bacterial cell wall components. *RSC Adv.* **2015,** *5* (81), 66476-66486.

42. Popov, P.; Honaker, L. W.; Kooijman, E. E.; Mann, E. K.; Jákli, A. I. A liquid crystal biosensor for specific detection of antigens. *Sens. Biosensing Res.* **2016**, *8*, 31-35.

43. Eimura, H.; Miller, D. S.; Wang, X.; Abbott, N. L.; Kato, T., Self-Assembly of Bioconjugated Amphiphilic Mesogens Having Specific Binding Moieties at Aqueous–Liquid Crystal Interfaces. *Chem. Mater.* **2016**, *28*, 1170-1178.

44. Das, D.; Sidiq, S.; Pal, S. K., A Simple Quantitative Method to Study Protein-Lipopolysaccharide Interactions by Using Liquid Crystals. *ChemPhysChem* **2015**, *16*, 753-760.

45. Pani, I.; Swasthi, H. M.; Mukhopadhyay, S.; Pal, S. K. Design of aqueous-liquid crystal interfaces to monitor protein aggregation at nanomolar concentrations. *J. Phys. Chem. C* **2019**, *123*, 1305-1312.

46. Price, A. D.; Schwartz, D. K. DNA Hybridization-Induced Reorientation of Liquid Crystal Anchoring at the Nematic Liquid Crystal/Aqueous Interface. *J. Am. Chem. Soc.* **2008**, *130*, 8188-8194.

47. Ranjbar, B.; Gill, P., Circular dichroism techniques: biomolecular and nanostructural analyses-a review. *Chem. Biol. Drug* **2009**, *74*(2), 101-120.

48. Frank, B.; Yin, X.; Schäferling, M.; Zhao, J.; Hein, S. M.; Braun, P. V.; Giessen, H.; Large-area 3D chiral plasmonic structures. *ACS Nano* **2013**, *7*(7), 6321-6329.

49. Lubitz, I.; Zikich, D.; Kotlyar, A., Specific high-affinity binding of thiazole orange to triplex and G-quadruplex DNA. *Biochemistry* **2010**, *49*(17), 3567-3574.

50. Borovok, N.; Molotsky, T.; Ghabboun, J.; Porath, D.; Kotlyar, A., Efficient procedure of preparation and properties of long uniform G4–DNA nanowires. *Anal. Biochem.* **2008**, *374*(1), 71-78.

Chapter 6

Summary

Amidst the diverse methodologies for scrutinizing various biomolecular phenomena, Liquid Crystals (LCs) stand out as exceptionally responsive interfaces for biomolecular recognition.[1] In comparison to more conventional techniques, encapsulating liquid crystals (LCs) in water yields a biomimetic interface that closely emulates biological systems.[1-3] This approach preserves the intricate features of such systems, encompassing dynamic behaviour, nanomolar concentrations, and considerations for labelling.[1-3] These LC-based optical amplifying interfaces exhibit compelling characteristics, including real-time responsiveness, simplicity, sensitivity, and cost-effectiveness, which are challenging to emulate with specific biophysical techniques.[1-3]

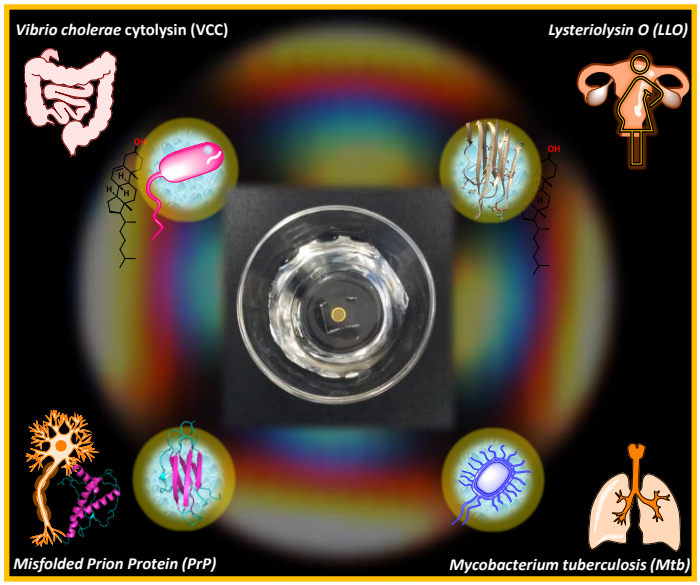

This thesis demonstrates the efficacy of thermotropic nematic LC for investigating specific toxins. Each of the four examples presented addresses a distinct fundamental challenge, showcasing how the interfacial properties of LC can be harnessed. In the initial three instances, LCs are employed to construct membrane mimics to examine lipid-toxin interactions, with implications for bacterial infections, neurodegenerative diseases, and cellular apoptosis. The fourth example reveals the potential of LCs in studying the spatiotemporal evolution of mycobacterial envelopes and the action of antimicrobial peptides as antibiotic synergists. These four diverse studies, utilizing the biointerface of LC, are unified by the overarching challenge of comprehending the self-assembly of LC molecules at biomolecular interfaces. This understanding is pivotal for designing LC-based biochemical sensors and gaining insights into toxin dynamism.

6.1. Comprehension

The discovery of the Liquid Crystal phase by Prof. Reinitzer in 1888 sparked a transformative shift in the display industry, opening new opportunities in optoelectronics and photonics.[1-4] Current research efforts dedicated to Liquid Crystals (LCs) challenge the capabilities of state-of-the-art devices and broaden the scope of their applications.

In recent decades, investigating LCs in sensing technology has yielded profound insights, particularly in elucidating the complexities of biological processes.[1, 2] The interfaces of LCs can be precisely tailored, either through chemical or physical means, facilitating the exploration of a diverse range of biomolecular interactions.[3-8] This adaptability has led to unexpected revelations, creating novel pathways for comprehending and manipulating biological phenomena. The instrumentation utilized in constructing sensors with LCs is characterized by its simplicity, yet it achieves exceptional sensitivity.[1-4] This unique combination allows LC-based sensors to surpass conventional techniques, providing superior performance in the realm of biomolecular sensing and analysis.[1-4] The ongoing scientific exploration of LCs continues to push the frontiers of technological innovation, offering abundant possibilities in the fields of materials science, biology, and beyond.[1-8]

In the aftermath of the COVID-19 pandemic, the contemporary landscape necessitates the development of straightforward technologies for detecting and studying various toxins pervasive in the environment. Motivated by this imperative, the research encapsulated in this thesis endeavours to showcase the utility of LCs in crafting functional interfaces conducive to the exploration of a diverse array of toxins. These applications extend beyond mere detection of biological analytes; they delve into the fundamental dynamics underlying their behaviour. Additionally, our efforts have been directed towards unravelling the intricate spatiotemporal evolutions occurring in mycobacterial envelopes and investigating the actions of antimicrobial peptides as antibiotic synergists. The subsequent section delves into the diverse applications of LCs, as exemplified in Chapters 2 to 4, expounding on their utility in varied contexts. The concluding remarks of each chapter are complemented by a brief discussion of the prospects within the realm of study. This work addresses the urgent need for advanced toxin detection technologies and contributes to the broader scientific understanding of complex biological interactions, positioning LCs as versatile tools in the ongoing pursuit of elucidating environmental challenges.

Pore-forming toxins (PFTs), produced by pathogenic bacteria, stand out as potent virulence factors due to their ability to induce cell death.[9, 10] A considerable subset of these toxins comprises β-barrel PFTs, which form transmembrane oligomeric pores within the membrane lipid bilayer in the presence of cholesterol.[9, 10] The mechanisms underlying pore formation involve intricately regulated events in the membrane environment, featuring substantial protein structure and organization alterations.[11, 12] Moreover, a coordinated interplay between protein and membrane lipid components emerges as pivotal in this process. Despite the profound impact of PFT-induced membrane damage, the specific details of alterations in membrane organization remain obscure in many instances.[11-14]

In **Chapter 2**, we endeavoured to elucidate the lipid membrane interactions of a β-barrel PFT, *Vibrio cholerae* cytolysin (VCC), leveraging LC-aqueous interfaces.[11] Our findings reveal the emergence of dendritic patterns upon introducing VCC to the cholesterol-embedded lipid over the LC film. In contrast, no LC reorientation was observed when VCC was introduced to the lipid-laden LC-aqueous interface devoid of cholesterol. Through epifluorescence and atomic force microscopy (AFM) imaging, we identified that VCC's interfacial binding with cholesterol-containing lipid-decorated LC induces the formation of fibrillar structures, conceivably mixed with lipids. Consequently, the underlying LC aligns along the VCC fibrils at the interface, resulting in a dendritic texture. Notably, the β-sheet-rich nature of the proteins manifests as dendritic patterns and exhibits robust interactions with lipids at the LC-aqueous interface. This observation underscores that the interfacial environment of lipid-laden LC induces the transformation of bound VCC into elongated fibrillar structures, a phenomenon not typically documented in conventional membrane lipid bilayers. Remarkably, the interaction of VCC with a thin layer of lipids assembled at the aqueous interface of LC induces fibrillar structure formation even at nanomolar concentrations. This work not only sheds light on the membrane-damaging action of β-PFTs but also establishes the aqueous interfaces of LC as a valuable platform for investigating the intricate details of changes and defects induced in membranes by membrane-interacting and membrane-damaging proteins, contributing to our broader understanding of these unique protein toxins.

Building upon the insights gleaned from preceding studies, the subsequent **Chapter 3** delves into an exploration of another pore-forming toxin, with a focus on unravelling the mechanistic intricacies underlying its interaction with membranes. Listeriolysin O (LLO), a

pivotal cholesterol-dependent cytolysin secreted by *Listeria monocytogenes*, disrupts phagosomal membranes through pore formation, contributing to pathogenesis.[14, 15] The ability of cholesterol-dependent cytolysins to recognize and bind to membrane cholesterol is a defining feature in their pathogenicity, setting them apart from other toxins.[14, 15] While the conservation of the cholesterol-recognition motif (CRM) has been identified as a prerequisite for membrane binding in some cholesterol-dependent cytolysins,[16] the role of CRM in LLO binding and pore formation remains ambiguous.

This investigation aims to scrutinize LLO-mediated lipid reconfigurations at physiological concentrations using the interfacial properties of a biomimetic LC-aqueous interface. The examination delves into the significance of CRM in protein structure and membrane dynamics regarding the cholesterol-mediated binding of LLO. Our findings indicate that CRM facilitates the binding of LLO to a distinctive amphipathic environment, particularly at low cholesterol levels. However, the removal or substitution of CRM significantly alters the threshold cholesterol level required for LLO activity. In summary, this study elucidates the sophisticated mechanism employed by LLO in binding to various membranes using the LC-aqueous interface as a potent hosting platform. The research highlights the diverse membrane-binding abilities of both LLO and its CRM mutant on lipid membranes hosted on LCs, underscoring the critical role of CRM in LLO binding. The results indicate the remodelling of lipid membranes containing 30 wt%-15 wt% cholesterol in zwitterionic lipids-PC to dendritic domains, indicative of the β-sheet-rich nature of LLO. Comparative analysis of the evolution rates of dendritic domains reveals the interplay of membrane dynamics and the role of CRM in modulating LLO binding to lipid membranes. At lower cholesterol concentrations, CRM mutations diminish LLO activity, in contrast to the heightened activity observed at higher cholesterol levels. The presence of elevated cholesterol in lipid membranes supports LLO by modulating lipid nature, thereby mitigating the impact of CRM mutations in LLO.

This study contributes valuable insights into the processes employed by LLO, shedding light on how Listeria elicits various host cell responses during infection at physiological concentrations. Overall, this research underscores the utility of the LC-aqueous interface as an augmentative tool for discerning differences in protein activity due to mutations in just two amino acids. In a broader context, this study significantly advances our understanding of pore-forming toxin-binding behaviour.

In our subsequent investigation (**Chapter 4**), we focused on prion diseases, a class of fatal neurodegenerative disorders characterized by the misfolding and aggregation of the prion protein (PrP).[17, 18] The cellular PrP is a glycosylphosphatidylinositol (GPI)-anchored, lipid raft-localized protein primarily expressed in the central nervous system.[18] The pathophysiology of PrP involves a significant conformational transformation from a primarily α-helical native state to a β-rich misfolded form, leading to the formation of protease-resistant amyloid-like aggregates.[19] These stable aggregates resist degradation, triggering a cascade of pathological events resulting in neuronal dysfunction, cell death, and the distinctive symptoms associated with prion diseases.[17-19] The self-propagating nature of the misfolded aggregates facilitates further conformational changes in normal PrP, perpetuating the disease process.[17-19]

In this study, we leveraged the interfacial properties of LCs to monitor the lipid membrane-induced conformational switching of PrP into β-rich amyloid fibrils.[17] The conformational switching and aggregation occurred at nanomolar protein concentrations, primarily driven by electrostatic interactions between PrP and lipid headgroups. Our LC-based methodology serves as a potent and sensitive tool for detecting and elucidating the molecular mechanisms of PrP misfolding mediated by lipid-protein interactions at the aqueous interface under physiological conditions. Our findings highlight the crucial role of electrostatic forces in guiding lipid-protein interactions during the initial binding, influencing PrP-lipid interactions at the interface, leading to an increased effective concentration of PrP and promoting short-range hydrophobic and protein-protein interactions. Consequently, the misfolding of PrP, induced by hydrophobic interactions with effective electrostatic charge neutralization, results in enhanced aggregation into oligomers.

We propose that at the LC-aqueous interface, these nanometre-sized oligomers function as colloidal particles, and the aggregation morphologies catalysed by chemoresponsive LC vary depending on the densities of oligomers at the interfaces. In summary, our study introduces an efficient LC-aqueous interfacial system to monitor a complex cascade of lipid-induced conformational switching and aggregation of PrP, demonstrating sensitivity toward non-covalent forces modulating lipid-protein interactions. Our results also revealed the remodelling of lipid membranes into dendritic domains during the interactions and recognized different membrane components-mediated steering of PrP either toward fibrillation or clustering at the LC-aqueous interface.

In conclusion, this study presents a straightforward strategy to investigate protein-lipid membrane interactions even at sub-micromolar concentrations. Furthermore, we envision that our approach can provide molecular insights into various neurodegenerative diseases resulting from lipid-mediated protein misfolding and amyloid formation.

Chapter 5 dealt with the antibiotic-resistant infectious tuberculosis associated with *Mycobacterium tuberculosis* (*Mtb*), which remains a significant global health challenge.[20-22] In this study, we employ the interfacial properties of LC to gain a comprehensive understanding of the spatiotemporal modifications occurring in the envelopes of *Mtb*. The optical responses of LC reveal a disorganization of outer membrane lipids relative to inner membrane lipids, highlighting the adaptability of *Mtb*. This adaptability is characterized by substantial evolutions in spatial envelope dynamics throughout the lifespan of the bacteria. Our investigation underscores *Mtb's* remarkable capacity to dynamically adjust lipid compositions, leading to variable membrane densities and charge distributions across different growth phases. These lipid adaptations are pivotal for the resilience of *Mtb* in adverse conditions and its resistance to drugs.

Notably, the outer membrane lipid (OML) consistently exhibits lower organization than the inner membrane lipid (IML) throughout various growth phases. Our study shows how different AMPs employ distinct mechanisms to disrupt bacterial membranes, with disruption achievable only at concentrations surpassing a specific threshold. Interestingly, during early bacterial growth, variations in density and charge modulation appear to mitigate the impact of AMPs. This suggests that combining aurein and maculatin may synergistically prove more efficient in dismantling bacterial envelopes. While our study primarily focuses on the organized inner membranes of bacteria, it lays the foundation for the development of a robust platform to investigate specific alterations and deficiencies induced in membranes by various antibiotics. This advancement contributes to a broader understanding of bacterial membrane-based therapeutic approaches.

This research emphasizes the ability of Australian frog antimicrobial peptides (AMPs), specifically aurein and maculatin, to enhance membrane permeability, thereby facilitating the entry of drugs into bacterial cells. The LC-biointerface serves as a sensitive tool to elucidate the molecular mechanisms behind AMP-mediated antibiotic sensitization of bacterial membranes under physiological conditions.

In conclusion, this research presents a straightforward approach to investigating bacterial lipid modulation and drug effects. We envision this strategy as a valuable tool for gaining molecular insights into antibiotic potentiators, with potential applications in point-of-care diagnostics and therapeutic interventions.

In a nutshell, LC materials are poised to revolutionize label-free diagnostics, particularly through the integration of smartphone-based technology with LC-based aptasensors and immunosensors.[1-3] This convergence holds the promise of creating clinically relevant diagnostic platforms. The aqueous interfaces of LC enable the amplification of biomolecular interactions into macroscopic signals, showcasing their potential in the last two decades for designing effective, rapid, and cost-efficient diagnostics.[1-3] Unlike many biosensors that rely on intricate assays and tend to be expensive, LC has proven to be an excellent candidate for biosensor materials. The utilization of LC-based biosensors can be instrumental in addressing the challenges associated with the affordability and accessibility of diagnostic tools.

Furthermore, the application of LC extends beyond diagnostics, as it holds significant potential for advancing the comprehension and design of stimuli-responsive scaffolds that mimic biological systems. Developing affordable diagnostic tools using LC becomes particularly relevant in providing decentralized care in regions with high populations, making a substantial contribution to healthcare solutions.

6.2. Acknowledgements

T.G. acknowledges powerpoint, chemdraw, pymol and chimera tools for various cartoons and protein structures used in the table of contents (TOC) graphics.

References

1. Lockwood, N.; Gupta, J.; Abbott, N., Self-assembly of amphiphiles, polymers and proteins at interfaces between thermotropic liquid crystals and aqueous phases. *Surf. Sci. Rep.* **2008,** *63* (6), 255-293.

2. Lowe, A. M.; Abbott, N. L., Liquid Crystalline Materials for Biological Applications. *Chem. Mater.* **2012,** *24* (5), 746-758.

3. Woltman, S. J.; Jay, G. D.; Crawford, G. P., Liquid-Crystal Materials Find a New Order in Biomedical Applications. *Nat. Mater.* **2007,** *6* (12), 929-38.

4. Collings, P. J.; Hird, M., *Introduction to Liquid Crystals: Chemistry and Physics (1st ed.)*. CRC Press: 1997.

5. Sadati, M.; Apik, A. I.; Armas-Perez, J. C.; Martinez-Gonzalez, J.; Hernandez-Ortiz, J. P.; Abbott, N. L.; de Pablo, J. J., Liquid Crystal Enabled Early Stage Detection of Beta Amyloid Formation on Lipid Monolayers. *Adv. Funct. Mater.* **2015,** *25* (38), 6050-6060.

6. Das, D.; Sidiq, S.; Pal, S. K., Design of bio-molecular interfaces using liquid crystals demonstrating endotoxin interactions with bacterial cell wall components. *RSC Adv.* **2015,** *5* (81), 66476-66486.

7. Wang, X.; Yang, P.; Mondiot, F.; Li, Y.; Miller, D. S.; Chen, Z.; Abbott, N. L., Interfacial ordering of thermotropic liquid crystals triggered by the secondary structures of oligopeptides. *Chem. Commun.* **2015,** *51* (94), 16844-7.

8. Tan, L. N.; Orler, V. J.; Abbott, N. L., Ordering transitions triggered by specific binding of vesicles to protein-decorated interfaces of thermotropic liquid crystals. *Langmuir* **2012,** *28* (15), 6364-76.

9. Gouaux, E., Channel-forming toxins: tales of transformation. *Curr. Opin. Struct. Biol.* **1997,** *7* (4), 566-73.

10. Parker, M. W.; Feil, S. C., Pore-forming protein toxins: from structure to function. *Prog. Biophys. Mol. Biol.* **2005,** *88* (1), 91-142.

11. De, S.; Olson, R., Crystal structure of the *Vibrio cholerae* cytolysin heptamer reveals common features among disparate pore-forming toxins. *Proc. Natl. Acad. Sci. U. S. A.* **2011,** *108* (18), 7385-90.

12. Zitzer, A.; Zitzer, O.; Bhakdi, S.; Palmer, M., Oligomerization of *Vibrio cholerae* cytolysin yields a pentameric pore and has a dual specificity for cholesterol and sphingolipids in the target membrane. *J. Biol. Chem.* **1999,** *274* (3), 1375-80.

13. Gupta, T.; Mondal, A. K.; Pani, I.; Chattopadhyay, K.; Pal, S. K., Elucidating liquid crystal-aqueous interface for the study of cholesterol-mediated action of a β-barrel pore forming toxin. *Soft Matter* **2022,** *18* (28), 5293-5301.

14. Lata, K.; Singh, M.; Chatterjee, S.; Chattopadhyay, K., Membrane Dynamics and Remodelling in Response to the Action of the Membrane-Damaging Pore-Forming Toxins. *J. Membr. Biol.* **2022,** *255* (2-3), 161-173.

15. Tweten, R. K., Cholesterol-dependent cytolysins, a family of versatile pore-forming toxins. *Infect. Immun.* **2005,** *73* (10), 6199-209.

16. Farrand, A. J.; LaChapelle, S.; Hotze, E. M.; Johnson, A. E.; Tweten, R. K., Only two amino acids are essential for cytolytic toxin recognition of cholesterol at the membrane surface. *Proc. Natl Acad. Sci. U. S. A.* **2010,** *107* (9), 4341-6.

17. Gupta, T.; Arora, L.; Mukhopadhyay, S.; Pal, S. K., Ultrasensitive detection of lipid-induced misfolding of the Prion Protein at the aqueous-liquid crystal interface. *J. Phys. Chem. Lett.* **2024***, 15,* 8, 2117–2122.

18. Prusiner, S. B., *Prion Biology and Diseases.* Gold Spring Harbour Laboratory Press: New York, 2017.

19. Wang, F.; Yang, F.; Hu, Y.; Wang, X.; Wang, X.; Jin, C.; Ma, J., Lipid interaction converts prion protein to a PrPSc-like proteinase K-resistant conformation under physiological conditions. *Biochemistry* **2007,** *46* (23), 7045-53.

20. Harding, E., WHO global progress report on tuberculosis elimination. *Lancet. Respir. Med.* **2020,** *8* (1), 19.

21. Hawkes, D. J.; Mak, J., Lipid membrane; a novel target for viral and bacterial pathogens. *Curr. Drug Targets* **2006,** *7* (12), 1615-21.

22. Mingeot-Leclercq, M. P.; Décout, J. L., Bacterial lipid membranes as promising targets to fight antimicrobial resistance, molecular foundations and illustration through the renewal of aminoglycoside antibiotics and emergence of amphiphilic aminoglycosides. *Med. Chem. Comm.* **2016,** *7* (4), 586-611.

List of Publications

1. Nandi, R.; Jain, V.; Devi, M.; **Gupta, T.**; Pal, S. K., Hydrogen bond assisted anchoring transitions in nematic liquid crystals at the aqueous interface. *Colloids Surf. A Physicochem. Eng. Asp.* **2021**, *625*, 126952.

2. **Gupta, T.**; Mondal A. K.; Pani I.; Chattopadhyay, K.; Pal S. K., Elucidating liquid crystal-aqueous interface for the study of cholesterol-mediated action of a β-barrel pore forming toxin. *Soft Matter* **2022**, *18*, 5293-5301.

3. Devi, M.; Sil, Soma; Pani I.; **Gupta T.**; Pal S. K., Design of liquid crystal-aqueous interface for detection of calcium ions using protein as recognition probe. *Liq. Cryst.* **2023**, DOI: 10.1080/02678292.2023.2266432.

4. **Gupta, T.**; Arora, L.; Mukhopadhyay, S.; Pal, S. K., Ultrasensitive detection of lipid-induced misfolding of the Prion Protein at the aqueous-liquid crystal interface. *J. Phys. Chem. Lett.* **2024**, *15*, 8, 2117–2122.

5. **Gupta, T.**; Lata, K., Chattopadhyay, K.; Pal, S. K., Investigating mutation and membrane guided action of Listeriolysin O at aqueous-Liquid Crystal Interface. (*Manuscript under revision in J. Mater. Chem. B*)

6. **Gupta, T.**; Menon P A.; Kapoor, S.; Pal, S. K., Liquid crystals-aqueous interfaces render selective detection of distinctive mycobacterial cell envelope responses. (*Manuscript submitted)*

Originality Reports and Copyrights

Overall Thesis

DrillBit Report

DrillBit

The Report is Generated by DrillBit Plagiarism Detection Software

Submission Information

Author Name	Tarang Gupta
Title	Toxin-Induced Ordering Transitions of Liquid Crystals at Biomolecular Interfaces
Paper/Submission ID	1815559
Submitted by	ph18066@iisermohali.ac.in
Submission Date	2024-05-16 16:20:08
Total Pages, Total Words	87, 26382
Document type	Thesis

Result Information

Similarity **13 %**

1 10 20 30 40 50 60 70 80 90

Turntin Report

ORIGINALITY REPORT

9%	4%	6%	2%
SIMILARITY INDEX	INTERNET SOURCES	PUBLICATIONS	STUDENT PAPERS

ELSEVIER LICENSE
TERMS AND CONDITIONS

May 24, 2024

This Agreement between Ms. Tarang gupta ("You") and Elsevier ("Elsevier") consists of your license details and the terms and conditions provided by Elsevier and Copyright Clearance Center.

License Number	5795290695055
License date	May 24, 2024
Licensed Content Publisher	Elsevier
Licensed Content Publication	Surface Science Reports
Licensed Content Title	Self-assembly of amphiphiles, polymers and proteins at interfaces between thermotropic liquid crystals and aqueous phases
Licensed Content Author	Nathan A. Lockwood,Jugal K. Gupta,Nicholas L. Abbott
Licensed Content Date	Jun 15, 2008
Licensed Content Volume	63
Licensed Content Issue	6
Licensed Content Pages	39
Start Page	255
End Page	293
Type of Use	reuse in a thesis/dissertation
Portion	figures/tables/illustrations
Number of figures/tables/illustrations	1
Format	both print and electronic
Are you the author of this Elsevier article?	No
Will you be translating?	No
Title of new work	Toxin-Induced Ordering Transitions of Liquid Crystals at Biomolecular Interfaces
Institution name	IISER Mohali
Expected presentation date	Jun 2024
Portions	Figure 3
Requestor Location	Ms. Tarang gupta 67, NEW Milap nagar, hissar road ambala city, HARYANA 134003 India Attn: IISER Mohali
Publisher Tax ID	GB 494 6272 12
Billing Type	Invoice
Billing Address	Ms. Tarang gupta 67, NEW Milap nagar, hissar road ambala city, India 134003 Attn: IISER Mohali
Total	**0.00 USD**

Issue 28, 2022

Previous Article | Next Article

From the journal:
Soft Matter

Elucidating liquid crystal-aqueous interface for the study of cholesterol-mediated action of a β-barrel pore forming toxin†

Check for updates

Tarang Gupta, ‡[a] Anish Kumar Mondal, ‡[b] Ipsita Pani, [a] Kausik Chattopadhyay*[b] and Santanu Kumar Pal *[a]

Author affiliations

Abstract

Pore-forming toxins (PFTs) produced by pathogenic bacteria serve as prominent virulence factors with potent cell-killing activity. Most of the β-barrel PFTs form transmembrane oligomeric pores in the membrane lipid bilayer in the presence of cholesterol. The pore-formation mechanisms of the PFTs highlight well-orchestrated regulated events in the membrane environment, which involve dramatic changes in the protein structure and

About | Cited by | Related

Gmail — Tarang Gupta <tarangguptachem@gmail.com>

Requesting publisher's permission to reuse full article in the author's dissertation
3 messages

Tarang Gupta <tarangguptachem@gmail.com> — Wed, Dec 6, 2023 at 11:54 AM
To: technicalsupport@rsc.org
Cc: ph18066@iisermohali.ac.in, RSC1@rsc.org

Dear sir/ma'am,

I am Tarang Gupta, a research scholar at IISER Mohali. I am requesting the rights and permission to reuse the full article (DOI https://doi.org/10.1039/D2SM00447J) in my PhD dissertation.

I have attached a print of the permission page which states that "If you are the author of this article, you do not need to request permission to reproduce figures and diagrams provided correct acknowledgement is given."

Is it sufficient to attach the following permission? Since I have to keep a copy of the copyright permission in my dissertation, I request you to help me with this. If anything else needs to be done, kindly let me know.

Thanks and Regards,

Tarang Gupta

PhD Scholar
Dr. Santanu Kumar Pal, IISER Mohali
Knowledge City, SAS nagar, 140306
Contact no. 7988947885

2 attachments

RSC.png
351K

Elucidating liquid crystal-aqueous interface for the study of cholesterol-mediated action of a β-barrel pore forming toxin - Soft Matter (RSC Publishing).pdf
1508K

Gmail

Tarang Gupta <tarangguptachem@gmail.com>

Requesting publisher's permission to reuse full article in the author's dissertation

CONTRACTS-COPYRIGHT (shared) <Contracts-Copyright@rsc.org>
To: "tarangguptachem@gmail.com" <tarangguptachem@gmail.com>

Wed, Dec 6, 2023 at 4:08 PM

Dear Tarang

Many thanks for your query below. You are not required to request formal permission to reuse your own article in your thesis, meaning you are free to do so provided that you provide the correct acknowledgement and check if permission is required for third party content in the article (e.g. figures from other publishers). In very general terms this is illustrated in the permissions flowchart on our website:

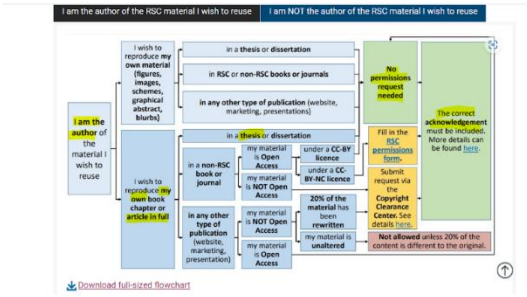

However you can use the text/this email below as evidence if required by your institution:

The Royal Society of Chemistry (RSC) hereby grants permission for the use of your paper(s) specified below in the printed and microfilm version of your thesis. You may also make available the PDF version of your paper(s) that the RSC sent to the corresponding author(s) of your paper(s) upon publication of the paper(s) in the following ways: in your thesis via any website that your university may have for the deposition of theses, via your university's Intranet or via your own personal website. We are however unable to grant you permission to include the PDF version of the paper(s) on its own in your institutional repository. The Royal Society of Chemistry is a signatory to the STM Guidelines on Permissions (available on request).

Please note that if the material specified below or any part of it appears with credit or acknowledgement to a third party then you must also secure permission from that third party before reproducing that material.

Please ensure that the thesis includes the correct acknowledgement (see http://rsc.li/permissions for details) and a link is included to the paper on the Royal Society of Chemistry's website.

Please also ensure that your co-authors are aware that you are including the paper in your thesis.

Best wishes

Becky

Becky Roberts
Contracts & Copyright Executive, Sales Operations

Royal Society of Chemistry

T: +44 (0) 1223 432304 | www.rsc.org

ROYAL SOCIETY OF CHEMISTRY

Ultrasensitive Detection of Lipid-Induced Misfolding of the Prion Protein at the Aqueous–Liquid Crystal Interface

Author: Tarang Gupta, Lisha Arora, Samrat Mukhopadhyay, et al
Publication: Journal of Physical Chemistry Letters
Publisher: American Chemical Society
Date: Feb 1, 2024

Gmail Tarang Gupta <tarangguptachem@gmail.com>

Query regarding copyrights to reuse full article in the author's dissertation

2 messages

Tarang Gupta <tarangguptachem@gmail.com> Thu, May 16, 2024 at 11:24 AM
To: Copyright@acs.org

Dear sir/ma'am,

I am Tarang Gupta, a research scholar at IISER Mohali. I am requesting the rights and permission to reuse the full article (DOI: https://doi.org/10.1021/acs.jpclett.3c02770) in my PhD dissertation.

I have attached a print of the permission page which states that "If you are the author of this article, you do not need to request permission to reproduce figures and diagrams provided correct acknowledgement is given."

Is it sufficient to attach the following permission? Since I have to keep a copy of the copyright permission in my dissertation, I request you to help me with this. If anything else needs to be done, kindly let me know.

Thanks and Regards,

Tarang Gupta

PhD Scholar
Dr. Santanu Kumar Pal, IISER Mohali
Knowledge City, SAS nagar, 140306
Contact no. 7988947885

Rightslink® by Copyright Clearance Center.pdf
190K

Gmail Tarang Gupta <tarangguptachem@gmail.com>

Query regarding copyrights to reuse full article in the author's dissertation

Copyright <Copyright@acs.org> Fri, May 17, 2024 at 5:03 PM
To: Tarang Gupta <tarangguptachem@gmail.com>, Copyright <Copyright@acs.org>

Dear Tarang Gupta,

In reference to your message below, the following is from the **American Chemical Society's Policy on Theses and Dissertations:**

This policy addresses permission to include **your article**(s) or portions of text from **your article**(s) in your thesis.

Reuse/Republication of the Entire Work in Theses or Collections: Authors may reuse all or part of the Submitted, Accepted or Published Work in a thesis or dissertation that the author writes and is required to submit to satisfy the criteria of degree-granting institutions. Such reuse is permitted subject to the ACS' "Ethical Guidelines to Publication of Chemical Research". Appropriate citation of the Published Work must be made as follows:

"Reprinted with permission from [COMPLETE REFERENCE CITATION]. Copyright [YEAR] American Chemical Society." Insert the appropriate wording in place of the capitalized words. Citation information may be found after the "Cite this:" heading below the title of the online version and at the bottom of **the first page of the pdf or print version of your ACS journal article**.

If the thesis or dissertation to be published is in electronic format, a direct link to the Published Work must also be included using the ACS Articles on Request author-directed link.

If your university requires you to obtain permission for manuscripts in ASAP status or final published articles, you must use the RightsLink permission system. **See RightsLink instructions at http://pubs.acs.org/page/copyright/permissions.html and make requests at the "Rights & Permissions" link under the title of the online version of the article.**

Submission to a Dissertation Distributor: If you plan to submit your thesis to UMI or to another dissertation distributor, you should not include the unpublished ACS paper in your thesis if the thesis will be disseminated electronically, until ACS has published your paper. After publication of the paper by ACS, you may release the entire thesis (**not the individual ACS article by itself**) for electronic dissemination through the distributor; ACS's copyright credit line should be printed on the first page of the ACS paper.

I hope this information is helpful.

Sincerely,

Keri Travis *(she/her)*

Copyright Specialist

Office of the Secretary & General Counsel

American Chemical Society

Conferences and Workshops

1. Oral presentation at 3rd International Conference on Nanomaterials in Biology (ICNB 2023) by IIT Gandhinagar in association with Soft Materials Research Society (SMRS), Jaipur, on "Ultrasensitive Detection of Lipid-Induced Misfolding of the Prion Protein at the Aqueous-Liquid Crystal Interface**".**

2. Poster presentation at 30th National Conference on Liquid Crystals (30th NCLC - 2023) by Andhra University, Visakhapatnam, Andhra Pradesh, in association with Indian Liquid Crystal Society.

3. Poster presentation at RSCPoster Twitter conference 2023.

4. Poster presentation at the 26th National Conference on Liquid Crystals (26th NCLC - 2019) by Chitkara University, Punjab, in association with the Indian Liquid Crystal Society.

5. Poster presentation at 29th Chemical Research Society of India- National Chemistry Symposium (CRSI-NSC) 2022 at IISER Mohali.

VITA

Tarang Gupta was born and raised in Ambala city in Haryana, where she completed her schooling and graduated. In 2015, she joined Punjabi University Patiala for her post-graduation in chemistry. After her M.Sc., she cleared the National Eligibility Test (NET) and was awarded a CSIR-Junior research fellowship (JRF). In Dec 2018, she joined IISER Mohali. She is now pursuing her PhD under Dr. Santanu Kumar Pal. Her research includes the design of stimuli-responsive interfaces formed between liquid crystals and aqueous phases for applications in label-free biosensing. During her PhD, she has presented oral and poster presentations at national and international conferences. She has authored and co-authored publications in reputed peer-reviewed international journals.